

Characterisation of the
biomechanical, passive, and active
properties of femur-tibia joint leg
muscles in the stick insect *Carausius*
morosus

Inaugural-Dissertation

zur

Erlangung des Doktorgrades

der Mathematisch-Naturwissenschaftlichen Fakultät

der Universität zu Köln

vorgelegt von

Christoph Guschlbauer

aus Wien

Köln

Februar 2009

Berichtersteller:
Prof. Dr. Ansgar Büschges
Prof. Dr. Peter Kloppenburg

Tag der mündlichen Prüfung:

30.04.2009

Abstract

The understanding of locomotive behaviour of an animal necessitates the knowledge not only about its neural activity but also about the transformation of this activity patterns into muscle activity. The stick insect is a well studied system with respect to its motor output which is shaped by the interplay between sensory signals, the central neural networks for each leg joint and the coordination between the legs. The muscles of the FT (femur-tibia) joint are described in their morphologies and their motoneuronal innervation patterns, however little is known about how motoneuronal stimulation affects their force development and shortening behaviour. One of the two muscles moving the joint is the extensor tibiae, which is particularly suitable for such an investigation as it features only three motoneurons that can be activated simultaneously, which comes close to a physiologically occurring activation pattern. Its antagonist, the flexor tibiae, has a more complex innervation and a biomechanical investigation is only reasonable at full motoneuronal recruitment. Muscle force and length changes were measured using a dual-mode lever system that was connected

to the cut muscle tendon.

Both tibial muscles of all legs were studied in terms of their geometry: extensor tibiae muscle length changes with the cosine of the FT joint angle, while flexor tibiae length changes with the negative cosine, except for extreme angles (close to 30° and 180°). For all three legs, effective flexor tibiae moment arm length (0.564 mm) is twice that of the extensor tibiae (0.282 mm). Flexor tibiae fibres are 1.5 times longer (2.11 mm) than extensor tibiae fibres (1.41 mm). Active isometric force measurements demonstrated that extensor tibiae single twitch force is notably smaller than its maximal tetanical force at 200 Hz (2-6 mN compared to 100-190 mN) and takes a long time to decrease completely (> 140 ms). Increasing either frequency or duration of the stimulation extends maximal force production and prolongs the relaxation time of the extensor tibiae. The muscle reveals 'latch' properties in response to a short-term increase in activation. Its working range is on the ascending limb of the force-length relationship (see Gordon et al. (1966b)) with a shift in maximum force development towards longer fibre lengths at lower activation. The passive static force increases exponentially with increasing stretch. Maximum forces of 5 mN for the extensor, and 15 mN for the flexor tibiae occur within the muscles' working ranges. The combined passive torques of both muscles determine the rest position of the joint without any muscle activity. Dynamically generated forces of both muscles can become as large as 50-70 mN when stretch ramps mimic a fast middle leg swing phase. FT joint torques alone (with ablated muscles) do not depend on FT joint angle, but on deflection amplitude and velocity. Isotonic force experiments using physiological activation patterns demonstrate that the extensor tibiae acts like a low-pass filter by contracting smoothly to fast instantaneous stimulation frequency changes. Hill hyperbolas at 200 Hz vary a great deal with respect to maximal force (P_0) but much less in terms of contraction velocity (V_0) for both tibial muscles. Maximally stimulated flexor tibiae muscles are on average 2.7 times stronger than extensor tibiae muscles (415 mN and 151 mN), but contract only 1.4 times faster ($6.05 \frac{mm}{s}$ and $4.39 \frac{mm}{s}$). The dependence of extensor tibiae V_0 and P_0 on stimulation frequency can be described with an exponential saturation curve. V_0 increases linearly with length within the muscle's working range. Loaded release experiments characterise extensor and flexor tibiae series elastic components as quadratic springs. The mean spring constant β of the flexor tibiae is 1.6 times larger than β of the extensor tibiae at maximal stimulation. Extensor tibiae stretch and relaxation ramps show that muscle relaxation time constant slowly changes with muscle

length, and thus muscle dynamics have a long-lasting dependence on muscle length history. High-speed video recordings show that changes in tibial movement dynamics match extensor tibiae relaxation changes at increasing stimulation duration.

Zusammenfassung

Um das Fortbewegungsverhalten eines Tieres verstehen zu können ist nicht nur die Kenntnis neuronaler Aktivität erforderlich, sondern auch die Umsetzung dieser Muster in Muskelaktivität. Die Stabheuschrecke stellt in Bezug auf die Erzeugung motoneuronaler Aktivität ein gut untersuchtes System dar. Diese motoneuronalen Aktivitätsmuster sind das Ergebnis des Zusammenspiels zwischen sensorischen Signalen, den zentralen neuronalen Netzwerken jedes Bein Gelenks und der Koordination der Beine untereinander. Die Muskeln des FT- (Femur-Tibia) Gelenks sind in ihrer Morphologie und der Art ihrer motoneuronalen Innervation beschrieben. Es ist jedoch wenig bekannt darüber, wie sich eine Stimulation ihrer Motoneurone in der Entwicklung von Kraft oder Verkürzung ihrer Fasern widerspiegelt. Einer der beiden Muskeln, die das Gelenk bewegen, ist der Extensor tibiae, der sich für eine derartige Untersuchung besonders gut eignet, da er nur drei Motoneurone besitzt, die simultan gereizt werden können. Dies kommt einem physiologischen Aktivierungsmuster recht nahe. Sein Antagonist, der Flexor tibiae, ist komplizierter innerviert und eine biomechanische Untersuchung ist ausschließlich bei Rekrutierung aller Motoneurone sinnvoll.

Muskelkraft und Muskellänge wurden mit einem 'dual-mode' Hebelarmsystem gemessen, welches mit der abgeschnittenen Muskelsehne verbunden wurde.

Beide tibiale Muskeln aller Beine wurden in Hinblick auf ihre Geometrie untersucht: Die Muskellänge des Extensor tibiae ändert sich mit dem Cosinus des FT-Gelenkwinkels, die des Flexor tibiae hingegen mit dem negativen Cosinus, ausser bei extremen Winkeln (nahe 30° oder 180°). Bei allen drei Beinen ist die effektive Hebelarmlänge des Flexor tibiae von 0.564 mm doppelt so lang wie die des Extensor tibiae (0.282 mm). Flexor tibiae Fasern sind mit 2.11 mm anderthalb mal so lang wie Extensor tibiae Fasern (1.41 mm). Messungen der aktiven Muskelkraft zeigen, dass die Einzelzuckungskraft des Extensor tibiae deutlich kleiner ist als seine maximale tetanische Kraft bei 200 Hz (2-6 mN im Vergleich zu 100-190 mN) und dass sie lange braucht, um wieder vollständig abzufallen (>140 ms). Erhöhung entweder der Frequenz oder der Dauer einer Reizung verlängert die Dauer maximal erzeugter Kraft und verlängert die Relaxationszeit des Extensor tibiae. Der Muskel zeigt 'Latch'-Eigenschaften sobald es zu kurzfristigen Aktivierungserhöhungen kommt. Sein Arbeitsbereich befindet sich auf der aufsteigenden Flanke der Kraft-Längen-Beziehung (siehe Gordon et al. (1966b)). Die Entwicklung maximaler Kraft ist bei niedriger Aktivierung zu größeren Faserlängen hin verschoben. Passive Kraft steigt mit wachsender Muskeldehnung exponentiell an. Innerhalb des Arbeitsbereichs treten maximale Kräfte von 5 mN beim Extensor und 15 mN beim Flexor tibiae auf. Die kombinierten passiven Drehmomente beider Muskeln bestimmen den Ruhewinkel des Gelenks, der sich ohne Muskelaktivierung einstellt. Dynamische passive Kräfte von Extensor und Flexor tibiae können 50-70 mN groß werden, wenn die Dehnungsrampen einer schnellen Schwingphase des Mittelbeins nachempfunden werden. Kräfte im Gelenk (also ohne Muskeln) sind unabhängig davon, welchen Winkel das FT-Gelenk beschreibt. Sie sind jedoch von der Amplitude und Geschwindigkeit tibialer Auslenkung abhängig. Der Extensor tibiae verhält sich bei physiologischer Aktivierung wie ein Tiefpassfilter: er zeigt einen glatten Kontraktionsverlauf bei schnellen Änderungen instantaner Reizfrequenz. Hill-Hyperbeln beider tibialer Muskeln zeigen große Variabilität in Hinsicht auf maximal erzeugte Kraft (P_0) aber variieren weit weniger in Hinsicht auf maximale Kontraktionsgeschwindigkeit (V_0) bei einer Reizfrequenz von 200 Hz. Maximal gereizte Flexor tibiae Muskeln sind im Schnitt 2.7 mal stärker als Extensor tibiae Muskeln (415 mN und 151 mN), verkürzen sich jedoch nur 1.4 mal schneller ($6.05 \frac{mm}{s}$ and $4.39 \frac{mm}{s}$). Die Abhängigkeit von V_0 und P_0 des Extensor tibiae kann mit einer exponentiellen

Sättigungskurve beschrieben werden. V_0 wächst linear mit der Muskellänge innerhalb des Arbeitsbereichs. Durch Experimente, bei denen der Muskel abrupt entlastet wird, kann man die serienelastische Komponente von Extensor und Flexor tibiae als quadratische Feder charakterisieren. Die Federkonstante β des Flexor tibiae ist im Durchschnitt um den Faktor 1.6 größer als die des Extensor tibiae. Reizung des Extensor tibiae mit Dehnungs- und Entspannungsrampen zeigen, dass sich die Zeitkonstante der Entspannung langsam mit der Muskellänge ändert und daher dynamische Eigenschaften des Muskels langanhaltend von vorigen Muskellängenänderungen abhängig sind. Hochgeschwindigkeitsvideoaufnahmen zeigen, dass bei Steigerung der Reizdauer Änderungen der Dynamik tibialer Bewegung mit Änderungen des Relaxationsverhaltens des Extensor tibiae einher gehen.

Contents

Abstract	1
Zusammenfassung	4
A. Introduction	11
B. Materials and Methods	21
1 Femur, muscle, fibre and sarcomere length measurements	22
2 Measurements with the Aurora 300B dual mode lever system	25
3 Animal preparation and dissection	27
4 Extracellular motoneuronal recording	27
5 Electrical stimulation of motoaxons	28
5.1 Recruitment of extensor tibiae motoneurons	28
5.2 Physiological stimulation of extensor motoneurons	32
5.3 Stimulation of flexor tibiae motoneurons	33
5.4 Isometric force experiments	33
5.5 Isotonic force experiments	34
6 Photo and video tracking of tibia movements	35
7 Data achievement, storage and evaluation	36
7.1 Statistics	36
C. Results	38
C1 Femoral geometry	39
1 Muscle length measurements of front, middle and hind leg tibial muscles	39
1.1 Relationship between resting muscle length and femur length .	39
1.2 Relationship between muscle length and FT-joint angle	40

1.3	Moment arm determination	41
2	Fibre length measurements of middle leg tibial muscles	42
3	Sarcomere length measurements of middle leg tibial muscles	43
4	Femoral cross-sectional area	48
C2	Force measurements in the isometric domain	49
1	Actively generated forces	49
1.1	Single twitch kinetics	49
1.2	Force kinetics at different activation	52
1.3	Post-stimulational force dynamics at different activation	53
1.4	Post-stimulational force dynamics at different stimulation duration	57
1.5	Force development in response to activation changes (latch)	58
1.6	The force-length relationship at different activation	62
C3	Passive forces I	68
1	Stretch experiments	68
1.1	Visco-elastic properties I	68
1.2	(Static) passive force-length relationship	71
1.3	Dynamic passive forces	73
2	Significance for tibial movements	76
3	FT-joint torques	78
C4	Force measurements in the isotonic domain	84
1	Muscle contractions in response to physiological stimulation	84
2	Loaded release experiments in response to tonical stimulation: the force-velocity relationship	89
2.1	The Hill hyperbola at maximal stimulation	91
2.2	Deviations from the hyperbolic shape	95
2.3	The Hill hyperbola at different activation levels	96
2.4	Activation dependent parameters	97
2.5	Length dependence of the maximal contraction velocity	99
3	Isometric and isotonic contraction dynamics at different muscle lengths	100
C5	Passive forces II	105
1	Series elasticity	105

1.1	Series elasticity of tibial muscles at maximal activation	105
1.2	Series elasticity of the extensor tibiae at different activation levels	108
2	Visco-elastic properties II: creep experiments	109
C6	Force generation under naturally occurring FT joint movement patterns	116
1	Extensor tibiae forces before, during and after simulated stance phase	116
2	Extensor tibiae forces at the simulated transition from swing to stance phase	122
3	Interaction of agonistic and antagonistic passively and actively generated forces during simulated swing and stance	126
3.1	Simulating tibial swing / stance phase	126
3.2	Simulated swing relaxation at maximal tibia extension	129
3.3	Simulated swing relaxation after hitting an obstacle	130
D.	Discussion	134
D1	Femoral geometry	136
D2	Force measurements in the isometric domain	142
D3	Passive forces I	155
D4	Force measurements in the isotonic domain	166
D5	Passive forces II	182
D6	Force generation under naturally occurring FT joint movement patterns	188
Appendix		197
1	Spike2 scripts	198
1.1	Sequencer scripts	198
1.2	Analytical script	204
Bibliography		205
	Abbreviations	220
	List of Publications	222
	Acknowledgements	225
	Erklärung	227
	Curriculum vitae	228

A. Introduction

Locomotion can be described as the translation of the center of mass through space along a path requiring the least expenditure of energy (Inman (1966); Mochon and McMahon (1980)). In doing so, an organism's nervous system is believed to represent a source of commands that are issued to the body as direct orders. However, rather than issuing direct commands, the nervous system can only make suggestions which are reconciled with the physics of the system and task at hand (Raibert and Hodgins (1993); Full and Farley (2000)). In terms of the integrated function of motor behaviour, the neural system and mechanical actuators rely heavily on each other's properties as well as their organisation (Ettema and Meijer (2000)). As neural and muscular systems coevolved, the activity of a motoneuron is likely to be tuned to the properties of the muscle it innervates in terms of its cellular properties for instance (Hooper et al. (2006)). Depending on their contraction dynamics, muscles can differ in their response to temporal components of the neural inputs they get (review in Hooper and Weaver (2000)). Prediction of movement from motoneuron spike activity alone is therefore impossible (Hooper et al. (2006)). Consequently, the combined knowledge about muscular properties together with the neural activity driving the muscle is necessary to describe appropriately how nervous systems generate motor output. Within the translation process of neuronal activity into movement, there are parameters on different organisation levels that can bear a high degree of complexity that needs to be considered. The number of motor units a muscle consists of (e.g. ~ 150 in the cat *soleus* muscle, Boyd and Davey (1968)) or the mechanics of power transmission (e.g. the morphological arrangement of the stick insect *retractor unguis* muscle, Radnikow and Bässler (1991)) are just two examples for parameters that can vary a lot in terms of their complexity (e.g. cockroach extensor muscles 177 and 179 are innervated by a single excitatory motoneuron, Pipa and Cook (1959)). Beyond that, many kinds of behaviour require an organised interplay of several muscles or even muscle groups. Some muscles feature the capacity to achieve context-dependent roles, like the posterior I1/I3/jaw complex in *Aplysia californica*, that can mediate biting and swallowing by changing the direction of force it exerts (Neustadter et al. (2007)). Another example is the metathoracic second tergocoxal muscle (Tcx2) in the locust *Schistocerca gregaria*, which acts as an indirect wing *levator* or as a coxal *remoter* (Malamud (1989); Malamud and Josephson (1991)). Muscles have the capacity to not only accelerate a mass, but also to avoid movements by braking or by resisting an external force (Hildebrand (1988)). Particular cockroach extensor muscles can operate as active dampers that only absorb energy during running (Full et al. (1998)) and stick insects can simultane-

ously exert braking and propulsive forces during part of each stride (Graham (1983)). Hence, interpretation of the neuromuscular transform requires knowledge about the functional context a muscle is implemented in. For this reason, it is advantageous to study muscle biomechanics in a well investigated system in terms of the neural patterns occurring during the behaviour in focus. Concerning locomotion, such an organism is the stick insect, *Carausius morosus* (Orlovsky et al. (1999); Büschges (2005); Ritzmann and Büschges (2007)). The walking movement of its legs can be separated in two sections: stance and swing. During stance, the leg has ground contact and during swing, the leg lifts off the ground (Cruse (1985a;b)). A characteristic motoneuronal activity can be attributed to both phases in the walking animal (Graham (1985); Büschges et al. (1994)). This motor output is the result of a complex interaction between local sensory feedback, central neural networks governing the individual leg joints, and coordinating signals between the legs (e.g. Bässler and Büschges (1998); Dürr et al. (2004); Büschges (2005); Gruhn et al. (2006); Borgmann et al. (2007)). The stick insect's femur-tibia (FT) joint, which is the functional knee-joint of the insect leg, is particularly well described in lots of aspects. Early examinations dealt with the joint's morphological organisation (Bässler (1967)). The motoneuronal innervation patterns of the muscles moving the joint (Bässler and Storrer (1980); Debrodt and Bässler (1989; 1990); Bässler et al. (1996)), the extensor and flexor tibiae, and the motor output controlling tibia movement during walking (Bässler (1993a); Büschges et al. (1994); Fischer et al. (2001)) are known, too. Some aspects of the control of these neural patterns including the activity of the central premotor networks (Bässler (1993a); Driesang and Büschges (1993); Büschges (1995b); Büschges et al. (2004)) were also revealed. In an attempt to relate specific sensory and neuronal mechanisms to the generation of the natural sequence of events forming the step cycle in a single leg, all previously collected knowledge was incorporated into the neuro-mechanical simulation of the stepping stick insect (Ekeberg et al. (2004)). However, the realisation of this simulation required not only the available information about neural activity but also the modelling of the simulated effectors, i.e. the muscles involved, by fixing the most important muscle physiological parameters defining them. At that time, those parameters were not yet measured. The search for information about 'typical insect leg muscles' led to the insight, that insect muscles can vary a lot in their properties (e.g. maximal force output). Especially the activation level of leg motoneuron pools during each locomotory duty cycle, i.e. how changes in motoneuron activity will affect muscle activation and thereby the movement amplitudes generated, shows large

discrepancies between species. Fig. A.1 presents the comparison of motoneuronal firing patterns of muscles involved in locomotion in three insect species (the fruitfly *Drosophila melanogaster*, the cockroach *Blaberus discoidalis* and the stick insect *Carausius morosus*) during physiological movements. Flight muscle b1 depicted in A.1a receives one action potential per wing stroke, hindleg extensor 179 shown in A.1b is activated by three or four action potentials per locomotory cycle (during fast running), whereas the middle leg extensor tibiae shown in A.1c carries out a swing phase with more than 30 action potentials of the fast motoneuron FETi (mean spike number per burst, see Hooper et al. (2007a)). Each muscle is designed for maximal power and efficiency in its important range of speed (Full et al. (1998)). The control of activation, i.e. the properties of force production and contraction related to the motoneuronal spike frequency, varies a lot between muscles and suggests their individual twitch-to-tetanus ratios to be very different among the three species shown. This ratio represents an essential muscle physiological parameter that indicates a muscle's capacity to finetune force and movement. The large differences in activation control between these three exemplary species highlights the urgency of muscle physiological investigations in the stick insect.

Hooper and colleagues demonstrated that extensor tibiae motoneuronal firing is highly variable (Hooper et al. (2006)). Measuring this variation on the effector level is the only way to tell whether this variation is really of physiological relevance for the animal. Given the well known neural aspects of stick insect leg motor control, understanding of the FT-joint control would therefore be greatly increased by examining the biomechanics of the joint's muscular system. Conveniently, the extensor tibiae represents a very suitable system for the investigation of muscle parameters: it is a pinnate muscle whose distal end is easily accessible by opening the femur with a few cuts and whose innervation is rather simple: one fast and one slow motoneuron (FETi and the SETi; Bässler and Storrer (1980)) and an additional inhibitory common inhibitor motoneuron (CI₁; Bässler et al. (1996); Bässler and Stein (1996)), that run in a single nerve (*nl3*, Marquardt (1940)). Its antagonist, the flexor tibiae is very different in terms of its innervation. It features more than twenty-five excitatory (Goldammer et al. (2007)) and two inhibitory motoneurons (Debrodt and Bässler (1990)) that run in a single nerve as well (*ncr*, Marquardt (1940)). Especially in the case of the flexor tibiae, controlled extracellular stimulation of a particular set of motoneurons is diffi-

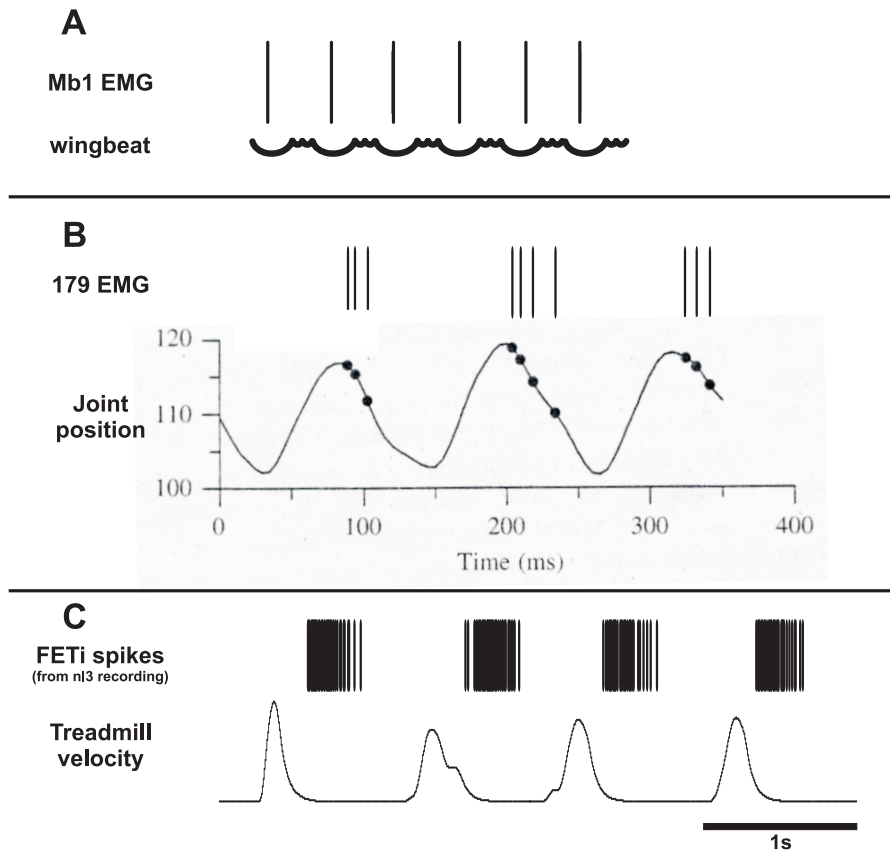


Figure A.1: Various forms of insect locomotion require different motoneuronal firing patterns. **a** The Mb1 motoneuron in *Drosophila melanogaster* spikes once every wingbeat cycle (modified from Heide and Götz (1996)). **b** The metathoracic trochanter-femoral extensor muscle 179 of *Blaberus discoidalis* fires either three or four action potentials per running cycle (modified from Full et al. (1998)). **c** The mesothoracic FETi motoneuron of *Carausius morosus* generates usually > 30 action potentials per swing phase (single middle leg preparation stepping on a treadmill, see Fischer et al. (2001)).

cult to achieve and the physiological relevance of such a recruitment pattern unclear. The number of possibilities in terms of motoneuronal activation patterns occurring in a behaviourally relevant situation is too large.

To overcome the difficulties of extracellular motoneuronal stimulation, the first tibial muscle force measurements were performed in response to movement of the chordotonal receptor apodeme, which acts as a feedback transducer measuring the angle between femur and tibia (Bässler (1965); Cruse and Storrer (1977)). The chordotonal organ is a position controller which works as a closed loop control system which enables the tibia to resist disturbance inputs (Bässler (1965; 1974); Cruse and Storrer

(1977)). Extensor and flexor tibiae act as the actuators within the mechanism, as their forces try to resist the artificial disturbance input (Cruse and Storrer (1977)). Initial measurements were made from the tibia (Bässler (1974)) and later from the extensor and flexor tibiae muscles separately (Storrer (1976); Cruse and Storrer (1977); Bässler (1983)). The reason for the avoidance of extracellular motoneuronal stimulation was justified with concerns towards the order of recruitment of extensor tibiae motoneurons. FETi has the largest diameter (Bässler and Storrer (1980)) and is therefore the first one to be recruited at *nl3* stimulation (for a detailed explanation, see Pearson et al. (1970); Stein and Pearson (1971)). Thus, extracellular SETi stimulation would always involve stimulating FETi as well, which was considered to be too far from a physiologically interesting situation and left the experimentators unsatisfied at that time. Consequently, measuring tibial muscle forces and length changes in response to direct motoneuronal stimulation was not taken into account.

However, a simultaneous extracellular stimulation of all extensor motoneurons comes actually quite close to a naturally occurring activation pattern. During walking, FETi, SETi and CI₁ are activated maximally during swing phase of the middle leg (Schmitz and Hassfeld (1989); Büschges et al. (1994)). In this context, CI₁ activity switches off force production of dually innervated fibres (Bässler et al. (1996); Bässler and Stein (1996)). Depending on the walking situation, extensor motoneurons can also be active during stance phase before the initiation of swing, although at a reduced level (Graham (1985); Schmitz and Hassfeld (1989); Büschges et al. (1994)). Simultaneous stimulation of all three extensor tibiae motoneurons via nerve *nl3* would therefore absolutely make sense and was chosen to be the right method to activate the extensor tibiae. Hence, by taking benefit of the knowledge available (see above), the middle leg extensor tibiae provides a lot of advantages that make it an ideal muscle physiological subject to study, which was done in the thesis at hand.

The muscle investigations presented in the *Results* section required a careful selection of the most relevant questions that need to be answered to improve understanding of stick insect walking, as muscle physiology in general is a very broad and complex field. It ranges from molecular studies on e.g. ATP-driven Ca²⁺-pump (Lou et al. (1997)) over force length measurements on highly specialised muscles that can be stretched nearly three times their resting length (Rose et al. (2001)) to the quantita-

tive description of the centre of gravity dynamics during the long jump take-off phase in humans (Seyfarth et al. (1999)). This thesis concentrates on the description of the main basic relationships that generally characterise a muscle and further deals with the interaction of characteristics and the development of individual parameters in a physiologically relevant context. The revelation of one of these basic characteristics, the so-called force-length relationship, was closely linked to the progressive exploration of structural processes within a sarcomere due to the development of techniques like electro microscopy. Those processes are summarised in the term 'sliding filament theory' (Huxley and Niedergerke (1954a); Huxley and Hanson (1954); Page and Huxley (1963)). A. E. Huxley and H. E. Huxley described the existence of cross-bridges as those structural elements, that are responsible for force generation and for the sliding of thick and thin filaments (Huxley (1957a;b)). The biochemical processes involved were termed 'power stroke'. Finally, the isometrically developed muscle forces at different fibre lengths could be explained by the number of attached cross-bridges and are described by the sarcomere model (Gordon et al. (1966b)). In order to interpret this force-length relationship, previous knowledge about the muscle length change within the working range of the limb, which is supposed to be moved, is required (Full et al. (1998)). This additional information is of particular importance as the muscle experiences length changes during every single contraction. Investigation of pinnate muscles like the extensor and flexor tibiae requires a further determination of the fibre length, as muscle length and fibre length are not the same, in contrast to parallel fibred muscles like e.g. the human *biceps brachii* muscle.

Another important muscle characteristic is the force-velocity relationship, which represents a fundamental property of the contractile system: the ability of a muscle to adjust its force to precisely match the load by varying the speed of shortening appropriately (Edman et al. (1997)). Fenn and Marsh (Fenn and Marsh (1935)) were the first to describe this relationship that was a few years later characterised by a rectangular hyperbola (Hill (1938)). This Hill curve defines a muscle's mechanical capacity - the maximum shortening velocity (V_0), the maximum stress (P_0) and the expected power output at any load less than P_0 or at any shortening velocity between 0 and V_0 (Edman and Josephson (2007)). Hill provided evidence that muscle shortening involves heat production, which is due to inner friction that a muscle needs to overcome during shortening. The heat production by the muscle is proportional to the amount of shortening, that the muscle experiences. The Hill-equation describes the interrelation-

ship between force, velocity and heat (Hill (1938)). Edman mentioned the possibility to use the force-velocity relationship as a relevant index of muscle activity (Edman et al. (1997)). Experiments on locust flight muscle (*Schistocerca gregaria*) showed that it was indeed possible to derive a so-called 'degree of activation' by releasing a muscle at different particular time points during a twitch (Malamud and Josephson (1991)). This is in line with A.V. Hill, who found out that this was a good method to determine when the muscle's ability to develop work output peaks. Interestingly, this peak arises much earlier than the maximal isometric force output (Hill (1938)). In this context, computer models present good means to evaluate the importance of a parameter in terms of comparing a situation where this parameter is implemented and another situation where it is omitted, as demonstrated by van Soest and Bobbert (van Soest and Bobbert (1993)). They could impressively show the actual importance of muscle's force-length and force-velocity characteristics in a human vertical jumping model and which sort of impact those characteristics have to a sudden perturbation. In general, muscle shortening represents a trade-off between the constraints of either moving fast or generating large power output. Elastic elements have the ability to uncouple muscle fibre shortening velocity from body movement to allow muscle fibres to operate more slowly, yet more strongly (Roberts and Marsh (2003)). Investigations on the *plantaris longus* muscle in the frog *Rana catesbeiana* reveals series elasticity to be essential to increase the mechanical work done in order to perform a fast and powerful movement at the same time (Roberts and Marsh (2003)). Passive elements like the series elasticity can have a major impact on locomotion behaviour. In the locust, passive torques have the capacity to lift even a loaded limb without any motoneuron activity: a large part of flexions and the initiation of extensions were attributable to passive forces (*Schistocerca gregaria*, Zakotnik et al. (2006)). The distribution of forces that arises during limb movement comprises not only the momentum of the actual mass that needs to be accelerated, but also the passive muscle forces of antagonistic muscle(s) and frictional joint forces, that have to be taken into account. The relevance of passive muscle forces scales with body size (Hooper et al. (2009)) and represents an essential movement and posture defining parameter in small animals like the stick insect. It was shown that loss of motoneuronal innervation in the extensor tibiae can be compensated (to some extent) by an increase in passive static tension, which can lead to a maintenance of walking behaviour (Bässler et al. (2007)). Thus, the knowledge about the neuromuscular transform represents only a part of the information that is needed to understand movement generation. Musculoskeletal units, leg segments,

and legs do much of the computations on their own by using segment mass, length, inertia, elasticity, and dampening as ‘primitives’ (Full and Farley (2000)). A mechanical system can react much faster to perturbations during rapid, rhythmic activity (Full and Koditschek (1999)). Nonetheless, passive dynamic control lacks the plasticity of active neural control, since suites of integrated structures which have evolved over millions of years take longer to modify (Full and Farley (2000)).

In addition to the questions that arise around the activation of a muscle and its passive behaviour, one crucial aspect of the above mentioned musculoskeletal units is their relaxation behaviour after active contraction. That is, a muscle can still exert force even though motoneuronal firing has ceased. In the isotonic force domain, the stick insect extensor tibiae takes on average 52 ms after a burst to start relaxing (Hooper et al. (2007a)). This becomes especially functionally relevant at step transitions, when a muscle’s relaxation has not finished and the antagonist muscle is about to be activated. In the stick insect, the transition from swing to stance features co-contraction in terms of an extensor and flexor tibiae activity overlap (single leg preparation in *Cuniculina impigra*, Fischer et al. (2001)). Antagonistic muscle co-contraction attributable to long muscle time constants facilitates substantial load compensation (Zakotnik et al. (2006)). The joint stiffness, that results from co-contraction, represents an important part of a successful control strategy. The level of co-contraction can vary with the history a muscle has experienced in terms of its previous activation or previously happened muscle length changes (see e.g. Ettema and Meijer (2000); Herzog et al. (2003); Ahn et al. (2006)).

The investigations in this thesis are presented and discussed in six chapters respectively. The stick insect FT joints of front-, middle- and hindleg were examined in respect to their geometrical characteristics. In the middle leg, femur and muscle cross-sectional area, fibre length and sarcomere length were determined for the extensor and flexor tibiae. Experiments determining statically and dynamically generated passive forces and testing creep behaviour were conducted on both tibial muscles of the middle leg as well. The middle leg extensor tibiae was investigated in respect to its twitch and tetanus kinetics, its relaxation dynamics at different activation levels, its latch properties and its force-length characteristic in the isometric domain. Experiments in the isotonic domain included force-velocity measurements at different

activation and length levels, the contraction behaviour in response to physiological input and series elasticity measurements at different activation levels. In the final part, the interaction of characteristics and the relaxation behaviour were investigated by mimicking physiologically occurring extensor muscle length changes. Video tracking of tibial movement should test whether the change in extensor tibiae relaxation dynamics after different activation durations is reflected in tibia movement. Due to the large amount of motoneurons, active middle leg flexor tibiae measurements were restricted to quick release experiments including the calculation of the parameters P_0 and V_0 and series elasticity determinations. These flexor nerve stimulations were exclusively conducted at maximum activation (i.e. entire motoneuronal recruitment and maximum stimulation frequency). The role of FT joint forces alone was examined by ablating both tibial muscles and deflecting the joint.

Some of the data shown in this thesis (parts of chapters C1, C2, C3, C4 and C5) were already published in Guschlbauer et al. (2007) (FT joint geometry of all legs, middle leg extensor tibiae single twitch and force-length relationship in terms of actively generated isometrical force and passive static tension, extensor tibiae Hill curves at different activation and maximal shortening velocities at different fibre lengths, extensor tibiae series elasticity at different activation). Other data shown (a part of chapter C3) are about to be published in parts of Hooper et al. (2009), where I appear as a contributing author (extensor and flexor tibiae passive static tension, flexor tibiae dynamically generated passive tension, joint deflections either intact, with muscles ablated or with joint tissue ablated). Some further measurements presented (a part of chapter C4) were the basis for the analysis shown in Hooper et al. (2006; 2007a;b), where I also appear as a contributing author (physiological stimulations of the extensor tibiae in the isotonic force domain).

B. Materials and Methods

Experiments were carried out on adult female stick insects of the species *Carausius morosus* Br. from a colony maintained at the University of Cologne. Animals were kept under artificial light conditions (12 h darkness, 12 hours light) and were fed with blackberry leaves (*Rubus fruticosus*). 10 sturdy-looking animals of the same size as used in the experiments had an average body length of 77.1 ± 2.28 mm and average weight of 940 ± 70 mg. All experiments were performed under daylight conditions (setup light, Olympus) and at room temperature (20-22°C).

1 Femur, muscle, fibre and sarcomere length measurements

The extensor and flexor tibiae muscles were exposed for length measurements by cutting a small window into the proximal and distal part of the femur. The red-coloured autotomal ring (Schindler (1979); Schmidt and Grund (2003)) was assigned as proximal end. Parts of the main leg trachea, the chordotonal organ and the first of three retractor unguis muscles (Radnikow and Bässler (1991)) were cut off and highly diluted 'Fast Green' (Sigma) was applied in most cases. Muscle length was calculated under the microscope by determining the distance from the insertion of the most proximal fibre to an orientation mark (see Fig. B.1, shown for the extensor tibiae) and adding the distance from this mark to the insertion of the most distal fibre into the tendon. The animal's abdomen was stimulated tactilely several times during a test series to make sure that the investigated muscle was tensed throughout (Bässler and Wegner (1983)). The tibia was moved on a plastic goniometer from 30° (maximally flexed) to 180° (maximally extended) and length measurements were taken in 10° intervals. This range (150°) is considered as the maximum working range of both tibial muscles (Storrer (1976); Cruse and Bartling (1995)). 90° was defined as the FT-joint angle at which both muscles are at their resting length for the stick insect (Friedrich (1932); Storrer (1976)) and for *Blaberus discoidalis* (Full et al. (1998); Ahn and Full (2002)). Femur cross sectional area was determined by cutting middle legs on the level of the mid-coxa. Sections of approximately 1 mm thickness were cut from the medial part of the femur with a razor blade (Rotbart).

Fibre length measurements were performed on muscles fixed in situ using 2.5% glutaraldehyde in phosphate buffer pH 7.4 (Watson and Pflüger (1994)) with the joint at the 90° position and the entire femur opened laterally. The animal was again stimulated tactilely several times during fixation (see above). Fibres were pulled from the proximal and medial parts of the femur because in these locations both muscles are primarily innervated by fast motoneurons (Bässler et al. (1996); Debrodt and Bässler (1989)). Muscle length changes and fibre length measurements were done using a 20x magnifying oculometer (Wild-Heerbrugg) at 25x magnification, femoral length was determined at 6x magnification. Calibration was done with a aluminium-ruler (estimated accuracy of 0.005 mm).

Two different methods were used measuring sarcomere length. In a first approach, middle leg FT-joints were set at angles of 30°, 90°, or 180°. The specimens were fixed in a mixture of 13% formaldehyde/ 59% ethanol/ 6% glacial acetic acid and embedded in paraffin. 15µm thick sagittal slices were made and stained with the fast Nissl procedure (Burck (1988)). Sarcomeres were visualised under a light microscope with a polaroid filter and measured with the analySIS software (Soft Imaging System, Olympus). The second approach consisted in staining extensor and flexor tibiae muscles with phalloidin (Phalloidin-FluoProbe 647H 650/670 nm) after fixing the femur as a whole in a mixture of 4% paraformaldehyde in 0.1 M sodium phosphate buffer (pH 7.4) and separating the muscles carefully afterwards from the femoral tissue. Phalloidin was dissolved in 1.5 ml methanol which results in a 6.6 nmol/ml phalloidin so-

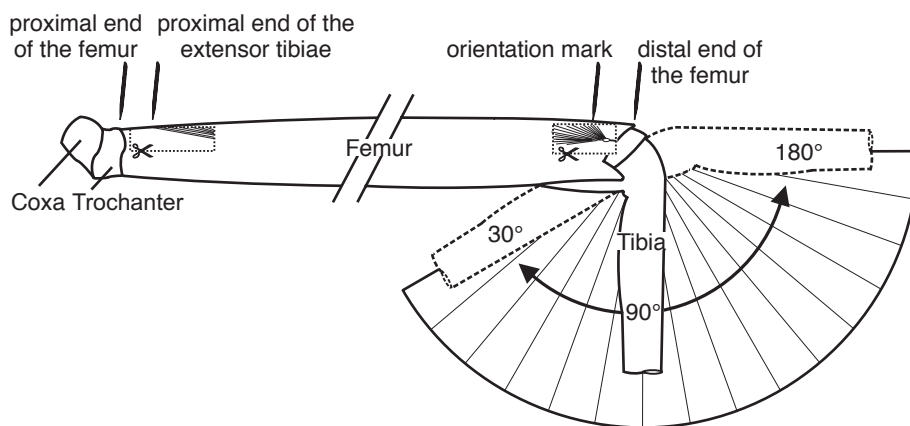


Figure B.1: Schematic representation of the geometrical arrangement of the femur-tibia joint in the stick insect middle leg. See text for details.

lution. $7.5\mu\text{l}$ of this solution were mixed with $400\mu\text{l}$ phosphate buffered saline (PBS). Muscles were incubated in a mixture of $0.16 \frac{\text{nmol}}{\text{ml}}$ phalloidin solution with 1% Triton-X in PBS for 15min (modified from Thuma (2007)). Concentrations of $0.32 \frac{\text{nmol}}{\text{ml}}$ and $0.08 \frac{\text{nmol}}{\text{ml}}$ were tested as well and led to worse results. Phalloidin stained sarcomere lengths were first measured at the actual contraction state when being fixed, that is at 30° and 180° FT-joint angle. Then, sarcomere lengths were determined by standardisation according to the instructions suggested by Thuma (2007), see Fig. B.2. The goal of such a normalisation procedure is to specify lengths independent from contraction state, because different muscles are known to have different sarcomere lengths. The comparison of sarcomere lengths between muscles therefore necessitates the reduction of a sarcomere to its own physical characteristics. This reduction provides an unambiguous anatomical base to determine sarcomere length independent from contraction state, because the standardised sarcomere length measures two times thin filament length.

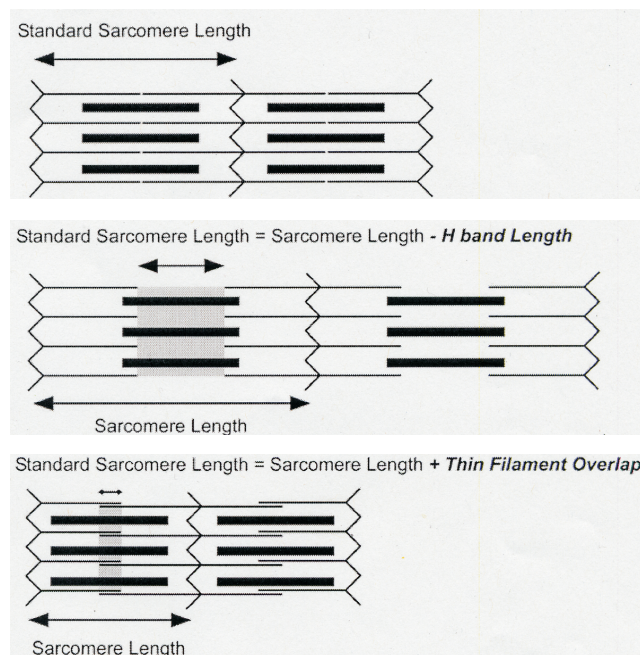


Figure B.2: *Standardisation of sarcomere length. Sarcomere lengths from the same type of muscle differ because of different muscle contraction states. To correct this, a standardisation protocol can be applied to each sarcomere length (modified after Thuma (2007)).*

2 Measurements with the Aurora 300B dual mode lever system

The 'Aurora 300B dual mode lever system' (Aurora Scientific Inc, Ontario, Canada) is a device enabling to measure and control both force and position simultaneously and to make the transition from force to position control with only small transients (Fig. B.3 shows a picture of the device). Forces of maximally 500 mN and length excursions of maximally 10 mm can be detected with a force signal resolution of 0.3 mN and a length signal resolution of 1 micron. Force step and length step response time are 1.3 ms and 1 ms respectively. It acts like a length controller that is precision force-limited and acts exclusively as a force controller if an external load attempts to pull harder than the set force level. Its servo motor has a preferred direction of force application although forces can be measured in both directions. Load should be attached to the lever arm such that a muscle contraction will pull the lever arm in a counterclockwise direction (when viewed from the shaft end of the motor).

The lever arm of the Aurora servo motor is 30 mm long and perforated at the tip. Its connection to a muscle is the combination of an u-shaped pin being glued to a cut thick insect pin being in turn glued to a 0.1 mm thin hook-shaped insect pin. A few experiments were done using a sterile silk thread (50 μm ; Resorbi, Nürnberg) in combination with a hook-shaped insect pin as link between lever arm and muscle. Force and position measurements with the lever system were mainly made on the extensor tibiae muscle of the middle leg, some experiments dealt with the flexor tibiae muscle's properties. The lever system was tuned so that length control was critically damped and inertia compensation was adjusted to minimise force transients using triangle waveforms as suggested in the Aurora's instruction manual.

For investigation of FT joint torques, a special lever arm was built (mechanics department of the Zoological institute, University of Cologne). Its effective moment arm length is 4.75 mm. The lever arm that was usually used narrows to the perforated tip and has an effective moment arm of 30 mm. A middle leg was cut on level of the mid-coxa and was fixed on the platform and positioned such that its FT joint rotational axis and its pivot was the same as the servo motor's. A plastic rod formed the connection between the lever arm and the tibia, with which it could be easily attached because



Figure B.3: The Aurora dual-mode lever arm system 300B (Aurora Scientific Inc.). The picture shows only the main device, i.e. the controller, not the servo motor.

of a notch that was slightly narrower than the average stick insect tibia (see Fig. B.4). Additionally, a drop of super glue (Loctite, Uhu Alleskleber) assured a good bond between tibia and the notch in the plastic rod. Finally, apodemes of both extensor and flexor tibiae were cut through the soft cuticle at the anatomical transition from femur to tibia with fine scissors.

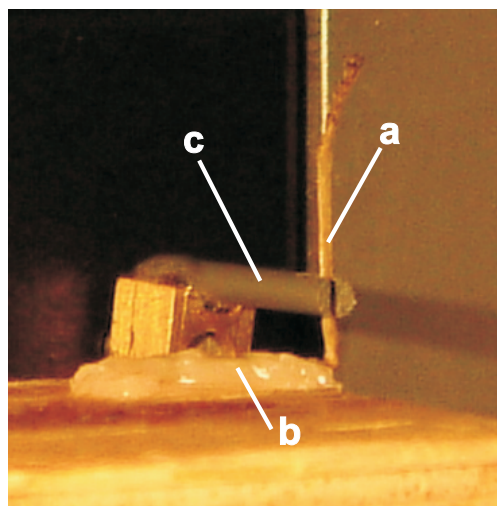


Figure B.4: Measuring FT-joint torques with a specialised device. *a* tibia, *b* femur embedded in dental cement, *c* modified lever arm (the lever arm that was usually used is depicted in Fig. B.7).

3 Animal preparation and dissection

All legs except one middle leg were cut at the level of the mid-coxa. The animal was treated according to the established procedures and was fixed dorsal side up on a balsa wood platform so that the tibia of the remaining leg was suspended above the edge of the platform in all extensor tibiae investigations. The tibia had to be cut in all flexor tibiae experiments. Coxa, trochanter, and femur were glued to the platform with dental cement (Protemp II, ESPE, St. Paul, MN, USA). The distal end of the femur was opened carefully to ensure that as many muscle fibres were left intact as possible. The femoral cavity was filled with ringer (NaCl 178.54 mM, HEPES 10 mM, CaCl₂ 7.51 mM, KCl 17.61 mM, MgCl₂ 25 mM) (Weidler and Diecke (1969)) several times during each experiment (see also Becht et al. (1960)). Muscle investigations were achieved by inserting the hook-shaped insect pin (described above) through the cut distal end of either the extensor or flexor tibiae distal muscle apodeme (see also Ahn et al. (2006)). Cutting of the apodeme was conducted under controlled conditions: muscle length was set to its corresponding length at a FT-joint angle of 90° at the beginning of each measurement. Flexor tibiae muscles were normally that strong that the hook-shaped pin had to be glued (Loctite 401, Uhu Alleskleber Super) to the apodeme in addition to the insertion through the tendon.

4 Extracellular motoneuronal recording

Nerves F2 and nl3, both containing the three extensor tibiae motoaxons, were recorded in different experiments *en passant* (Schmitz et al. (1991)) with a monopolar hook electrode filled with silicone paste (high-viscosity, Bayer), modified by the mechanics department of the Zoological institute, University of Cologne. A fine polyethylene tube can be slid on the nerve, which can in turn be isolated with the silicone paste. A silver wire (0.25 mm in width) served as a reference electrode. The signal was either preamped with a battery-powered optocoupler (100x) or by a 'Ultra low noise preamplifier MA103' (50x), boosted by an AC-filter amplifier (20x or 50x) and sampled by an AD-converter (Cambridge Electronics 1401) with 12500 Hz. The filter range settings of the booster were usually 150 Hz-9500 Hz.

Nerve activity could be made audible by a monitor (1278), that was amplified with a DC filter amplifier (1274A). All devices were built in the electronics department of the

Zoological insitute of the University of Cologne when not noted differently.

5 Electrical stimulation of motoaxons

5.1 Recruitment of extensor tibiae motoneurons

Most experiments were done on the extensor tibiae muscle because it is innervated by only three motoneurons (Bässler and Storrer (1980)), all of which have their axons in nerve *nl3* (nomenclature according to Marquardt (1940)). After opening the thorax dorsally and removing the gut, fat, and connective tissue to expose the mesothoracic ganglion, a bipolar hook electrode was placed under nerve *nl3* (Marquardt (1940)). The nerve was crushed proximally with a foreceps and isolated with white vaseline (Engelhard Arzneimittel GmbH & CoKG, Niederdorfelden). In order to measure either the tension or the muscle length change of the middle leg extensor tibiae, the axons of its innervating motoneurons, the FETi, SETi, and CI₁ were stimulated via a stimulation isolation unit putting out current ('Universal stimulus isolator Model 401'). Due to their differing axon diameters (Bässler and Storrer (1980)), the three motoneurons can be sequentially activated by increasing stimulation strength; FETi has the lowest threshold (Fig. B.5 a(i) and a(iiii)), SETi the next highest (Fig. B.5 a(ii) and a(iiii)), and CI₁ the highest (Fig. B.5 a(iii) and a(iiii)). The determination of the appropriate current pulse amplitude to use in the nerve stimulation was complicated by a conflict between 1) the desire to routinely stimulate all three motoneurons (FETi, SETi, and CI₁) and 2) the desire to keep the current amplitude low enough that the nerve could be repeatedly stimulated over long periods without damage. This issue was even more difficult to resolve because the dissection required to allow extracellular recordings from the extensor nerve F2 in the distal femur close to the muscle (which is required to test whether all three axons are being stimulated) inevitably damaged some more distal muscle fibres which are mostly dually innervated (Bässler et al. (1996)) and also added considerable time to the dissection procedure. It was consequently not possible to both perform the long experiments on undamaged muscles and to check if all three motoaxons were being stimulated in the same preparation. To overcome these difficulties, 15 experiments were performed using a dissection enabling to record extracellularly from the F2 nerve, where the relative thresholds of the three motor units were measured. Since these experiments were also short, forces

could be measured that the muscle produced as the number of stimulated nerve units changed (due to the inevitable muscle fibre damage, in all cases less than the usually detected forces reported in the Results part). In five of these experiments stimulating the nerve at 1.5 fold the threshold for visible twitches resulted in reliable stimulation of all three motor axons. In eight experiments, stimulation at this level was not sufficient to reliably activate the two smaller fibres (typically SETi but not CI₁ was reliably activated). However, increasing the stimulation amplitude in these experiments showed that (presumably because FETi induces by far the largest twitches, and because in most of these cases SETi was already being activated at the 1.5 stimulation level), when a sufficient stimulation amplitude was achieved to activate the other two units completely, this induced negligible changes (in 7 preparations none, in one 3%) in muscle force production. Fig. B.5 b(i)-(iiii) shows forces and F2-recordings in response to a 50 Hz stimulation pulse train of a representative experiment. In Fig. B.5 b(i), 75% of the pulses excited FETi and 25% FETi and SETi. In In Fig. B.5 b(ii), 50% of the stimuli elicited FETi and 50% FETi, SETi and CI₁. Fig. B.5 b(iii), shows recruitment of all three motor units with every pulse, doubling the current amplitude in Fig. B.5 b(iiii), shows no further increase in force. In the remaining two experiments stimulating the additional two units resulted in an increase in muscle force of 20±4%. These experiments also showed that stimulating the motor nerve with current pulses 1.5 times larger than the visible twitch threshold for long periods of time did not induce any sign of nerve damage (e.g., an increase in stimulation failures). These control experiments thus showed that in 90% of preparations stimulating n13 with a current amplitude 1.5 times greater than the FETi threshold either resulted in activation of all three motor axons or, if not, that the failure to activate SETi and CI₁ completely had a negligible effect on muscle force production. In the remaining 10% of preparations, the lack of the SETi and CI₁ only induced a modest decrease in measured muscle force. These observations led to the decision to simply set the amplitude of the current pulses to approximately 50% above threshold generating a visible twitch (Malamud and Josephson (1991)). Pulse trains of different frequencies could be either applied with a SPIKE2 sequencer program or with a 'Universal digital stimulator MS501' triggered by a SPIKE2 sequencer script in intervals of at least 30 seconds to assure inter-trial muscle recovery. Pulse duration was 0.5 ms in all experiments (Josephson (1985); Stevenson and Josephson (1990); Malamud and Josephson (1991); Full et al. (1998); Ahn and Full (2002); Ahn et al. (2006)).

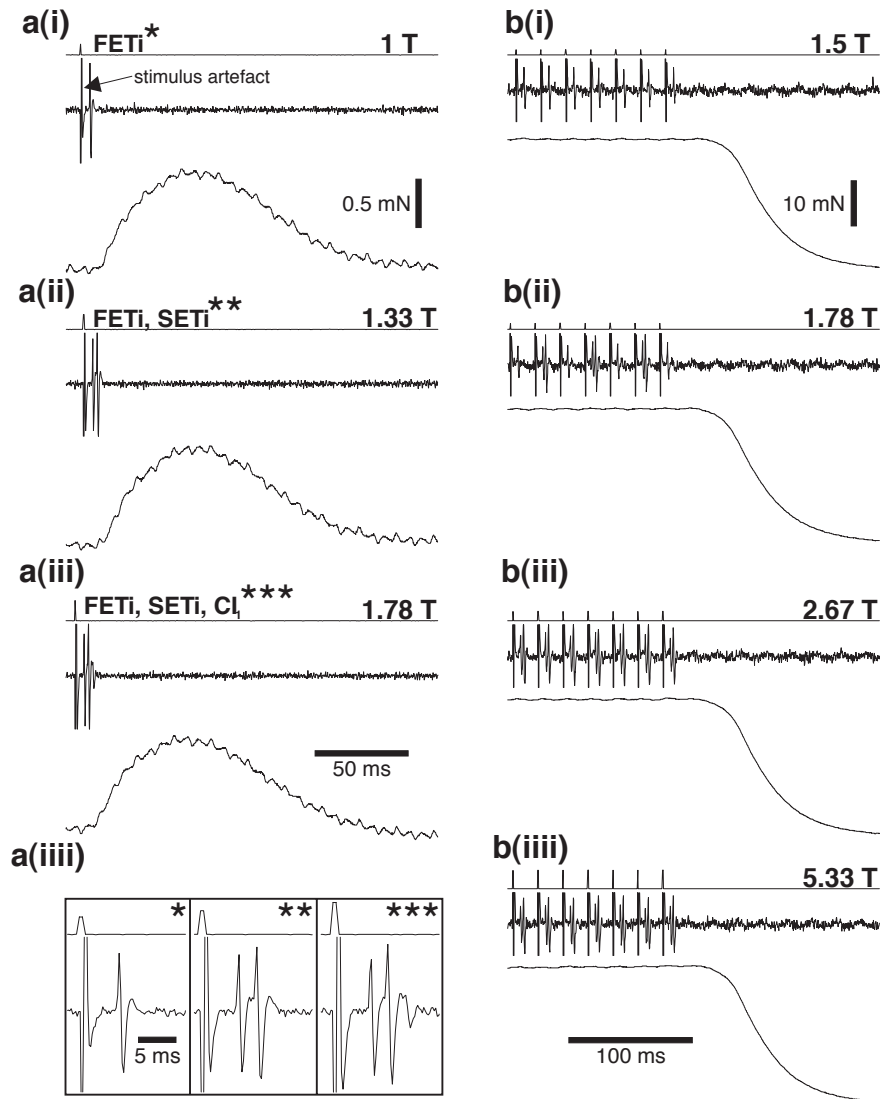


Figure B.5: Isometric forces induced in the middle leg extensor tibiae muscle by electrical stimulation of nerve nL3 with different current amplitudes. In all panels the top trace is a stimulus monitor (note pulse height changes as stimulus amplitude was increased), the second trace is an extracellular recording of nerve nL3, and the third trace is muscle force. **a(i)-a(iii)** show sequential recruitment of FETi (**a(i)**), FETi and SETi (**a(ii)**) and FETi, SETi and CI1 (**a(iii)**) recorded in extensor leg nerve F2 in response to single stimuli. **a(iiii)**: An enlarged version of the recordings showing the sequential addition of new units. 1 T was 0.0023 mA. **b(i)-b(iiii)** show F2-recordings and forces in response to a 50 Hz pulse train. In **b(i)**, 75% of the pulses excited FETi and 25% FETi and SETi. In **b(ii)**, 50% of the stimuli elicited FETi and 50% FETi, SETi and CI1. **b(iii)** shows recruitment of all three motor units with every pulse. Doubling the current amplitude (**b(iiii)**) induced no further increase in force. In this experiment the SETi spikes were of larger amplitude than FETi spikes. This is uncommon and likely because nerve F2 was recorded very distally in the femur. In all panels the electrical disturbance in the nerve recording that coincides with the stimulus is a stimulus artifact, not an action potential (arrow in **a(i)**).

Figs. B.6 (scheme) and B.7 (photograph) summarise the above described. All experiments examining muscle force were based on this setup configuration.

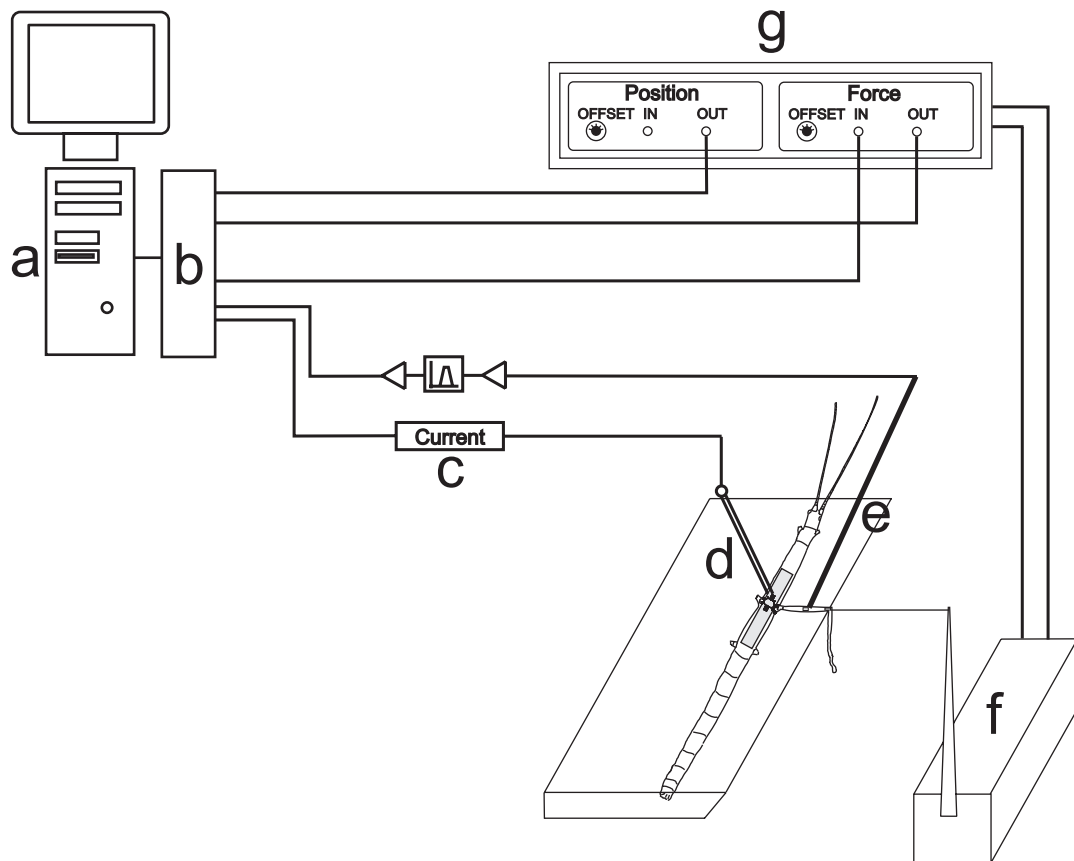


Figure B.6: *Experimental overview. a Computer, b AD-converter, c stimulation isolation unit, d bipolar electrode on either nerve nl3 (extensor tibiae stimulation) or ncr (flexor tibiae stimulation), e monopolar recording electrode on nerve F2, f Aurora servo motor, g Aurora control device.*

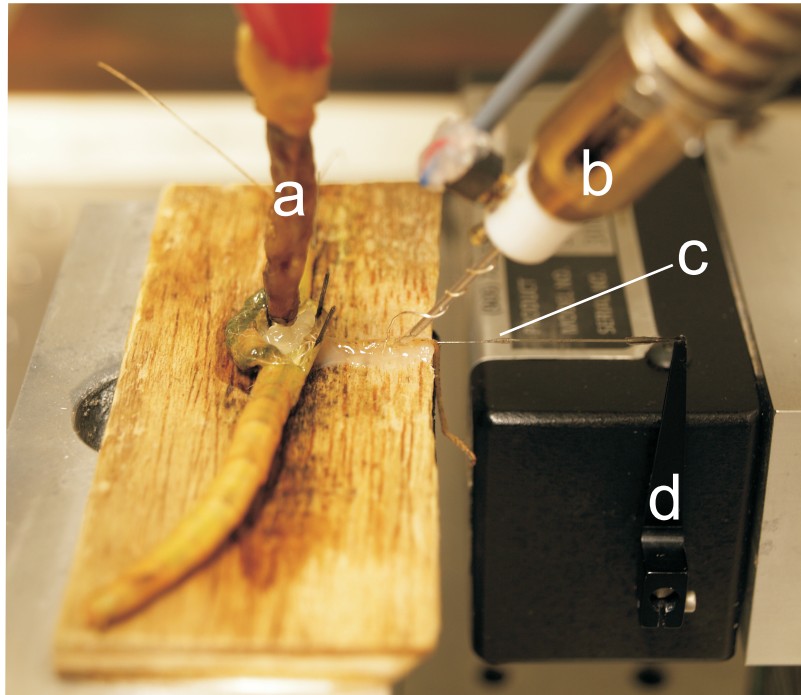


Figure B.7: Photo showing the setup for all experiments dealing with muscle force and/or muscle length. **a** bipolar hook electrode stimulating either *nl3* or *ncr*, **b** monopolar hook electrode, recording F2 (used in 15 control experiments) **c** combination of an insect pin glued to a thin hook-shaped insect pin inserting either the end of the cut extensor or flexor tibiae tendon, **d** lever arm being part of the Aurora servo motor (black).

5.2 Physiological stimulation of extensor motoneurons

Physiological stimulation of the extensor muscle could be achieved by initially recording *nl3* activity with a monopolar hook electrode while the right middle leg of a stick insect performed step-like movements on a treadband (N=1, see Fig. B.8). For a detailed description of the single leg preparation see Fischer et al. (2001). The treadband consisted basically of crepe paper being driven by two engines (Gabriel et al. (2003); Gabriel (2005); Gabriel and Büschges (2007)). On each engine axis, a plastic cylinder was mounted. On one of the two engines was used as a tachometer to register treadband velocity. These recordings were further analysed by sorting out FETi motoneuron action potentials with the SPIKE2 software, marking those as events and using them as triggers to stimulate nerve *nl3* (see above) of a different animal. Muscular output was exclusively investigated in the isotonic domain setting the force output on the servo motor manually as high that total muscular relaxation between the putative step-like

movements (visible as contractions) could be accomplished.

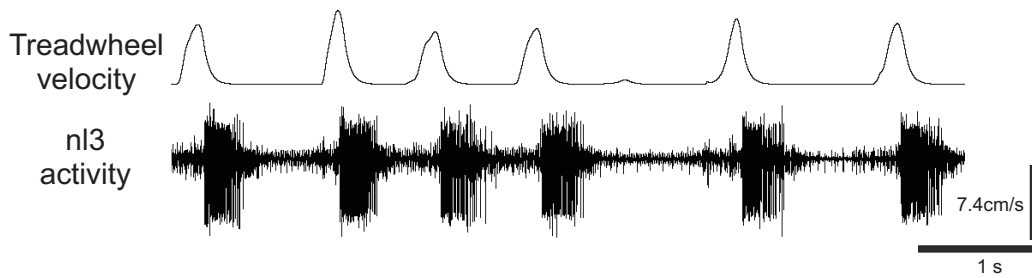


Figure B.8: Recorded extensor nerve (*nl3*) activity while a stick insect performed step-like movements on the treadwheel shown in the lower trace (for a detailed description of the single leg preparation, see Fischer et al. (2001)). Velocity of the treadwheel's tachometer is displayed in the upper trace.

5.3 Stimulation of flexor tibiae motoneurons

The flexor tibiae muscle is innervated by about 14 motoneurons running in nerve *ncr* (Storrer et al. (1986); Debrodtt and Bässler (1989); Gabriel et al. (2003)). Recent investigations resulted in an even larger number of flexor tibiae motoneurons (18-27, $N=8$; Goldammer et al. (2007)). Thus, extracellular stimulation of this muscle is complicated to achieve, therefore only a few experimental paradigms carried out on the extensor tibiae were conducted on the flexor tibiae as well. A bipolar hook electrode was placed under nerve *ncr*, crushed proximally and isolated with vaseline (as described for nerve *nl3*). At the beginning of each experiment in the isotonic force domain, stimulation amplitude was increased until isometric force showed no further increase and force development showed no visible stimulation failure. Sequential recruitment was mainly tested investigating single twitches. As maximal output by the MICRO1401 A/D converter (Cambridge Electronic Design Limited; Cambridge, UK) was limited to 5 V (i.e. maximally 250 mN force application on the Aurora's lever arm), the force output was amplified with an amplifier / signal conditioner MA102 by factor 2 (500 mN is the Aurora's maximal measuring capacity). Detected flexor tibiae forces were not exceeding this value.

5.4 Isometric force experiments

Experiments to determine the active and passive force-length characteristics according to Gordon and colleagues (Gordon et al. (1966b)) were carried out as follows:

muscle length was manually set to a FT joint angle of 90° at the beginning, defined as the muscle's resting length l_0 (see above). It was then released 0.75 mm ($0.5 l_0$) and subsequently stretched in coarse steps (mostly 0.15 mm) with sequencer-generated ramps of $0.05 \frac{\text{mm}}{\text{s}}$ up to 0.75 mm beyond the muscle's resting length (ca. $1.5 l_0$). In a different approach, the focus was on examining force development within the muscle's working range using small ramps (0.05 mm) within the range of ca. $0.8 l_0$ to ca. $1.2 l_0$ to obtain a more accurate screening. Actively generated forces were investigated with a paradigm of different stimulation frequencies at each length position after having relaxed. For isometric force experiments, the influence of filament overlap on force generation was examined by stretching the muscle in ramps of different size over a range of 1.5 mm using a SPIKE2 sequencer script (see Appendix). The stimulation protocol was carried out at each muscle length.

5.5 Isotonic force experiments

Force-velocity curves (Hill-curves) were obtained according to the established procedures (Edman et al. (1976); Edman (1979; 1988); Malamud and Josephson (1991); Edman and Curtin (2001)). For isotonic force experiments, the influence of load on contraction velocity and muscle series elasticity was determined by application of different force levels on the lever arm during tetanus using a SPIKE2 sequencer script (see Appendix). Extensor muscles were stimulated to reach steady-state contraction under isometric conditions and then allowed to shorten under isotonic conditions against a variety of sequencer-generated counter force levels. Lengthening of the muscle was accomplished with stretches while applying sequencer-generated load levels larger than the tetanical steady-state contraction force.

Caution was taken that the variation of tetanical steady-state force before the switch to force control (for a given stimulation frequency) was not exceeding 15% for all contractions used for further data evaluation (see also Ahn et al. (2006)). The bigger the difference between tetanical force (P_0) and force level applied, the more the muscle went bad (observed in numerous experiments). Therefore, experiments were generally designed the following way: load levels were applied rather randomly between $0.25 P_0$ and $1 P_0$, load levels $< 0.25 P_0$ were applied at the end of an experiment. Switching from force to length control involved a sudden increase in force applied on

the lever arm. This abrupt step was most often filtered with an ‘amplifier / signal conditioner MA102’ or a ‘DC filter amplifier 1274A’.

6 Photo and video tracking of tibia movements

Movement still photographs of the FT joint were taken in two different ways. Passive movements were tracked by pinching cut middle legs horizontally into a clamp (without gravitational effects). A digital camera (Fuji FinePix S602) was placed on a tripod above the leg’s FT joint. Pictures were evaluated using the CorelDRAW software: cursors could be tilted to the desired angle in order to lay on top of the tibia picture in focus with an estimated accuracy of 1° . Muscles were ablated by cutting the tendon at the most distal part of the femur without previous dissection, the transitional part from femur to tibia has a very thin cuticle and is well accessible.

Tibia movement dynamics were tracked using a VGA highspeed camera (‘AVT Marlin F-033C’) and pictures were taken in 10 ms intervals. Nerve stimulation (200 Hz pulses) of either *nl3* (extensor tibiae) or *ncr* (flexor tibiae) and video tracking were triggered by a ‘Universal Digital Stimulator MS501’. The antagonistic nerve (either *nl3* or *ncr*) was crushed or cut to avoid reflex behaviour (Bässler and Büschges (1998)). Each frame was triggered individually by a 100Hz pulse train that was gated manually. Nerve stimulation started with a 50 ms delay to have at least 5 single pictures of the non-moving tibia as a reference point. Pictures were evaluated in CorelDRAW in the same way described for the photos taken with the digital camera ‘Fuji FinePix S602’ (see Fig. B.9).

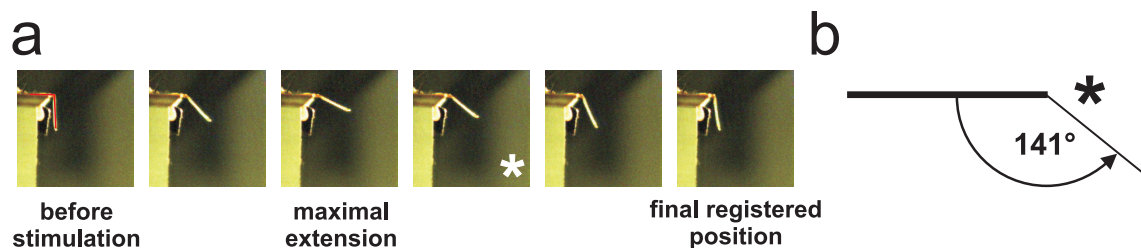


Figure B.9: (a) Single still photographs of a tibia movement high-speed video track with the FT-joint highlighted with red lines at the leftmost picture. The example shows stimulation with 80 spikes. Angular evaluation of the asterisk marked picture is displayed in (b): FT joint angle was measured by setting cursors in the CorelDRAW software.

7 Data achievement, storage and evaluation

Data was recorded on a PC using a MICRO1401 A/D converter with SPIKE2-software (both Cambridge Electronic Design Limited; Cambridge, UK). The stiffness of the measuring system was measured by connecting the insect pin directly to the base of the platform. It was greater than $7500 \frac{mN}{mm}$ and can therefore be neglected in our measurements. Jewell and Wilkie discuss the influence of the compliance of the measuring device thoroughly (Jewell and Wilkie (1958)). For most of the data analysis, custom SPIKE2 script programs were written (see *Appendix*). Plotting, curve fitting, and error evaluation were performed in ORIGIN 6.0 (Microcal. Software Inc, Northampton, MA, USA) except for the RC-type growth and exponential decay fits performed in GNU PLOT. This PhD-thesis was written with the L^AT_EX software.

7.1 Statistics

Mean values were compared using ORIGIN's

either unpaired

$$t = \frac{(\bar{x}_1 - \bar{x}_2 - d_0)}{\sqrt{s^2 \left(\frac{1}{n_1} + \frac{1}{n_2} \right)}}$$

or paired

$$t = \frac{\bar{D} - d_0}{S_D}$$

two sample t-test.

(\bar{x}_n is mean of sample group n , d_0 is a specific value, s is the S.D., n_n is number of sample group n , \bar{D} is the mean difference.)

Regression analysis was used to determine linear correlation between two variables. The ORIGIN 6.0 software used the least squares method to calculate the slope and provided the correlation coefficient (R value) and the p-value (probability, that R=0). Means, samples and correlation coefficients were regarded as significantly different from zero or each other at $p < 0.05$. The following symbols show the level of statistical

significance: (-) not significant; (*) $0.01 \leq p < 0.05$; (**) $0.001 \leq p < 0.01$; (***) $p < 0.001$. In the text, N gives the number of experiments or animals while n gives the sample size. All data were calculated as mean \pm S.D. *R*-values or *R*²-values are specified additionally when it was reasonable.

C. Results

C1 Femoral geometry

The 'Results' part is generally structured in the following way: the majority of the thesis' topics were examined on the extensor tibiae of the middle leg, some of those topics were also examined on the flexor tibiae of the middle leg. Muscle data is therefore presented first for the extensor tibiae and subsequently for the flexor tibiae whenever there was data collected. Front, middle and hind leg data are presented, when available, for both muscles when indicated.

1 Muscle length measurements of front, middle and hind leg tibial muscles

1.1 Relationship between resting muscle length and femur length

Resting muscle length was measured (at 90° joint angle, see 'Materials and Methods') of flexor and extensor tibiae for the front (flexor N=3, extensor N=3), middle (flexor N=5, extensor N=8) and hind legs (flexor N=3, extensor N=3, Fig. C.1). The linear regression of this data showed in 5 cases a significant dependence of muscle length on femur length (*, $p < 0.05$ or better), only the flexor tibiae front leg data showed no significant dependence. The dependence was simplified in Fig. C.1 for all legs to a pure proportionality forcing the regression lines through the origin (dotted lines, see also Tab. C.1). For comparison, the 1:1 proportion (solid line) is included.

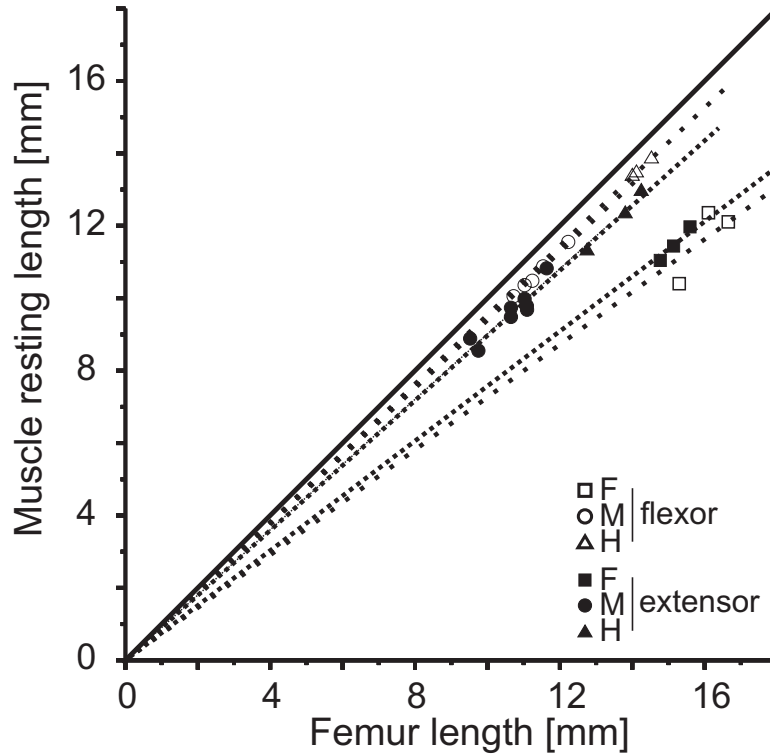


Figure C.1: Relationship between muscle resting length and femur length in front leg (squares), middle leg (circles) and hind leg (triangles). Data points for the extensor tibiae are represented by filled symbols, data points for flexor tibiae are represented by open symbols. The dotted lines give the linear fit under the assumption of pure proportionality between muscle length and femur length. For comparison the 1:1 proportion is added as a solid line. Values are shown in Tab. C.1.

Table C.1: Relationship between muscle length and femur length. Mean percentages arise from the slopes of linear fits forced through the origin (all significant, * ($p < 0.05$ or better) with the exception of flexor tibiae front leg data not being significant (-).

	Percentage of femur length	N
Extensor tibiae FL ■	75.7 ± 0.6	3
Extensor tibiae ML ●	90.1 ± 0.9	8
Extensor tibiae HL ▲	89.7 ± 0.7	3
Flexor tibiae FL □	72.7 ± 2.5	3
Flexor tibiae ML ○	94 ± 0.2	5
Flexor tibiae HL △	95.4 ± 0	3

1.2 Relationship between muscle length and FT-joint angle

From the resting position of 90° , the length change of the tibial muscles as a function of FT-joint angle was investigated. Given a fixed moment arm length of H, the length

change should have the form of $x = H \cdot \cos(\alpha)$, where α is FT joint angle. Fig. C.2 shows the normalised data compared to the cosine function. For the extensor muscle changes in joint angle depend on $+\cos(\alpha)$, for the flexor muscle on $-\cos(\alpha)$ (the sign difference arises from the fact that extension shortens the extensor muscle and lengthens the flexor tibiae). Normalised datapoints show good accordance with the additionally displays cosine function within a range from 50-160°. At extreme FT joint angles (< 50° and > 160°), datapoints tend to deviate slightly from the cosine function, which makes sense in respect to tibia movement mechanics (see ‘Discussion’).

1.3 Moment arm determination

The slope of the plots of muscle length versus $\cos(\alpha)$ is equivalent to the moment arm, because of $moment\ arm\ length = \frac{\Delta\ muscle\ length}{\cos(\alpha)}$. Fig. C.3 shows that the flexor

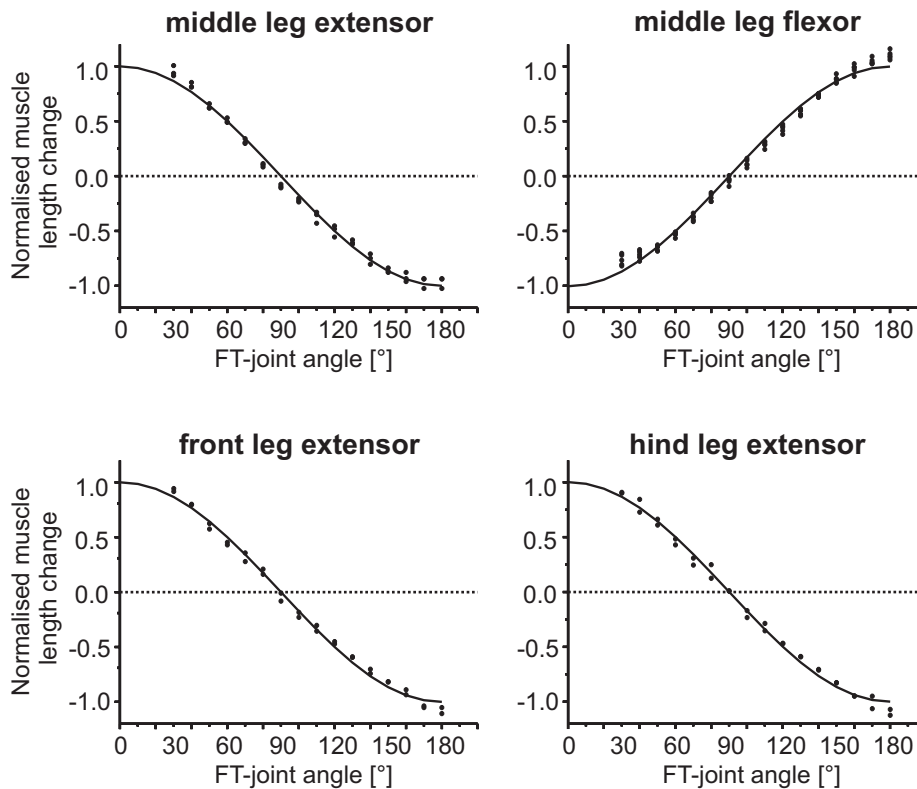


Figure C.2: Normalised muscle length change as a function of FT-joint angle. Extensor data are shown compared with $+\cos(\alpha)$ flexor data are compared with $-\cos(\alpha)$ (solid lines).

muscle moment arms of all leg joints are about two times larger than the extensor muscle moment arms (mean flexor moment arm length, 0.56 ± 0.04 mm, $N=7$ and mean extensor moment arm length 0.28 ± 0.02 mm, $N=7$).

2 Fibre length measurements of middle leg tibial muscles

As in all orthopteran legs, both the extensor and flexor tibiae of the stick insect are pinnate muscles (Storrer (1976)). This fibre arrangement markedly presents an advantage in terms of effective muscle cross-sectional area and maximum muscle force (Hildebrand (1988)) but decreases effective muscle length and maximum contraction velocity. Given a mean fibre diameter of 0.125 mm (Bässler and Storrer (1980)), and a mean of 156 fibres per muscle ($N=4$; min. $n=146$, max. $n=172$) an estimated mean cross-sectional area of the extensor tibiae muscle is 1.91 mm². As the extensor tibiae fills out about the upper third of the femur (3D-reconstruction model of Ulrich Bässler; Bässler et al. (1996)), the lower two thirds of the femur can be attributed to the flexor

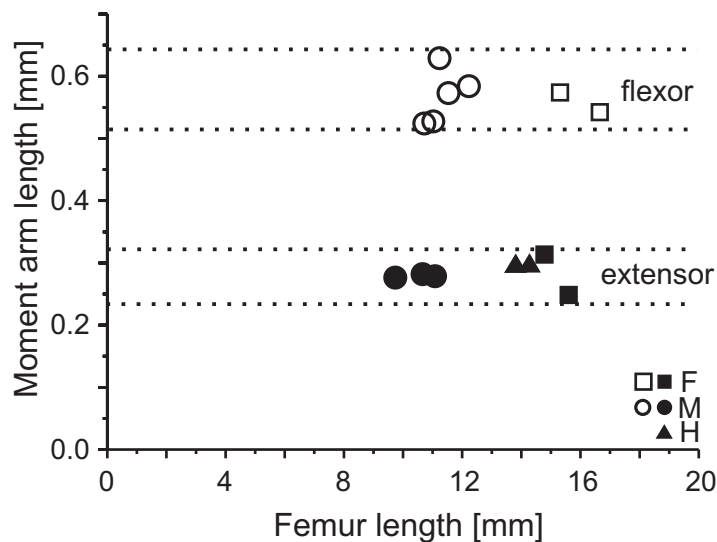


Figure C.3: Relation between femur-tibia joint moment arm and femur length. Note that moment arm does not depend on femur length. Closed symbols are data from extensor muscles from 2 front legs (squares), 2 hind legs (triangles), and 3 middle legs (circles), while open symbols are data for flexor tibiae muscles from 5 middle legs (circles) and two front legs (triangles).

tibiae, which is therefore estimated to have a cross-sectional area of 4 mm². For pinnate muscles, length changes of the muscle as a whole do not lead to the same changes in muscle fibre length; muscle fibre length instead varies with muscle length times the cosine of the pinnation angle, which in return varies as muscle length changes. For the extensor tibiae, a range of angles from 8.2 - 12° for the proximal and 10.2 - 15.6° for the medial fibres can be found within physiological muscle lengths. For the flexor tibiae, a range of 11.1 - 12.9° for the proximal and 12.4 - 15.4° for the medial part of the fibres can be determined. These calculations are based on the determination of fibre length (see next paragraph) and the distance from the tendon to the cuticle (where the fibres are attached). Calculation of errors was conducted using Pythagoras' law: the cosine correction was only 3.7% for the extensor and 2.9% for the flexor tibiae for the largest angle, so a correction can be neglected (i.e. the muscle fibres were treated as though they were arranged parallel to the muscle longitudinal axis in both cases).

The analysis of the relation between fibre length and muscle length is depicted in Fig. C.4. Proximal fibres of the extensor tibiae muscle had a mean length of 1.47 ± 0.21 mm (N=5) and are about 0.13 mm longer than the medial muscle fibres (N=5). From these results, a mean fibre length of the extensor tibiae was 1.41 ± 0.23 mm. In contrast, flexor tibiae proximal fibres had a mean length of 2.0 ± 0.32 mm (N=4) and are about 0.21 mm shorter than the medial fibres (N=4). The mean fibre length of the flexor tibiae is therefore 2.11 ± 0.30 mm. Regression analysis of this data showed a significant linear dependence of fibre length on extensor muscle length (*, $p \leq 0.03$), whereas no such dependence was detected for flexor tibiae muscle fibres (see dotted regression lines).

3 Sarcomere length measurements of middle leg tibial muscles

The following data set on sarcomere length represents a preliminary version, the investigation is not finalised yet. Because of sarcomeres being the fundamental functional units that a muscle consists of, an initial characterisation was carried out that is supposed to prompt future work. The ultimate goal of these examinations was to

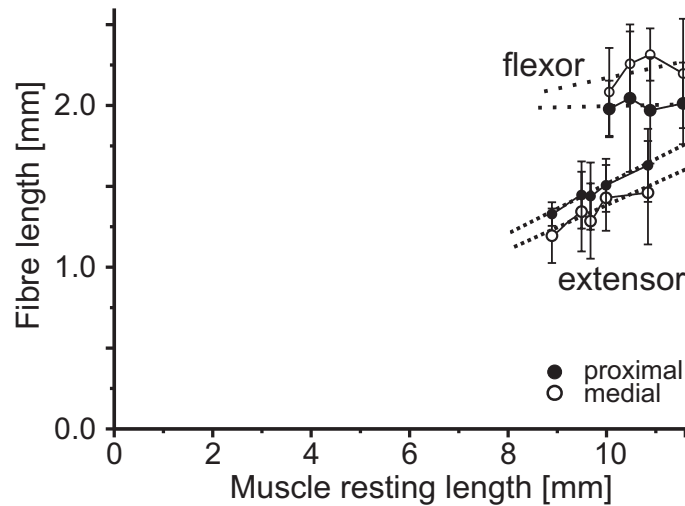


Figure C.4: Relation between middle leg muscle resting length and fibre length. Extensor muscle fibre length depends on muscle resting length (*, $p \leq 0.03$), whereas no such dependence is present in the flexor muscle (-, $p \geq 0.05$, dotted regression lines). Open circles denote data from medial muscle fibres, filled circles from proximal ones. Data are means \pm S.D. from nine animals ($N=9$).

relate a gross leg property (i.e. the joint angle) to a microscopic muscle property (i.e. the sarcomere length). The relevant question was as follows: Does the percent length change that extensor and flexor tibiae fibres experience within the physiological working range of 150° match the percent length change that the sarcomeres of these fibres experience? It was first attempted to measure sarcomere length with the muscle fibres being fast Nissl stained (Burck (1988)). Proximal and medial parts of the extensor and flexor tibiae fibres were investigated because of being predominately innervated by fast motoneurons (Debrodt and Bässler (1989); Bässler et al. (1996)). The study was not satisfactory, as only the dark A-bands (overlap of thick and thin filaments) and the much brighter I-bands (only thin filaments with the Z-lines in between) could be distinguished. The treatment that was necessary for the fast Nissl stainings involved drying, paraffin embedding and sectioning into $15 \mu\text{m}$ slices (see 'Materials and Methods' section). It is very likely that this whole procedure led to deformations of the stained sarcomeres. Hence, the method was considered to be inappropriate because the visibility of structures was limited and analysis of the stained material was questionable.

Further stainings were accomplished. Phalloidin stains F-Actin (Thuma (2007)) and is easier to handle because it does not require sectioning of the specimen and fibres

can be directly scanned on the Laser Scanning Microscope (LSM). Phalloidin stainings have a much greater visibility and therefore allow the discrimination of Z lines, thin filament overlap and H-Bands, see Fig. C.5a-c.

Measurements were taken from extensor and flexor tibiae fibres at 30° and 180° FT joint angle (see Fig. C.6a(i), a(ii), b(i), b(ii) and Tab. C.2). Extensor tibiae sarcomeres have a length of $7.50 \pm 0.75 \mu\text{m}$ (N=1, n=114) at 30° and a length of $6.21 \pm 0.38 \mu\text{m}$ (N=1, n=97) at 180°. Flexor tibiae sarcomeres have a length of $5.16 \pm 0.16 \mu\text{m}$ (N=1, n=60) at 30° and a length of $9.16 \pm 0.46 \mu\text{m}$ (N=1, n=31) at 180°. For extensor tibiae fibres, the ratio $\frac{Fl\ at\ 30\ deg}{Fl\ at\ 180\ deg}$ is 1.46 (calculated with a mean fibre length of 1.41 mm at 90° FT joint angle and a mean moment arm length of 0.282 mm) and the corresponding ratio for the sarcomeres $\frac{Sl\ at\ 30\ deg}{Sl\ at\ 180\ deg}$ is 1.21: sarcomeres experience 25 % less relative length change than fibres. For flexor tibiae fibres, the ratio $\frac{Fl\ at\ 180\ deg}{Fl\ at\ 30\ deg}$ is 1.65 (calculated with a mean fibre length of 2.11 mm at 90° FT joint angle and a mean moment arm length of 0.564 mm) and the corresponding ratio for the sarcomeres $\frac{Sl\ at\ 180\ deg}{Sl\ at\ 30\ deg}$ is 1.78: sarcomeres experience 13 % more relative length change than fibres. The length changes of the fibre do not match the sarcomere length changes, but the calculated values are close enough to make the conclusion that there is a gross correlation between fibre and sarcomere length changes. The results suggest that there might be muscle properties (e.g. cuticle or tendon proteins) that involve processes that could lead to the calculated mismatches. Further examinations should clarify whether this mismatch is detectable in more muscles.

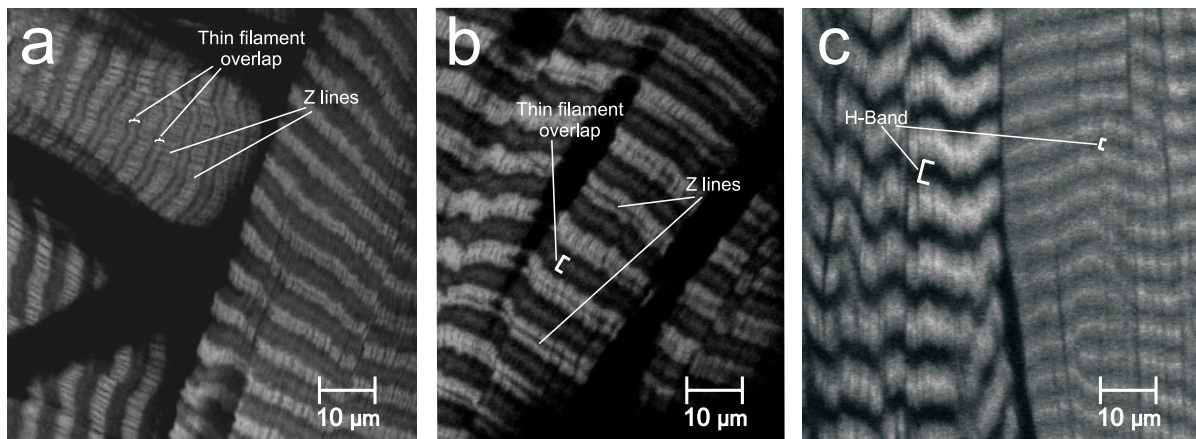


Figure C.5: LSM (laser scanning microscope) pictures showing either thin filament overlap (a, b) or occurrence of an H-band (c) in extensor and flexor tibiae fibres after phalloidin treatment.

In addition to the question whether sarcomeres of both tibial muscles experience the same length changes than the fibres, another topic needs to be clarified: are the structural components of the sarcomeres built the same way in extensor and flexor tibiae? Is there a way to determine sarcomere length independent from contraction state? A standardisation of sarcomere lengths (see Thuma (2007)) can answer these questions and allows to compare a) different muscles of one kind (e.g. extensor tibiae fixed at 30° and 180°) and b) muscles of different kinds (e.g. extensor tibiae fixed at 30° and flexor tibiae fixed at 30°). This normalisation procedure reduces each sarcomere to two times thin filament length (see ‘Materials and Methods’ section). The visibility of structures and therefore the possibility to distinguish between sarcomere elements allowed a standardisation of sarcomere length (see above).

Fig. C.5 shows the discrimination of individual phalloidin-stained sarcomere structures enabling to conduct measurements (both extensor and flexor tibiae sarcomeres, fixed at 30° and at 180° FT joint angle shown in Fig. C.6a(i), a(ii), b(i) and b(ii)). Standardised extensor tibiae sarcomere lengths (twice thin filament length) are $5.67 \pm 0.66 \mu\text{m}$ (N=1, n=114) at 30° and $5.17 \pm 0.46 \mu\text{m}$ (N=1, n=97) at 180°. An unpaired t-test results in a *** difference. Standardised flexor tibiae sarcomere lengths are $6.63 \pm 0.25 \mu\text{m}$ (N=1, n=60) at 30° and $7.22 \pm 0.44 \mu\text{m}$ (N=1, n=31) at 180°. An unpaired t-test results in a *** difference. Interestingly, flexor tibiae sarcomeres fixed at 30° show thin filament overlap (Fig. Fig. C.6b(i)), whereas extensor tibiae sarcomeres fixed at 180° do not show thin filament overlap (Fig. C.6a(i)). For both muscles, the standardised

FT-joint angle [°]	extensor tibiae		flexor tibiae	
	FI	SI	FI	SI
180	1.13 mm	6.21 μm	2.67 mm	9.16 μm
30	1.65 mm	7.50 μm	1.62 mm	5.16 μm
$\frac{\text{length at stretched state}}{\text{length at contracted state}}$	1.46	1.21	1.65	1.78

Table C.2: Analysis of extensor and flexor tibiae sarcomere phalloidin stainings. Fibre lengths (FI=fibre length) at 30° and 180° (1.41 mm for the extensor and 2.11 mm for the flexor tibiae at 90° FT joint angle) were calculated using the effective moment arm length of extensor (0.282 mm) and flexor tibiae (0.564 mm). Sarcomere lengths (SI=sarcomere length) were measured individually. Extensor tibiae sarcomeres at 30°: N=1, n=114; extensor tibiae sarcomeres at 180°: N=1, n=97; flexor tibiae sarcomeres at 30°: N=1, n=60; flexor tibiae sarcomeres at 180°: N=1, n=31).

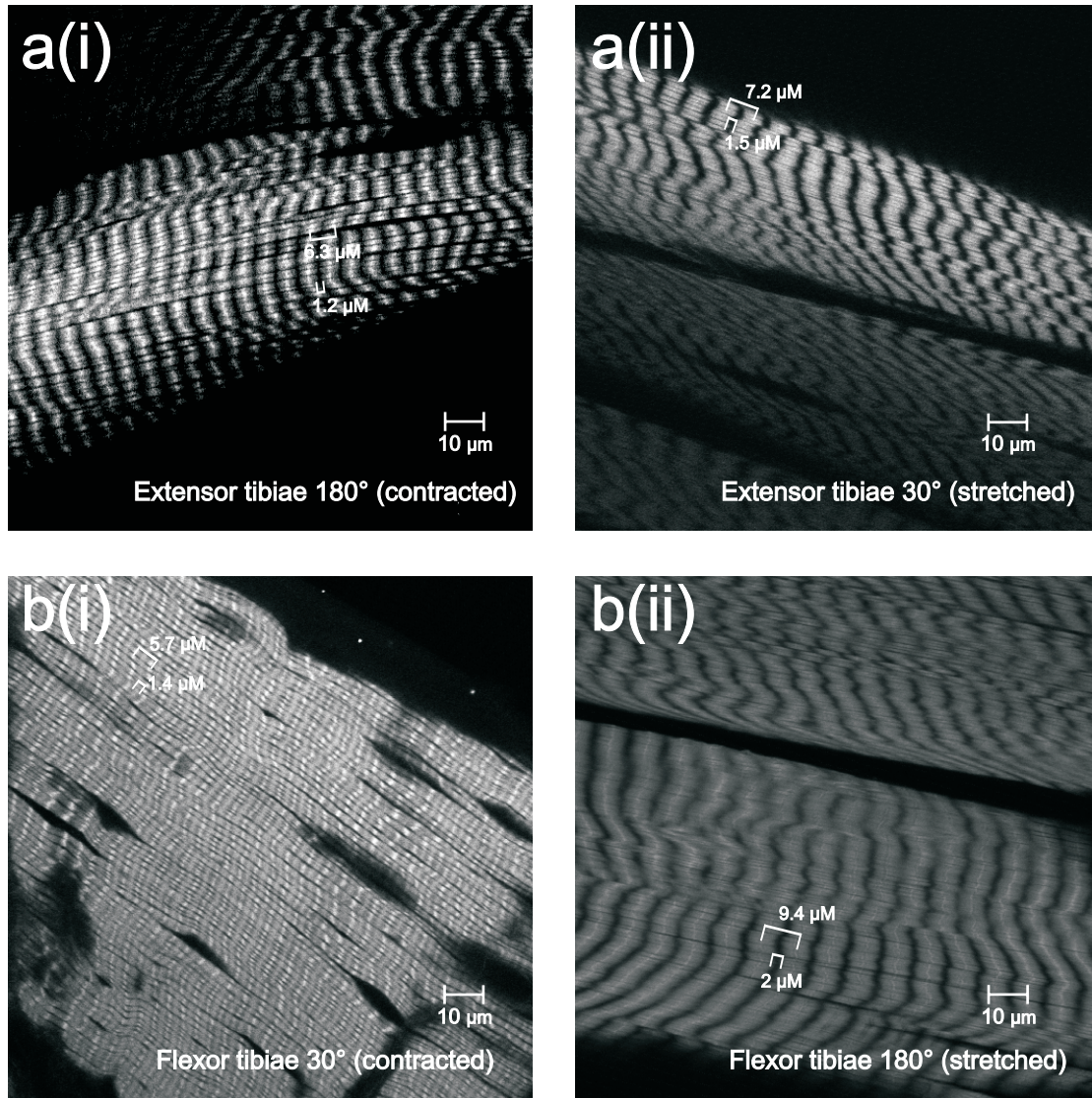


Figure C.6: LSM sarcomere length measurements on extensor (**a(i)** and **a(ii)**) and flexor tibiae muscles (**b(i)** and **b(ii)**). The fibres were fixed *in situ* at either 30° or 180° FT joint angle. Standardised sarcomere length could be calculated as described in Thuma (2007).

length value is smaller when calculated from the more contracted state compared to the calculation from the more stretched state. Because even at rest there is some thin-to-thick filament interaction, these increases in thin filament length as muscle fibre length increases suggest that the thin filaments may have substantial elasticity. The total of standardised extensor tibiae sarcomere lengths was tested to be highly significantly different (***) from the total of standardised flexor tibiae sarcomere lengths, see Fig. C.7. Mean standardised extensor tibiae sarcomere length is 5.42 μm , mean flexor

tibiae sarcomere length is $6.93 \mu m$. These data suggest that extensor and flexor tibiae sarcomeres are structurally different.

4 Femoral cross-sectional area

When cutting a middle leg femur with a razor blade (Rotbart), one gets an approximately elliptical cross-sectional area.

Using the following equation for an elliptical area

$$A = \frac{a \cdot b \cdot \pi}{4} \quad (\text{with } A = \text{elliptical area, } a = \text{length, } b = \text{width})$$

gives $A = 0.524 \pm 0.078 \text{ mm}^2$ (N=3), representing mean middle leg femur cross-sectional area.

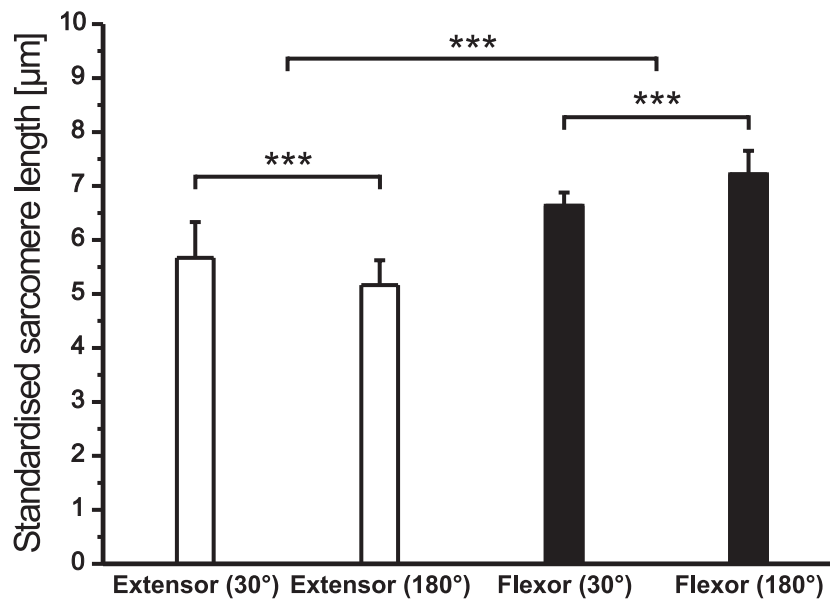


Figure C.7: Extensor and flexor tibiae standardised sarcomere length measurements with fibres fixed at 30° FT joint angle and 180° . Unpaired *t*-tests show extensor tibiae standardised sarcomere lengths at 30° to be highly significantly different (***, $p < 0.001$) from standardised sarcomere lengths at 180° and flexor tibiae standardised sarcomere lengths at 30° to be highly significantly different (***, $p < 0.001$) from standardised sarcomere lengths at 180° . Additionally, the total of extensor tibiae standardised sarcomere lengths is highly significantly different (***, $p < 0.001$) from the total of flexor tibiae standardised sarcomere lengths. See text for mean lengths \pm S.D.

C2 Force measurements in the isometric domain

1 Actively generated forces

Extensor tibiae motoneurons were stimulated with single pulses (Fig. C.8) and tonically at frequencies ranging from 30 Hz to 200 Hz (see Fig. C.11). The maximum frequency of 200 Hz was chosen because this is in the range of maximum frequency that FETi generates during the swing phase of stepping movements (Hooper et al. (2007a); Guschlbauer et al. (2007), 150 Hz in *Blaberus discoidalis* (Ahn et al. (2006))). Flexor tibiae motoneurons were mainly stimulated with single pulses (Fig. C.9). Homogeneous stimulation of a particular set of motoneurons was possible in only a few cases using high frequencies without visible stimulation failures in the force trace (C.12). The dual-mode lever system was used exclusively as a force transducer in this chapter.

1.1 Single twitch kinetics

Twitch kinetic measurements included the time to peak force (T_{max}), time to 50% relaxation (T_{50off}) and time to 90% relaxation (T_{90off}), all calculated relative to the force onset.

As described in ‘Materials and Methods’, suprathreshold extensor tibiae nerve stimulation led to one force amplitude (Fig. C.8), because stimulation current should have



Figure C.8: Average time course of an exemplary single twitch of the extensor tibiae ($N=1$, $n=43$).

Table C.3: Extensor tibiae single twitch kinetics.

Latency[ms]	P_{max} [mN]	T_{max} [ms]	T_{50off} [ms]	T_{90off} [ms]	N
8.5 ± 1.80	2.6 ± 2.45	26.41 ± 6.3	60.69 ± 15.65	149.89 ± 67.93	12

stimulated mostly all three motoneurons (Bässler and Storrer (1980)). Eventual stimulation of only the fast motoneuron could have altered force amplitude only very modestly. In contrast, five different flexor tibiae force amplitudes could be determined by continuous increase of stimulation current amplitude in one animal tested in respect to this issue (Fig. C.4). Latency of force onset becomes smaller as a consequence of the putative sequential recruitment of more fast motor units. Motoaxons with a smaller axon diameter need higher current amplitudes to be activated. The conduction velocity of an axon is proportional to the square root of the axon diameter (Hodgkin and Huxley (1952); Stein and Pearson (1971); Pearson et al. (1970)). For the extensor tibiae, the rough size proportions of the three motoneurons (see ‘Materials and Methods’) are known from Bässler (1977); Bässler and Storrer (1980). Maximal force (P_{max}) is within a similar range than the extensor tibiae twitch P_{max} (2.6 ± 2.45 mN) for the first three single twitch amplitudes (Tabs. C.3 and C.4, lines 1-3). Further increase of stimulation current leads to doubling of P_{max} (Tab. C.4, line 4). Single twitch kinetics (recruitments 1-4) show flexor tibiae fibres to be nearly 3 times faster reaching P_{max} (8-10 ms compared to 26 ms, Tabs. C.3 and C.4) and to be 3-6 times faster relaxing, depending on the recruitment level (24-51 ms compared to 150 ms). The reduction in muscle force to prestimulus levels after twitch took in general about 250 ms for the extensor tibiae, and 60 ms for the flexor tibiae. Maximal extracellular electrically achieved flexor tibiae twitch force (Tab. C.4, line 5) must be described separately be-

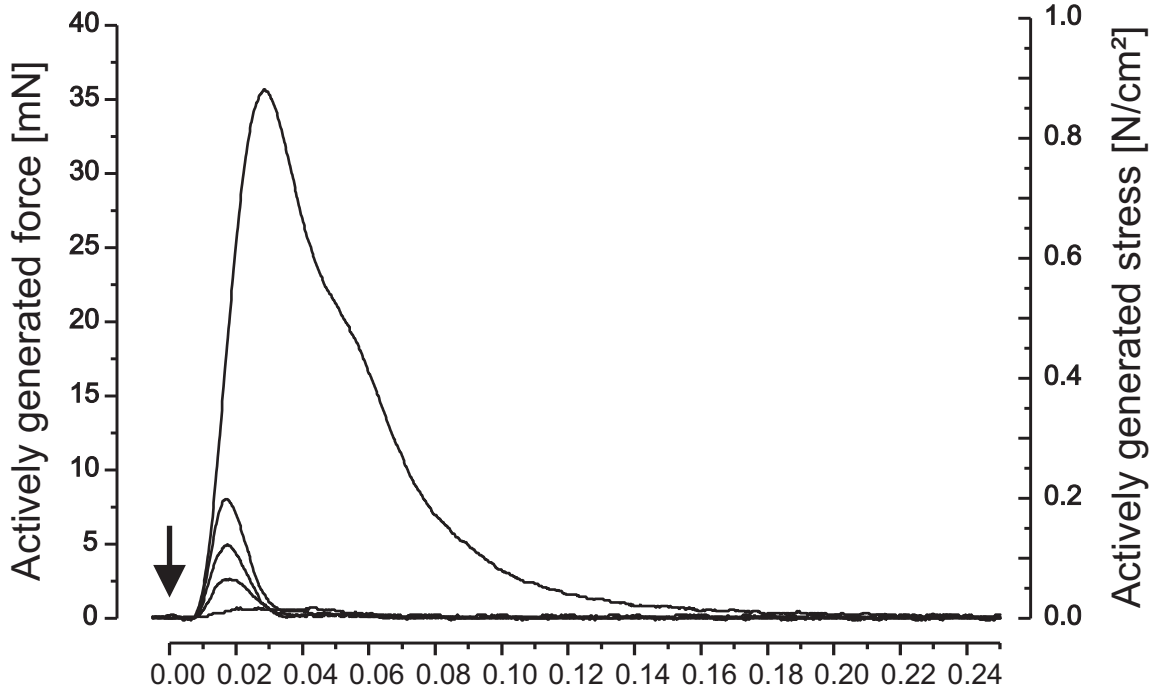


Figure C.9: Different flexor tibiae single twitch force amplitudes suggesting sequential motoneuronal recruitment as stimulation current was continuously increased (starting with 0 mA) until single twitch force was not becoming bigger (no ncr recording). As in Fig. C.8, the arrow marks the stimulation onset.

cause of its exceptionally large amplitude. P_{max} is 14 times bigger than extensor tibiae twitches ($N=2$, one example shown) but kinetics are rather similar for T_{max} and T_{50off} (21 ms compared to 26 ms and 50 ms compared to 60 ms). T_{90off} is 0.6 times faster (90 ms compared to 150 ms) but muscle force takes nearly 200 ms to reach prestimulus levels, compared to 250 ms in the extensor tibiae. The force trace in Fig. C.9 shows a little shoulder at about 0.06 ms which is likely to represent the force decay of slower relaxing fibres that were co-stimulated.

Table C.4: Flexor single twitch kinetics at different recruitment of motor units in one animal.

	Latency [ms]	P_{max} [mN]	T_{max} [ms]	T_{50off} [ms]	T_{90off} [ms]
1	11.6	0.6	8	30	51
2	8.4	2.6	9	19	29
3	8.4	4.9	10	17	23
4	8.2	8	9	16	24
5	7.8	35.5	21	50	90

The remarkably high contraction amplitude (N=2) led to further investigations. Continuous stimulation with 0.2 Hz shows a steady decrease of P_{max} that can be described with a power function ($y = x^a$). Continuous stimulation with 1 Hz shows a faster decrease (Fig. C.10a(i), both force traces are temporally set to zero). Log-log application of maximal force (ordinate) and time (abscissa) proves the force decays to be power-function-like because $y = x^a$ gives $\log(y) = a \cdot \log(x)$ and the decays can be fit with linear regressions (***, Fig. C.10a(ii)) with a R=0.961 for the fit of the 0.2 Hz stimulation data and R=0.978 for the fit of the 1 Hz data). However, the decays have fairly different slopes (-0.0803 and -0.0730). Lin-lin plotting of maximal force vs. pulse count (instead of time) on the abscissa was done in order to test whether the persistent force decrease is a temporal or an event-driven effect (Fig. C.10b(i)). The similarity of the linear regression slopes (-0.0826 compared to -0.0829) shown in Fig. C.10b(ii) suggests that force decreases with each pulse, no matter at which frequency. There seems to be no regeneration within the next 4 s.

1.2 Force kinetics at different activation

At 30-50 Hz stimulation frequency, twitch contractions merged into an incomplete tetanus in all preparations (N=38; Tab. C.5). The summated "steady-state" force amplitude of the resulting contractions varied between preparations (see Tab. C.6 and Fig. C.24). At 80 Hz and higher stimulation frequencies, tetanus was complete in all preparations. At higher stimulation frequencies, the force level only increased slightly with increasing stimulation frequency (Fig. C.11, Tab. C.5) and was maximal with no further increase at 200 Hz. Maximum force values from 9 preparations are given in Tab. C.6.

Summated steady-state force of the flexor tibiae was exclusively tested upon 200 Hz stimulation (see chapter 'Force in the isotonic domain'). However, in one case it was possible to achieve a nearly twofold variation of the isometric contraction amplitude by variation of the stimulation current amplitude (Fig. C.12). Gradation of stimulus amplitude is difficult because the activation thresholds of the flexor tibiae motoneu-

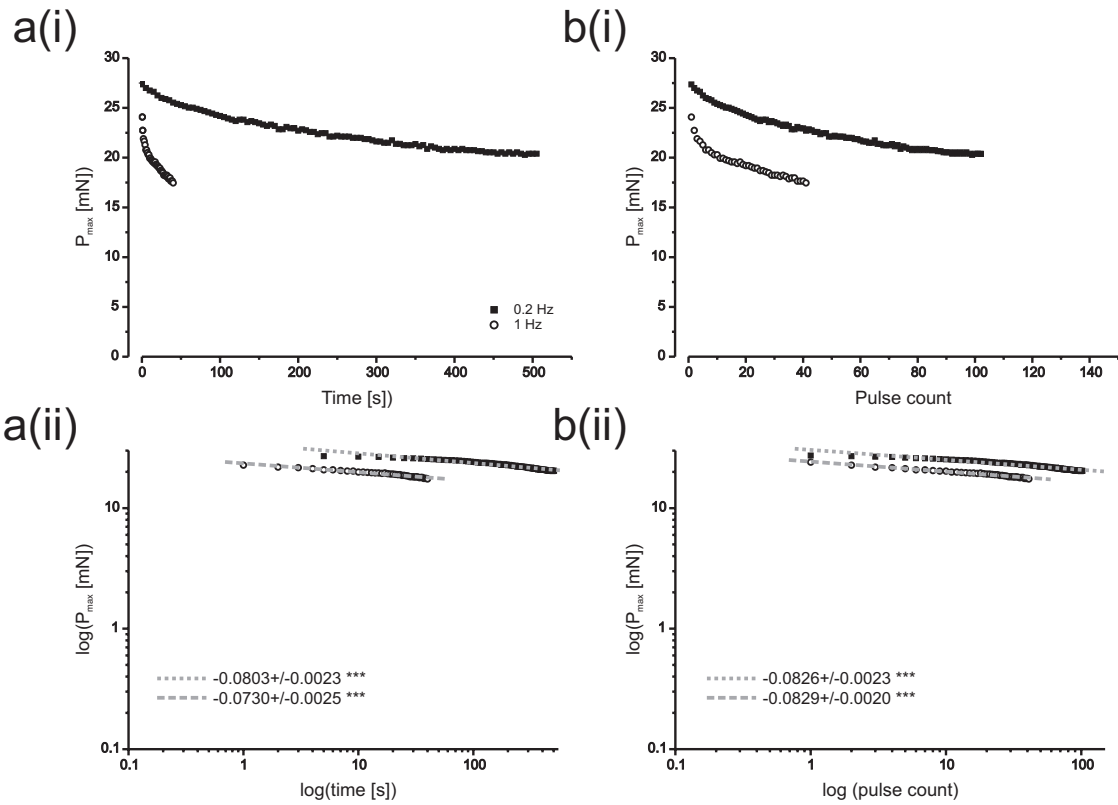


Figure C.10: Continuous decrease of maximal flexor tibiae twitch force at continuous stimulation with 0.2 Hz (filled circles) and 1 Hz (open circles) in one exemplary experiment ($N=1$). Note that the force level at each frequency is slightly different (3 to 4 mN). Data in **a(i)** and **b(i)** are shown as lin-lin plot (linear scaled abscissa and ordinate), data in **a(ii)** and **b(ii)** are depicted as log-log plot (logarithmic scaled abscissa and ordinate). The fact that the data can be fitted well by linear regressions (***) ($p < 0.001$), shows that P_{max} decreases in a power-function-like manner and suggests the decrease to be rather pulse count dependent than time dependent (compare R-values of **b(ii)** to **a(ii)**, legend displayed in the plot).

rons are often at close quarters. Thus, homogenous force generation is difficult to achieve without stimulation failures.

1.3 Post-stimulational force dynamics at different activation

Isometric force generation of the middle leg extensor tibiae is characterised by a noticeably long lasting P_{max} after the end of stimulation followed by a slow relaxation phase, illustrated in Fig. C.13. In this example, force takes > 500 ms to decline completely.

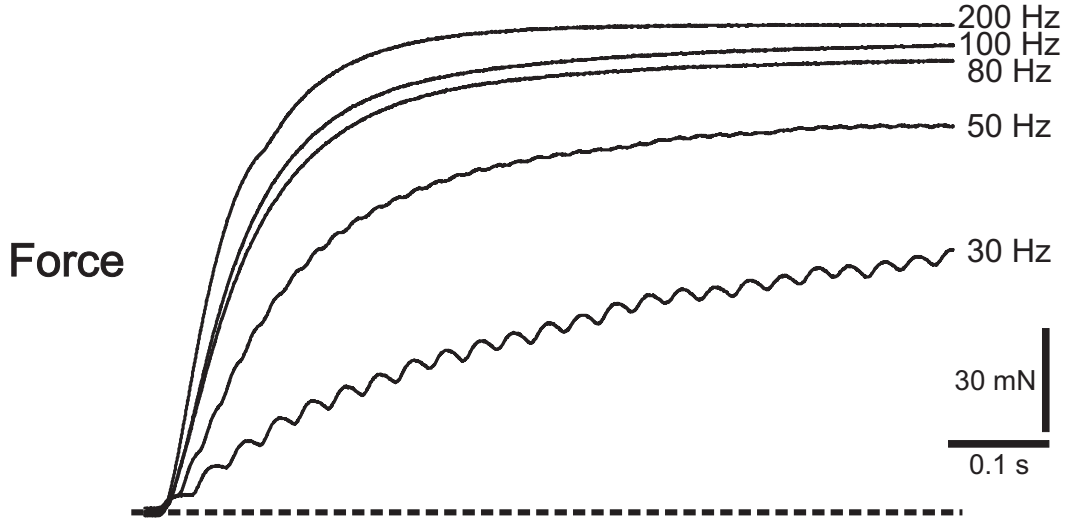


Figure C.11: Force development generated upon repetitive stimulation with differing stimulation frequencies between 30 Hz and 200 Hz (values in Tab. C.5).

Table C.5: Extensor tibiae tetanus / stress kinetics at different activation levels (N=1 shown exemplarily).

	P_0 [mN] / [$N \cdot cm^{-2}$]	$T_{0.5 P_0}$ [ms]	$T_{0.9 P_0}$ [ms]
30 Hz	84 / 4.39	264	632
50 Hz	115 / 6.01	116	245
80 Hz	134 / 7.00	85	173
100 Hz	140 / 7.31	81	164
200 Hz	144 / 7.52	64	132

Considering the fact that most physiologically occurring middle leg swing phases have a duration < 0.2 s (Gabriel et al. (2003); Gabriel and Büschges (2007)), the course of isometric force after the end of stimulation is a relevant task. Hooper and colleagues (Hooper et al. (2007a)) found muscle time constants in isotonic contractions to be different during contraction from during relaxation. Their results show a mean relaxation τ of 0.055 s (N=7) in response to naturally occurring stimulation input and a sustained duration of P_{max} (they called it ‘delay to rapid relaxation’) of 0.064 ± 0.014 s (N=7). I wondered how long it takes for the extensor tibiae to relax after having generated force in the **isometric** domain at different activation levels (in comparison to **isotonic** experiments performed by Hooper et al.). The persistence of P_{max} after stimulation end was examined as well.

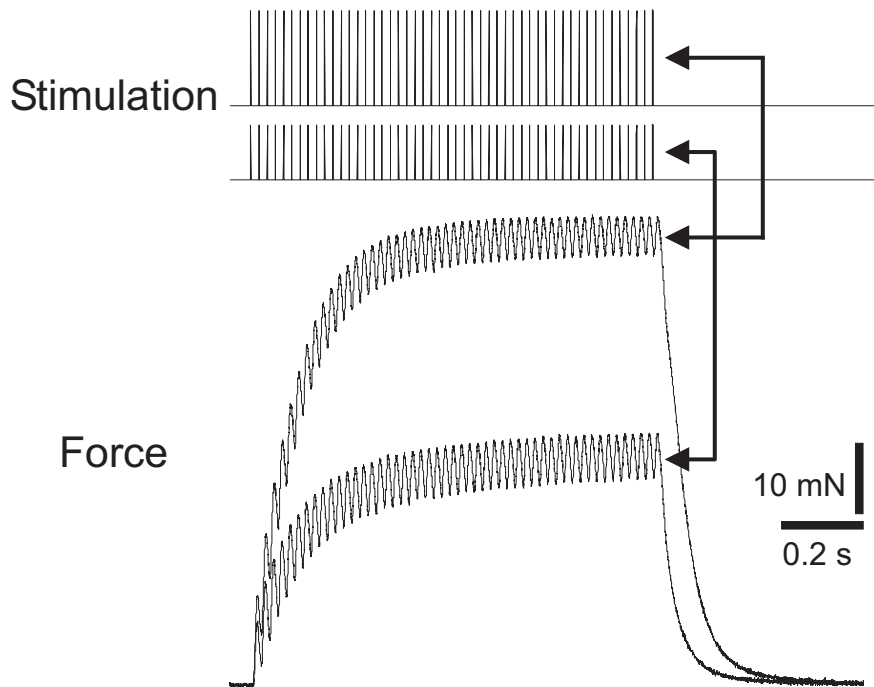


Figure C.12: Different flexor tibiae force development upon 50 Hz stimulation at two different stimulation current amplitudes. Arrows indicate that the lower current amplitude elicited a smaller isometric force response and the higher current amplitude a larger response.

Following Hooper et al. (Hooper et al. (2007a)), relaxation time constants were determined by fitting the data with the equation $A = A_0 \cdot e^{-\frac{t}{\tau}}$. This is in good agreement with examinations from Jewell and Wilkie, who report that the tension fall in the *sartorius* muscle of the frog *Rana temporaria* becomes exponential (Jewell and Wilkie (1960)). Fitting started at 95 % P_{max} (see Fig. C.14) and ended about 0.1 s after reaching prestimulus force levels. 95 % seemed reasonable as a start because the transition from maximal force generation to force decay is rather smooth than abrupt. Ca^{2+} takes a few milliseconds to be pumped back into the sarcoplasmic reticulum (Abbot (1973); White and Thorson (1975)).

Data was fitted consistently for isometric contractions of different stimulation frequency (exemplary fits see Fig. C.15a). Persistence of P_{max} was calculated by measuring the time after the last stimulation pulse and the intersection where the exponential decay fit and the straight line that extends P_{max} meet (see Fig. C.15b).

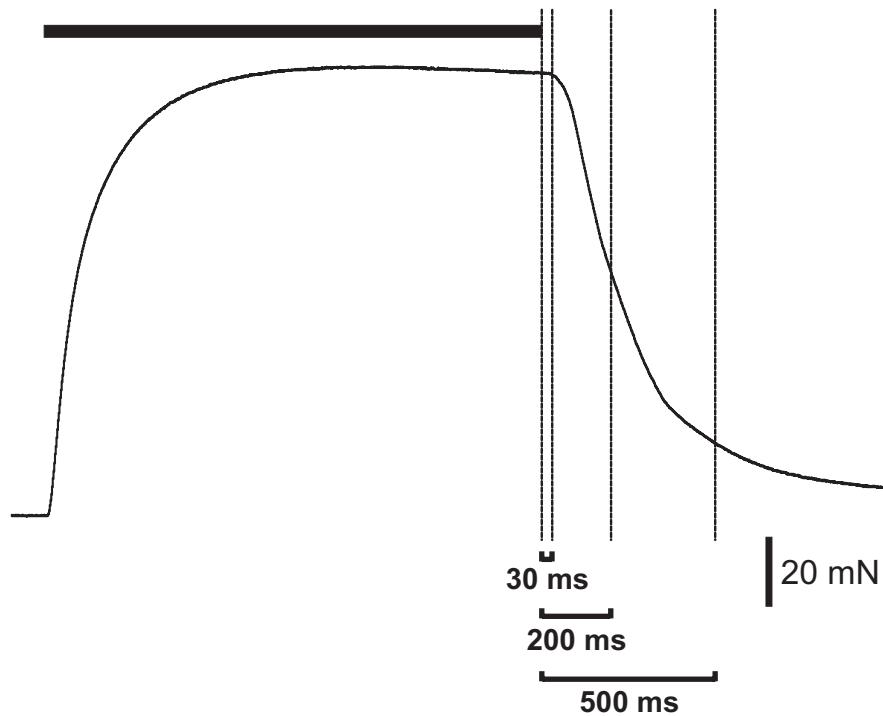


Figure C.13: Extensor tibiae isometric contraction force takes almost 1 s to reach prestimulus levels. 30 ms after the end of stimulation, P_{max} has not decreased at all. After 500 ms, P_{max} has decreased 50 %.

Seven extensor tibiae muscles (N=7) were tested in respect to their relaxation time constants, sustained P_{max} -durations and P_{max} . Data were depicted as absolute values (Fig.C.16a(i), b(i) and c(i)) and as relative datapoints normalised to the maximal value (=1.0) in a(ii), b(ii) and c(ii), because of the high degree of variation between animals. In all experiments, relaxation τ and the sustained P_{max} -duration increased with increasing stimulation frequency. Both normalised datapools could be fitted with a linear regression (both $***$, $R=0.814$ for the normalised relaxation τ data and $R=0.714$ for the sustained P_{max} - duration data) and increased by $0.2 \frac{\%}{\text{Hz}}$. The relationship between P_{max} and stimulation frequency can be described with an exponential saturation curve: the higher the activation, the less increase of P_{max} .

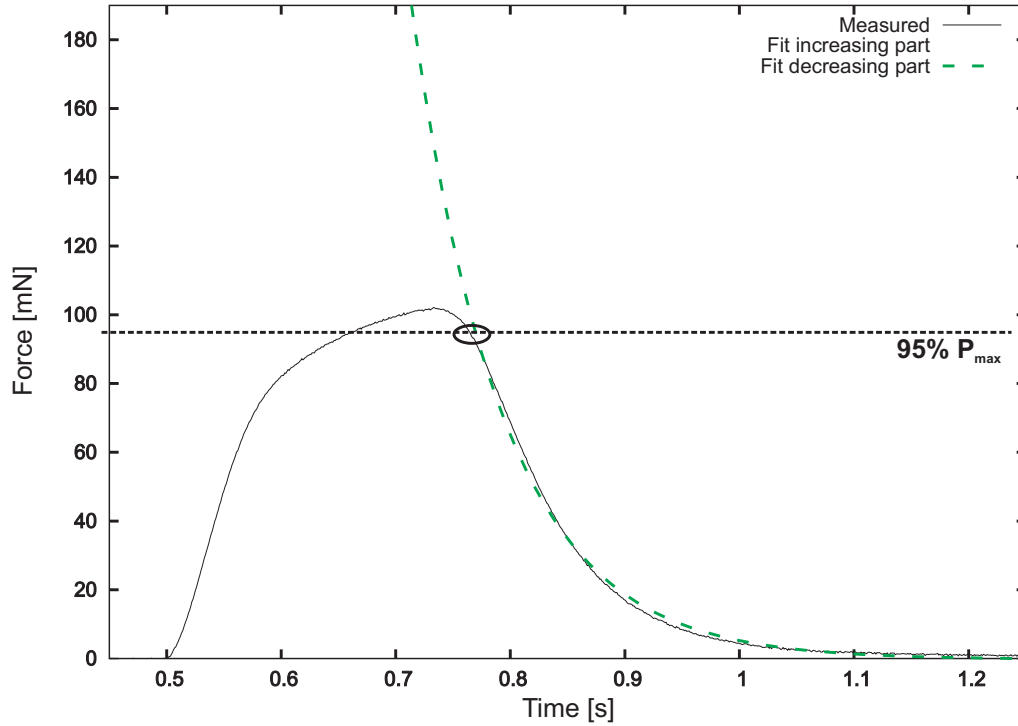


Figure C.14: Exemplary exponential decay fitting extensor tibiae relaxation after an isometric contraction. Fits ($A = A_0 \cdot e^{-\frac{t}{\tau}}$) started at 95 % P_{max} , indicated by the dashed line crossing the force trace and emphasised by the oval.

1.4 Post-stimulational force dynamics at different stimulation duration

In the same way than described in section 1.3, relaxation τ , sustained duration of P_{max} and P_{max} were tested in terms of their dependence on pulse number. Fig. C.17 shows the overlay of seven isometric contractions in response to 200 Hz stimulation with 20, 40, 60, 80, 100, 120 and 140 spikes that were triggered to the end of the last stimulation pulse (arrow in Fig. C.17).

Data from five extensor tibiae muscles (N=5) are depicted as absolute values (Fig. C.18a(i), b(i) and c(i)) and as relative datapoints normalised to the maximal value (=1.0) in a(ii), b(ii) and c(ii). In all experiments, relaxation τ , the sustained P_{max} -duration and P_{max} increased with increasing pulse number. All three normalised datapools were fitted with a linear regression that proved to be significant ($p < 0.5$ or better). Relaxation τ data increased by $0.7 \frac{\%}{pulse}$ (***, R=0.748), sustained P_{max} -duration

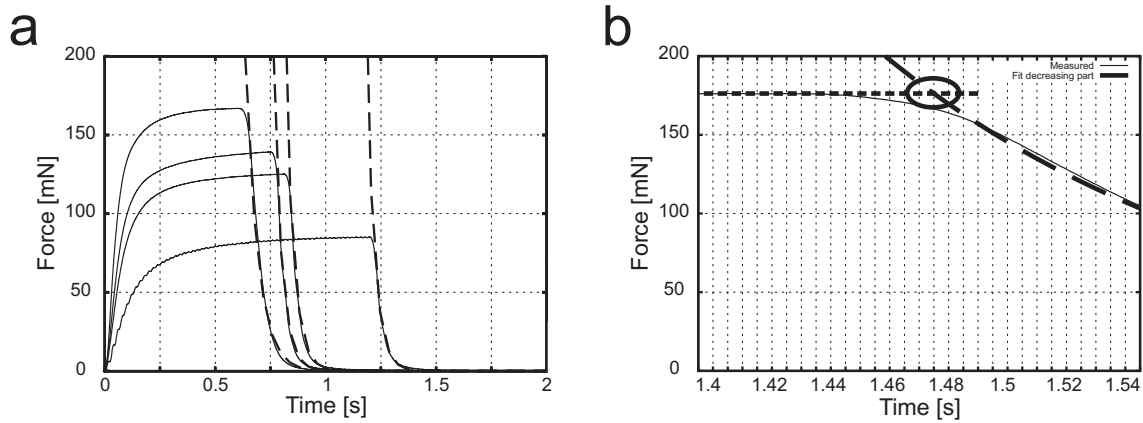


Figure C.15: **(a)** Exponential decay fits of the relaxation phase of isometric contractions at different stimulation frequencies (30, 50, 80, 200 Hz) for one exemplary animal ($N=1$). **(b)** The intersection of an isometric contraction's P_{max} extension line and its relaxation phase's exponential decay fit marks the end of the persisting P_{max} phase.

increased by $0.4 \frac{\%}{pulse}$ (***, $R=0.794$) and P_{max} showed a weak increase of $0.1 \frac{\%}{pulse}$ (*, $R=0.437$).

1.5 Force development in response to activation changes (latch)

Blaschko and Kahn (Blaschko et al. (1931)) reported that the force plateau of a crustacean muscle stimulated repetitively at a low frequency becomes higher if the muscle had been stimulated with a brief intercalated high frequency burst prior to returning to the original low frequency. Wilson and Larimer (Wilson and Larimer (1968)) termed the phenomenon “catch-like” effect because “catch” was restricted to smooth muscle and because the catch-like contraction requires neuronal activity to maintain it. Finally, the catch-like effect (or sometimes termed “latch”) could also be found in a crustacean muscle involved in walking movements (Günzel and Rathmayer (1994)). Such a ‘residual force enhancement’ could also be detected in the middle leg extensor tibiae. In a series of experiments, the extent of this catch-like effect was characterised in the extensor tibiae.

Fig. C.19a and b demonstrates the basic phenomenon: two muscles were stimulated isometrically with 33 Hz pulses and for a short term, frequency was increased to 200 Hz (30 pulses). After the switch back to a stimulation frequency of 33 Hz, force was

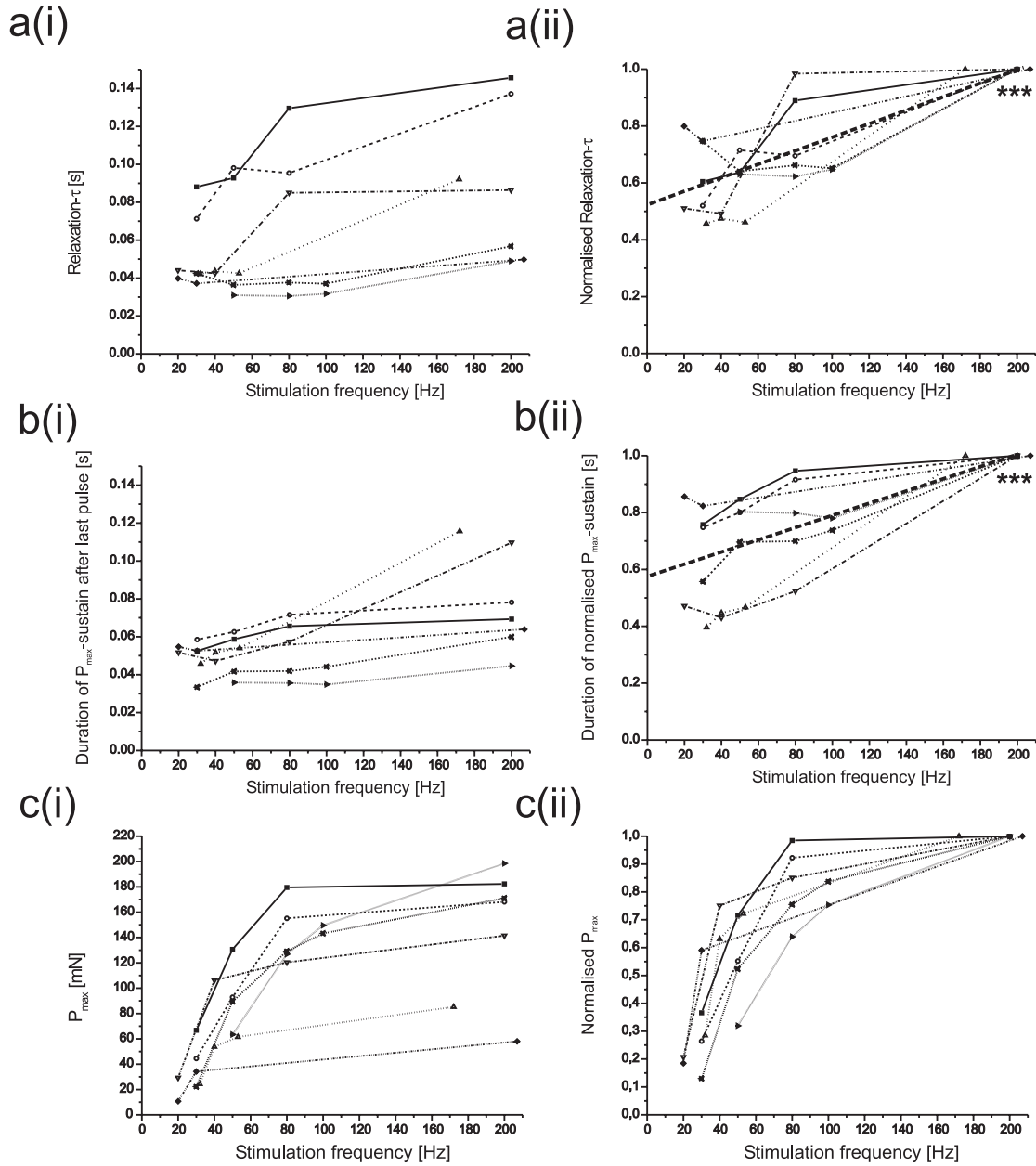


Figure C.16: Changing of relaxation time constants, post-stimulatory maximal force sustain and P_{max} with different activation in seven animals ($N=7$, $n=28$). Data was normalised in **a(ii)**, **b(ii)** and **c(ii)** to the maximal value (=1.0).

enhanced by 23 % in **(a)** and by 17 % in **(b)** compared to a contraction with continuous 33 Hz stimulation (cambered brackets) and remained enhanced for the rest of the low-frequent stimulation (3 s).

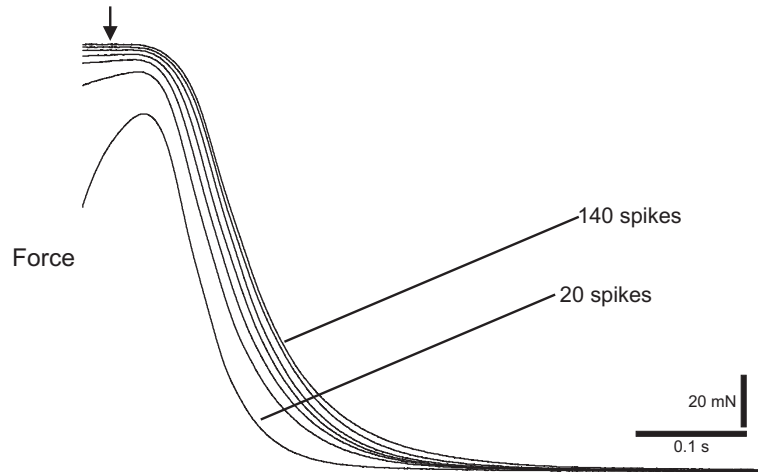


Figure C.17: End of contraction and succeeding relaxation phase after 200 Hz stimulation with 20 (indicated), 40, 60, 80, 100, 120 and 140 (indicated) pulses in one exemplary animal ($N=1$). The arrow marks the end of stimulation.

Further investigations focussed on the effect's dependence on stimulation frequency (Fig. C.20). Muscles were initially always stimulated at 33 Hz and 20 pulses of 33, 40, 60, 80 or 100 Hz were applied subsequently. After that, stimulation continued again at 33 Hz (C.20a). Fig. C.20b shows two experiments, where P_{Peak} , measured at the end of the high-frequency stimulation (circles), and P_{end} , forces measured at the end of low-frequency stimulation (triangles), appear to be enhanced the higher the frequency. Normalised data in (c), 100% relative force = P_{33Hz} , describe the consequences of a high-frequency insertion: P_{Peak} increased by $2.1 \frac{\%}{Hz}$ (**, normalised force at 100 Hz was 175% of P_{33Hz} in one experiment and 300% of P_{33Hz} in the other) . P_{end} at 100 Hz increased by $0.36 \frac{\%}{Hz}$ (**, 125% of P_{33Hz} in both experiments).

The next set of experiments investigated the effect's dependence on pulse number (Fig. C.21). Like in Fig. C.20, muscles were stimulated at 33 Hz. Insertions consisted of 100 Hz stimulations with 3, 5, 10, 12, 15, 20 or 30 pulses (Fig. C.21a). Similar to C.20, P_{Peak} and P_{end} increase with pulse number (Fig. C.21b). Normalised data (c) show P_{Peak} to increase by $6.39 \frac{\%}{pulse\ number}$ (***, $R=0.973$, $n=13$) and P_{end} to increase by $0.89 \frac{\%}{pulse\ number}$ (***, $R=0.902$, $n=14$).

The catch-like effect was finally examined on its potential to compensate for a force

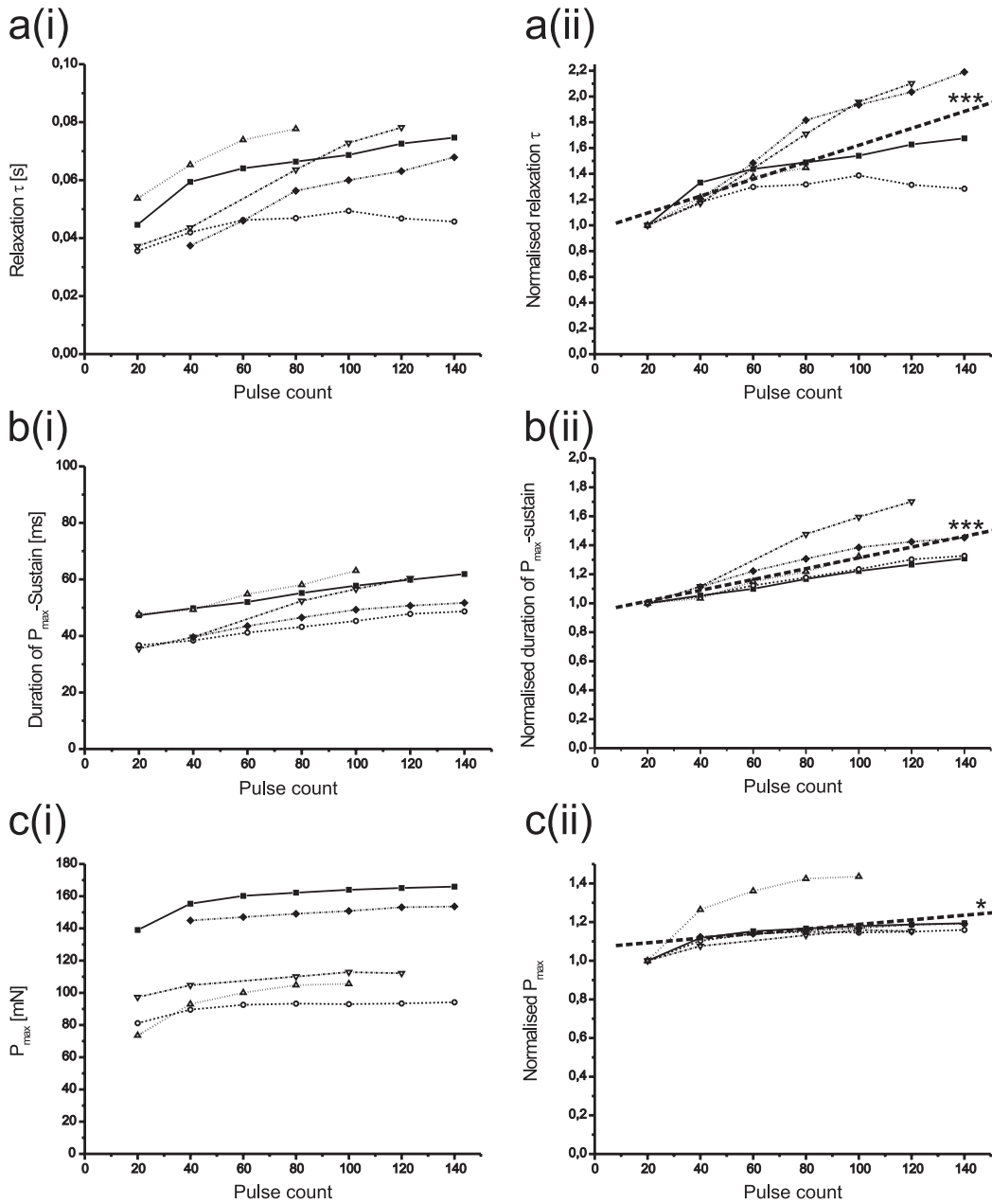


Figure C.18: Changing of relaxation time constants and of post-stimulational maximal force sustain with different activation duration in seven animals ($N=7$, $n=30$). Data was normalised in **a(ii)**, **b(ii)** and **c(ii)** to the maximal value ($=1.0$).

drop during stimulation gaps. The procedure followed the principles of the previous investigations shown in Figs. C.20 and C.21: 33 Hz stimulation was interrupted by a brief 20 pulse at 100 Hz stimulation. Additionally, stimulation gaps of various duration were included: 0 s, 0.05 s, 0.1s and 0.15 s (Fig. C.22). Data was normalised to

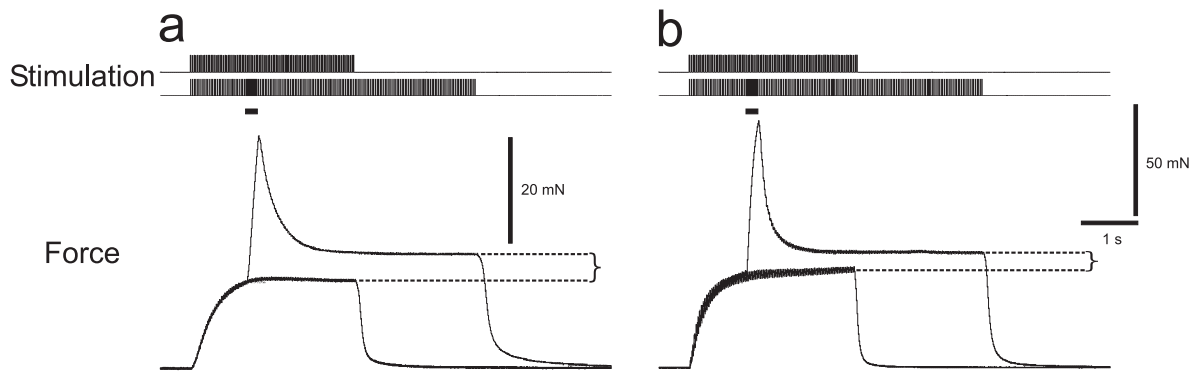


Figure C.19: *a, b*: Persisting force increase in response to a short-term 100 Hz burst ($N=2$). The force increase marked by the cambered brackets represents the 'catch-like effect', also termed 'latch'.

$P_{33\text{Hz}}$ measured right before high frequency stimulation started (=100 %). Gap duration could be as long as 0.1 s and was still 'compensated' by the force enhancement after the high frequency burst (Fig. C.22b, $N=2$). Force dropped below $P_{33\text{Hz}}$ when the stimulation gap exceeded 0.1 s ($N=1$).

1.6 The force-length relationship at different activation

The isometric force generated by a muscle depends on motoneuron firing rate and muscle length because of the overlap of the filaments changes as muscle length changes (Gordon et al. (1966b); Rack and Westbury (1969); Brown et al. (1999); Brown and Loeb (1999)). The dependence of extensor tibiae muscle force upon these parameters was therefore tested by stimulating the muscle with single stimuli, intermediate (10-80 Hz) and high (200 Hz) frequency tonic stimulations.

Fig. C.23 shows (middle leg) extensor tibiae single twitch force, isometric force at 50 Hz stimulation frequency and at 200 Hz versus muscle fibre length. Besides the expected general length dependence based on filament overlap (Gordon et al. (1966b)), it becomes apparent that the dependence of force generation on fibre length and stimulation frequency varied between experiments. In the single twitch measurements, maximum force varied 8-fold ($1.7\text{-}13\text{ mN} / 0.09\text{-}0.68\text{ } \frac{\text{N}}{\text{cm}^2}$), for the 50 Hz stimulation 5-fold ($23.4\text{-}114.9\text{ mN} / 1.22\text{-}6.00\text{ } \frac{\text{N}}{\text{cm}^2}$) and for the 200 Hz stimulation 2.7 fold ($61.8\text{-}165.6\text{ mN} / 3.23\text{-}8.65\text{ } \frac{\text{N}}{\text{cm}^2}$) (see also Tab. C.6).

RESULTS

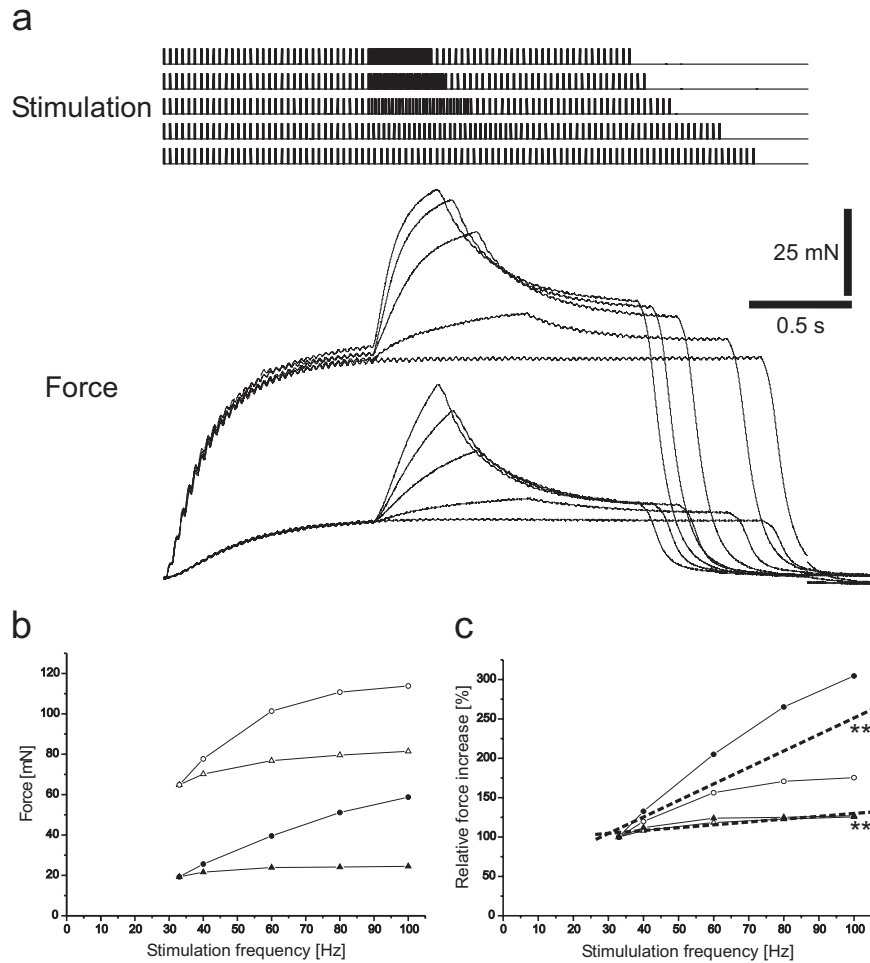


Figure C.20: **(a)** Latch in response to short-term stimulation of different frequency (20 pulses of 33, 40, 60, 80 and 100 Hz; $N=2$, $n=10$). **(b)**, **(c)** Circles represent forces (P_{Peak}) measured at the end of high-frequency stimulation, triangles represent forces measured at the end of the second part of low-frequency stimulation (P_{End}). Open symbols denote experiment 1, filled symbols experiment 2. P_{Peak} and P_{End} are enhanced with increasing frequency (**, $R=0.802$ for P_{Peak} and **, $R=0.898$ for P_{End}). Data are illustrated relative to non-stop 33 Hz stimulation (= 100% relative force, P_{33Hz}). For details see text.

Whereas the 200 Hz length dependencies shows maximum muscle force in the upper third of the working range, the curves with lower stimulation frequencies show a tendency of shifted maximum force up to more elongated fibre lengths (Fig. C.23). This shift is known from other muscles (cat, *soleus* muscle: Rack and Westbury (1969); cat, *caudofemoralis* muscle: Brown et al. (1999); Brown and Loeb (1999)).

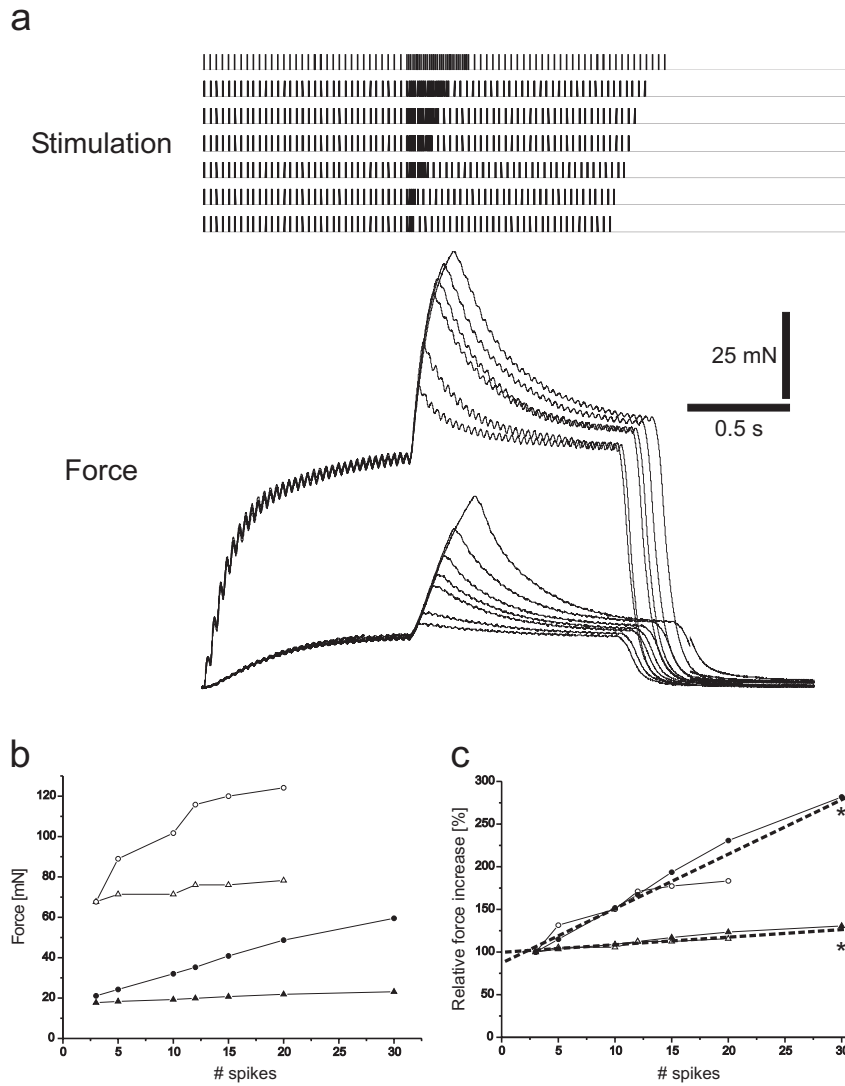


Figure C.21: **(a)** Latch in response to short-term 100 Hz stimulation of different spikenumber (3, 5, 10, 12, 15, 20 and 30 pulses; $N=2$, $n=27$). **(b)**, **(c)** Circles represent forces (P_{peak}) measured at the end of high-frequency stimulation, triangles represent forces measured at the end of the second part of low-frequency stimulation (P_{end}). Open symbols denote experiment 1, filled symbols experiment 2. P_{peak} and P_{end} are enhanced with increasing pulse number (dashed lines indicate linear regressions, *** ($p < 0.001$), $R=0.973$ for P_{peak} and ***, $R=0.902$ for P_{end}). Data are illustrated relative to non-stop 33 Hz stimulation with an insertion of 3 pulses at 100 Hz (= 100% relative force, P_{33Hz}). For details see text.

In addition, the extent of this shift could vary between experiments: two examples with maximal and minimal frequency dependence of the length at which the muscle develops maximum force are depicted in Fig. C.24 **a**, **b**.

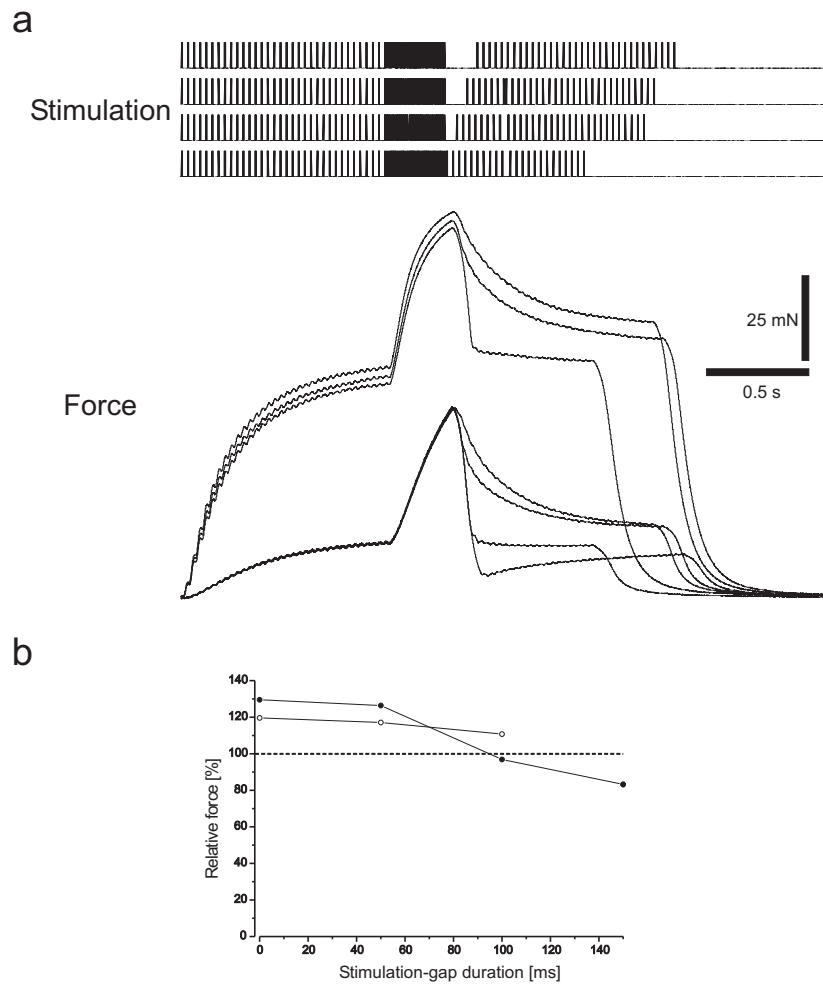
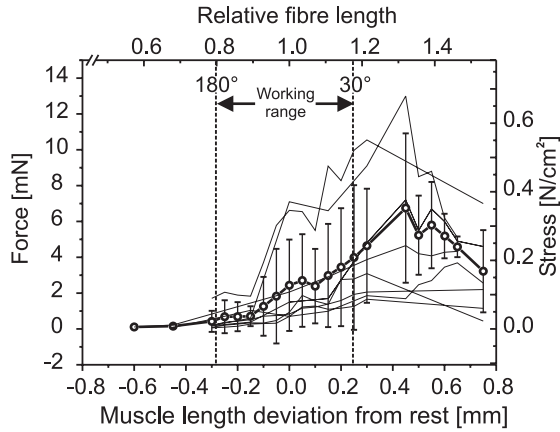
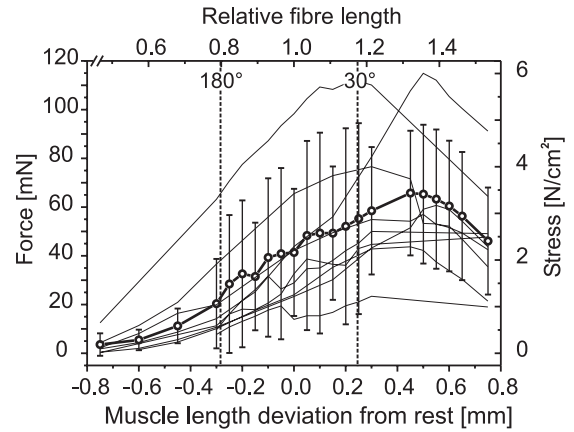


Figure C.22: Latch in response to short-term 100 Hz stimulation consisting of 20 pulses. Gaps of different duration (0 s, 0.05 s, 0.1 s and 0.15 s) were inserted after the high frequency burst ($N=2$, $n=7$). The dashed line indicates $P_{33\text{Hz}}$ measured right before high frequency stimulation (= 100% relative force).

Single Twitch



50 Hz



200 Hz

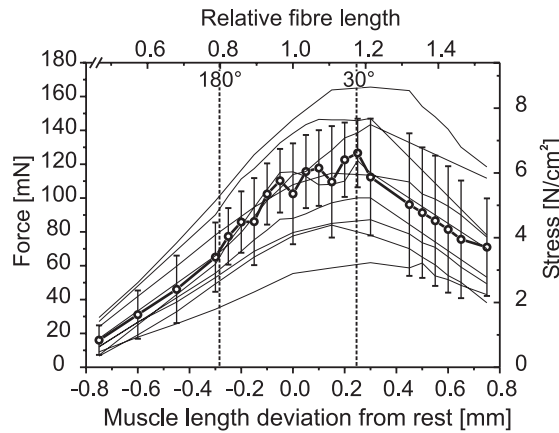


Figure C.23: Isometric force (mN, left ordinate) as a function of muscle stretch (mm, lower abscissa) and relative fibre length top abscissa). Values for single twitch ($N=8$), 50 Hz ($N=9$) and 200 Hz ($N=9$), see maximum values in Tab. C.6. For comparison with other muscles, the right ordinate shows stress ($\frac{N}{cm^2}$). The working range from 180° (fully stretched joint angle) to 30° (maximal physiologically flexed joint angle) is marked. Please note that the number for individual means can differ, for single twitch measurements $3 \leq N \leq 9$, for 50 Hz and 200 Hz measurements $5 \leq N \leq 9$.

RESULTS

Table C.6: Variation of frequency-dependent maximum force / stress development in nine animals (N=9).

Twitch force [mN] / [$\frac{N}{cm^2}$]	50 Hz Force [mN] / [$\frac{N}{cm^2}$]	200 Hz Force [mN] / [$\frac{N}{cm^2}$]
-	43.7 / 2.28	84 / 4.39
7.2 / 0.38	114.9 / 6.00	165.6 / 8.65
13 / 0.68	57 / 2.98	61.8 / 3.23
3.69 / 0.19	60.7 / 3.17	114.7 / 5.99
4.65 / 0.24	76.6 / 4.00	84.2 / 4.56
3.09 / 0.16	23.4 / 1.22	100.1 / 5.23
2.06 / 0.11	50 / 2.61	143.4 / 7.49
1.66 / 0.09	44.7 / 2.34	122.1 / 6.38
10.55 / 0.55	111.7 / 5.84	147.1 / 7.69
5.7 ± 44.15 / 0.3 ± 0.22	64.74 ± 31.04 / 3.38 ± 1.62	114 ± 33.96 / 5.96 ± 1.77

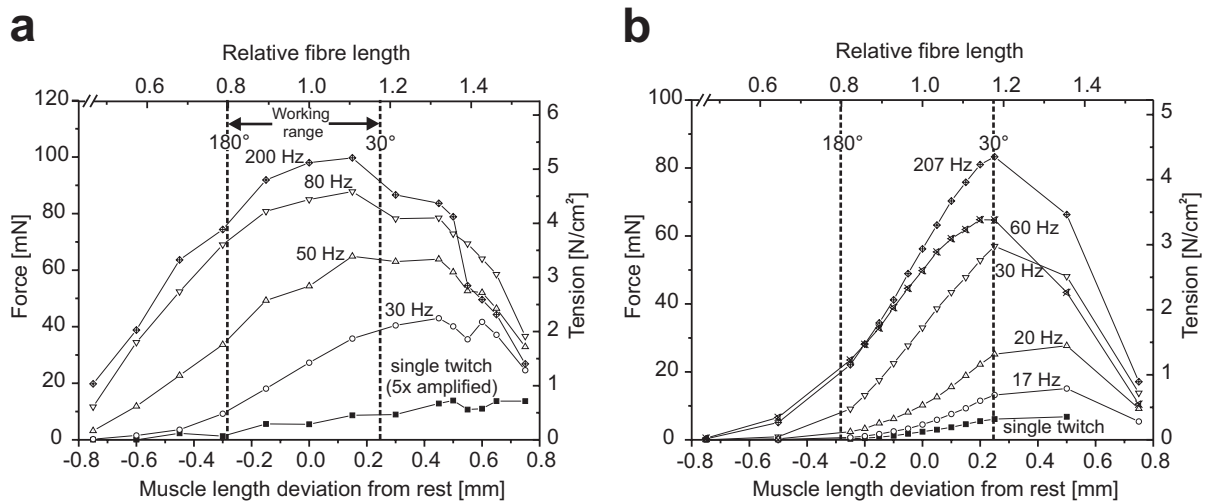


Figure C.24: Two extreme examples of extensor tibiae muscle single twitch and tetanical forces as a function of muscle stretch. With increasing stimulation frequency, the maximum force in (a) moves markedly towards shorter lengths while the shift in (b) is much less prominent. Axes are displayed like in Fig. C.23.

C3 Passive forces I

1 Stretch experiments

Stretching an unexcited muscle with a step-like displacement stimulus from its resting position leads immediately to a large force increase followed by a much slower force decrease as soon as the displacement stimulus has reached its final position. The response can be separated into a dynamic part with a subsequent decrease becoming by and by an approximate constant static part. Theoretically, following Maxwell's spring-dashpot model, the stretch of an infinite number of parallel elements leads to an infinitely large force increase. This can be avoided by stretching the muscle with moderately fast ramps: Fig. C.25 shows the dynamic part with the relaxation onset exemplified for an extensor tibiae muscle. Within the displayed time frame, the muscle has not yet reached an almost steady-state force value.

1.1 Visco-elastic properties I

The resting tension of a stretched muscle exhibits a phasic-tonic time course due to its visco-elastic properties (Fig. C.25; Bässler and Wegner (1983); Malamud (1989)). In response to a length step stimulus (i.e. an infinitely fast stretch against a velocity proportional friction), the muscle acts instantaneously like a spring. Hooke's law $F = d \cdot \Delta l$ describes this interrelation: the restoring force of a spring is proportional to the displacement of the force application point against the force direction. Due to the muscle being viscous at the same time, the dynamically generated force in response to such a step stimulus stretch becomes (theoretically) infinitely large because the

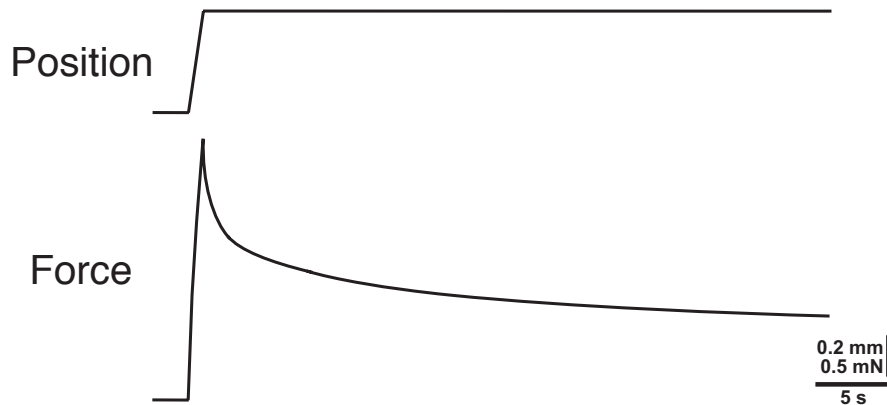


Figure C.25: *Passive force development of an unstimulated, denervated middle leg extensor tibiae. Time course of passive force induced by a ramp stretch of 0.5 mm amplitude in 1s. Note the dynamic nature of the force change and its subsequent relaxation at maintained stretch.*

mathematical term $P = C \cdot t^{-k} \rightarrow \infty$ if $t = 0$ (see Thorson and Biederman-Thorson (1974)). As soon as this instantaneous displacement ends, the muscle starts to flow, like a dashpot whose pistons are moving in oil. In contrast to this viscous muscle property, a pure spring would hold the force. Thus, such muscle properties can be described as “visco-” (like a liquid) “-elastic” (like a spring): the muscle is neither a real solid body, nor a real liquid. In contrast to a length step stimulus, the passive muscle response to a ramp stretch must be described with the term $P = C \cdot t^{1-k}$, it represents the integral of the length step stimulus response. As the displacement is not instantaneous, the flowing process is happening simultaneously with the stretch. Taking a closer look at such a phasic-tonic time course (Fig. C.26a) reveals two things:

First of all, log-log (double logarithmic) application shows that both increase and decrease are linear (***, $R=0.973$ for the increase fit and $R=-0.934$ for the decrease fit, Fig. C.26b). This means that the course of force development follows a power function characteristic. The muscle response increase follows the equation $P = C \cdot t^{1-k}$ and the decrease describes again a power function characteristic of the form $P = C \cdot t^{-k}$ after ~ 10 times the ramp duration. Thorson and Biedermann-Thorson (Thorson and Biederman-Thorson (1974)) showed that processes with a slowly decaying time constant can well be described with a power-function characteristic in general. The exponent k can be derived from conversion and gives the slope: $\log\left(\frac{P}{C}\right) = -k \cdot \log(t)$. The constant C defines the sensitivity in response to stretch and describes the stiffness of the system. Secondly, the exponents of increase and decrease are different: $k = -0.21$ for the increase and $k = 0.16$ for the decrease.

45 min recording after a large stretch shows that the force decrease is a continuous process that becomes persistently slower and slower but will eventually never stop (Fig. C.27a). Theoretically, the force should reach zero in infinity. There is no evidence for a non-zero asymptote - implying that the resting tension in the stretched muscle would eventually decay almost completely (from experiments on *Schistocerca americana*, Malamud (1989)). The powerfunction character of this force development becomes even more evident at log-log application on a long time axis (45 min), the linear decrease fit has an R value of 0.997 (***) . The fact that such a muscle would flow “forever” and that it never reaches steady-state force confirms the fact that the muscle is not a real solid body.

Another special property of the relaxation after stretch is the fact, that active muscle contraction does not affect the passive force time course (Fig. C.28). This suggests active force generation and developed muscle resting tension to be two processes that run in parallel.

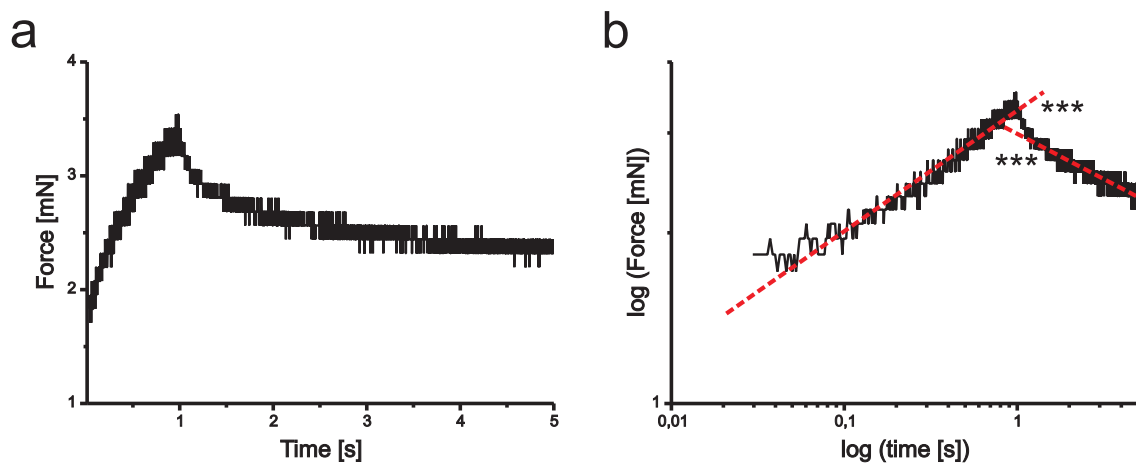


Figure C.26: Force time course of an extensor tibiae muscle with (a) double linear and (b) double logarithmic scaling during muscle stretch (1 s duration).

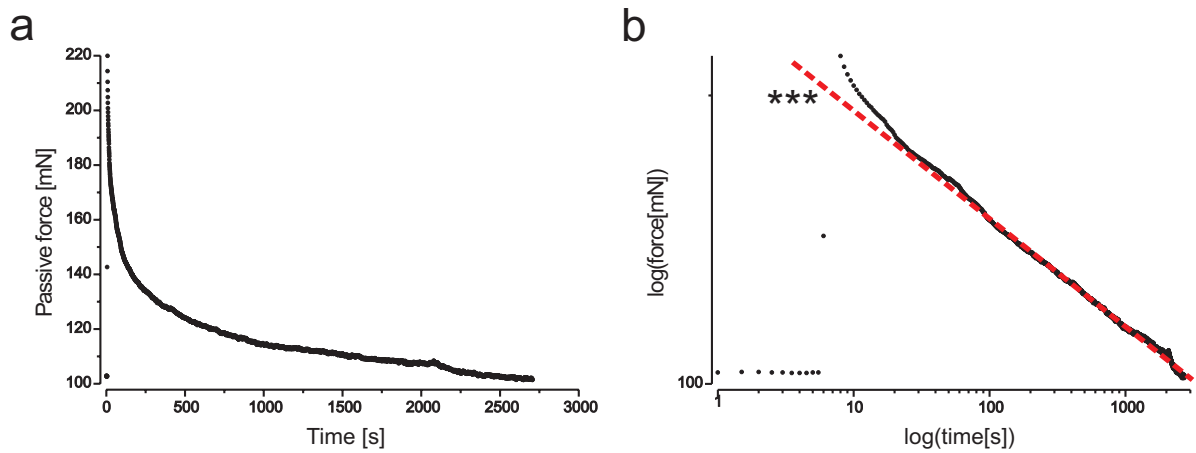


Figure C.27: Force time course of a flexor tibiae muscle with (a) double linear and (b) double logarithmic scaling during muscle stretch (1 s duration). The muscle had a prestretch of 0.7 mm relative to muscle resting length at 90° FT-joint angle.

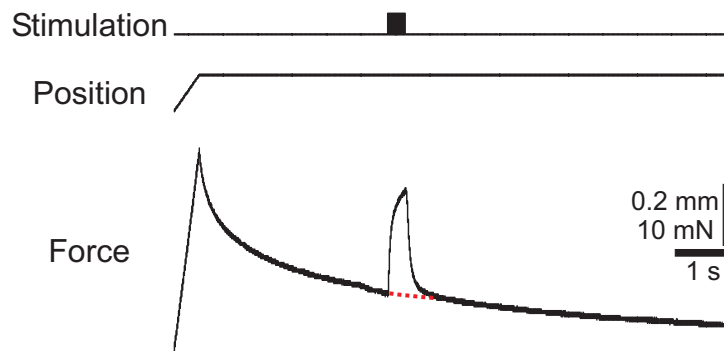


Figure C.28: Muscle stimulation during muscle relaxation a few seconds after a stretch. Passive force decreases despite of the occurrence of an isometric contraction in the same way than without. The dotted red line denotes intrapolated passive muscle force decrease without stimulation (see Figs. C.25, C.26 and C.27).

1.2 (Static) passive force-length relationship

The resting (passive) tension of the middle leg extensor tibiae muscle was measured by lengthening the muscle with linear ramps (described in ‘Materials and Methods’) beginning at its most relaxed state ((muscle length at 90°) - (0.75 mm)). Fig. C.29 illustrates the experimental procedure.

The phasic component amplitude of the response was defined to be the peak force induced by the stretch and, somewhat simplified, the tonic tension to be the force at which the rate of change of force was smaller than ~ 0.3 mN per minute. Both

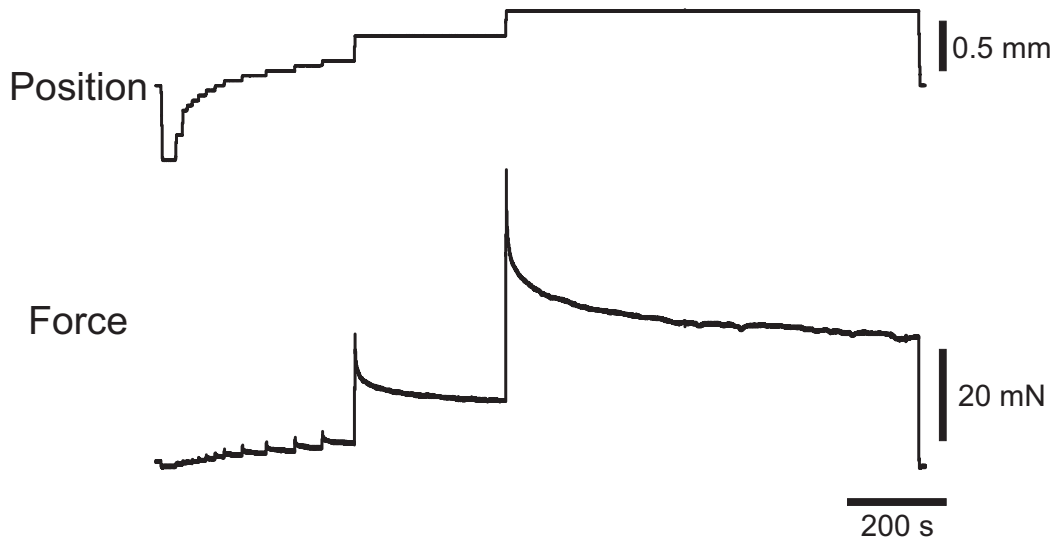


Figure C.29: *Passive force development of an exemplary unstimulated, denervated middle leg extensor tibiae in response to ramps starting at -0.75 mm and ending at +0.75 mm (0mm = rest length at 90°).*

phasic and tonic component amplitude increased with increasing muscle stretch (Fig. C.29). Fig. C.30 shows tonic force versus muscle length for ten extensor tibiae muscles (N=10) and shows that passive tension increases from 0 mN at -0.75 mm to about 30 mN at +0.75 mm (0 mm = resting length) in an exponential-like way (semi-logarithmic plotting results in a linear passive tension increase). When leaving the innervation of the extensor tibiae muscle via nerve *nl3* intact, passive tension was 2 mN higher as compared to the denervated situation (see Fig. C.30) throughout the muscle's working range (FT-joint angle between 30° and 180°, data not shown).

Passive tension was measured in both extensor and flexor tibiae of the middle leg in order to predict the equilibrium angle of the FT joint (Fig. C.31a). The range of angles where forces are about the same for both muscles (the intersection of the means) represents the predicted FT joint angle during rest. If the passive muscle forces were the main driving force for the passive tibia movement, FT joint rest angle should be around 65-80°. In Fig. C.31b, forces were expressed as muscle torques acting on the joint. This was done by taking the different moment arms (0.282 mm for the extensor and 0.564 mm for the flexor tibiae, see chapter C1) into account and by considering that the effectiveness of the moment arm is zero at 0° and 180° FT joint angle and is maximal at 90°. The intersection of the means is at around 55-65°, thus the FT joint rest angle that was predicted by plotting muscle **forces** shifts slightly towards a more

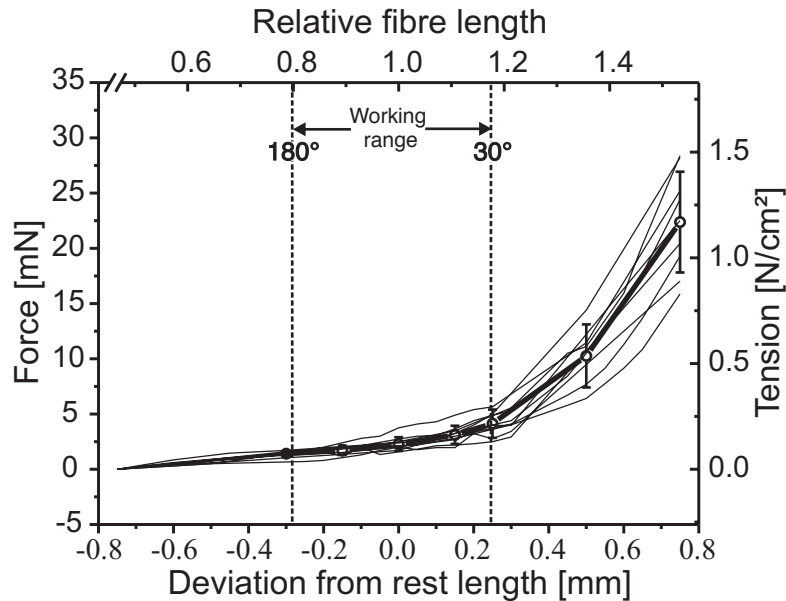


Figure C.30: Passive forces of the unstimulated, denervated middle leg extensor tibiae. Tonic resting force versus muscle length. Data from $N=10$ experiments (see text for details). Please note that the number for individual means can differ ($6 \leq N \leq 10$).

flexed position when doing calculations with the **torques** acting on the joint.

1.3 Dynamic passive forces

As described above, tibial muscle resting tension appears to be never in a real steady state. Swing phase duration in a free walking stick insect can become as fast as 0.1 to 0.12 s (Cruse (1985a), Büschges and Schmitz (1991); Büschges (1995b)). As the muscle acts like a spring in response to stretch, i.e. fast extension movements like a swing phase for instance, the dynamically achieved passive force e.g. of the flexor tibiae can become very large. Focussing on the FT joint, the swing phase in the stick insect middle leg is mainly determined by activity of the extensor tibiae (Fischer et al. (2001); Schmidt et al. (2001)). The passive force of the flexor tibiae is therefore the main movement opposing force considering the fact that the tibia mass is that light that its inertia does not really matter (tibia and tarsus: 3.3 ± 0.2 mg, $N=5$). Passive flexor tibiae force amplitude was therefore investigated with ramps simulating swing phase in amplitude and duration (Fig. C.32).

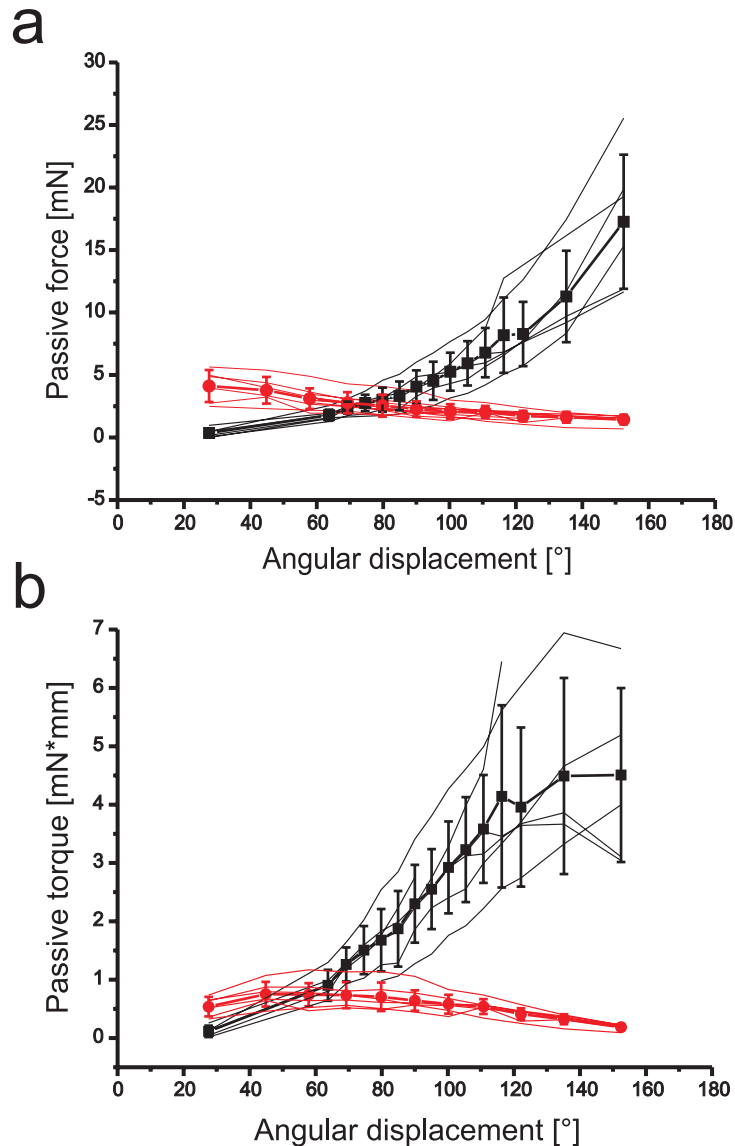


Figure C.31: Passive static denervated extensor (data shown in red, $N=10$) and flexor tibiae (data shown in black, $N=6$) forces (a) and torques (b) within the physiological working range (30° to 160°). Thin solid lines represent single measurements, bold lines the calculated mean \pm S.D. The torques were calculated using the effective moment arm lengths of extensor (0.282 mm) and flexor tibiae (0.564 mm) dependent on joint angle, i.e. being 100 % effective at 90° FT joint angle and 0 % effective at 0° and 180° FT joint angle.

From Cruse and Bartling (1995); v. Uckermann and Büschges (2008); Wendler (1977), maximal FT joint angle displacement during swing was estimated ($50 - 60^\circ$) and maximal resulting flexor tibiae muscle length change calculated (0.5 mm, considering a moment arm length of 0.564 mm, see chapter C1). As swing movements do not always start at the same FT joint angle, two different joint angles were taken as swing

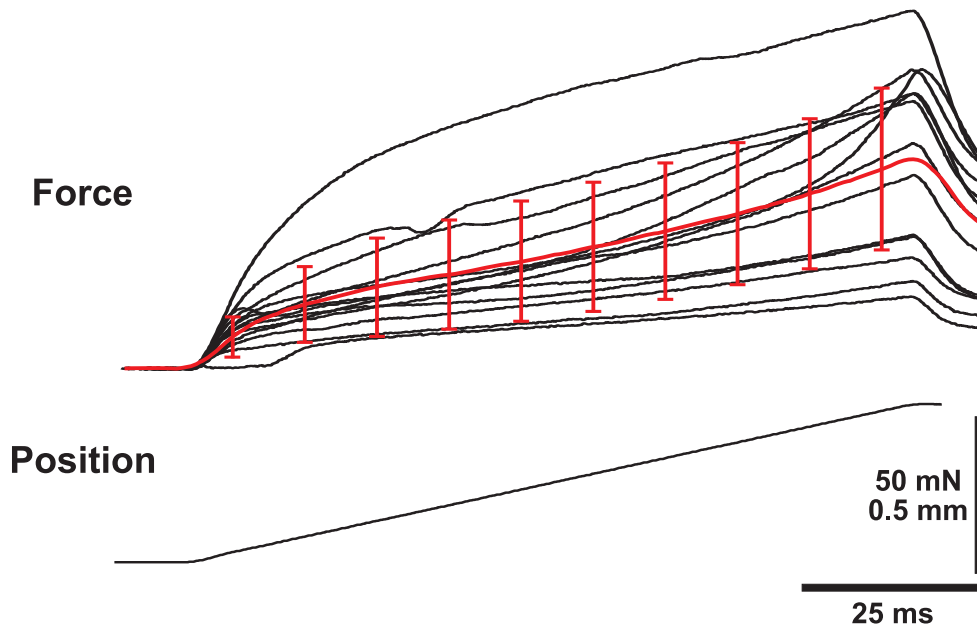


Figure C.32: Passive dynamic force in 13 flexor tibiae muscles in response to a muscle stretch mimicking swing phase tibia movement in duration and amplitude (0.5 mm in 0.1 s, $N=13$). Flexor tibiae muscle stretch started at 90° . Additionally, mean passive force \pm S.D. are displayed in red.

start: 90° and 60° . Resulting forces were 68.56 ± 27.92 mN when starting at 90° ($N=13$) and 40.37 ± 14.09 mN when starting at 60° ($N=9$), see Fig. C.33a. An unpaired t-test showed that the values were significantly different (*, $p < 0.02$). In addition, passive extensor tibiae force was measured in few animals for comparison. Interestingly, resulting forces when starting at 90° with the same ramps than applied for the flexor tibiae were 64.02 ± 12.22 mN ($N=5$) and were statistically not different (-, $P \geq 0.05$) from flexor tibiae forces starting at the same angle (Fig. C.33b).

Passively generated flexor tibiae force was further investigated with ramps of the same duration (0.1 s), but different amplitude (Fig. C.34). In two experiments performed, passive muscle force increased almost linear in one case and almost exponential in the other. More ramp amplitudes in more animals would have to be made in order to draw a clear conclusion.

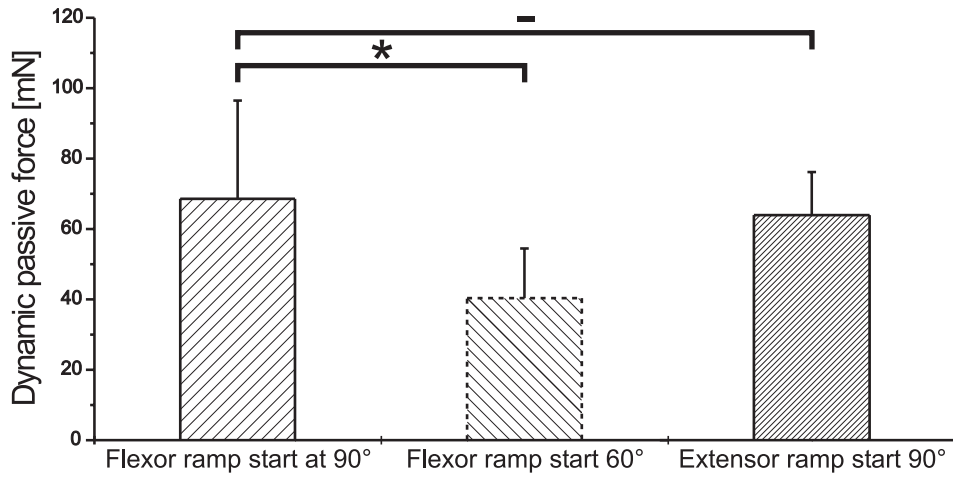


Figure C.33: *Passive dynamic flexor and extensor tibiae forces in response to muscle stretch. Flexor tibiae force development in response to ramps starting at 90° FT joint angle (N=13) is significantly different from forces in response to ramps starting at 60°, N=9 (*, $p < 0.02$). Flexor (N=13, see above) and extensor tibiae force (N=5) in response to ramps starting at 90° are statistically not different from one another (-, $p \geq 0.05$). Mean values are shown \pm S.D.*

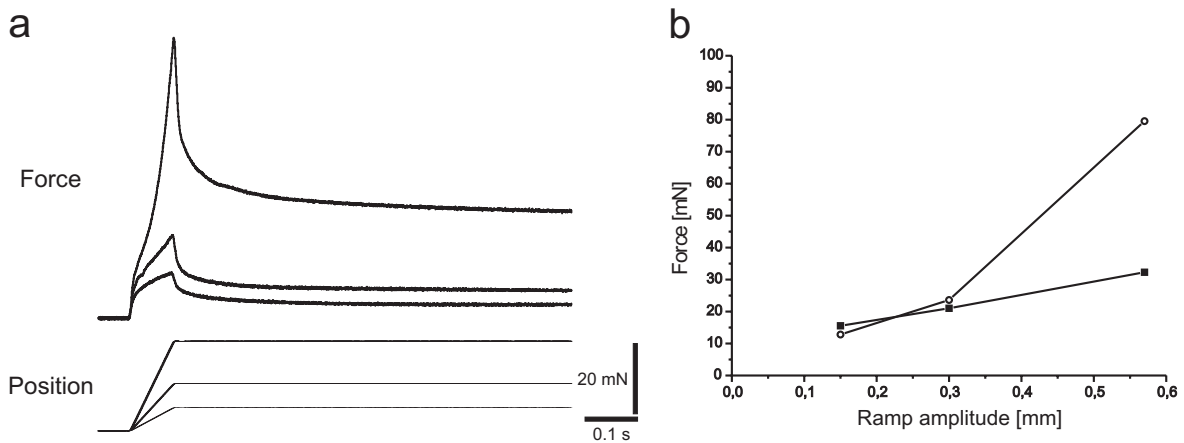


Figure C.34: *(a) Passive dynamic flexor tibiae force in response to different muscle stretch amplitudes: 0.15, 0.3, 0.57 mm (N=2, represented by two different symbols). Ramp duration was 0.1 s throughout. (b) In these exemplary experiments, the relationship between maximally dynamically reached forces and the ramp stretch amplitude is either linear or exponential-like.*

2 Significance for tibial movements

The predicted range of equilibrium FT joint angles shown in Fig. C.31 suggests passive forces to be the crucial actuators determining tibia position during inactivity of extensor and flexor tibiae. Photographed tibia displacement with successive muscle ablation of a cut leg should test that to be true or not.

After either tibia extension or tibia flexion of a cut leg with both muscles intact in one exemplary animal (N=1), the tibia returns to nearly 90° with a tendency towards slight flexion ($89 \pm 1^\circ$ after extension, $76 \pm 1^\circ$ after flexion, Fig. C.35a). Ablation of the flexor tibiae does solely alter the tibia position after previous extension, only little after previous flexion ($156 \pm 13^\circ$ after extension, $87 \pm 5^\circ$ after flexion, Fig.C.35b). After ablation of both muscles, the tibia moved only little from the position where it was put at ($141 \pm 7^\circ$ after extension, $53 \pm 5^\circ$ after flexion, Fig.C.35c). Rotating the joint (so that gravitational force would matter) did not affect the measured angles. The static passive forces shown in Figs. C.30 and C.31 are larger than the 0.03 mN force of gravity on the mass of tibia and tarsus (3.3 ± 0.2 mg, N=5; see above).

Locusts are known to store large forces in elastic distortions of the tendons and the femoral cuticle when large forces are generated in femoral muscles, e.g. in prepa-

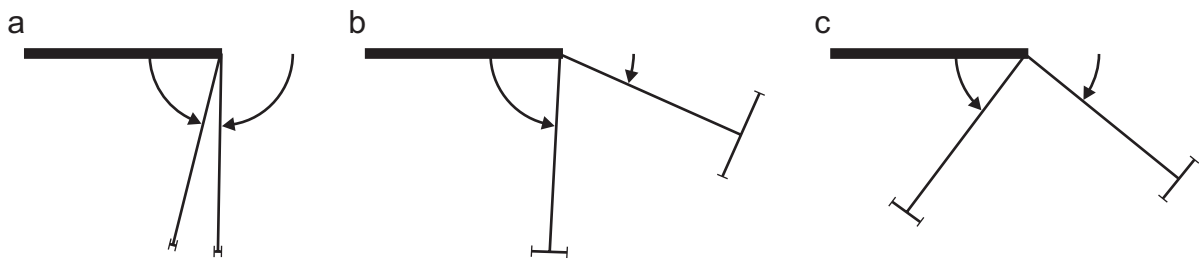


Figure C.35: Mean tibia positions \pm S.D. in one exemplary animal (N=1) with intact muscles (a), the flexor tibiae tendon cut (b), both extensor and flexor tibiae tendon cut (c). The bold line represents the femur, the thinner line represents the tibia. Arrows mark previous tibial extension (to 180° , n=5 in every experiment) or flexion (to 30° , n=5 in every experiment).

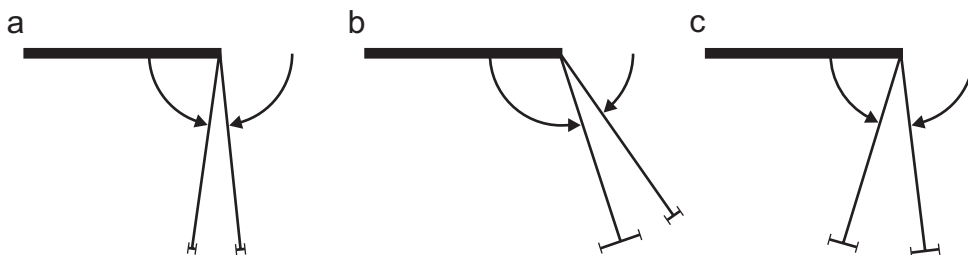


Figure C.36: Mean tibia positions \pm S.D. in one exemplary animal (N=1) with intact joint tissues (a), the outer (extensor tibiae) FT joint tissue ablated (b), both inner (flexor tibiae) and outer (extensor tibiae) FT joint tissues ablated (c). Arrows mark previous tibial extension (to 180° , n=5 in every experiment) or flexion (to 30° , n=5 in every experiment).

ration to jumping and kicking, with the dorsal distal femur cuticle being crumpled (Sasaki and Burrows (2003)). Thus, similar to investigating the relevance of passive muscular input, successive ablation of extensor and flexor femoral FT joint cuticles should examine their relevance for tibia rest position after previous extension and flexion in one exemplary animal (N=1). Tibia return positions after previous extension and flexion (Fig. C.36a) are very similar to the ones shown in Fig. C.35a), both tibia return positions are slightly shifted towards more extension in this example ($96 \pm 1^\circ$ after extension, $82 \pm 1^\circ$ after flexion). Ablation of the extensor tibiae joint cuticle (tendon still intact) shifts return angles after both extension and flexion towards larger FT joint angles ($125 \pm 2^\circ$ after extension, $108 \pm 6^\circ$ after flexion, Fig.C.36b). Ablation of both joint cuticles leads to rather similar tibia return positions to the situation when joint cuticles were intact ($97 \pm 4^\circ$ with previous extension and $73 \pm 4^\circ$ with previous flexion, Fig.C.36c).

The two presented series of experiments serve as examples. Tibial positioning after extension and flexion in intact legs was evaluated in two animals (see above), another five animals (altogether N=7, in every experiment n=5 for extension and flexion respectively) showed very similar results: almost 90° after previous extension and slightly flexed after previous flexion.

3 FT-joint torques

Movement of a limb is determined by active agonistic and simultaneously occurring passive antagonistic forces. As described in section 2 of this chapter, the tibia is that light that gravity forces and inertia do not really matter. Passive forces appear to become movement determinant the smaller the animal (Hooper et al. (2009)) and legs of arthropods such a locusts and spiders have been shown to be highly resilient, storing and returning as much as 90% of the energy invested to deflect them (Dudek and Full (2006); Bennet-Clark (1975); Katz and Gosline (1994); Blickhan (1986); Sensenig and Shultz (2003)). Thus, FT-joint torques were investigated with a special lever arm mounted on the Aurora's servo motor (see 'Materials and Methods'). In order to do so, the tibia was deflected either starting from the 90° FT joint angle position with fast ramps of different amplitude (0.2° to 3.8°) or it was first moved to the desired angle (82° to 98°) and then deflected with ramps of the same amplitude (0.2°). Fig. C.37a

shows the general measurement procedure of displacing the tibia with a ramp step. Fig. C.37b shows deflection from 89.7° to 90.3° (**(b(i))**) and from 90.3° to 89.7° (**(b(ii))**). Deflection from 88.1° to 91.9° is depicted in (**(c(i))**) and from 91.9° to 88.1° in (**(c(ii))**). Specialisation of the lever arm designed for the investigation of joint torques would have required a new tuning of the Aurora control device, especially in respect to inertia compensation as this was done with the usually used lever arm shown in 'Materials and Methods', Fig. B.7. This led to the decision to conduct additional torque measurements with the same stimulation paradigm as with no tibia attached, just the measuring device alone. This control measurement (red trace in Fig. C.37b(i) to c(ii)) was subtracted from the regular measurement with the tibia attached (green trace) which results in the black trace. The initial overshoot in response to the displacement step proves to be an artefact, most likely because the Aurora tuning has not been adapted to the specialised lever arm. What remains after subtraction is a constant force elevation with a small initial oscillation when step-ramping in one direction (tibia extension, arrow up in **(a)**) and force decrease when step-ramping in the other (tibia flexion, arrow down in **(a)**). The difference between torques measured at tibia extension and torques measured at tibia flexion represents the joint stiffness at a given deflection.

In a first approach, it was tested whether joint torque was dependent on FT joint angle. The tibia was moved to various joint angles and 0.2° step ramps were applied. Fig. C.38a shows joint torques where the device torque alone was not subtracted (N=7, n=55). Device torques alone are displayed as big closed symbols connected with a bold line (N=1, n=17 in total i.e. including all angles). At 90°, several measurements were done before and after tibia extension and flexion (see indicated standard deviations in **(a)**). **(b)** shows resulting joint torques, calculated from subtraction of the device torques. As no visibly detectable trend was identifiable, means of all measurements were taken and t-tested with control measurements of the device, shown in **(c)**. The measurements are highly significant different from one another (***) , so it was reasonable to calculate the mean joint torque (device torque alone subtracted). It was tested whether torque measurements changed linearly with tibia extension and flexion. In order to do so, torque responses to tibia flexions were plotted as if the deflection stimulus were an extension (e.g. a torque measurement at 86° was plotted at 94°, **(d)**). Linear regression indicates the increase slope to be barely significant with a

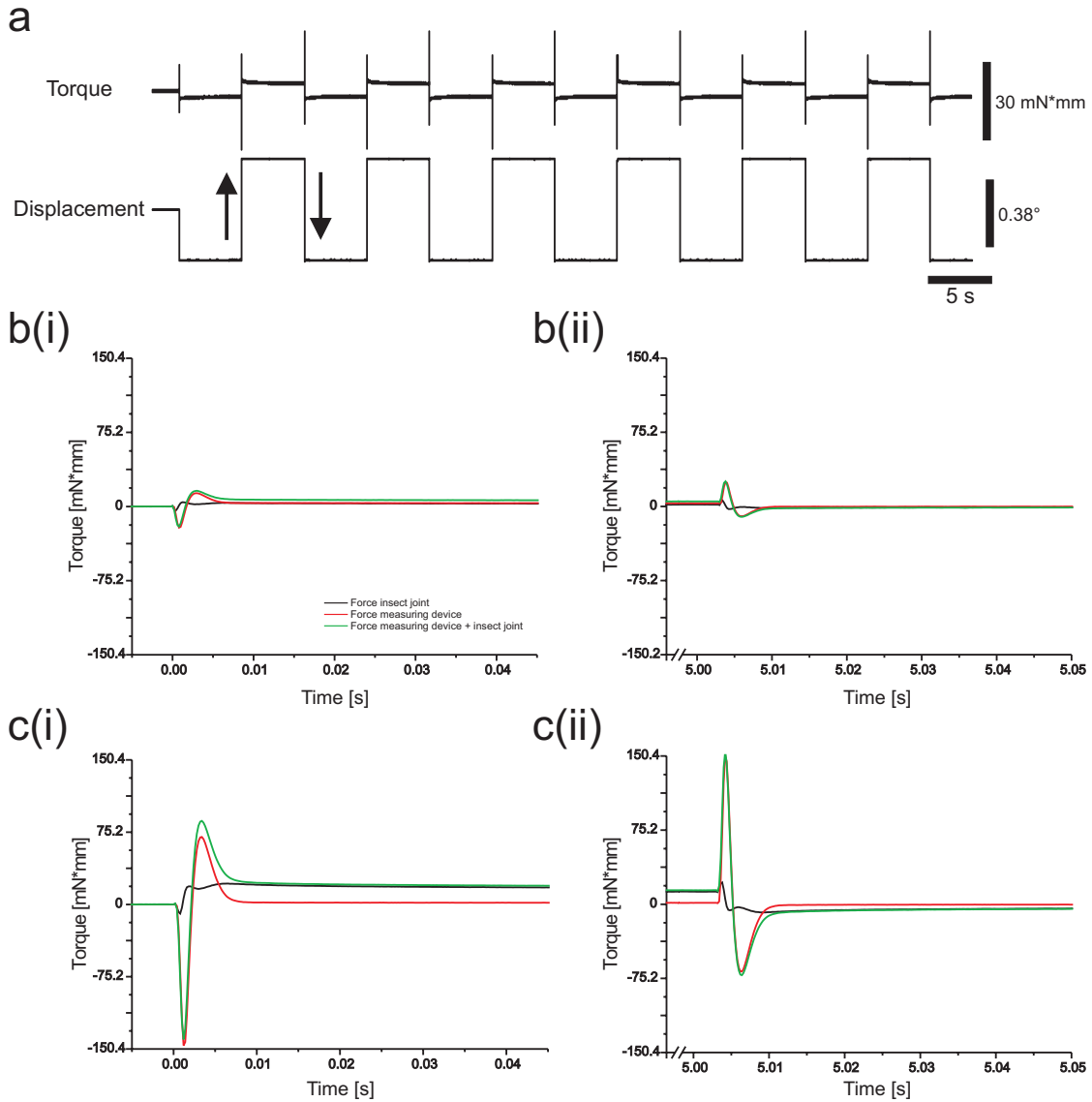


Figure C.37: Exemplary FT-joint torque in response to angular displacement (a), the measuring device's lever arm length of 4.75 mm is taken into account. Tibia deflection from 89.7° to 90.3° (b(i)) and from 88.1° to 91.9° (c(i)) and back (b(ii)) and c(ii)). Displacement trace not shown. Green trace: measurement of joint torque including torques arising from the measuring device; red trace: measurement of the device only; black trace: red trace subtracted from green trace, i.e. calculated joint torques.

small R-value (*, $0.04 \leq p < 0.05$, $R = 0.32$). Thus, within the range of angles tested, joint torques have a weak trend to increase with the tibia being either more extended or more flexed compared to torque at 90° with a slope of $0.011 \frac{mN \cdot mm}{deg}$. In spite of this weak trend, the mean joint torque was measured ($0.068 \pm 0.057 mN \cdot mm$). The data are very scattered, as indicated by the large S.D. and the low R-value (see above).

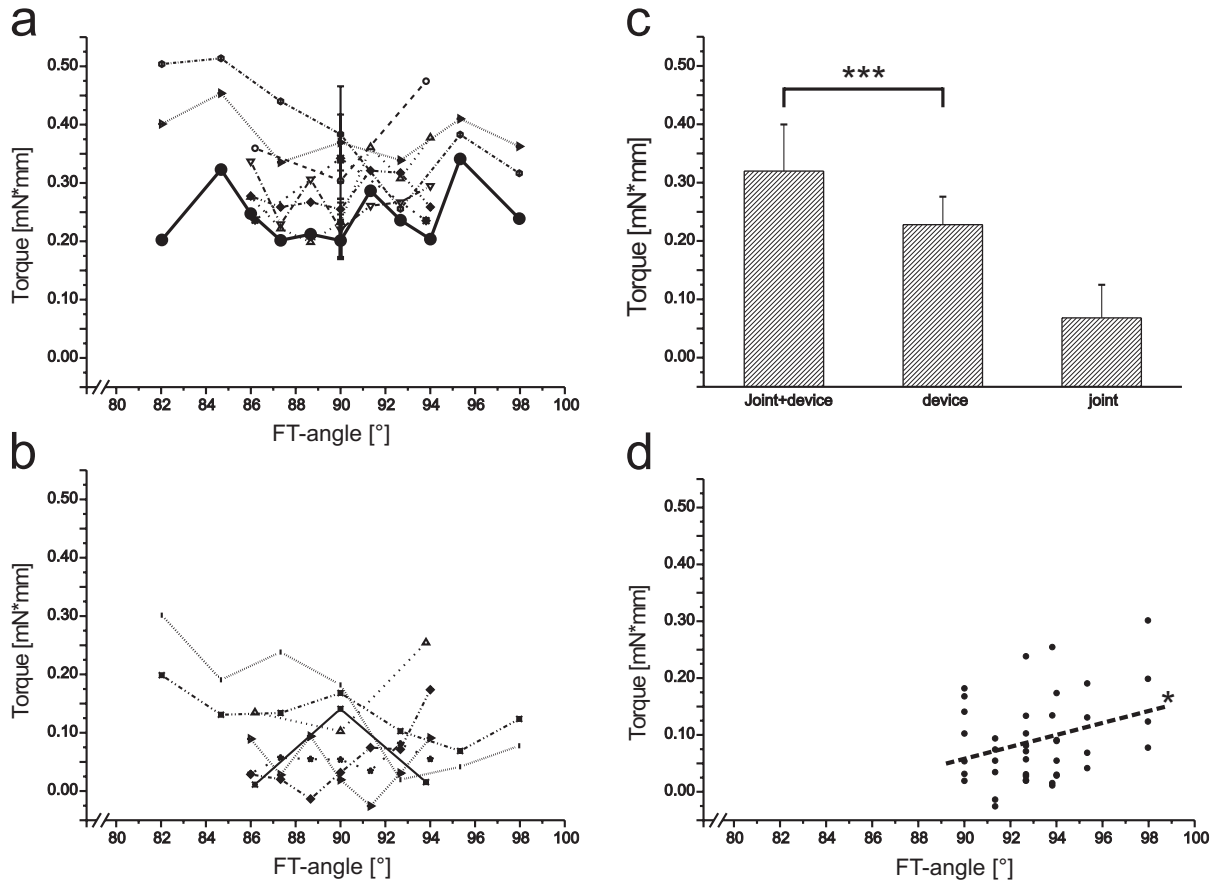


Figure C.38: FT-joint torque in response to 0.2° deflection measured at different joint angles. **(a)** Joint torques, where device torques alone are not subtracted (small symbols, thin lines; $N=7$, $n=55$) and device torques alone (big closed circles, bold lines; $N=1$, $n=17$ in total i.e. including all angles). **(b)** Calculated joint torques from subtraction of device torques alone. **(c)** Mean values of joint torque, where device torque alone is not subtracted (first column), joint torque alone (second column) and calculated joint torque, without device torque alone (third column). An unpaired t -test reveals joint torque, where device torque alone is not subtracted and device torque alone to be highly significantly different (***). **(d)** When torque responses to tibia flexions were plotted as if the deflection stimulus were an extension (see text), joint torque in response to 0.2° deflection increases significantly (*, $p \leq 0.04$).

In the next step, it was tested whether joint torque was dependent on deflection amplitude. The tibia was moved in fast ramps of different amplitude and speed (0.2° to 3.8° ramps in 0.2 ms). As described in the displacement trace in Fig. C.37a, the tibia was deflected in both directions from 90° . Fig. C.39a shows this deflection from 90° : the larger the angular displacement, the larger the torque generation relative to 90° ($0.5 \frac{mN \cdot mm}{deg}$). In C.39b, the absolute torque generation is plotted vs. the relative angular displacement, i.e. the difference between tibia extension and tibia flexion angle. Again, torques measured with the device alone are shown as big closed symbols

connected with a bold line.

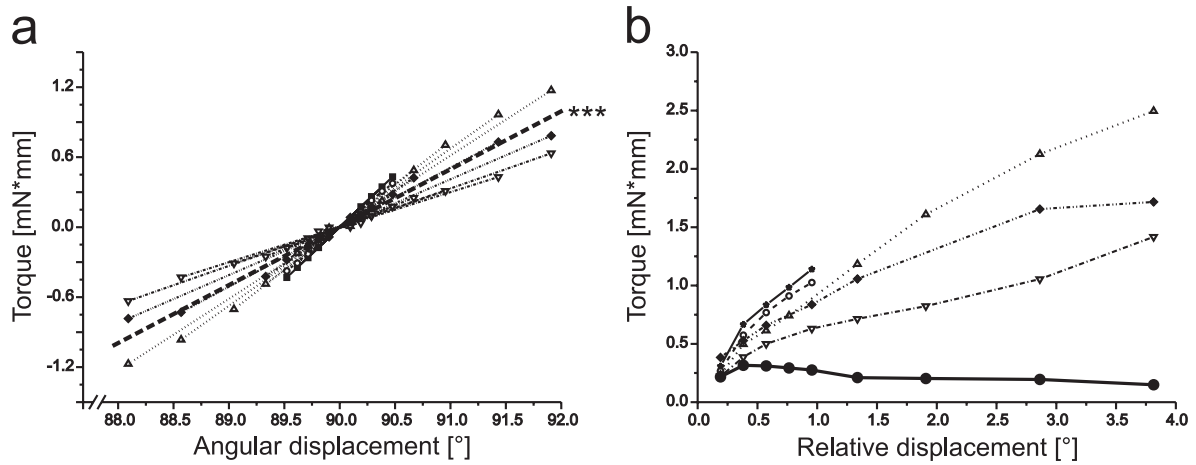


Figure C.39: FT joint torque vs. absolute and relative angular displacement. (a) shows the calculated torque generation (with the subtracted device torque) as function of the absolute angular displacement. Linear regression is depicted as bold dashed line ($0.5 \frac{\text{mN}\cdot\text{mm}}{\text{deg}}$, ***, $R = 0.951$). (b) shows torque generation including measuring device torques (all symbols except for big filled circles; $N=5$, $n=33$). Torques measured with the device alone are depicted as big filled circles, connected with a bold line ($N=1$, $n=7$).

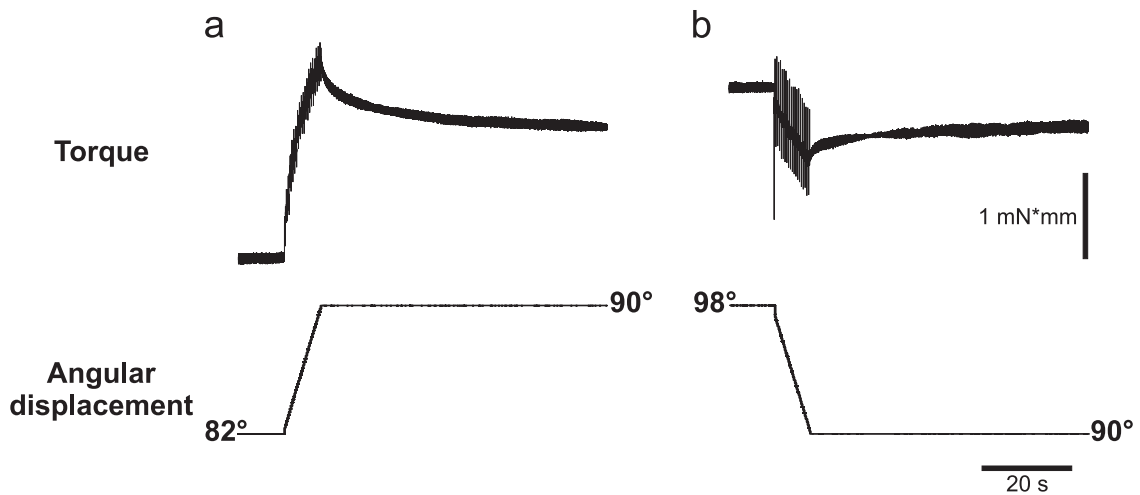


Figure C.40: Viscoelasticity of the FT joint. Tibial angular displacement causes a joint torque increase (a) / decrease (b) as long as the ramp lasts. Joint torque starts to decrease (a) / increase (b) as soon as the displacement ends.

To summarise, the FT joint features no clear spring properties because the same displacement conducted at different joint angles shows hardly a trend. Nevertheless,

there is a dynamic force component because the joint responds with an increase in force the faster the tibial displacement, it acts like an attenuator (Fig. C.40 **a** and **b**). As described above (section 1.1), tibial muscles feature visco-elastic properties and so does the FT joint. Interestingly, the net dynamically generated torque development at tibia extension (**a**) is larger than at tibia flexion (**b**).

C4 Force measurements in the isotonic domain

1 Muscle contractions in response to physiological stimulation

Investigation of muscle properties using tonic stimulation input is important to measure characteristics like twitch kinetics or the active force length curve demonstrated in chapter C2, because it is in most cases advantageous to have control upon the input parameters. However, when measuring muscular output, it is also essential to know the mechanisms allowing the animal to transform motoneuronal input into muscle contractions. Hooper et al. (Hooper et al. (2006; 2007a;b)) found several mechanisms, a few are presented here.

As described in 'Materials and Methods', contractions from five animals in response to 87 stimulation regimes of extensor tibiae motoneurons collected from a single leg preparation were investigated. Fig. C.41a shows FETi motoneuron action potential count for each performed step-like movement. Mean spike number was 44.2 ± 20.0 per step-like movement (**a**). Distribution of step-like movements vs. spike number was Gaussian-like (fit not shown) with the peak at the mean (**b**). Most steps had spike numbers ranging from 20 to 60 spikes.

Mean burst duration was 0.41 ± 0.24 s per step-like movement (Fig. C.42a). Very similar to Fig.C.41, distribution of step-like movements was Gaussian-like with a maxi-

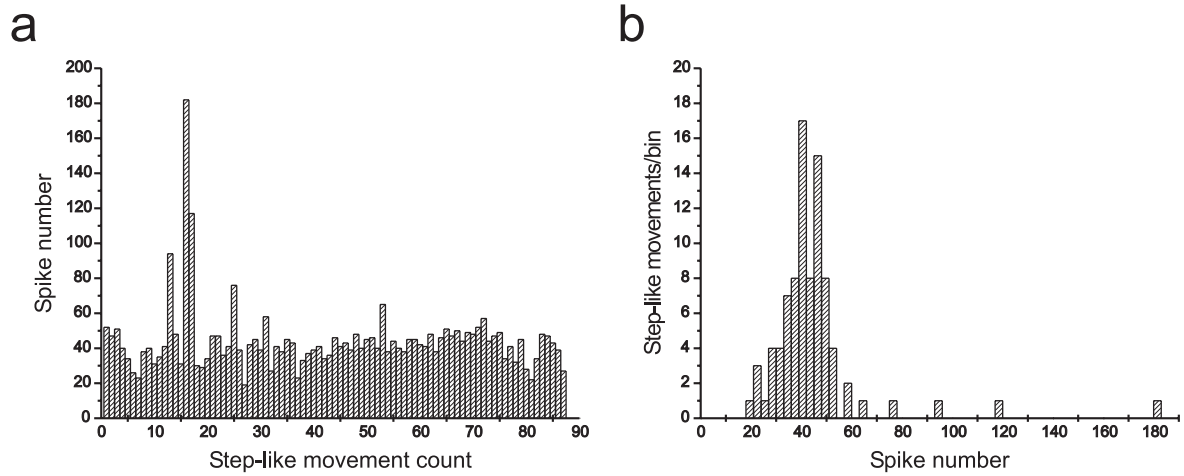


Figure C.41: FETi motoneuron spike numbers while performing step-like movements on the treadmill ($N=1$, $n=87$). Spike number per step-like movement shown in chronological order within the recording experiment (a) and distribution of step-like movements/bin vs. spike number (b, bin width = 3 spikes).

around the mean (Fig. C.42b; fit not shown). A few step-like movements had burst durations > 1 s.

Mean interburst interval, i.e. stance phase duration, was 2.30 ± 3.58 s including all step-like movements ($n=87$, Fig. C.43a). According to Hooper et al. (Hooper et al. (2006)), step-like movements with interburst interval durations > 2 s were not taken into account for calculations of the mean which becomes therefore much shorter: 0.77

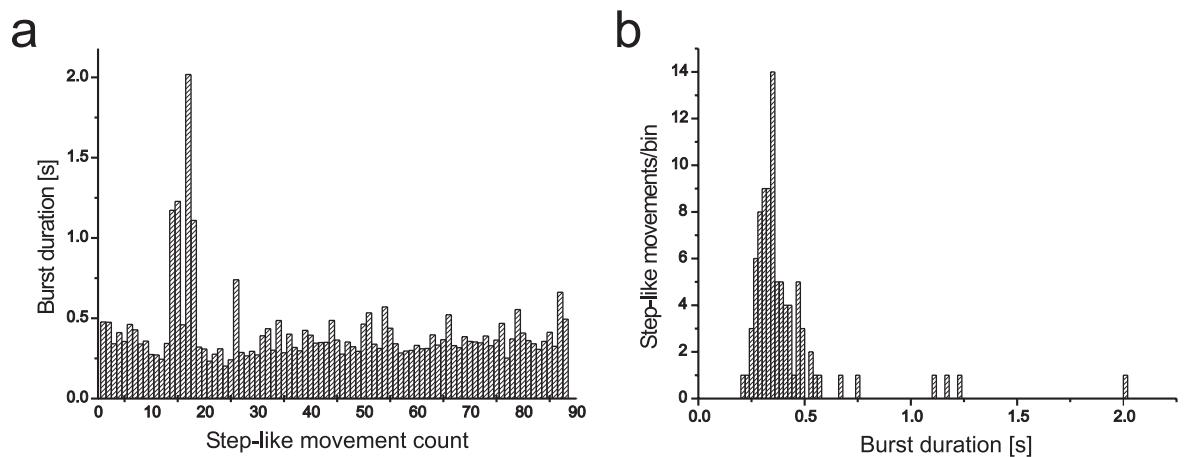


Figure C.42: FETi motoneuron burst duration during step-like movements on the treadmill ($n=87$). Burst duration per step-like movement shown in chronological order within the recording experiment (a) and distribution of step-like movements/bin (b, bin width = 0.02 s).

± 0.39 s ($n=65$). This selection was conducted to make sure that only interburst intervals within a robust walking sequence of about 1 s (Hooper et al. (2006)) were taken. It was arbitrarily chosen that the animal was very probably quiescent at interburst intervals > 2 s. Distribution is much more scattered than for spike count and burst duration, but has also a very distinct maximum around the mean showing the majority of intervals having a duration < 3 s (Fig. C.43b).

Fig. C.44 shows contractions of five extensor tibiae muscles in response to two exemplary, randomly picked stimulation patterns from physiological step-like movements. The individual contractions respond in a similar way and have the same triangular shape. Contraction velocities (the slope of the position signals) and amplitudes are less consistent between animals.

Contraction shape can vary a lot in response to physiological stimulation with patterns from locomotory movements. The observed contraction shapes found (Fig. C.45) include: trapezoidal-like shape (a), triangular-like shape (b), multi-slope decay (c), (d) and multi-slope increase (e). This figure as well as the following figures show data from one animal ($N=1$, picked randomly) for the sake of phenomenon description, as experiments from five animals ($N=5$) were consistent.

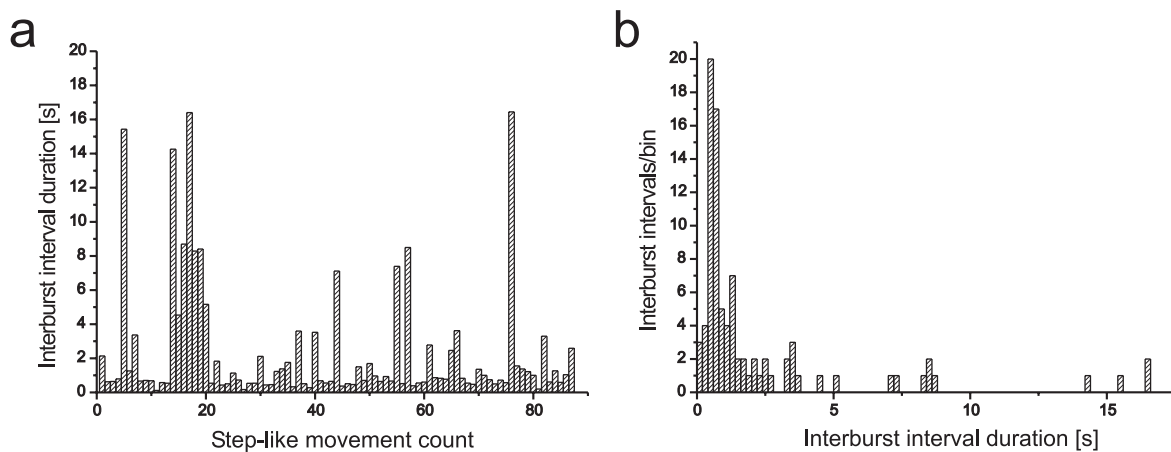


Figure C.43: *FETi* motoneuron interburst interval duration during step-like movements on the treadmill ($n=87$). Interburst interval duration per step-like movement shown in chronological order within the recording experiment (a) and distribution of step-like movements/bin (b, bin width = 0.2 s).

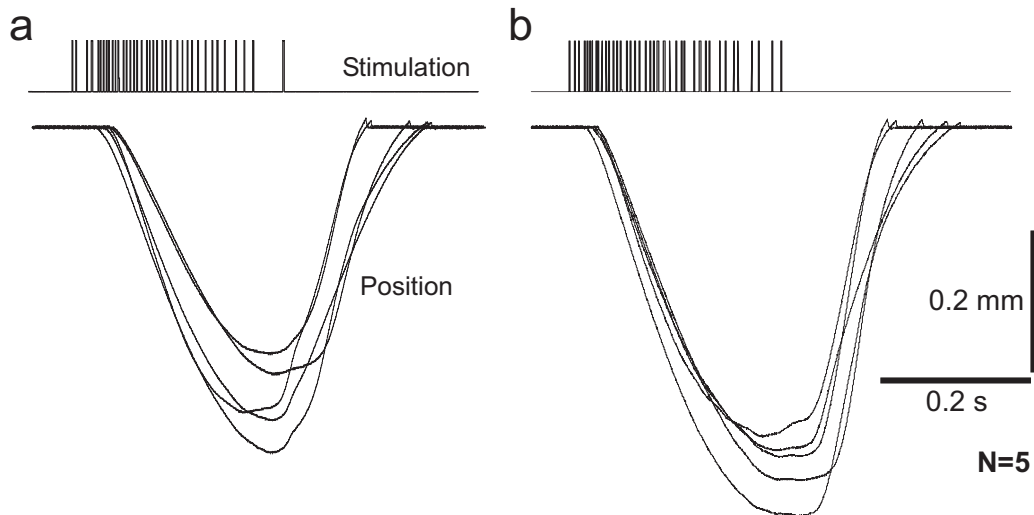


Figure C.44: Overlay of isotonic contractions of extensors tibiae in response to physiological stimulation representing two randomly picked step-like movements (**a** and **b**, $N=5$). Contraction movement delay arises from muscle force being initially weaker than Aurora lever arm load (min. 3.05 mN, max. 15.72 mN).

Visual inspection of physiologically evoked contractions (Figs. C.44 and C.45) suggests that the muscle acts like a lowpass filter: contraction shapes look very smooth even though most spike patterns are rather ragged (Hooper et al. (2006; 2007a)). This raggedness becomes even clearer when the instantaneous frequency of the physiological stimulation is additionally depicted (Fig. C.46). The three contractions shown are very similar in their contraction amplitude and shape, although their stimulation patterns look rather different and very ragged in terms of the spikes' instantaneous frequency patterns.

Fig. C.47 shows the stimulation (upper trace), the stimulation smoothed with a time constant of 0.07 s (like Borgmann et al. (2007)) in the middle trace and the isotonic muscle contraction in the lower trace, in this case inverted, i.e. muscle shortening is shown as a positive deflection for better comparison. The apparent similarity between the smoothed stimulation trace and the inverted position in examples (**a**) to (**c**) demonstrates the lowpass filter properties of the extensor tibiae: smoothed stimulation is reproduced in shape and amplitude in the position trace. Especially Fig. C.47c shows that the relative amplitudes between individual stimulations of the smoothed stimulation trace match the relative position amplitudes.

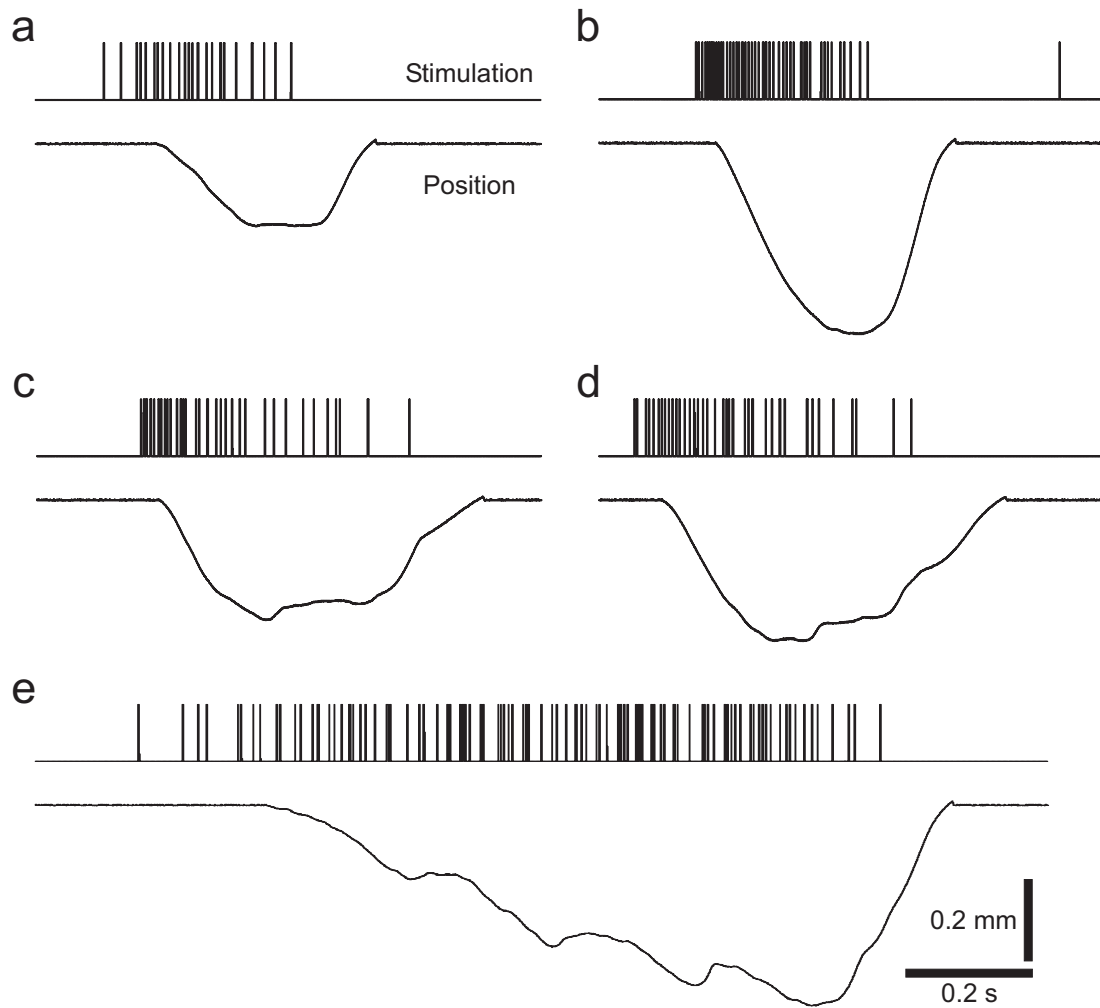


Figure C.45: *a-e*: Various shapes of contractions in response to physiological stimulation. See text for details.

To quantify this match, the integral of randomly picked contractions was calculated and plotted vs. the integral of the smoothed physiological stimulation patterns (Fig. C.48, $n=63$ from five animals, $N=5$). Linear regression fitting the data (all fits ***; minimal R value=0.914, maximal R value=0.992) confirms the visual similarity between contraction and smoothed stimulation shown in Fig. (a) to (c). This is in good agreement with the analysis of these experiments, which was carried out by Hooper and colleagues (Hooper et al. (2007a)). They demonstrated that the extensor tibiae acts like a slow filter on the time scale of burst interspike intervals (5-10 ms).

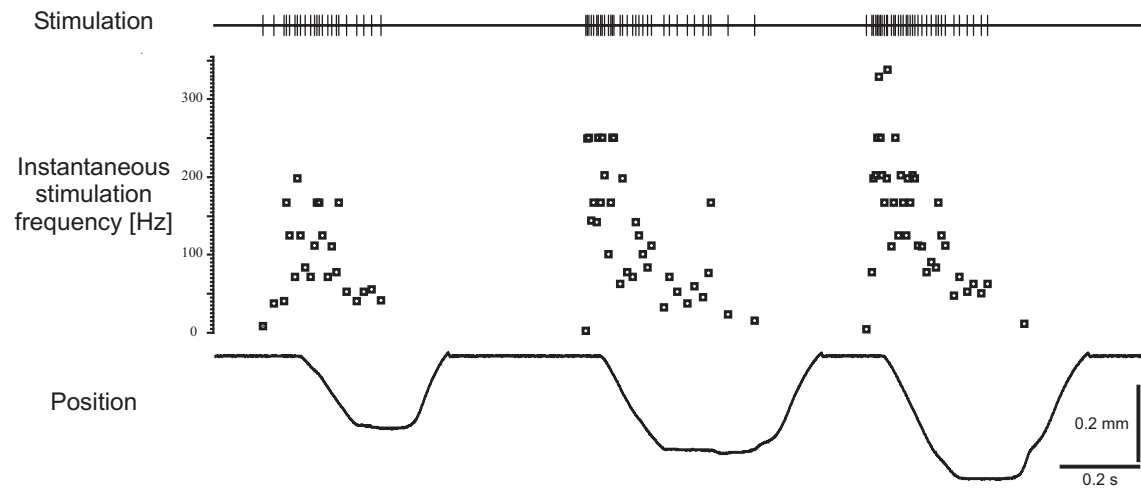


Figure C.46: *Stimulation (upper trace), stimulation's instantaneous frequency (middle trace) and resulting contraction (lower trace). Illustrated are three randomly picked contractions showing similar contraction shape and amplitude.*

2 Loaded release experiments in response to tonical stimulation: the force-velocity relationship

Chapters C2 and C3 deal with muscle activity under isometric steady state conditions. However in physiological situations, a muscle has to work steadily under changing load and changing length conditions. It is thus essential to describe the muscle's dynamic properties, in order to understand its biological functions and to build predictive muscle models (Zajac (1989); Ekeberg (2002); Ekeberg et al. (2004)). Loaded-release experiments are particularly useful for measuring these dynamic characteristics. In these experiments, a muscle is stimulated tonically to reach steady-state contraction under isometric conditions and then allowed to shorten under isotonic conditions against a variety of counter force levels. Typically, such an investigation aims for getting the relationship between a muscle's force and contraction velocity at a particular stimulation paradigm, first described by A.V. Hill (Hill (1938)). Fig. C.49a shows an example of the experimental paradigm. The activated muscle responds to the switch to isotonic conditions (arrow in Fig. C.49b, which represents the enlargement of the data within the bracket 'b' on the top of Fig. C.49a) in two distinct phases: an abrupt initial shortening ('I' in Fig. C.49b), followed by a subsequent smooth length change, representing the actual active contraction ('II' in Fig. C.49b). The first response is due to the series elastic properties of the muscle (Jewell and Wilkie

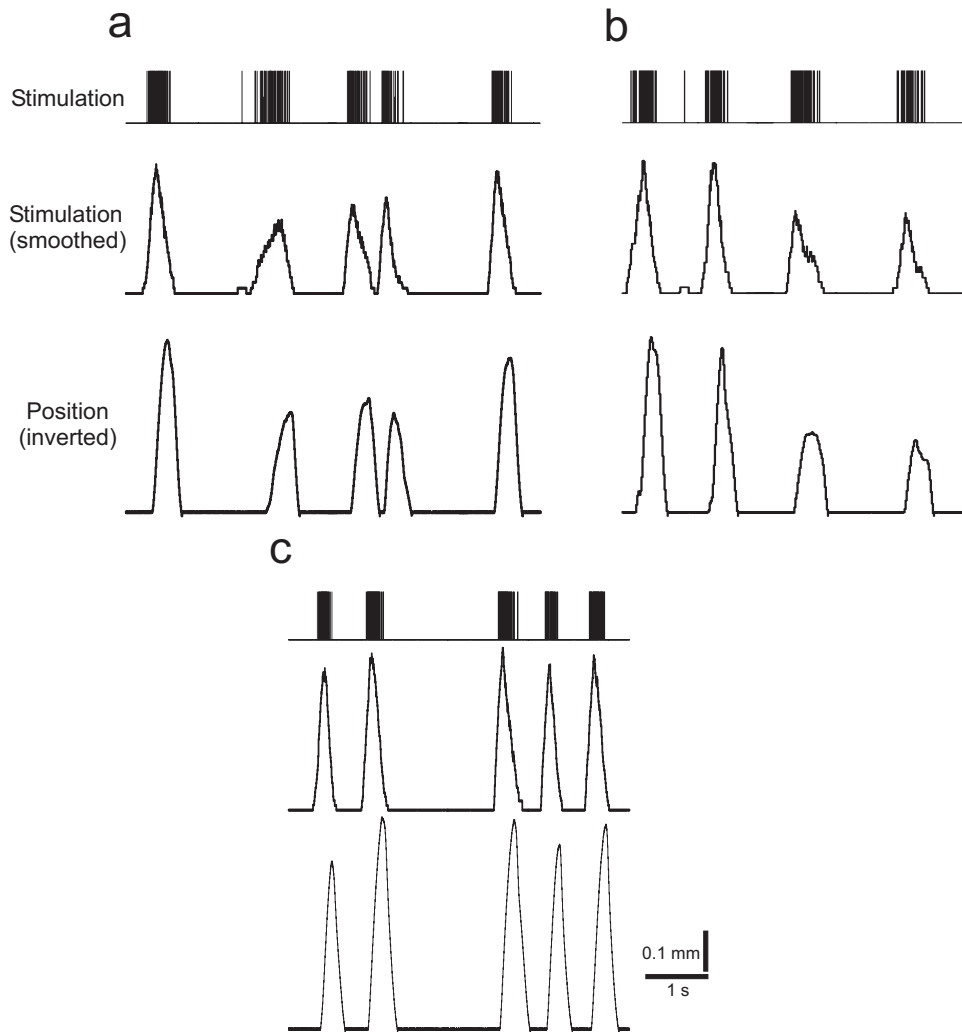


Figure C.47: *a-c* Physiological extensor tibiae stimulation (*a* previous *nl3* recording from an animal performing step-like movements on a treadmill) untreated (upper trace) and smoothed (middle trace) and the resulting muscle contraction (lower trace) in one exemplary animal ($N=1$). The time constant of the smoothing was 0.07 s (Borgmann et al. (2007)). The contraction delay comes from the fact that the muscle first had to overcome a counterforce of 9.52 mN (see text for details).

(1958)), and will be dealt on in the *Results* chapter C5. The subsequent slow contraction, which is initially accompanied by some oscillations (White and Thorson (1975); Edman (1988); Edman and Curtin (2001); Siebert and Blickhan (2003)) is characterised by an almost linear initial time course followed by a late, saturating approach to its final length. The velocity of the linear phases of the contraction represents the maximum contraction velocity of the muscle for a given activation and load level (see the different traces in Fig. C.49a). A time span of 50 ms immediately after the end of the oscillations was chosen to be representative for calculating maximum contraction ve-

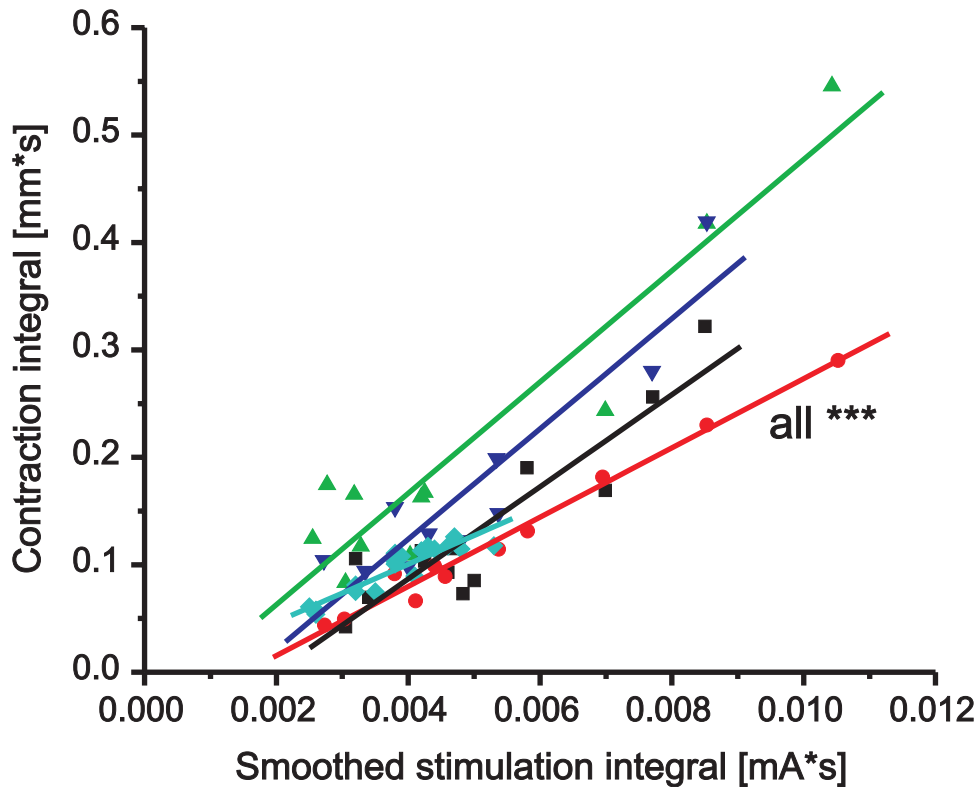


Figure C.48: Plotting the smoothed physiological stimulation integral vs. the contraction position integral results in highly significant correlations in all of the five animals tested (all fits ***; minimal R value=0.914, maximal R value=0.992; $n=63$, $N=5$).

locity: plotting this calculated shortening velocity vs. the isotonic force level gives the muscle's force-velocity characteristic, the Hill-curve (Hill (1938)). The duration of the oscillations varied with the given load level and the stimulation frequency: it ranged from 17.4 ± 4.16 ms for 30 Hz ($N=5$) up to 24.5 ± 6.75 ms at 200 Hz ($N=6$).

2.1 The Hill hyperbola at maximal stimulation

Fig. C.50 shows extensor tibiae force-velocity data at 200 Hz stimulation frequency and fits of these data to the Hill-hyperbola from seven experiments ($N=7$, $n=73$; fitting performed in ORIGIN with HyperbolaGen).

$$(V + b) \cdot (P + a) = b \cdot (P_0 + a) \quad (1)$$

where V represents velocity, P force, P_0 the isometric force just prior to the switch to

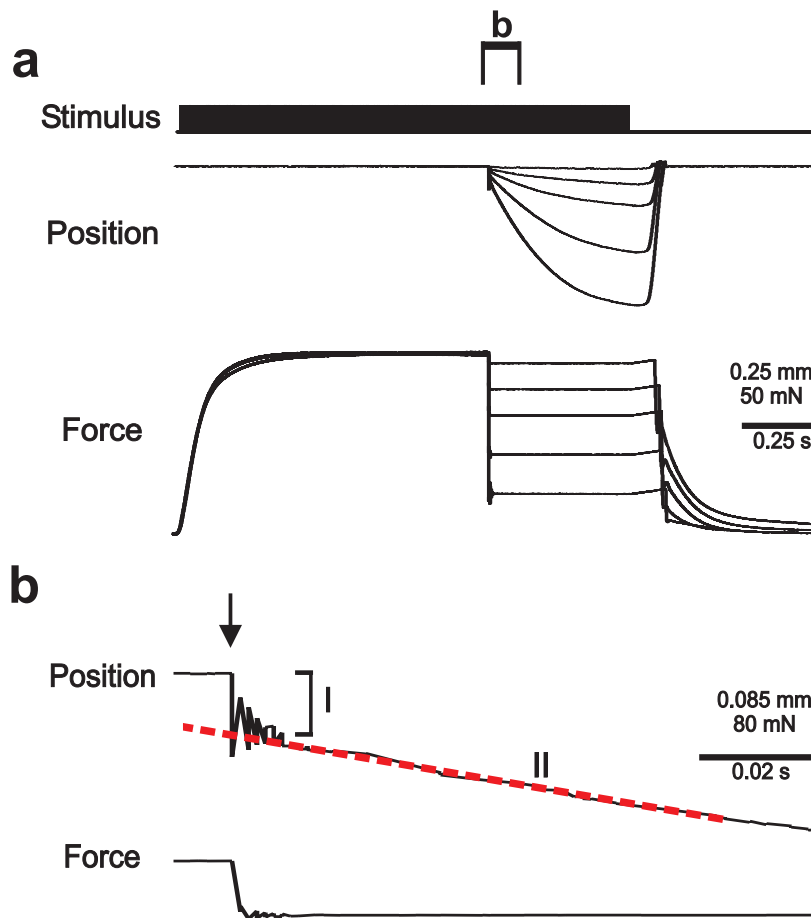


Figure C.49: The loaded release experiment. (a) Response of a tetanically activated muscle to a switch from isometric to isotonic conditions with counter forces less than the force the muscle had developed during its isometric contraction (different force traces in a). The bracket on top ('b') marks the time frame in which position control switches to force control and the data is shown enlarged in (b): The muscle shows an abrupt length change (bracket 'I') followed by a smooth initially linear contraction ('II'), see text for details.

isotonic conditions, and "b" and "a" the asymptotes (lying at negative values of P and V).

These data are clearly well fit by a hyperbola (mean $R^2=0.996 \pm 0.006$). Different muscles show considerable variation in P_0 and a smaller variation in V_0 , the latter being the maximum contraction velocity without load. This variability can be removed by normalising the Hill-equation to P_0 and V_0 in order to emphasize potential systematic similarities:

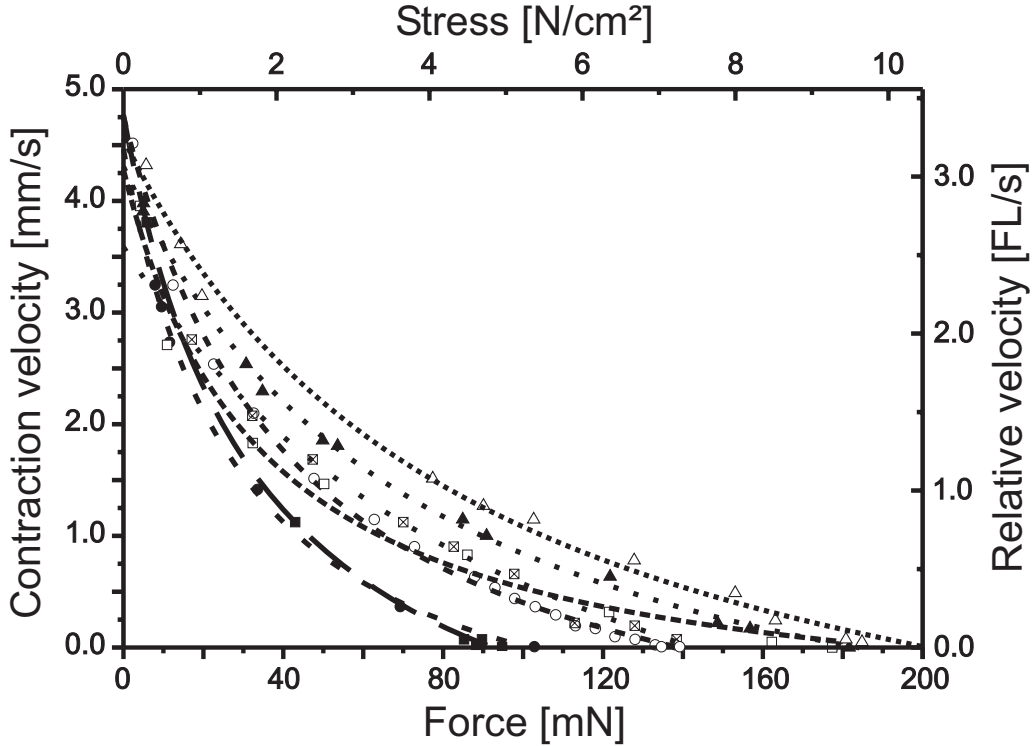


Figure C.50: Variability of the force-velocity characteristic of the extensor tibiae muscle at 200 Hz stimulation frequency ($N=7$, $n=73$; values in Tab. C.7).

$$\left(V \frac{V}{V_0} + c\right) \cdot \left(\frac{P}{P_0} + c\right) = c \cdot (1 + c) \quad (2)$$

This normalised version of the Hill-hyperbola gives a common value for the asymptotes $c = \frac{b}{V_0} = \frac{a}{P_0}$; the reciprocal value $\frac{1}{c}$ can serve as a measure for the curvature of the Hill-hyperbola (Josephson (1993)). Tab. C.7 gives the values V_0 , P_0 , c and R^2 for the measurements shown in Fig. C.50.

Flexor tibiae force-velocity data from eight animals ($N=8$, $n=135$) reveal mainly two facts (Fig. C.51): first at all, flexor tibiae max. forces are much larger than extensor tibiae forces (414.93 compared to 150.69 gives nearly the 2.8 fold, see Tabs. C.7 and C.8). However, normalised to cross-sectional area, max. flexor tibiae stresses are only 1.3 fold larger than extensor tibiae max. stresses. Secondly, flexor tibiae max. contraction velocities are 1.4 fold larger than in the extensor tibiae, see Tabs. C.7 and C.8. However, normalised to fibre length, max. flexor tibiae contraction velocities are only 0.9 fold the extensor tibiae stresses. Altogether, normalisation of both force and velocity demonstrates that the values of extensor and flexor tibiae cover a similar range.

Table C.7: Extensor tibiae maximum force / stress, maximum velocity, curvature and R^2 -value of the Hill hyperbola in seven animals (N=7). Values were calculated from the fit (HyperbolaGen, ORIGIN).

P_0 [mN] / [$\frac{N}{cm^2}$]	V_0 [$\frac{mm}{s}$] / [$\frac{FL}{s}$]	c	R^2
101.04 / 5.28	4.46 / 3.17	0.28	0.999
92.54 / 4.83	4.77 / 3.39	0.36	1
138.84 / 7.25	4.75 / 3.38	0.31	0.998
194.41 / 10.16	4.28 / 3.04	0.18	0.983
183.74 / 9.60	4.31 / 3.07	0.41	0.999
201.62 / 10.53	4.56 / 3.24	0.44	0.995
142.66 / 7.45	3.59 / 2.55	0.76	0.999
150.69 ± 44.06 / 7.87 ± 2.3	4.39 ± 0.4 / 3.12 ± 0.29	0.39 ± 0.18	0.996 ± 0.006

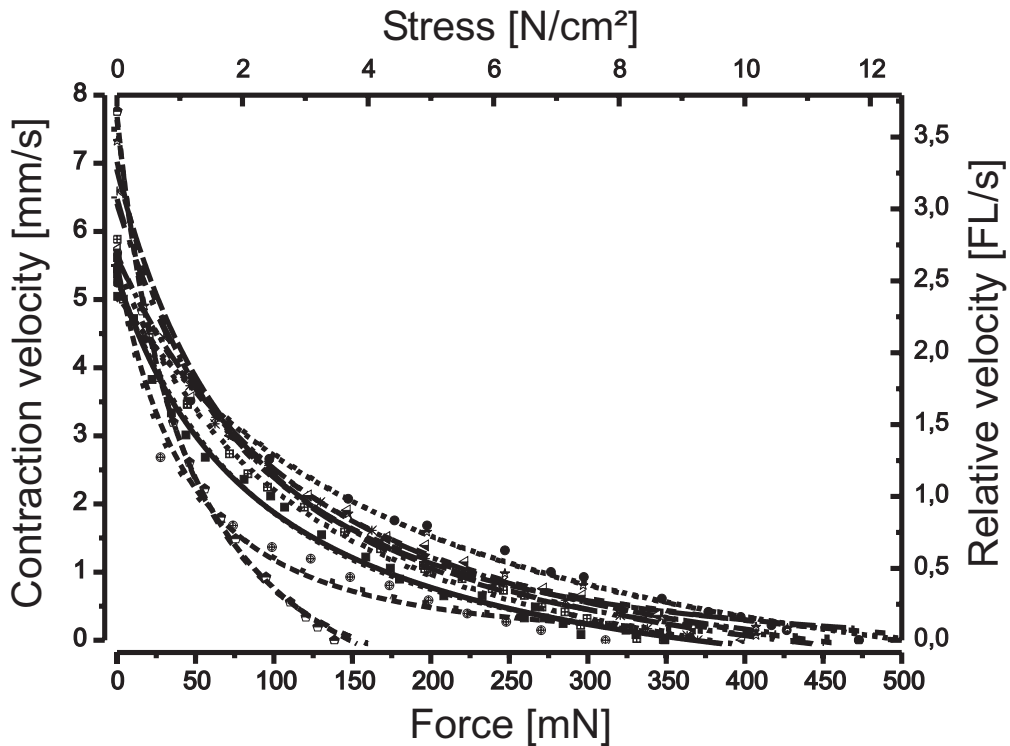


Figure C.51: Variability of the force-velocity characteristic of the flexor tibiae muscle (N=8, n=135; values in Tab. C.8).

Table C.8: Flexor tibiae maximum force / stress, maximum velocity, curvature and R^2 -value of the Hill hyperbola in eight animals (N=8). Values were calculated from the fit (HyperbolaGen, ORIGIN).

P_0 [mN] / [$\frac{N}{cm^2}$]	V_0 [$\frac{mm}{s}$] / [$\frac{FL}{s}$]	c	R^2
367.23 / 9.18	5.34 / 2.53	0.25	0.994
502.15 / 12.55	5.07 / 2.4	0.4	0.995
376.65 / 9.42	5.51 / 2.61	0.32	0.997
503.71 / 12.59	5.61 / 2.66	0.07	0.987
148.21 / 3.71	7.68 / 3.64	0.3	0.998
555.16 / 13.88	7.02 / 3.33	0.13	0.987
442.5 / 11.06	5.66 / 2.68	0.3	0.997
423.85 / 10.6	6.48 / 3.07	0.22	0.996
414.93 ± 125.85 / 10.37 ± 3.15	6.05 ± 0.92 / 2.87 ± 0.43	0.25 ± 0.11	0.994 ± 0.004

2.2 Deviations from the hyperbolic shape

As reported by Edman and colleagues (Edman et al. (1976)) and Edman (Edman (1988)), deviations of the Hill-curve from the hyperbolic shape in the region of high forces (P near P_0) at low contraction velocities can also be found for tibial muscles. The measured contraction velocities in this region lie systematically below the hyperbolic fit function. To demonstrate this for one exemplary experiment shown in Fig. C.50, force values were normalised to P_0 (open circles in Fig. C.52). In this figure, the depicted hyperbola represents data fit exclusively for values $< 0.65P_0$. Measured velocities $> 0.65P_0$ deviate clearly from the hyperbolic fit. Edman et al. (Edman et al. (1976)) and Edman (Edman (1988)) showed also that this deviation persisted for values of $\frac{P}{P_0} > 1$ (negative contraction velocities, i.e. stretch). It seemed therefore reasonable to conduct a set of six similar experiments, changing from tetanical isometric contraction to loads higher than P_0 , resulting in a “loaded stretch”, where the muscle is stretched with a given force and stretch velocity is measured (Fig. C.52, filled circles to the right of $\frac{P}{P_0}=1$).

As maximum contraction velocity V_0 in all experiments did not scatter very much, the collected original velocity data was put as a function of $\frac{P}{P_0}$ in one diagram. The composite picture demonstrates that the Hill-curve does not intersect the abscissa with a non zero slope (as the hyperbola would) but that the zero intersection is instead sigmoidal with an almost horizontal tangent.

Deviations from the hyperbolic shape can also be found for the flexor tibiae. Fig.

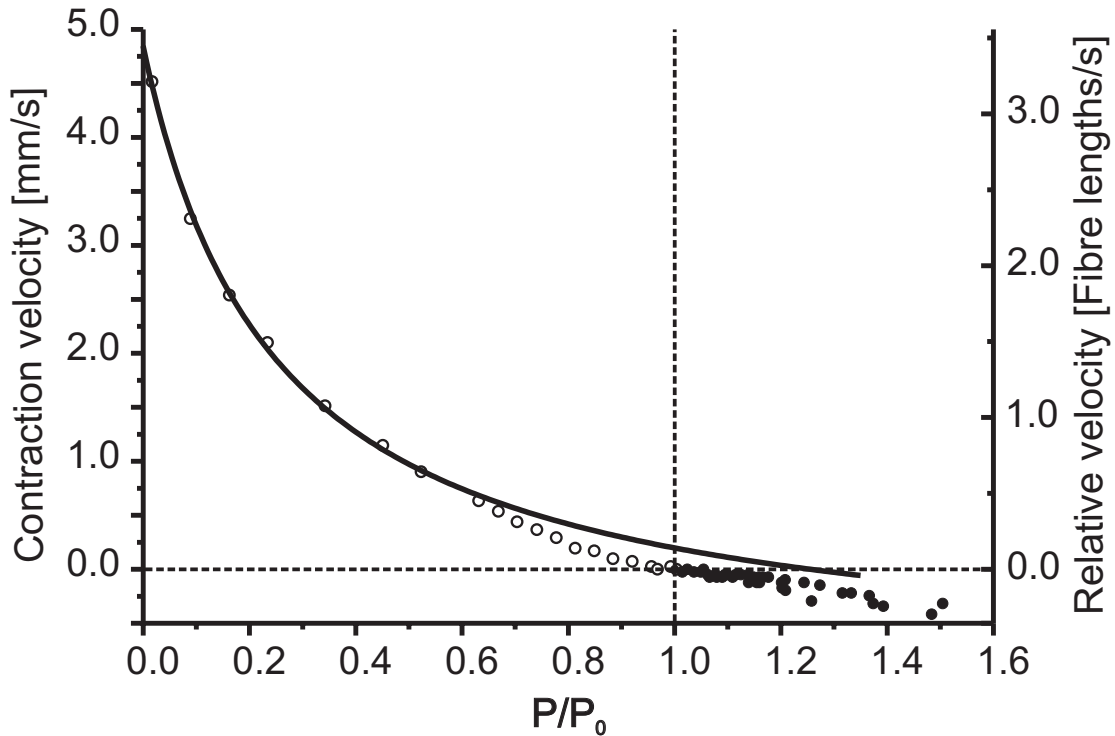


Figure C.52: Deviation of the force-velocity curve (solid line) from hyperbolic shape in the region of $\frac{P}{P_0}$ between 0.6 and 1 for one typical experiment (open circles). The extensor tibiae muscle was activated with a stimulation frequency of 200 Hz. In the region $\frac{P}{P_0} > 1$ force-velocity measurements are shown under stretch (filled circles, data from 6 experiments) to demonstrate the sigmoid zero crossing of the Hill-hyperbola. The force axis was normalised to the maximum isometric contraction force P_0 .

C.53 shows an example where this deviation is obvious for values in the region of $\frac{P}{P_0}$ between 0.6 and 1, when only data $< 0.65P_0$ were fitted. Even though the figure shows only one experiment, the deviation is very likely to be found in all measurements (N=8), probably not always starting at datapoints $> 0.65P_0$. In the example shown (Fig. C.53), datapoints are visibly shifted towards smaller contraction velocities, as was also shown for the extensor tibiae in Fig. C.52.

2.3 The Hill hyperbola at different activation levels

Muscle activation is controlled by motoneuron spike frequency. Thus, the influence of stimulation frequency on the Hill characteristic was systematically investigated. Fig. C.54 shows an example of the Hill-curves obtained from different stimulation

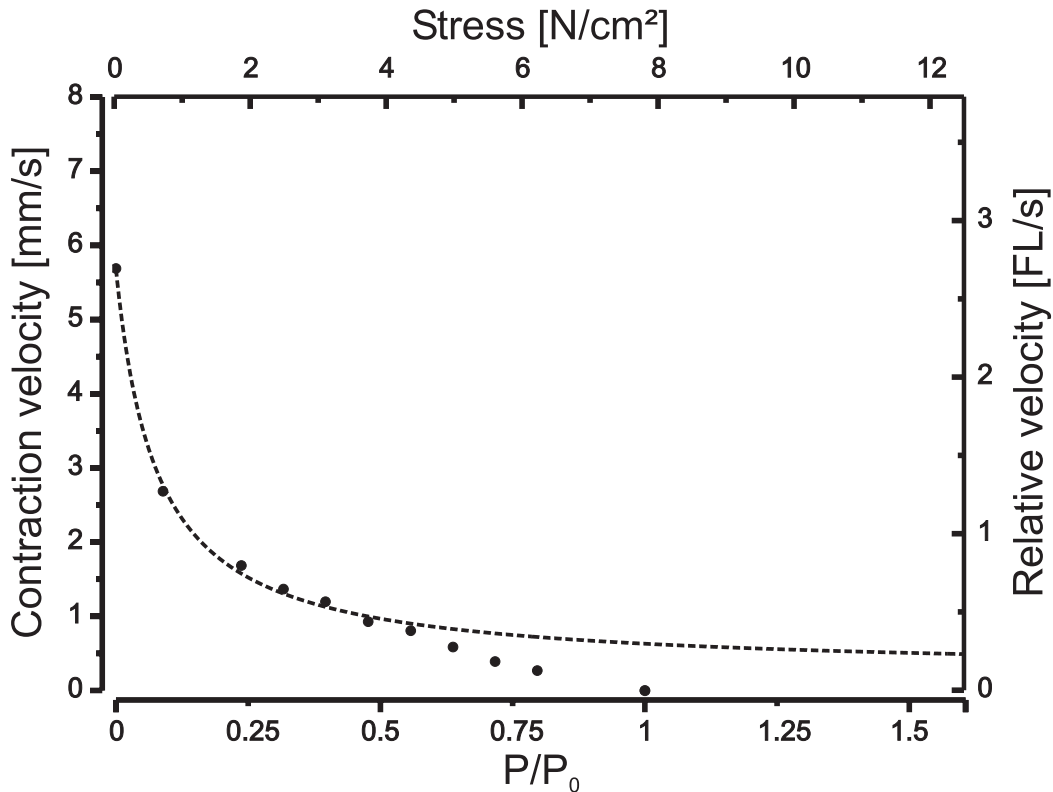


Figure C.53: Deviation of the force-velocity curve (dashed line) from the hyperbolic shape in the region of $\frac{P}{P_0}$ between 0.6 and 1 for one typical experiment. The flexor tibiae muscle was activated with a stimulation frequency of 200 Hz.

frequencies. It is apparent that both V_0 and P_0 strongly increase with increased stimulation frequency (see also Tab. C.9) leading to an almost concentric alignment of the individual fitted hyperbolas. Fig. C.54 demonstrates this for one exemplary experiment ($N=1$), one other experiment was conducted showing basically the same coherence (not shown, in total $N=2$).

2.4 Activation dependent parameters

Plotting P_0 versus stimulation frequency (Fig. C.55a, $N=11$) for the different experiments reveals two main characteristics. First of all, P_0 shows a sharp increase at low frequencies between about 20 Hz and 80 Hz, and then saturates (reaches an unchanging maximum) at stimulation frequencies larger than 100 Hz, as could already

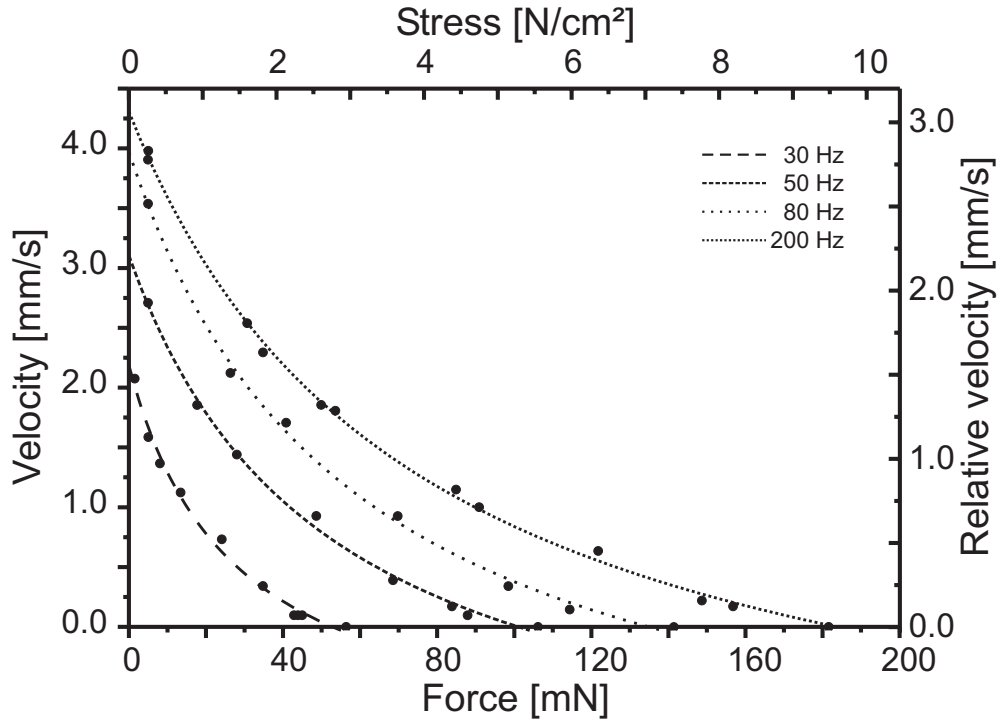


Figure C.54: Hill curves of the extensor tibiae muscle at different stimulation frequencies from one animal ($N=1$, values in Tab. C.9).

Table C.9: Maximum force / stress, maximum velocity, curvature and R^2 -value of the Hill hyperbola in the extensor tibiae muscle at different activation in an exemplary animal.

	P_0 [mN] / [$N \cdot cm^{-2}$]	V_0 [$mm \cdot s^{-1}$] / [$FL \cdot s^{-1}$]	c	R^2
30 Hz	52.82 / 2.76	2.19 / 1.56	0.51	0.993
50 Hz	101.1 / 5.28	3.11 / 2.21	0.5	0.997
80 Hz	134.97 / 7.05	3.97 / 2.82	0.43	0.997
200 Hz	183.74 / 9.60	4.31 / 3.07	0.41	0.999

be observed in Fig. C.16 in chapter C2. Secondly, the maximum saturated force at maximum stimulation frequency (in this case 200 Hz) varies from about 100 mN up to 190 mN in the different muscles examined. Fitting these data with an exponential saturation curve $P_0 = P_{0_{max}}(1 - e^{-\frac{f}{f_0}})$ in which $P_{0_{max}}$ is the saturation value and f_0 is the frequency at which the curve has reached $1 - \frac{1}{e}$ of its saturation level gave R^2 values of 0.90 ± 0.047 (min. 0.83, max. 0.98) and a mean f_0 of 56.6 ± 17.2 Hz ($N=11$). The steepest and the shallowest fit to the data as well as the mean \pm S.D. are added.

Plotting V_0 versus frequency can be fitted with a similar function and shows a nearly identical dependence with an even higher mean R^2 of 0.93 ± 0.06 (min 0.86, max 0.98)

and a similar mean f_0 of 57.7 ± 17.9 Hz (Fig. C.55b, N=5). Again the steepest and the shallowest fit as well as the mean \pm S.D. are shown.

The paired data of V_0 and P_0 in the individual experiments showed in all cases a significant positive correlation (*, $p < 0.03$, Fig C.55c, N=5). The ratio $\frac{V_0}{P_0}$ of the maximum values of P_0 and V_0 at 200 Hz correlate well with the slopes of the regression lines (*, $p < 0.05$).

Neither a correlation could be found between the frequency constants f_0 of the corresponding P_0 and V_0 fits of the individual experiments, nor between the f_0 values and the P_0 and V_0 values. At present, a similar analysis is not possible for the curvature parameter 'c'. This mostly arises from the fact that only a limited number of values for 'c' were gathered, since the focus was rather to look for pairs of V_0 and P_0 and not for the complete Hill-curve in most cases. The available data do not show a systematic change of 'c' with stimulation frequency (not shown). The mean evaluated 'c' value was 0.5 ± 0.22 (N=14).

2.5 Length dependence of the maximal contraction velocity

Measuring the Hill-curves at different muscle lengths and under minimal load demonstrates how maximum contraction velocity V_0 depends on muscle length. Two experiments were performed to investigate this topic (Fig. C.56). One experiment was conducted with 200 Hz and with 50 Hz stimulation frequency and with a rest load of 0.7 mN compared to a maximum isometric force of 69 (35) mN at 200 (50) Hz (filled symbols). The other experiment was done solely at 200 Hz (open symbols) at a rest load of 4.5 mN compared to the maximum isometric force of 140 mN. Similar to the force-length characteristics (Fig. C.23,C.24) the velocity-length curves show a monotonic and nearly linear increase within the muscle's working range, followed by a plateau at longer fibre lengths.

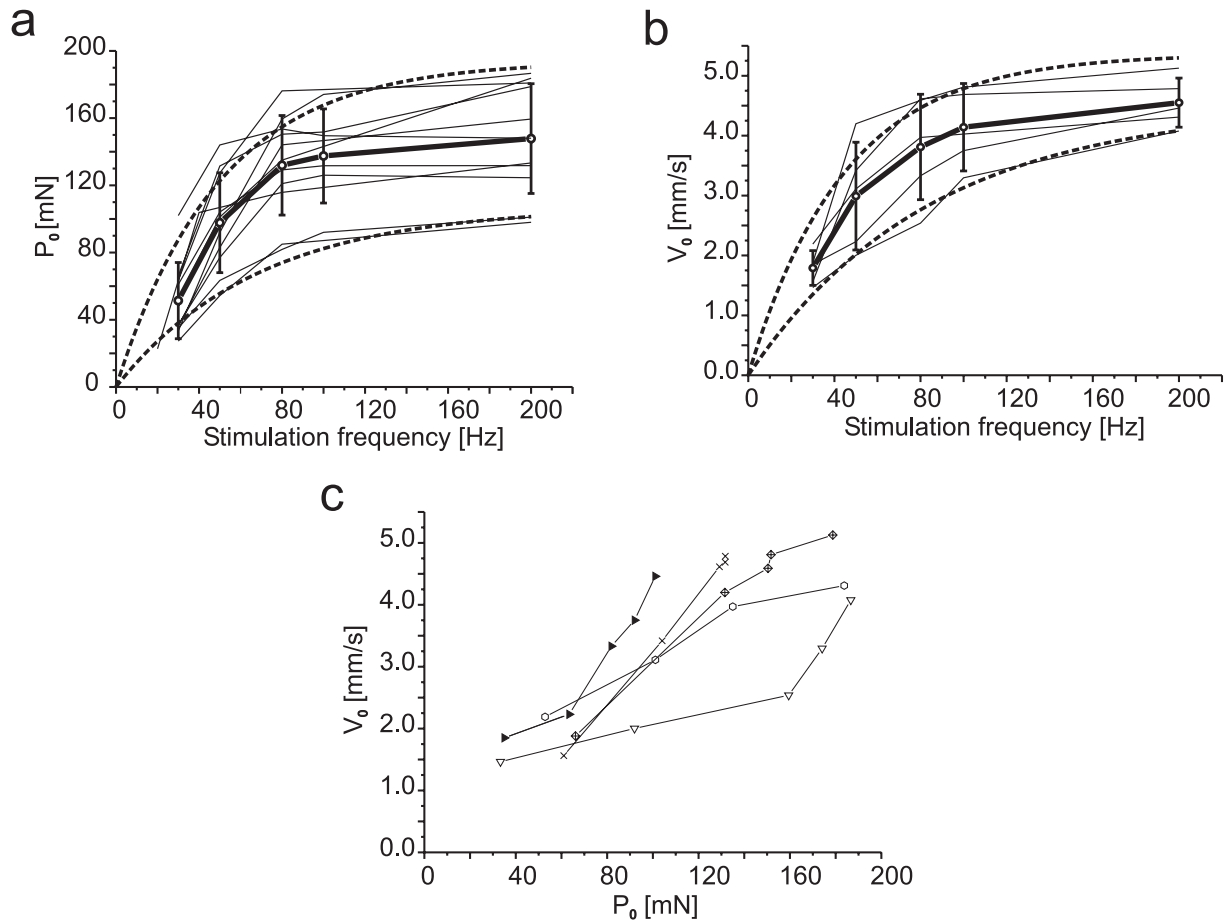


Figure C.55: Dependence of the Hill-curve parameters on stimulation frequency in the extensor tibiae muscle. **a** Dependence of the isometric force P_0 on stimulation frequency ($N=11$). **b** Dependence of maximum contraction velocity V_0 on stimulation frequency ($N=5$). For both diagrams the data of each experiment were fitted by an exponential saturation function leading to the same mean 'frequency-constant' f_0 of about 60 Hz for both dependencies. In both panels **a** and **b** the dotted lines show most shallow and steepest fits and bold lines show mean \pm S.D. Please note that the number for individual means can differ (in Fig. **a**: $6 \leq N \leq 9$, in Fig. **b**: $4 \leq N \leq 5$). **c** Coupling of maximum contraction velocity V_0 with isometric force P_0 under variation of stimulation frequencies ($N=5$). The values of each set of experiments are marked by connecting straight lines. For all individual experiments the data showed a significant correlation ($p < 0.05$). Note that the maximum values V_0 and P_0 at 200 Hz for each experiment determine roughly the overall slopes of the diagrams. See text for details.

3 Isometric and isotonic contraction dynamics at different muscle lengths

Following Gordon et al. (Gordon et al. (1966b)), parts of chapter C2 dealt with the relationship between actively generated force and fibre length (sarcomere length to

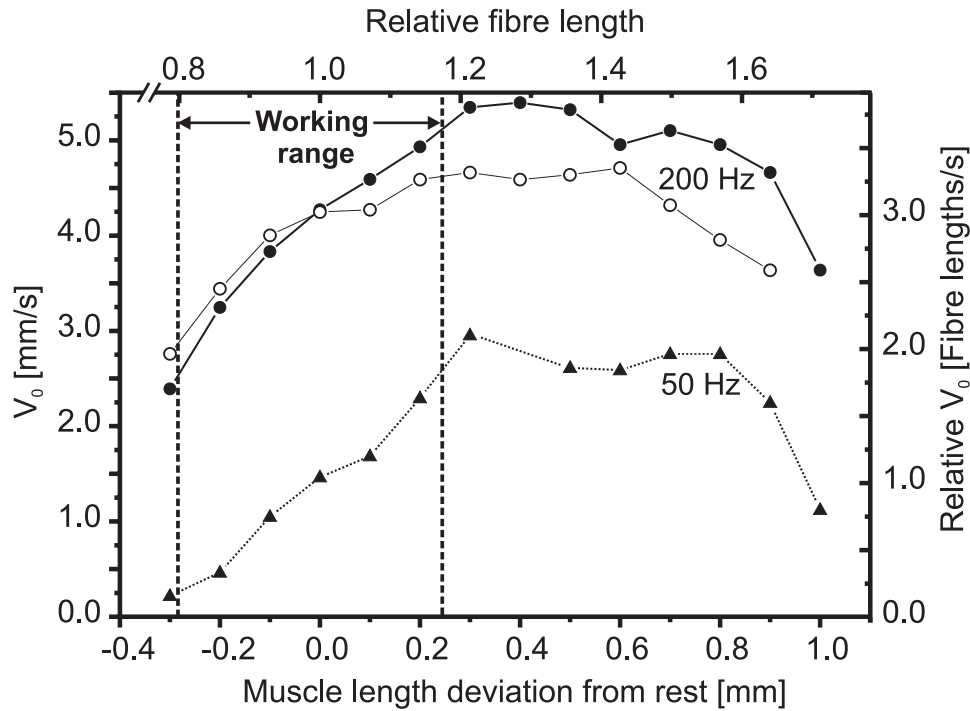


Figure C.56: Length dependence of maximum contraction velocity V_0 in the extensor tibiae ($N=2$): one experiment was done at 200 Hz and at 50 Hz stimulation frequency (filled symbols). The other experiment was done only at 200 Hz (open symbols). See text for details.

be precise). In addition, data in chapter C3 demonstrated that passive static muscle forces increases exponentially with increasing muscle stretch. The following investigations went one step further, as not only absolute active force at a particular length was measured, but also the velocity of the force development. This was performed at two different muscle lengths within the extensor tibiae's working range. Fig. C.57a(i) shows two data sets: an extensor tibiae muscle was stretched 0.175 mm more than its length at 90° (red trace) and 0.125 mm less than its length at 90° (black trace) and was stimulated with a 50 Hz pulse series at both muscle lengths. The measurements result in isometric forces (intersections with the ordinate) of 0.18 mN (passive) and 94.6 mN (active) in the less stretched state (black trace) and 3.11 mN (passive) and 117.97 mN (active) in the more stretched state (red trace). The passive and active force increase at the more stretched position compared to the less stretched position agrees with previously shown data in chapters C2 and C3 and the force-length examinations of Gordon et al. (Gordon et al. (1966b)). In addition, velocity of the force increase is presented that was gained by differentiating the force recording in SPIKE2

(time constant of 0.015 s). Force increase accelerates within the first two stimulation pulses to maximum velocity at both muscle length states (stretched and relaxed). At 20 mN, velocity becomes continuously smaller until it reaches P_{max} in both isometric contractions. Individual pulses are visible because the tetanus is not totally fused at 50 Hz. Force increase velocity demonstrates to be 55 % larger in the stretched muscle compared to the muscle being more relaxed ($912.5 \frac{mN}{s}$, red trace and $588 \frac{mN}{s}$, black trace).

From experiments conducted in the isotonic domain (muscle shortening was conducted against a load being approximately equal to the passive tension at the respective length), velocity of the muscle's displacement is illustrated in Fig. C.57a(ii): exactly like the force increase's velocity, maximal displacement velocity is reached within the first two stimulation pulses at both contraction states. However, different from force increase's velocity, maximal displacement velocity is in the muscle's stretched state only 7 % larger than in the relaxed one ($3.14 \frac{mm}{s}$ and $2.94 \frac{mm}{s}$). After having reached maximum, displacement velocity becomes continuously smaller, like the force velocity depicted in a(i), until it reaches its end position, i.e. the muscle length where the maximal filament overlap is obtained.

The combination of a(i) and a(ii) is illustrated in a figure basically showing three different planes: using an algorithm by S. L. Hooper (Hooper et al., in preparation), velocities can be depicted as arrows (Fig. C.57b). The length and width of an arrow is a measure for the velocity amplitude at a given point. Making the assumption that the increase branches of the force velocity vs. force and the displacement vs. displacement velocity plots can be attributed to Ca^{2+} influx, arrows are exclusively shown starting at maximal velocity. The figure demonstrates clearly that a muscle at a physiologically stretched state generates more active and passive force isometrically (as would be expected from chapters C2 and C3) and performs to an equal degree more length change than a relaxed muscle. The ratios of those isometric forces and those isotonic displacements ($\frac{muscle_{stretched}}{muscle_{relaxed}}$) are very similar: 1.22 for the isometric forces and 1.26 for the isotonic displacements.

Force velocity and contraction velocity play a major role when it comes to movement control. Dean (Dean (1984)) found stick insect protractor muscles to maintain suitable

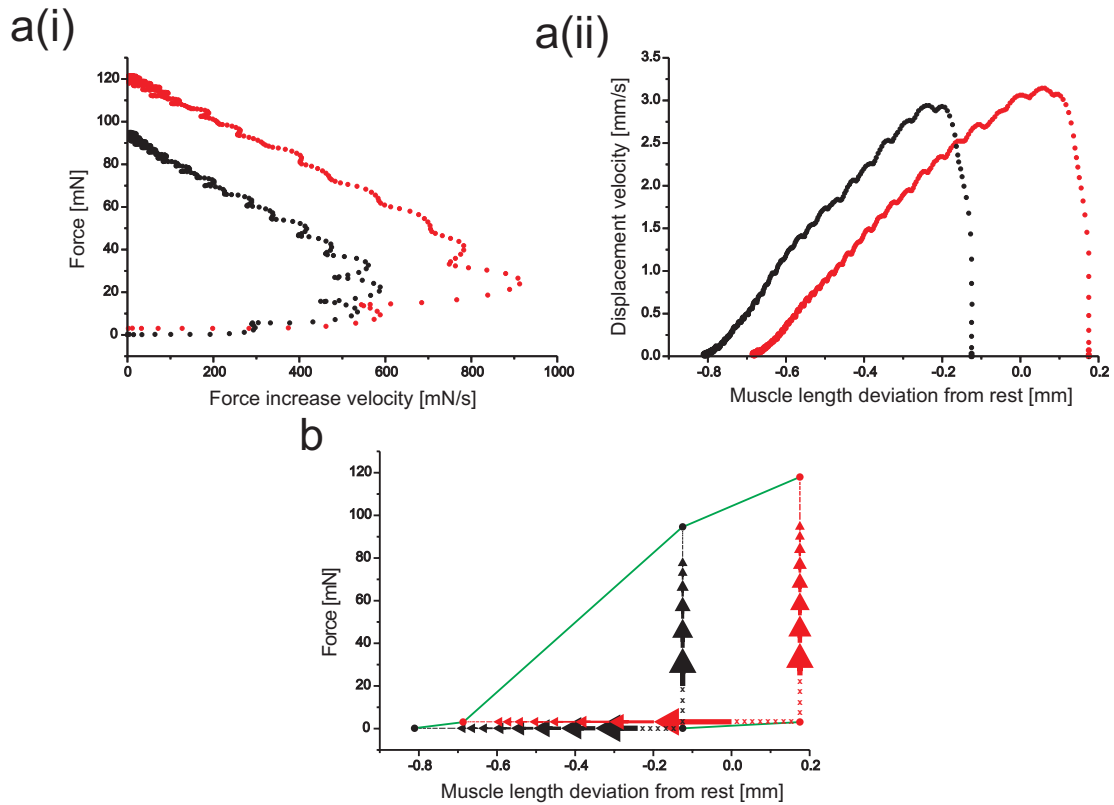


Figure C.57: Force increase velocity (**a(i)**) and displacement velocity (**a(ii)**) at two different lengths in the extensor tibiae muscle (red depicted data 0.175 mm stretched, black depicted data 0.125 mm relaxed; 0 mm = muscle length at 90°). Contraction velocities were calculated by differentiating the force and position recordings in SPIKE2 with a time constant of 0.015 s. (**b**) Active and passive forces, displacements and velocities expressed as arrows from **a(i)** and **a(ii)**. Width and length of the arrows were calculated using an algorithm by S.L. Hooper (Hooper et al., in preparation) and correspond to the force or muscle length velocity respectively.

speeds in the presence of increased loads. He interpreted his finding to show this property to rely on positive feedback reflexes. The continuous movement of the leg through sudden load changes indicated an adaption to the new load within 20 ms. The next set of experiments should test whether this phenomenon can be attributed to a feedback mechanism of a control circuit or whether this could rather represent a muscle property.

An extensor tibiae muscle was stimulated at 100 Hz and got clamped on two different force levels (P_1 and P_2) so that it could shorten isotonically after the time t_0 : its maximal contraction amplitude was larger at the small force level P_1 and smaller at the higher load level P_2 (Fig.C.58a). The shapes of the two contractions are very sim-

ilar: the muscle shortens fast at the beginning, slows down afterwards and saturates finally because of maximal degree of thin and thick filament overlap. In a second approach (Fig.C.58b), the same muscle is first clamped to P_1 and force is switched to P_2 after 0.125 s (t_1). The muscle shortens initially as fast as in (a) and continues shortening, but slower, after the switch to P_2 . The contraction represents basically the combination of the two muscle shortenings depicted in (a). When the muscle is clamped to P_1 and is switched to P_2 after 0.92 s (t_2), the muscle does not continue to shorten: it lengthens immediately and ends at the same contraction amplitude that is reached when switching to P_2 earlier (t_1 or t_0). This contraction represents also the combination of the two shortenings depicted in (a), with the discrepancy in the time of the switch: as long as the muscle is in the phase of continuous shortening (t_1), a switch to a higher force level will not stop this muscle from shortening. As soon as a saturation of the shortening process is reached, or nearly reached (t_2), the muscle will lengthen. This mechanism was verified in four animals (N=4), data from one animal was taken for illustration.

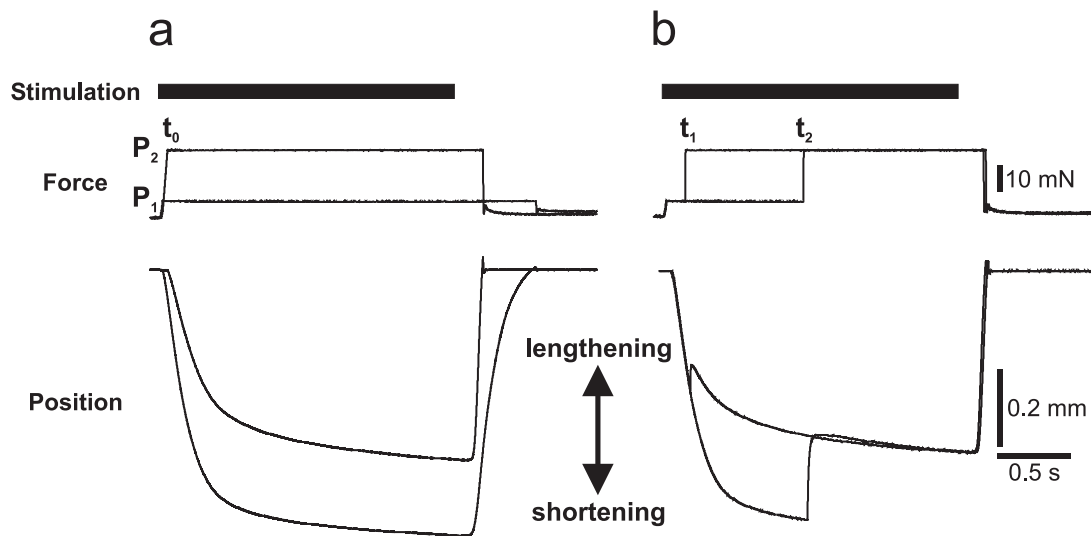


Figure C.58: Loading at different times during shortening of the extensor tibiae muscle (t_0, t_1, t_2). (a) Isotonic contractions at two different load levels ($P_1 < P_2$). (b) Increase of load ($P_1 \rightarrow P_2$) at the beginning of an isotonic contraction (t_1) leads to a continuation of shortening, the same load increase later in the contraction (t_2) leads to a sudden muscle lengthening.

C5 Passive forces II

1 Series elasticity

1.1 Series elasticity of tibial muscles at maximal activation

The loaded release experiment shown in Fig. C.49a demonstrated that two things happen when a tetanically stimulated muscle is all of a sudden allowed to shorten: first, the muscle in focus experiences a very fast abrupt length change (bracket at 'I' in Fig. C.49b). Only after that, the muscle shortens actively due to sliding filaments ('II' in Fig. C.49b). Chapter 3 dealt with this **second** length change in detail. This section investigates the **first** length change.

To analyse the series elasticity (spring constant) of both tibial muscles, the isotonic force change in the loaded release experiment (steps in the force trace in Fig. C.49a) is plotted versus the associated fast initial length change. Similar to series elasticity measurements in the river toad (*depressor mandibulae* muscles in *Bufo alvarius*, Lappin et al. (2006)), data was calculated by extrapolation of the slope that determines shortening velocity (see chapter C4): the length difference between this extrapolated slope and the muscle length before switching to force control at the time of the switch represents the fast shortening of the series elastic component at a given load level (see Fig. C.49b). The SPIKE2 script performing this calculation is added in the Appendix. In order to obtain a force-length characteristic comparable with similar measurements in literature (Wilkie (1956); Jewell and Wilkie (1958)) and with technical spring characteristics, the data are presented in the following way: the plot shows the independent, controlled force at the ordinate, the resultant length change on the abscissa for maximal muscle activation, i.e. 200 Hz. The origin length (0 mm) for every set of data was

the initial length of the isometric contracted muscle, and muscle shortenings are thus plotted as negative values. The starting force value in each experiment is the tetanical isometric force at 200 Hz. Each force step is plotted from this starting point, leading to a sequence of diminishing forces versus the more and more shortening length of the releasing muscle. Plotted data of each individual experiment can be fitted best with a 2nd order polynomial fit in ORIGIN, the series elasticity can therefore be described with a quadratic spring. Parabolic fits depicted in Figs. C.59 and C.60 were cut at the minimum (the apex), data can only be described with one leg of a parabola. From the simplified equation $P(x) = \beta \cdot x^2$, the quadratic spring constant is represented by the value for β . Extensor tibiae measurements at 200 Hz illustrated in Fig. C.59 reveal an average β of $14948 \pm 2590 \frac{mN}{mm^2}$, the mean $R^2 - value$ is 0.997 ± 0.002 (N=5, n=59). All fits are highly significant (***)

For the flexor tibiae (Fig. C.60), 200 Hz measurements reveal a mean β of $24515 \pm 5241 \frac{mN}{mm^2}$, the mean $R^2 - value$ is 0.995 ± 0.002 (N=8, n=135). All fits are highly significant

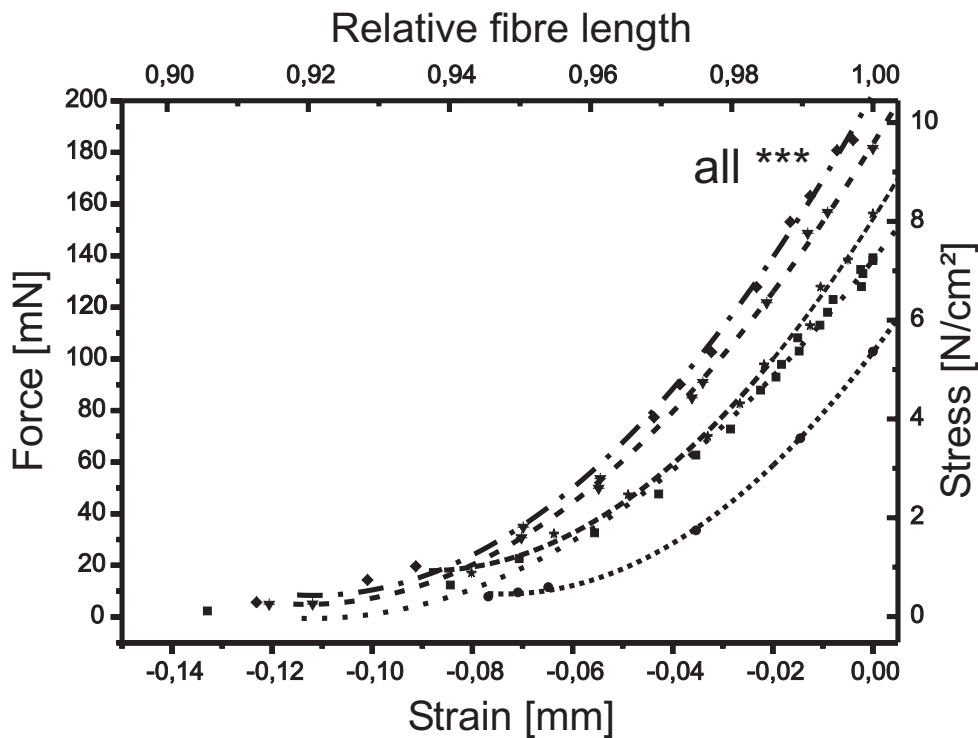


Figure C.59: Nonlinear extensor tibiae series elasticity measurements at 200 Hz (N=5, n=59). Each experiment is marked by a different symbol, data fits of individual experiments (performed in ORIGIN) differ in line shape. Fits show were all highly significant (***) with min. R=0.996 and max. R=0.999.

(***). β of the flexor tibiae is 1.64 times larger than β of the extensor tibiae.

For better comparison, a second abscissa and ordinate are depicted in Figs. C.59 and C.60. Conveniently, β was additionally calculated taking the different fibre lengths (1.41 mm for the extensor and 2.11 mm for the flexor, see chapter C1) and the muscle's different cross-sectional areas (1.94 mm² for the extensor tibiae and estimated 4 mm² for the flexor tibiae, see chapter C1) into account, which gives $\frac{P(x)}{A} = \beta^* \cdot \left(\frac{x}{Fl}\right)^2$ (A = cross-sectional area, Fl = fibre length). Calculated this way, β^* s of both muscles (i.e. the modified β s) are $15322 \pm 2655 \frac{mN}{mm^2}$ for the extensor and $27285 \pm 5833 \frac{mN}{mm^2}$ for the flexor tibiae. β^* of the flexor tibiae is 1.8 times larger than β^* of the extensor tibiae.

The extensor tibiae muscle was also exposed to forces $> P_0$. Fig. C.61 shows data from shortening (N=1) and lengthening (N=1) measurements in the strain range from -0.05 to 0.05 mm (N=2): the series elastic component lengthens in a similar way than it

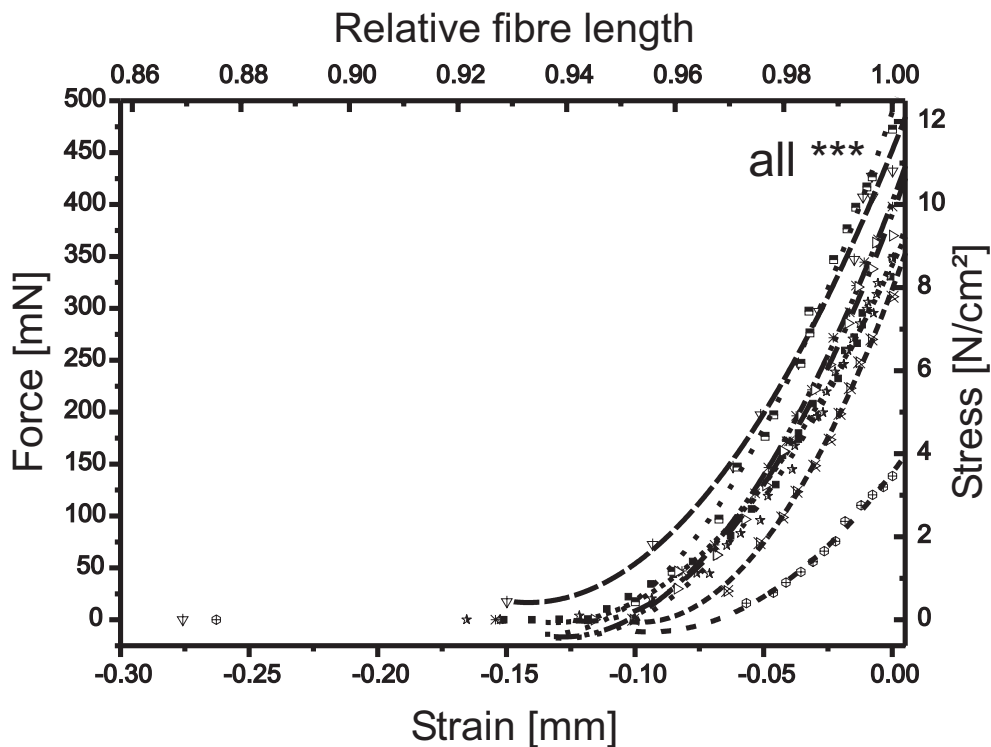


Figure C.60: Nonlinear flexor tibiae series elasticity measurements at 200 Hz (N=8, n=135). Each experiment is marked by a different symbol, data fits of individual experiments (performed in ORIGIN) differ in line shape. Fits were all highly significant (***) with min. R=0.991 and max. R=0.998.

shortens during a quick release, but with inverted sign. The muscle keeps its stiffness, at least at small forces $> P_0$ (40 mN in this case).

1.2 Series elasticity of the extensor tibiae at different activation levels

Figs. C.59, C.60 and C.61 demonstrate that the series elasticities of tibial muscles are nonlinear and that stiffness increases with increasing stretch. Now, the series elasticity of the extensor tibiae was further examined in terms of its dependence on stimulation frequency. In Fig. C.62a, the starting force value in each experiment is the tetanical isometric force at each given stimulation frequency. Consideration of these curves shows that the curve generated by 30 Hz stimulation, with its maximum force of 60 mN, has the same shape as the 60 mN portions of the curves generated by the 50, 80, and 200 Hz stimuli. These data can therefore be combined by translocating the 30, 50 and 80 Hz curves to the left so that they overlay the 200 Hz, maximum force curve (see also Jewell and Wilkie (1958) for further discussion on this issue). When

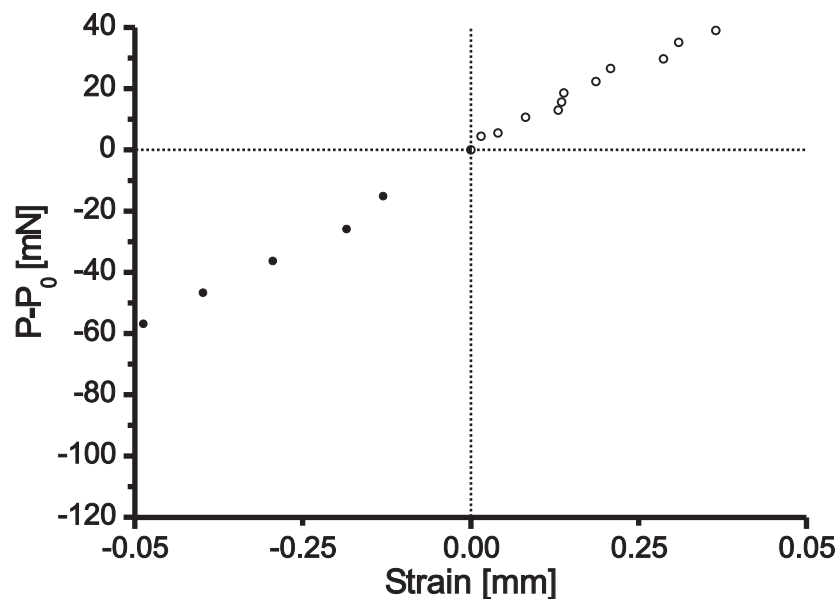


Figure C.61: Extensor tibiae series elasticity measurements at 200 Hz $< P_0$ (closed circles, $N=1$) and $> P_0$ (open circles, $N=1$). Depicted are strains ranging from -0.05 mm to 0.05 mm. In order to compare data of different extensor tibiae muscles, application on the ordinate shows $P - P_0$ and strain to be zero at P_0 for both experiments.

doing so, demonstrated in Fig. C.62b, all force-length curves can be fitted by a single parabola. In the illustrated experiment (Fig. C.62b), β was $13900 \frac{mN}{mm^2}$; maximum stiffness reached $3150 \frac{mN}{mm}$. It is currently unclear if the spring constant varies with muscle length, further investigations would be needed to answer this question.

2 Visco-elastic properties II: creep experiments

Chapter 1.6 shows the viscoelastic nature of tibial muscles by ‘*deformation with a constant rate of strain*’, where the strain is increased linearly with time and the stress is measured as a function of time. The reverse can be achieved by suddenly applying stress and maintaining constant while strain is measured as a function of time (after Ferry (1961)). Such experiments are called ‘*creep*’ experiments are a usual technique in materials science.

Fig. C.63a illustrates the procedure of such an experiment: a denervated extensor tibiae muscle is minimally lengthened by stretch and by simultaneously clamping force just above the muscle’s resting force level. When the clamped force level suddenly increases, the muscle responds with a “creeping” strain increase (trace ‘1’ in Fig. C.63a). When the muscle is unloaded 10 s later, the muscle does not return to its original length. The course of this reverse deformation is called ‘*creep recovery*’. Again 10 s later (trace ‘2’ in Fig. C.63a), the muscle is loaded in the same way again and responds with a length change that is much smaller than before. Again, unloading 10 s afterwards does not reestablish the length value before the first loading. Fig. C.63b shows that the measured strains can be well described with a power-function characteristic because the data can be fitted with a highly significant linear regression in log-log application in both ways (all ***, loading $R=0.985$ and later $R=0.999$; unloading $R=-0.896$ and later $R=-0.881$).

Fig. C.64 illustrates different forms of creep occurring in different materials:

(a) shows strain to return to its initial value after any time: after t_1 , when an equilibrium compliance is not yet reached or after t_2 , when an equilibrium compliance is obtained in the example. Creep and creep recovery can be described with the same func-

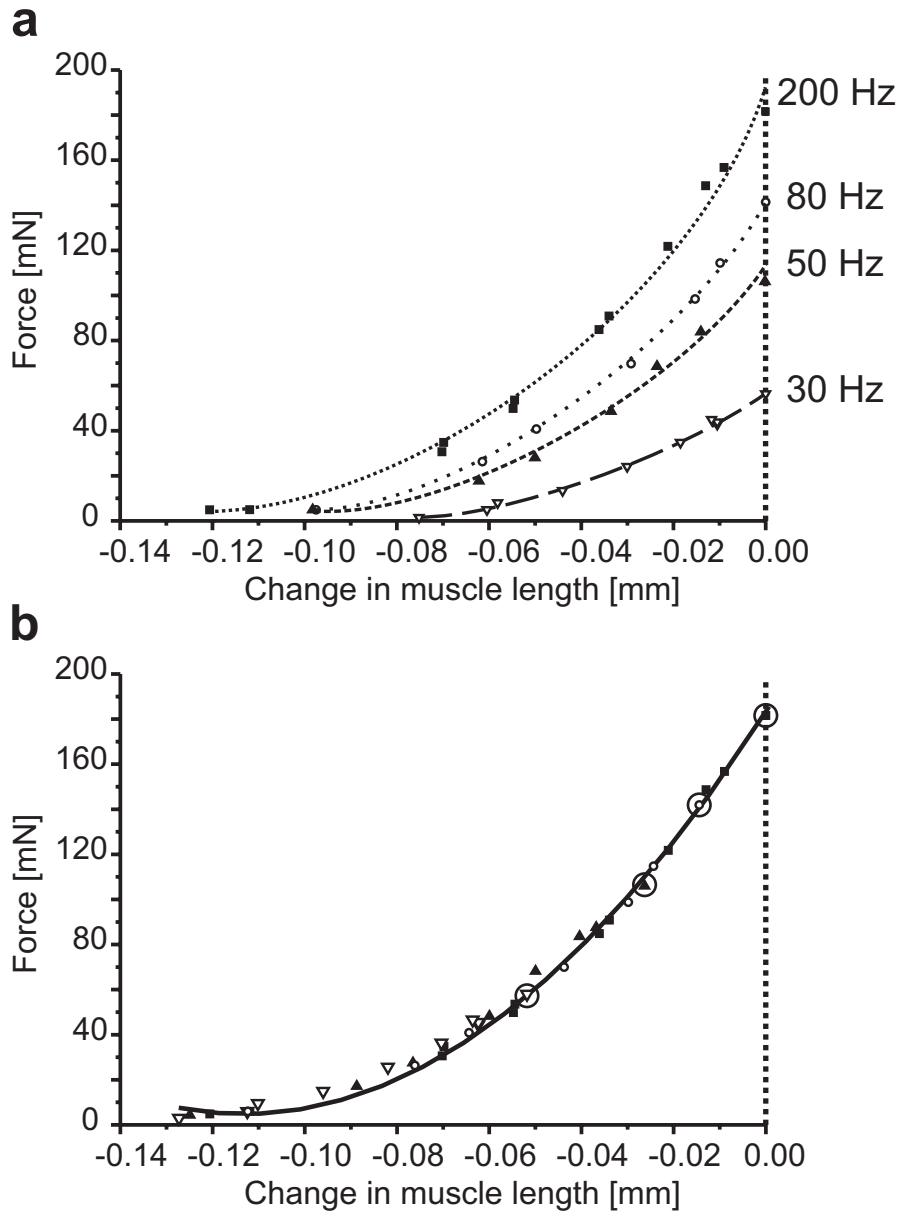


Figure C.62: Nonlinear spring-characteristics of the series elasticity in the extensor tibiae using different activation levels. **a** Fast length change in the loaded release experiment starting from different tetanical force levels. Depicted is the change in force over the resultant change in length. **b** Common parabola fit for all shifted curves in **a**.

tion, just sign is inverted. Thus, for small deformations (i.e. as long as the material does not break), a constant strain value is reached and creep recovers in a *crosslinked polymer* to 100 % (after Ferry (1961)).

(b) shows strain not to return to its initial value, creep does not recover totally. A

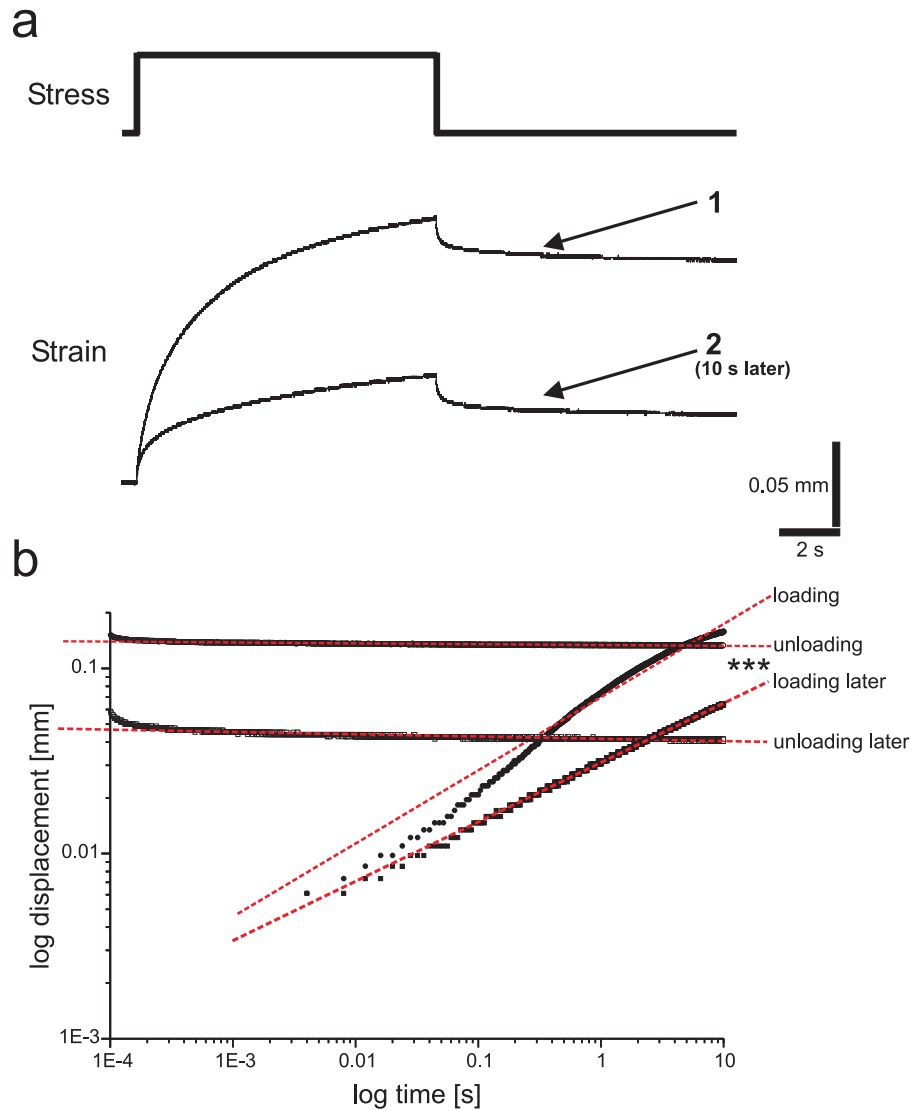


Figure C.63: *Passive extensor tibiae creep.* (a) 10 s of stress application and 10 s of release (trace '1'), repeated once (trace '2'). The second load application leads to a smaller strain increase. (b) Double-logarithmic plotting of the data shows that strain increase (creep) and decrease (creep recovery) can be fitted well with linear regressions, i.e. the courses follow a power-function characteristic (all ***).

small deformation leads to a creep approaching a constant value plus a viscous flow contribution. This viscous flow is responsible that the material does not totally recover. This is an example for an *uncrosslinked polymer*, whose threadlike molecules are not permanently attached to each other and which has no equilibrium compliance (after Ferry (1961)).

(c) shows creep in the extensor tibiae: here, it looks like an equilibrium compliance

is reached (an additional exponential RC-type growth fit is depicted), but creep does not totally recover nevertheless. The material nature of the extensor tibiae appears to be sort of inbetween the materials described in **(a)** and **(b)**. Its measured properties cannot be described satisfactorily with a linear power function model.

The above described creep properties raise the question whether it is possible for the muscle to recover from creep or whether this is an irreversible process, suggesting material damage. Fig. C.65 shows creep and incomplete creep recovery. During the recovery a short burst is applied and leads to a large contraction because the load pulling on the muscle was just slightly larger than the muscle's resting tension. After the contraction, the muscle creeps to its initial strain value (and further) again suggesting that there is no real steady state where passive tension is at steady-state. Finally, creep is reversible and muscle strain can be reset by active thick and thin filament slide.

The description and comparison of materials with creep experiments was also taken on a more quantitative level. Muscle strain and stress clamp were applied simultaneously, on one hand resulting in a few milliseconds of oscillations (Fig. C.66a), on the other hand having the advantage to measure under controlled conditions, because the initial muscle length is always the same. The time range used for calculations was in all quantitative creep examinations 85 ms. A test linear fit with a time range of 850 ms (not shown) resulted only in a slight increase of the R value. Taking such a large time range for analysis had the disadvantage, that muscle strain at large muscle stress levels could not be analysed because muscle stretch was chosen to be not too large in order to prevent muscle damage, and therefore 85 ms were chosen for determinations. As shown in Fig.C.63b, the strain courses in response to the stress levels depicted in the upper trace of Fig. C.66a are linear (all fits *** with R values ≥ 0.992), demonstrating that the courses follow powerfunction-characteristics of the form $L = C \cdot t^k$ (in comparison to this **force** step stimulus, the **length** step stimulus reponse follows $P = C \cdot t^{-k}$, see chapter C3). Conversion gives $\log(L) = \log(C) + k \cdot \log(t)$. k is the slope and $\log(C)$ the intersection with the ordinate in Fig. C.66b. C represents the amplification and should be changing with increasing stress, which is obvious from Fig. C.66b. k should be independent from stress which can also be reconstructed from Fig. C.66b, as the slopes are apparently parallel to one another.

RESULTS

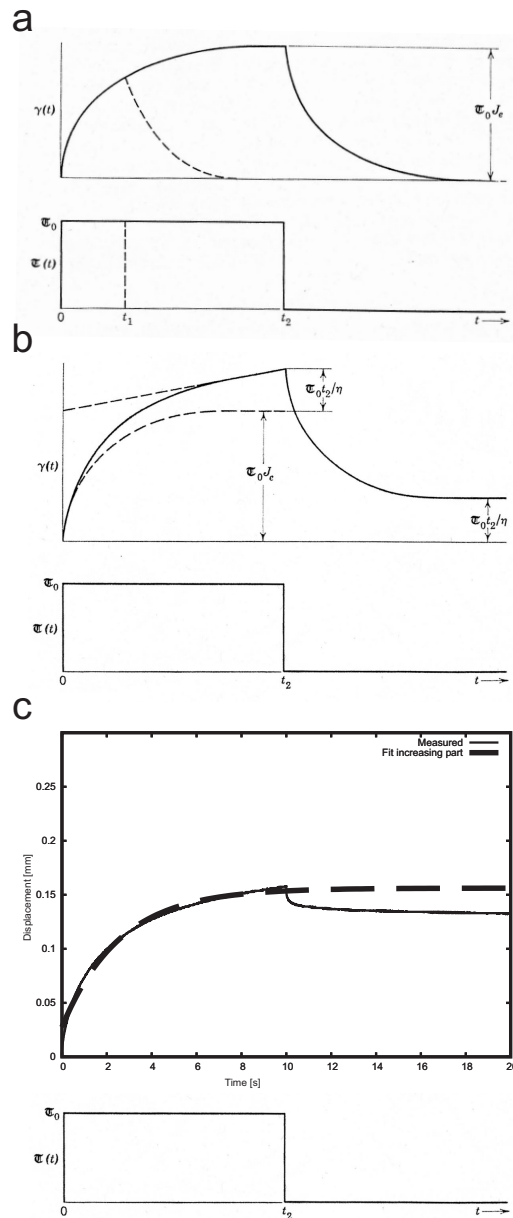


Figure C.64: Shear creep and creep recovery shown schematically for (a) a cross-linked polymer, (b) an uncross-linked polymer, (c) the extensor tibiae. (a) and (b) are adapted after Ferry (1961). The dashed line in (c) denotes an exponential RC-type growth fit.

Creeps were measured of two extensor-flexor tibiae pairs, i.e. one pair from one animal respectively ($N=2$, $n=4$). In order to compare the material properties of both muscles, strains were expressed as the ratio $\frac{C [mm]}{\text{Fibre length} [mm]}$ and are therefore nondimensional (for fibre lengths, see chapter C1). Stresses were expressed as the ratio

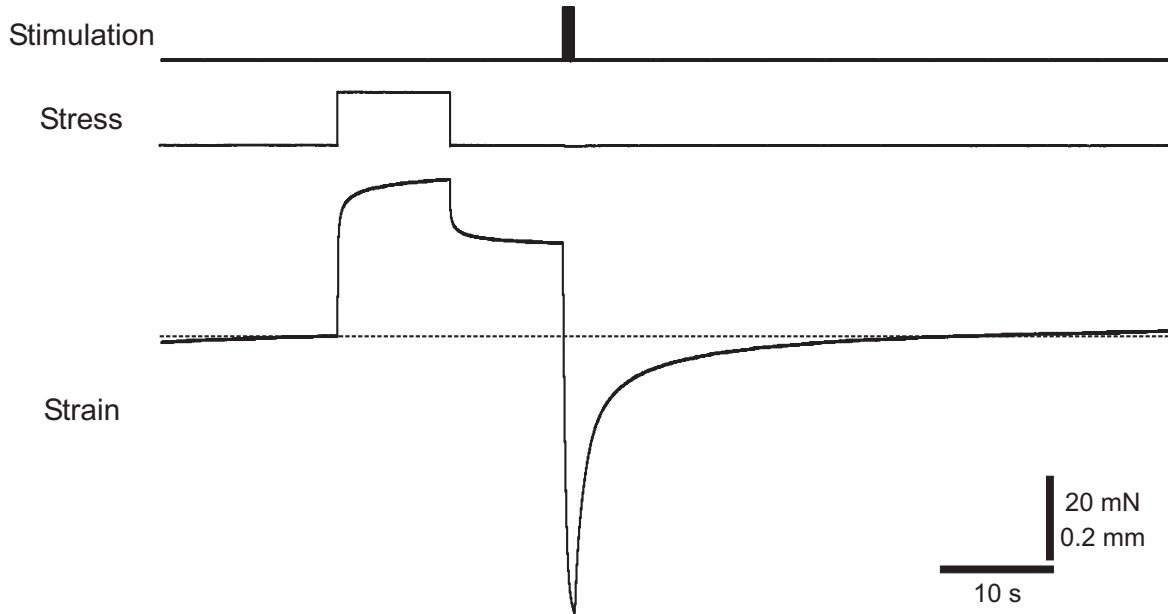


Figure C.65: Short high frequency stimulation resets extensor tibiae muscle length after load.

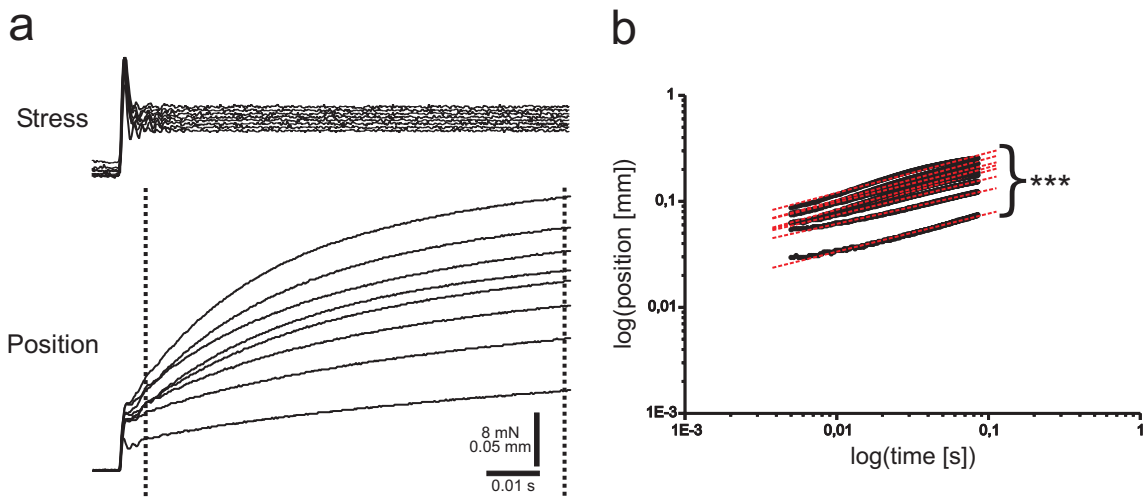


Figure C.66: Exemplary creep experiment. (a) Stress is applied to a passive muscle during simultaneous muscle stretch (upper trace). The resulting muscle creep is measured (lower trace). The vertical dashed lines indicate the time range used for calculations (in all experiments 85 ms). (b) Double logarithmic plot showing the power-function characteristics of the creeps depicted in (a) as the different creep courses have a linear developing (all linear regression fits $***$, $p < 0.001$).

$\frac{P [N]}{\text{Muscle cross-sectional area [cm}^2]}$ (for cross-sectional areas, see chapter C1). The slope $\frac{\text{Strain}}{\text{Stress}}$ gives the muscle's compliance. When plotting so (Fig. C.67a and b), two different results arise. For one muscle pair (a), the compliance of extensor and flexor tibiae match very well: $2.51 \frac{\text{cm}^2}{\text{N}}$ for the extensor tibiae ($***$, $R=0.998$) and $2.08 \frac{\text{cm}^2}{\text{N}}$ for the

flexor tibiae (***, $R=0.990$). For the other muscle pair (**b**), compliances differ a lot: $0.60 \frac{cm^2}{N}$ for the extensor tibiae (***, $R=0.974$) and $2.45 \frac{cm^2}{N}$ (***, $R=0.995$) for the flexor tibiae, the latter being in the same range of compliances than the other muscle pair (in **a**) measured.

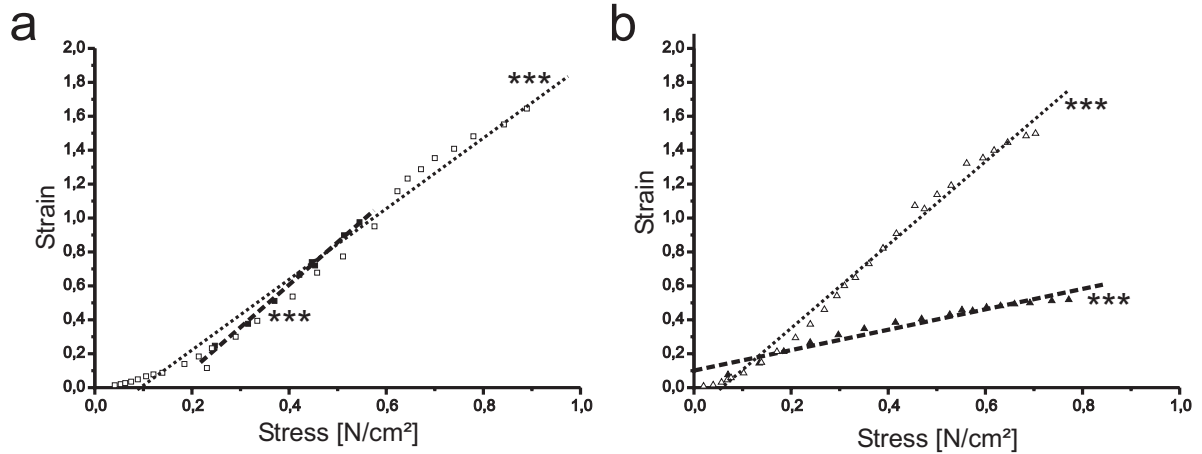


Figure C.67: Analysed creep experiments of two pairs of extensor and flexor tibiae ($N=2$, filled symbols mark extensor tibiae, open symbols mark flexor tibiae data). The time range for calculation was 85 ms for all samples. The $\frac{Strain}{Stress}$ ratio represents each muscle's compliance. Dashed lines denote extensor tibiae linear regressions (***, $R=0.998$ ($n=8$) in **a** and ***, $R=0.974$ ($n=17$) in **b**). Dotted lines denote flexor tibiae linear regressions (***, $R=0.990$ ($n=26$) in **a** and ***, $R=0.995$ ($n=27$) in **b**).

C6 Force generation under naturally occurring FT joint movement patterns

1 Extensor tibiae forces before, during and after simulated stance phase

Measuring isometric forces in animals provides the required information to characterise a muscle (chapter C2) and to be able to implement it into a model (e.g. Zajac and Gordon (1989); Brown and Loeb (2000c;b); Wagner et al. (2005)). However, exertion of pure isometric force is an almost theoretical case in stick insects, the length of a muscle is only seldom in a steady state during tetanical contraction, in humans as well (e.g. when picking up a heavy weight). This section deals with the changes of muscle contraction dynamics (force development and relaxation) and the changes of P_{max} involved when muscle length is changing.

Fig. C.68 illustrates the experimental procedure: short 200 Hz bursts were applied before muscle stretch (1), during muscle stretch (2), after muscle stretch (3-5), during muscle release (7), after muscle release (7-10). Stimulations had always the same pulse number (50), bursts 3-5 and 7-10 were equally separated by 10 s.

Calculation of active muscle forces was achieved by subtracting passive muscle force from the overall force. Fig. C.69 illustrates the subtraction procedure: referring to

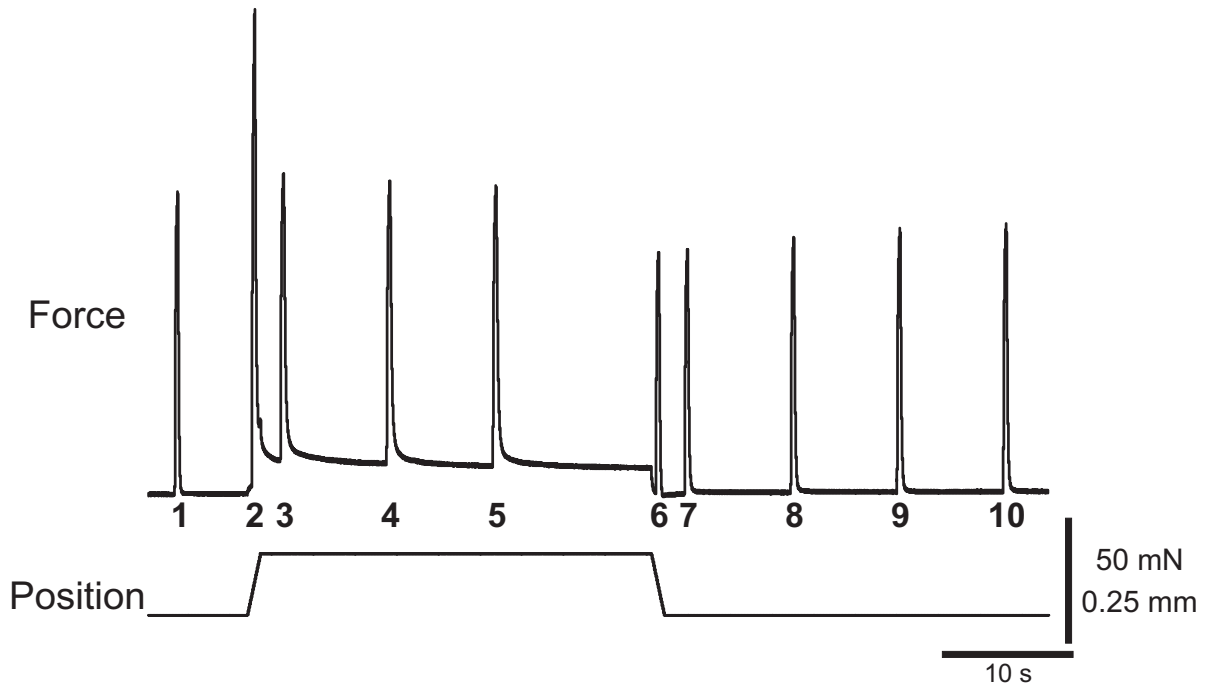


Figure C.68: Different extensor tibiae force development before and while stretching and while and after releasing the muscle. Contractions are numbered from 1-10, stimulation bursts not shown.

chapter C3, the course of dynamic passive muscle force development can be estimated by connecting start and end point in the force recording trace during simultaneous stimulation and stretch. The dashed line depicts the actual putative passive force course, that can be estimated from the experiments carried out in chapter C3. The muscle normally acts like a spring and force develops with $P(t) = C \cdot t^{-k}$. Representing passive force development with a straight line is a rather simple approximation (dotted line in C.69a). The calculated force development is shown in Fig. C.69b.

Relaxation phases were fitted with exponential decays in the same way than described in chapter C2. Additionally, rising phases were fitted with an exponential RC-type growth of the form $A = A_0(1 - e^{-\frac{t}{\tau}})$, starting at 5 % P_{max} instead of 95 % P_{max} when fitting relaxations (Fig. C.70, see also Hooper et al. (2007a)).

To give an example, fig. C.71 shows the active forces (calculated from previously subtracting passive force, see Fig. C.69) before, during and after 0.5 mm muscle stretch, i.e. contractions 1-3 in Fig. C.68. P_{max} increases during stretch (2) and is slightly in-

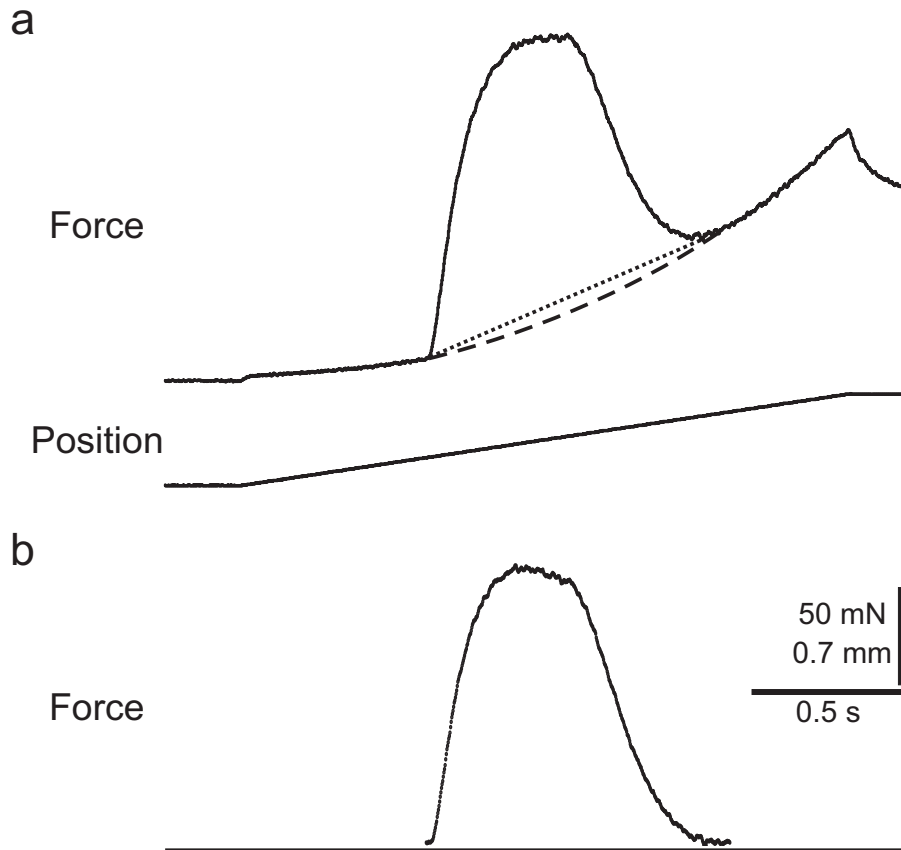


Figure C.69: Calculation of active isometric force development by subtracting passive forces (dashed line in (a) denotes putative dynamic passive force generation, the dotted line in (b) denotes passive force approximation by simple interpolation).

creased after stretch (3) compared to prestretch (1). The slopes of force increase and decay appear to be affected as well (red fits: exponential RC-type growth fit, green fits: exponential decay fits).

Fig. C.72 illustrates the occurring effects in response to 1s ramps of different amplitude (0.1, 0.25, 0.5, 0.75 mm, in total N=5). Time constants of exponential RC-type growth fits vary a lot between experiments: at prestretch (1), min. 0.040 s, max. 0.069 s (a(i)). This makes a general description of the effect difficult. Normalised data (Fig. C.72 a(ii)) show mostly a slight increase of τ during stretch (2), tendencies of a continuing increase after stretch (3-5) and nearly prestretch levels after (relaxation (7-10) with the relaxation ramp (6) showing τ values between after stretch and after relaxation values. τ increases a little during contractions 7-10. In general, the described effects appear to be rather weak and are the more pronounced, the more the muscle was

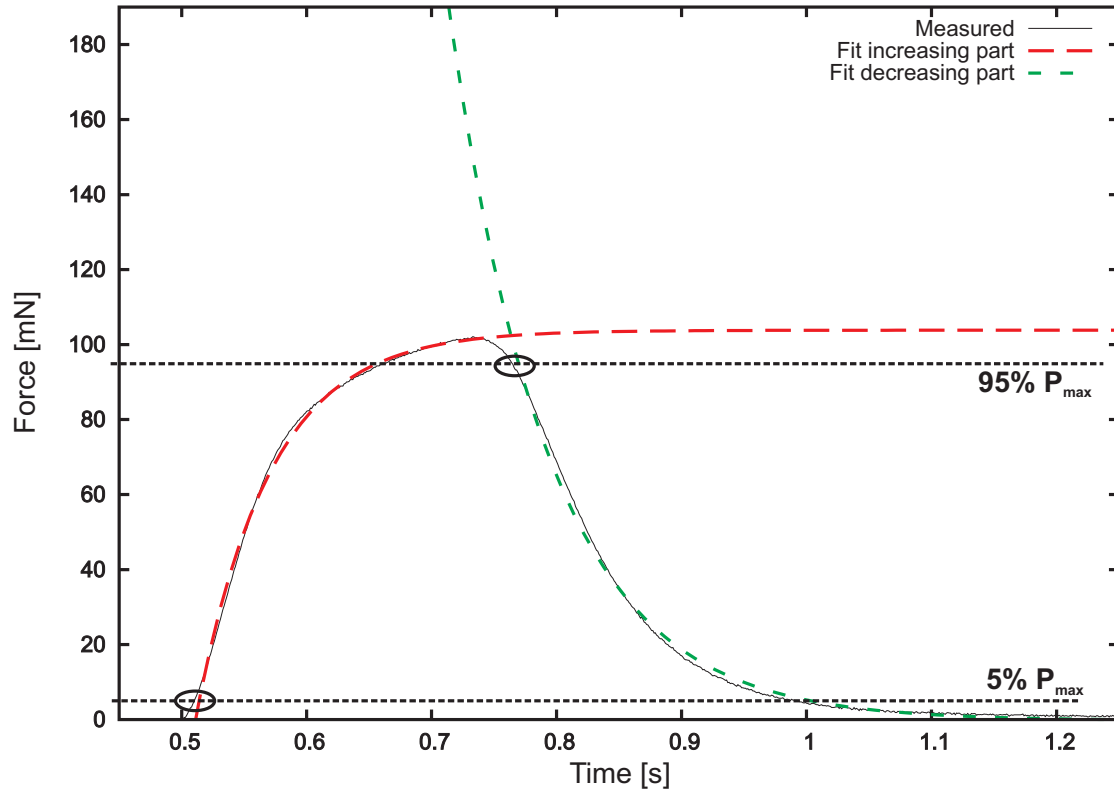


Figure C.70: Calculation of the exponential RC-type growth ($A = A_0(1 - e^{-\frac{t}{\tau}})$) fits and exponential decay ($A = A_0e^{-\frac{t}{\tau}}$) fits starting at 5% P_{max} and 95% P_{max} respectively, indicated by two ovals.

stretched.

This is different for relaxation phase time constants: prestretch values are much less scattered (min. 0.055 s, max. 0.066 s) and muscle stretch causes are very distinct increase in all experiments (Fig. C.72b(i)). Relaxation causes in turn a very clear drop to prestretch levels. After relaxation, τ remains rather stable with a little tendency to decrease at small stretch (0.1, 0.25 mm) and to increase at larger stretch (0.5, 0.75 mm). As described for the force increase time constant, effects are more distinct, the more the muscle was stretched (comparing the green data points (0.75 mm ramp amplitude) with the light blue ones (0.1 mm ramp amplitude) in b(ii)).

The course of P_{max} can be very well described with the characteristics presented in chapters C4 and C5: prestretch P_{max} shows the large variation between animals that was already described in previous chapters (min. 99.45 mN, max. 156.01 mN, Fig.

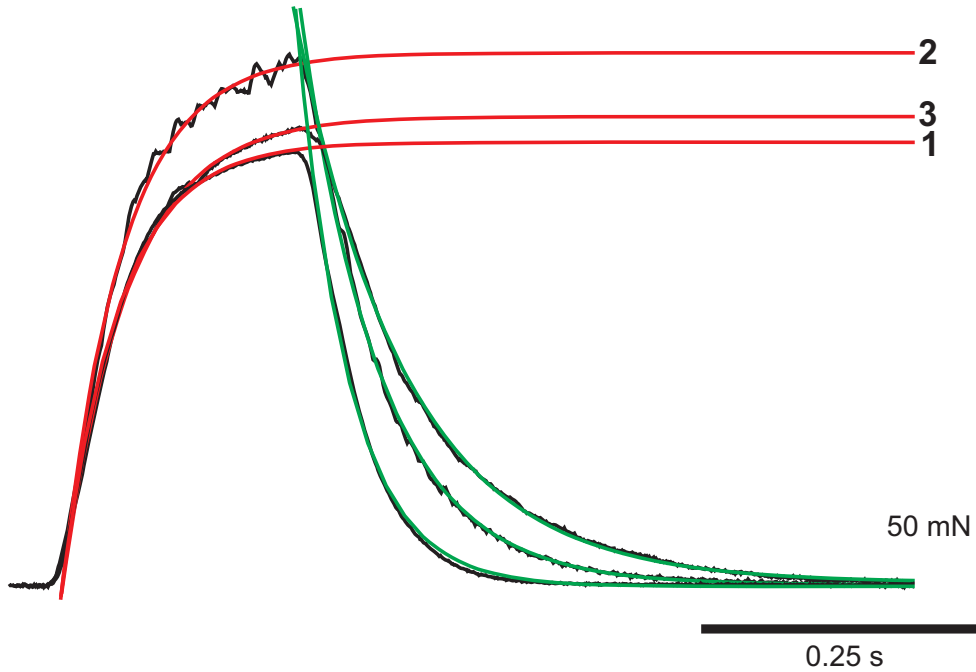


Figure C.71: Overlaid isometric contractions 1, 2 and 3 and their fits. Red solid lines denote exponential RC-type growth fits, green solid lines denote exponential decay fits.

C.72c(i)). Muscle stretch causes an immediate increase of P_{max} because of the negative shortening (i.e. ‘positive lengthening’) velocity applied to the muscle during contraction. The double hyperbolic characteristic shown in Fig. C.52 predicts an increase of 50 % when muscle is lengthened with velocities between 0.25 to 0.75 $\frac{mm}{s}$. This is exactly what happens: the higher the lengthening velocity, the bigger the increase of P_{max} (datapoints at (2) in c(ii)). After stretch, P_{max} remains rather stable at the same P_{max} -level following the force-length characteristic (chapter C2): 0.25 mm stretch elicits the largest increase, 0.5 mm stretch causes already a slight P_{max} decrease. This is what data in Figs. C.23 and C.24 in chapter 4 would predict because of the descending limb of the force-length relationship. This becomes even more distinct at larger stretch (0.75 mm): P_{max} is decreased to about 50 %. During and after relaxation, P_{max} -values are approximately at prestretch levels, with a tendency to increase slightly when previously applied stretch amplitude was large (green and red trace in c(ii)).

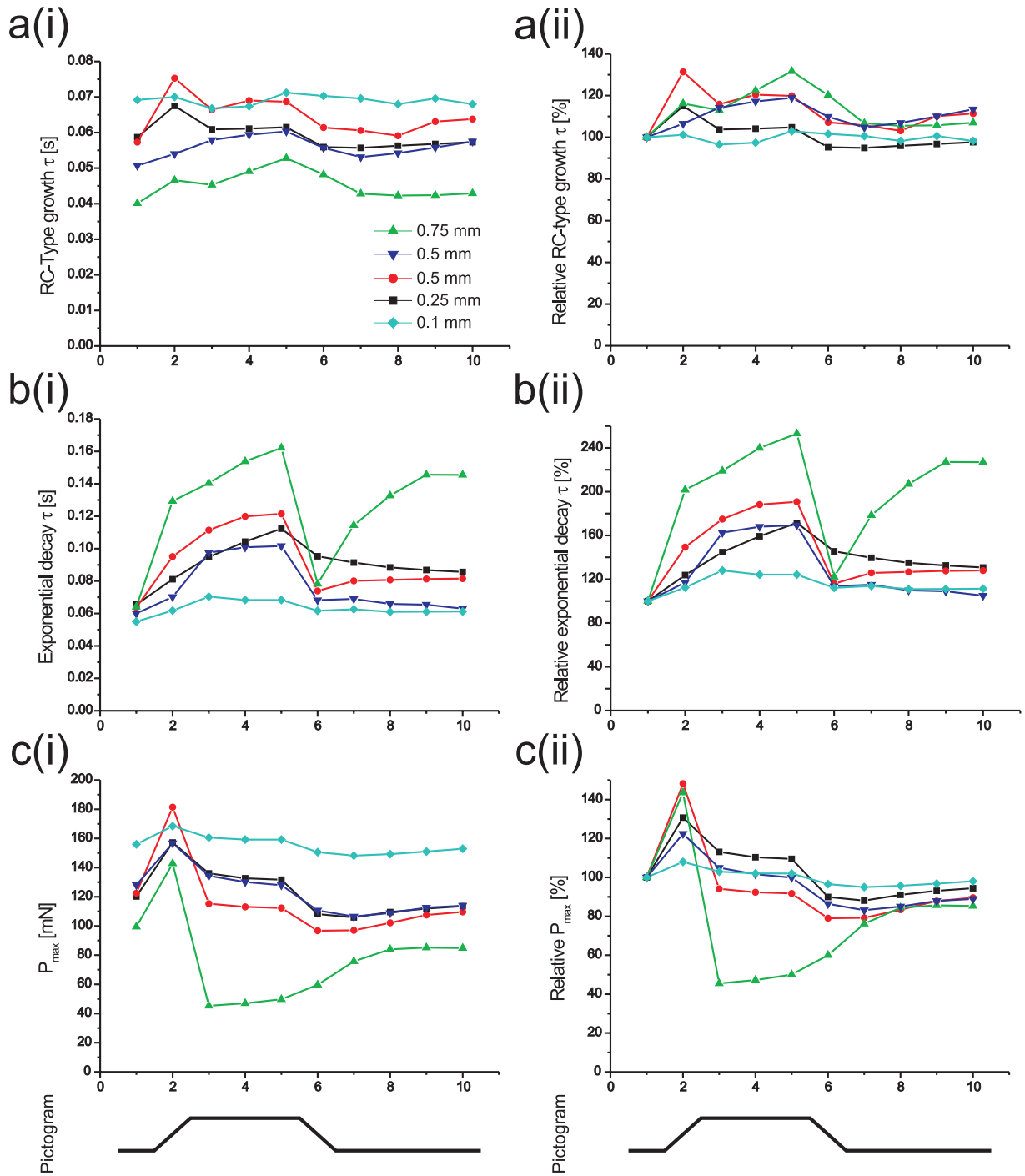


Figure C.72: Time constants of RC-type growth (a(i) and a(ii)), exponential decay (b(i) and b(ii)) and P_{max} (c(i) and c(ii)) at different muscle lengths (see Fig. C.68). Ramp amplitudes depicted in a(i) as legend: 0.1 to 0.75 mm. Left column depicts absolute data values, right column shows data that were normalised to prestretch values. All stretch and relaxation ramps had a duration of 1 s.

2 Extensor tibiae forces at the simulated transition from swing to stance phase

Development of forces was measured in all kinds of ways within this thesis. It turns out that the time period after the end of motoneuronal input (e.g. stimulation pulses) is crucial for antagonistic movement because the agonistic muscle does not start to relax immediately and because relaxation can become very slow, depending on the circumstances (see above and data in chapter C2).

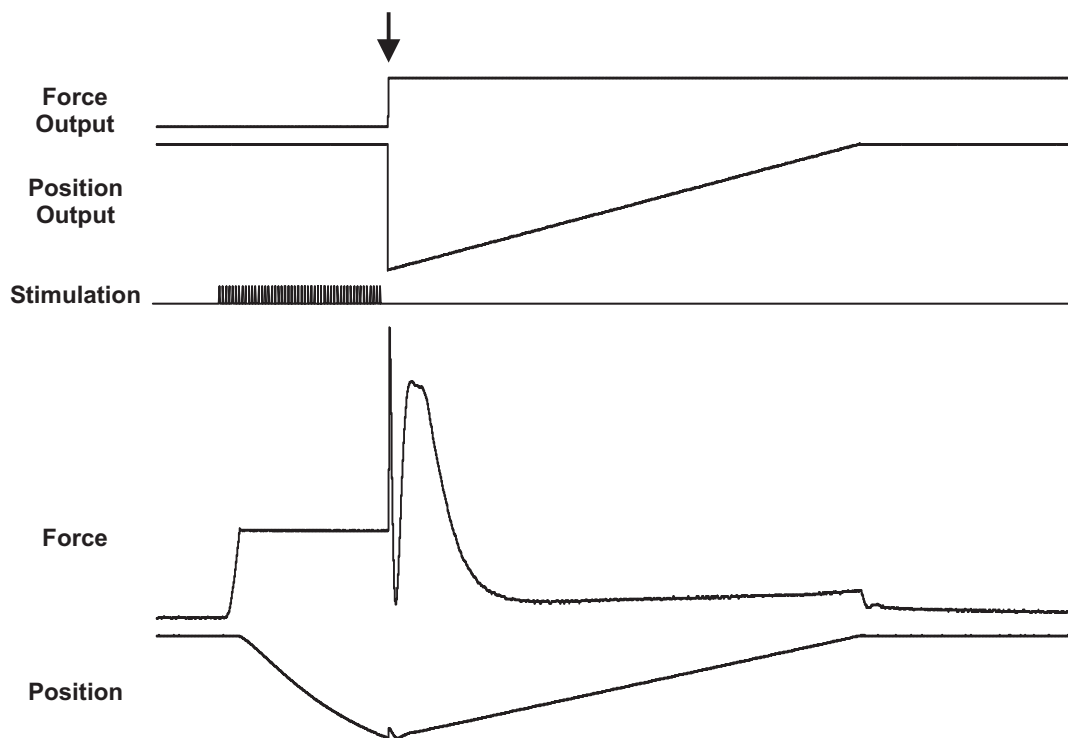


Figure C.73: Overview of the experimental time course. The extensor tibiae develops isometric force in response to a tonic stimulation burst initially and starts to shorten isotonicly when the developed force becomes larger than the force applied on the lever arm of the Aurora's servo motor. A ramp mimicking antagonistic muscle movement pulls the muscle back to its initial position at a desired point in time (marked as arrow) with the desired velocity. The amount of force generated during a ramp of constant velocity is termed 'isovelocity force'. The switch from force to length control is accompanied by a large force artefact and small position artefact. Additionally, force and position output are also depicted. In the experiment, it was essential to record these traces as well, because the programmed sequencer script involved these recordings (see Appendix section).

The following set of experiments deals also with this transition: the period of time, where limb movement is first determined by agonistic muscle shortening (e.g. tibial

extension) subsequently switching to limb movement being determined by antagonistic muscle shortening (e.g. tibial flexion). Fig. C.73 shows the experimental procedure investigating this topic: an extensor tibiae muscle is stimulated tonically at 200 Hz and develops force isometrically until it becomes stronger than the force applied on the Aurora's lever arm. As a consequence, it starts to shorten isotonicly. At a given time (arrow in Fig. C.73), slightly before or after the stimulation's last pulse, the muscle is stretched by a ramp of desired speed back to its pre-stimulus length. Thus, two parameters were altered: start time of the ramp and ramp speed. Unfortunately, the fast switch from force to length control involves a relatively large artefact in the force trace and a small one in the position trace. Smoothing of the force signal (see 'Materials and Methods') could not reduce the size of this artefact.

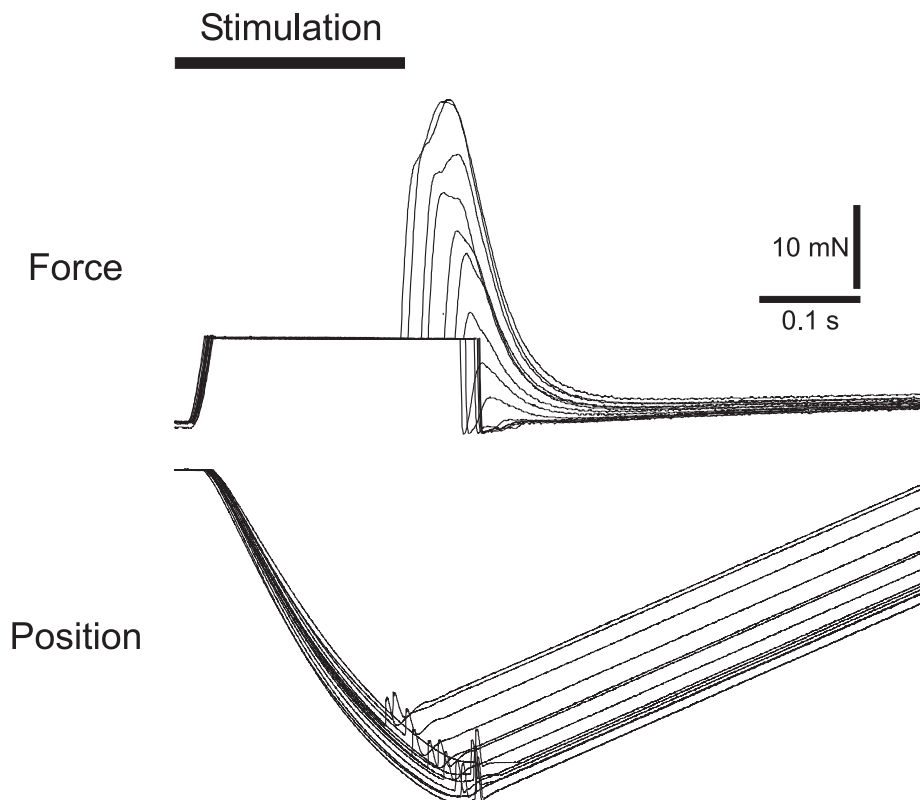


Figure C.74: Multiple overlay of active isovelocity forces occurring in response to ramps starting at different times relative to the end of the muscle stimulation ($N=1$, $n=11$). Artefacts (see Fig. C.73) were removed.

Fig. C.74 shows multiple, overdrawn isovelocity force traces in response to ramps starting at different times during and after stimulation, ramp speed was in this exam-

ple $0.66 \frac{mm}{s}$ ($N=1, n=11$). At ramp starts > 0.08 s after the last stimulation pulse, force has diminished almost completely.

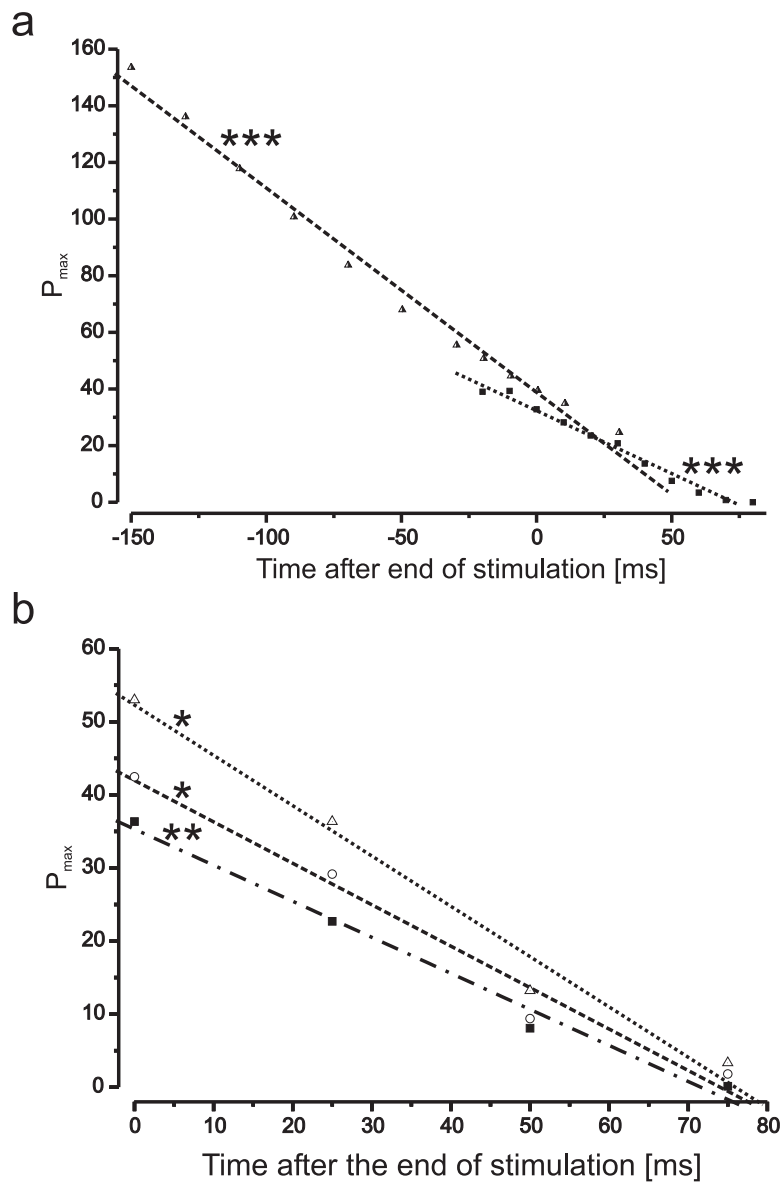


Figure C.75: Maximally actively generated forces occurring in response to different ramp speeds with linear fits. (a) $0.86 \frac{mm}{s}$ (dashed line, *** $p < 0.001$; $N=1, n=12$) and $0.66 \frac{mm}{s}$ (dotted line, *** $p < 0.001$; $N=1, n=11$). (b) From one exemplary animal ($N=1$): $0.33 \frac{mm}{s}$ (dashed-dotted line, ** $p = 0.007$, $n=4$), $0.66 \frac{mm}{s}$ (dashed line, * $p = 0.013$, $n=4$) and $1.32 \frac{mm}{s}$ (dotted line, * $p = 0.010$, $n=4$). All stimulations consisted of 50 pulses at 200 Hz.

Fig. C.75 shows evaluations of experiments, where ramps were started throughout the second half of stimulation (-0.15 s to 0 s (a)) and after the stimulation until ramp

stretch could not anymore elicit any measureable forces (0 s to 0.08 s, **(b)**). Time = 0 s corresponds to the time of the last stimulation pulse in each single experiment. The earlier the ramp start, the larger the maximal force response (P_{max}). After stimulation, force occurrence arises from the slow force decrease of isotonic contractions (Hooper et al. (2007a)) combined with the effect of lengthening a muscle that still tries to shorten further, see Hill characteristics at negative contraction velocities (chapter C4). This characteristic explains P_{max} to be larger at faster ramps mimicking faster stance phases (see C.75b). The faster the ramp, the steeper the slope of the linear data fits ($-0.493 \frac{mN}{ms}$ at $0.33 \frac{mm}{s}$, $-0.567 \frac{mN}{ms}$ at $0.66 \frac{mm}{s}$ and $-0.689 \frac{mN}{ms}$ at $1.32 \frac{mm}{s}$). Up to 75 ms after the last stimulation pulse, the extensor tibiae shows force development in response to a ramp resetting the muscle to its original position. After 80 ms, the muscle ceases to generate force, even when being stretched with the fastest ramp ($1.32 \frac{mm}{s}$).

From the insights gained in chapter C3 (that passive muscle forces can play a major role), it was necessary to look at the passive dynamic force development involved as well. Fig. C.33 demonstrated that passive dynamic forces of extensor and flexor tibiae can become remarkably large (> 50 mN when stretched fast starting at 90° FT joint angle). Passive force responses to the same ramp stretch velocities which were used in Fig. C.75b ($0.33 \frac{mm}{s}$, $0.66 \frac{mm}{s}$, $1.32 \frac{mm}{s}$) are displayed in Fig. C.76: maximal dynamically generated force was 6.26 ± 0.31 mN (N=1, n=5) in response to the fastest ramp.

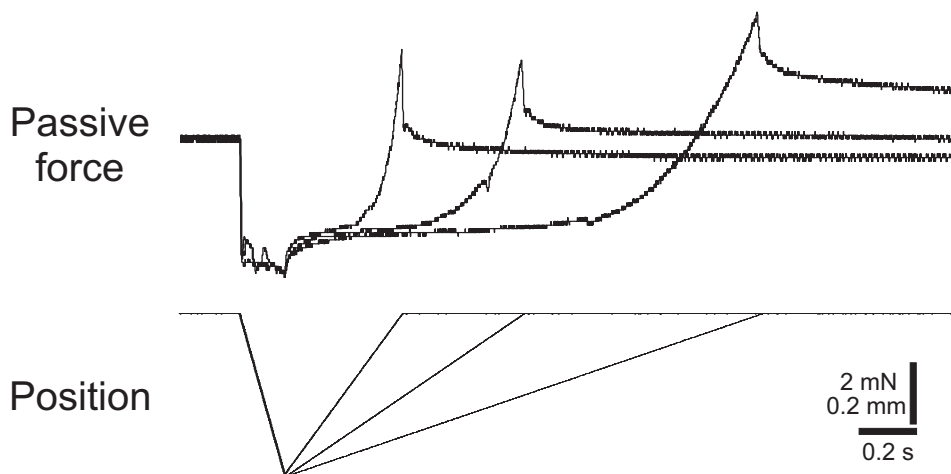


Figure C.76: Multiple overlay of passive isovelocity forces occurring in response to ramps of different speed ($0.33 \frac{mm}{s}$, $0.66 \frac{mm}{s}$, $1.32 \frac{mm}{s}$).

3 Interaction of agonistic and antagonistic passively and actively generated forces during simulated swing and stance

Chapters C2-C5 dealt with the descriptions of either isometric passive, isometric active, isotonic passive or isotonic active forces. Measurements were all done by directly measuring at the muscle (either extensor or flexor tibiae) and different issues were highlighted in a very isolated way. In order to get a broader picture, the following experiments were conducted while leaving the whole middle leg intact, either the extensor tibiae nerve nl3 or the flexor tibiae nerve ncr were stimulated with 200 Hz and tibia movement dynamics were tracked with a highspeed camera (see 'Materials and Methods' section).

3.1 Simulating tibial swing / stance phase

Different numbers of pulses were tested and FT joint angular displacements were tracked vs. time. Fig. C.77 illustrates the fast tibial movement beginning in all experiments at 0.06 s, i.e. 0.01 s after stimulation begin (the first 50 ms tracked the resting leg before stimulation begin). This is consistent with the twitch latency determinations shown in Tabs. C.3 and C.4. Initial tibia position in extensor tibiae experiments was found to be $102.2 \pm 0.3^\circ$ (N=1, n=3) and $88.6 \pm 2.9^\circ$ (N=1, n=3) in flexor tibiae experiments. A paired t-test showed the values to be significantly different from each other (*, $p < 0.02$). Thus, as antagonistic innervation was either crushed or cut (see *Materials and Methods* section), the lack of antagonistic tonic motoneuronal firing seems to have an impact on tibia rest position. Either when the extensor tibiae was silent (resulting in a more flexed tibia rest position) or when the flexor tibiae was silent (resulting in a more extended tibia rest position). The tibia appears to be extended and flexed with approximately the same speed because the individual angular increasing (at extensor tibiae stimulation) and angular decreasing phases (at flexor tibiae stimulation) in Fig. C.77a parallel each other until the maximal deflection is reached for each stimulation. This maximal deflection is 30° to 180° , which is consistent with the maximal physiological working range (see above). At stimulation of both extensor and flexor tibiae, relaxation (i.e. when the tibia starts to return to its rest position) after 20 pulse stimulation starts after the same time t_1 (see Fig. a). When a maximal angle is reached and

RESULTS

the tibia cannot be extended or flexed further, the tibia remains at the same position and starts to relax when stimulation is over (extensor tibiae at 40 pulses and flexor tibiae at 30 pulses).

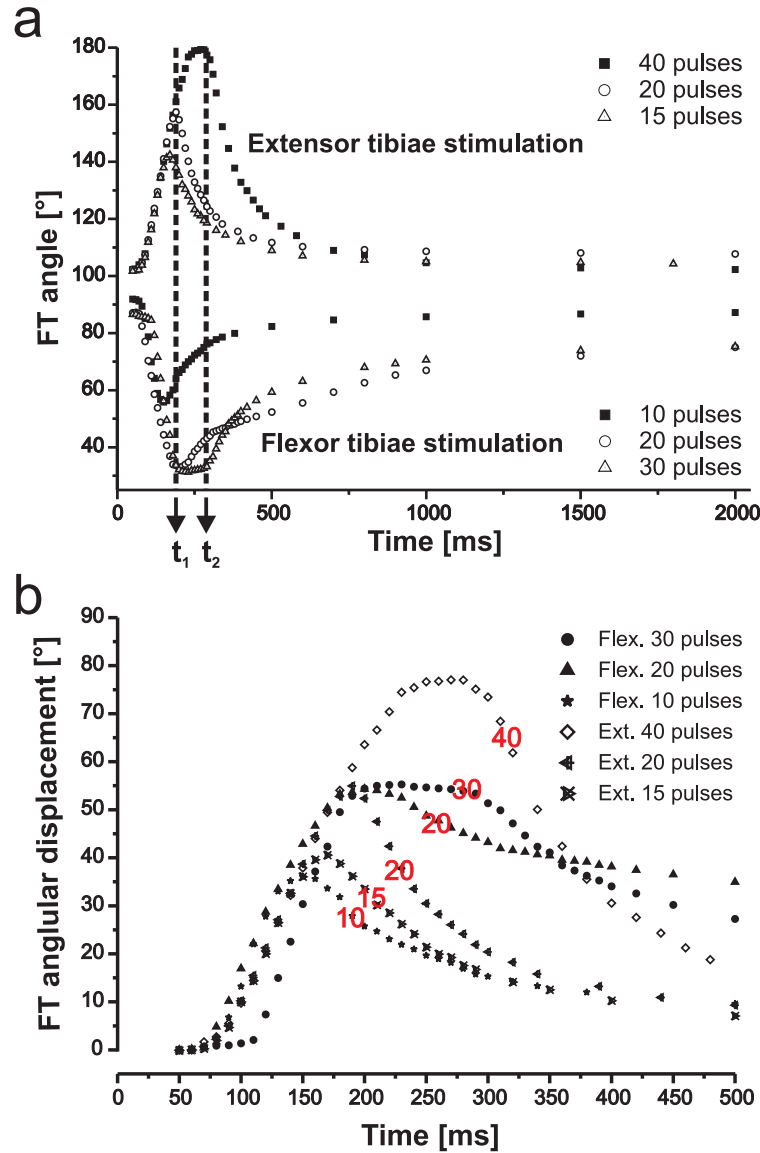


Figure C.77: Video analysis of tibia movement during and after 200 Hz stimulation of either extensor ($N=1$; 15, 20, 40 pulses) or flexor tibiae ($N=1$; 10, 20, 30 pulses). (a) Absolute tibial deflections over time. t_1 marks relaxation starts after 20 spike duration of extension and flexion respectively and t_2 after maximal extension and flexion. (b) Relative angular displacement over time. Numbers in red denote stimulation pulse number. The relaxation start of the stimulated muscle (i.e. when the tibia starts to return to its rest position) is consistent with the stimulation pulse number, no matter what muscle (extensor or flexor tibiae) was activated.

t_2 marks the relaxation start after having reached maximal possible angular deflection. The whole relaxation time course (until 2000 ms) looks as if it were exponential, but semi-logarithmic plotting did not confirm that (not shown). Maximal tibial extension is obtained after 40 pulses, maximal tibial flexion is obtained after 20 pulses.

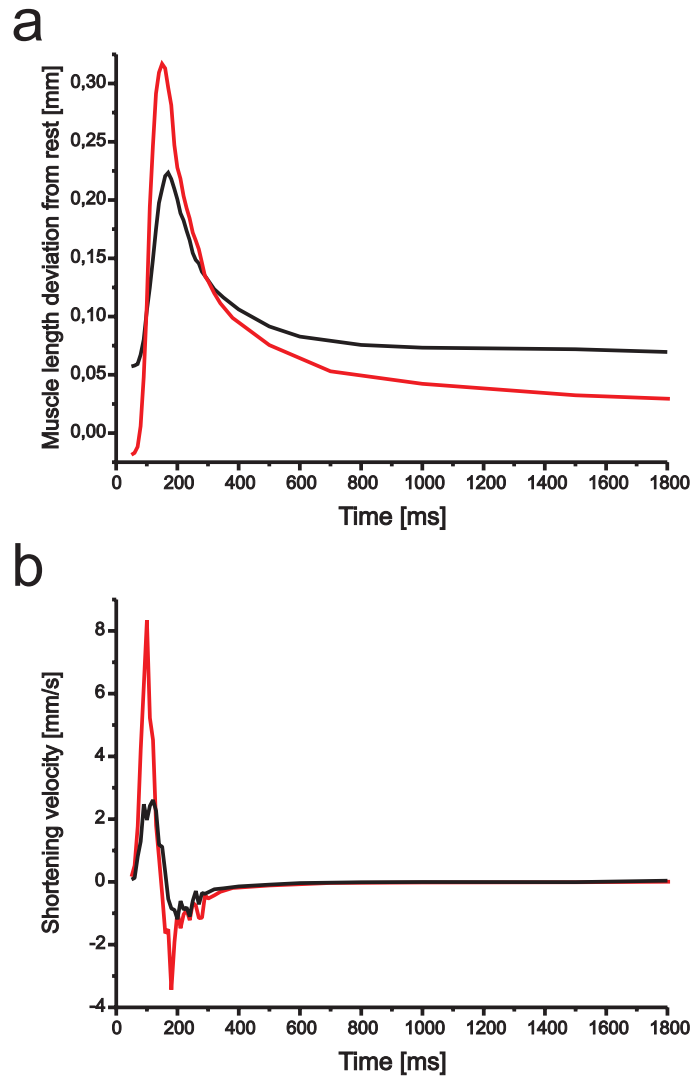


Figure C.78: Calculated extensor and flexor tibiae muscle length deviation from rest vs. time (a) and the movement's shortening velocities vs. time (b). The example shows extensor tibiae stimulation with 15 pulses (black solid lines in (a) and (b)) and flexor tibiae stimulation with 10 pulses (red solid lines in (a) and (b)). Shortening velocity data are gained from calculation of the slopes between datapoints (1st order derivation) in (a) without any smoothing.

Fig. C.77b shows the first 0.5 s of all tibial displacement traces starting at 0°: no matter if extensor or flexor tibiae was stimulated, relaxation start is pulse number dependent,

i.e. post-flexion relaxation after 10 pulses starts before post-extension relaxation after 20 pulses etc. Time courses of tibial angular displacement at extensor tibiae stimulation with 15 pulses and of flexor tibiae stimulation with 10 pulses are rather similar (see Fig. C.77b), but the actual calculated muscle length changes vs. time for both muscles under consideration of their individual moment arm lengths look very different (Fig. C.78a).

The flexor tibiae experiences a much larger length change than the extensor tibiae but peaks at nearly the same time. Thus, the **mean** shortening velocity of the flexor tibiae is supposed to be twice as large compared to the extensor tibiae when its moment arm is twice as long. Nonetheless, the **maximal** calculated shortening velocities of extensor and flexor tibiae can vary far more than twofold, which is illustrated in Fig. C.78b: the flexor tibiae reaches a maximum velocity of $8.34 \frac{mm}{s}$ after 100 ms and the extensor tibiae reaches a maximum velocity of $2.61 \frac{mm}{s}$ after 120 ms.

3.2 Simulated swing relaxation at maximal tibia extension

The next approach was to test whether pulse number has an impact on the tibial return dynamics after extension, given the maximal tibial extension angle is the same at all stimulations. Stimulation consisted of either 20, 40, 60, 80, 100, 120 or 140 pulses at 200 Hz with the antagonist's nerve (*ncr*) being cut, a paradigm already used in section 1.4 of chapter C2. The idea was to stimulate the muscle long enough to make it extend the tibia maximally (180°) and to stimulate it then even further. Fig. C.79a shows neither 20 pulse stimulation to be sufficient to extend the tibia maximally (max. angle 145°), nor 40 pulse stimulation (max angle 176°). 60 pulses and more led to a complete extension and even further. Interestingly and not expected, the tibia can be extended more than 180° when stimulation is continuing (maximally 184°). In Fig. C.79b, tibia movement is translated into extensor tibiae muscle length ($90^\circ = \text{rest angle} = 0$). Chapter C1 described the relation between muscle length and joint angle in great detail and showed that muscle length deviated from the cosine course in the range of extreme angles, i.e. 30° and 180° . This deviation is necessary because the joint would not be able to move if the two limbs of a joint (femur and tibia) were in line with the operating force vectors ('mechanical dead centre'). As the tibia can hardly be returned in such extreme positions ($175\text{-}185^\circ$, Fig. C.79a), the different relaxation time courses

in response to different stimulation durations depicted in Fig. C.79a and b are hard to interpret because it is not clear whether this movement dynamics effect comes from the fact that the joint is close to being in a dead centre or whether this effect arises from the increasing τ described in chapter C2.

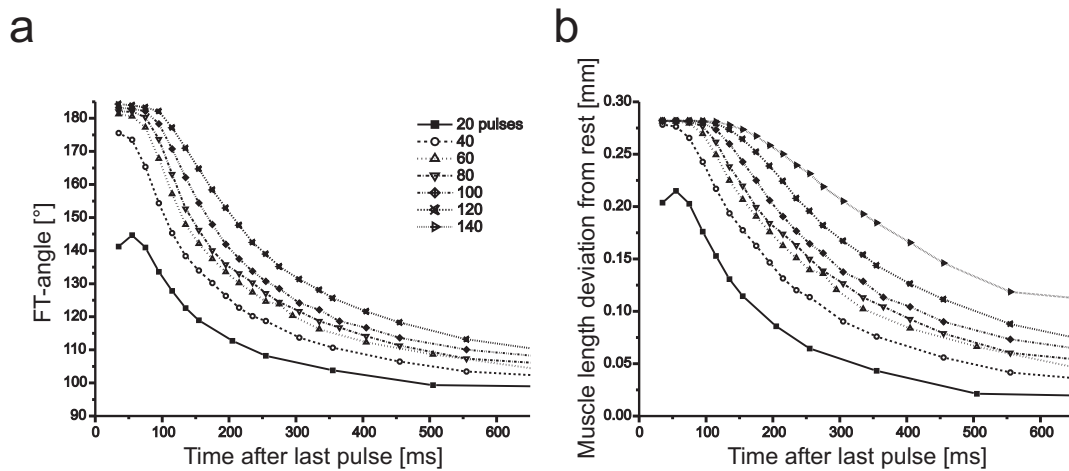


Figure C.79: (a) FT joint angle plotted over time after the last 200 Hz stimulation pulse (pulse number legend is displayed as well). Additionally (b), extensor tibiae muscle length was plotted vs. time under consideration of extensor tibiae moment arm length (0.282 mm, see chapter C1). Moment arm length was calculated to be maximal at 185°: 5° were subtracted from all calculated joint angles because of the muscle being close to a mechanical dead centre (see text for details).

3.3 Simulated swing relaxation after hitting an obstacle

As could already be demonstrated in chapter C2, different stimulation durations have an impact on the subsequent muscle relaxation phase and on the delay of this relaxation in the isometric domain. The above described experiments attempted to test this aspect on a more physiological level, i.e. a real tibia movement. The aim of this study was to look whether prolonged extensor tibiae activity is reflected not only in longer muscle relaxation, but also in longer tibia restoring dynamics. As middle leg swing phases vary in the number of action potentials generated by the FETi motoneuron (see chapter 4), it needs to be clarified to which extent the subsequent tibia movement dynamics are biased by this fact. The previous examination (Fig. C.79a and b) could not satisfactorily answer this question, because maximal possible tibia extension involves mechanical difficulties that complicate interpretation of the results (see above). In order to overcome the difficulties of a mechanical dead centre, the exper-

imental approach was slightly changed in the following investigation. In contrast to the previous study, extreme tibia extension ($> 140^\circ$ FT joint angle) was blocked with a heavy pen (Faber-Castell) mounted on a micromanipulator (see Fig. C.80, exp. 1). With this setting, the tibia position from which the tibia restoring process started was always the same, no matter how long the extensor tibiae muscle was stimulated. The stimulation paradigm was the same as in the previous section.

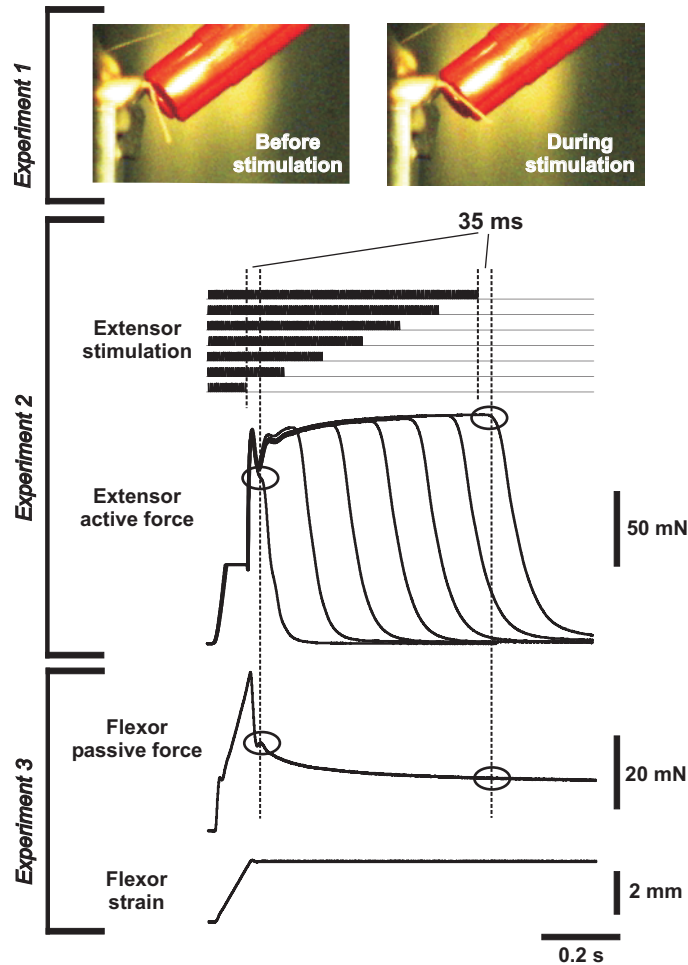


Figure C.80: Combination of three kinds of experiments: (exp. 1) High-speed video tracking of tibia movement achieved by 200 Hz extensor tibiae stimulation of different duration (20-140 pulses). Extreme tibia movement is blocked by a heavy pen (Faber-Castell). Two still photographs are shown: before stimulation begin and during stimulation when the tibia is blocked by the pen. (exp. 2) Isometric force measurement at 200 Hz stimulation of different duration (20-140 pulses). (exp. 3) Measuring passive flexor tibiae force by muscle stretch mimicking tibia movement in amplitude and duration (0.28 mm in 0.09 s, adjusted amplitude and time to exp.1). Exps. (2) and (3) are on the same time scale, the dashed lines indicate time after the stimulation end at 20 and 140 pulses as well as 35 ms after, as this was the relaxation movement begin at all stimulations.

In Fig. C.81, exp. 1, tibia relaxation angles were plotted vs. time after the last stimulation pulse: the relaxation movement starts later and is slower the longer the muscle was stimulated.

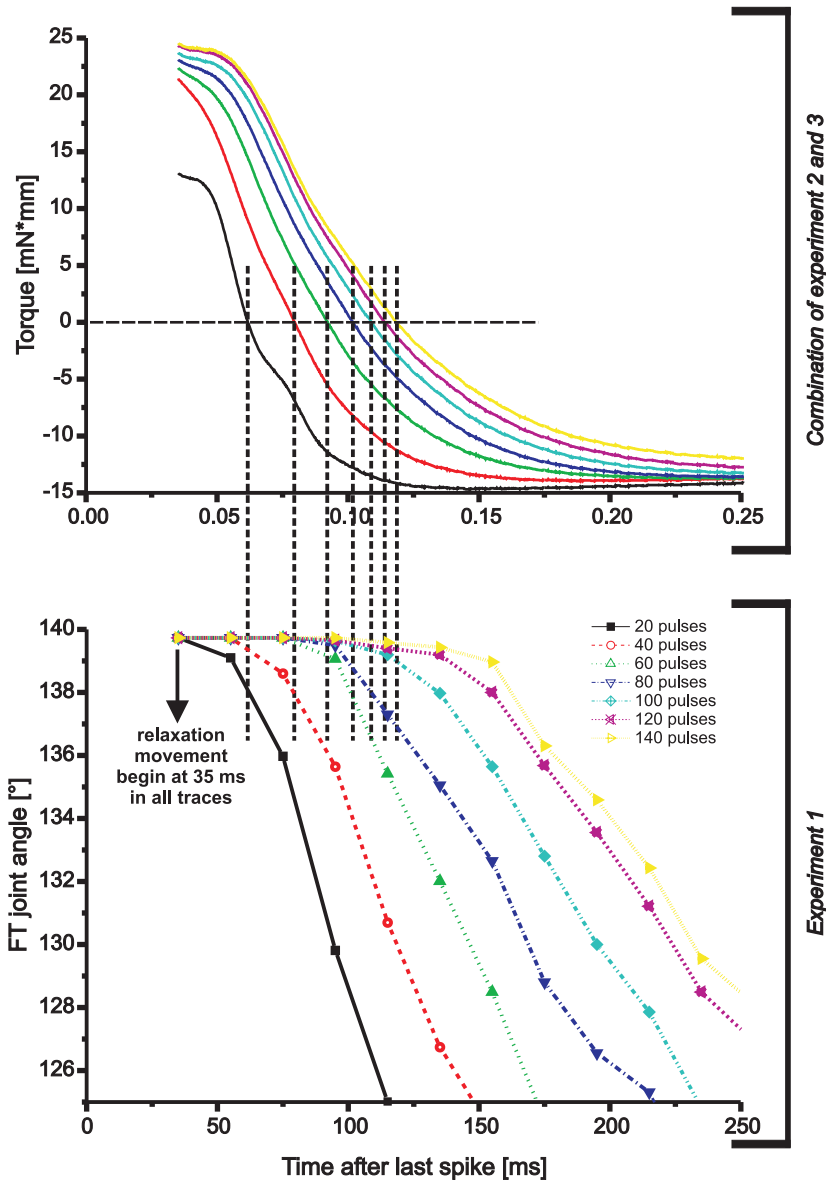


Figure C.81: Combination of three kinds of experiments. (exp. 1, lowest trace) Analysis of high-speed video tracking of tibia movement achieved by 200 Hz extensor tibiae stimulation of different duration (20-140 spikes). (exps. 2 and 3, shown above) Calculated torques (subtraction of passive flexor tibiae forces of the active extensor tibiae forces shown in Fig. C.80) taking extensor and flexor tibiae moment arm lengths into account (see chapter C1).

As limb relaxation in general involves the interaction of agonistic and antagonistic

muscles, isometric extensor tibiae force at 200 Hz stimulation of different duration (20-140 spikes) was measured (Fig. C.80, exp. 2) and, additionally, the flexor tibiae was stretched with a ramp mimicking tibia extension amplitude and duration tracked by the camera (Fig. C.80, exp. 3). With the intention to reconstruct tibial relaxation dynamics, subtractions of passive flexor torques from the active extensor torques are displayed in Fig. C.81, the combination of exps. 2 and 3. Comparison of the times where the individual torque traces cross 0 mN*mm with the movement traces shown underneath (Fig. C.81, exp. 1) shows satisfying accordance. The stimulation-history dependent effect being an intrinsic property of the extensor tibiae affects the different tibial movement return dynamics. Magnitude and time course of passive flexor forces give a good reference point in order to understand the actual begin of relaxation.

D. Discussion

Biomechanical muscle investigations were performed in order to characterise mainly the extensor tibiae, and in parts the flexor tibiae, of the stick insect *Carausius morosus*. The basic idea of these examinations consisted in the desire to understand the operation of a neuromuscular system (i.e. examining motoneuron output and muscular properties in a functional context) by taking a simply innervated leg muscle (Blickhan et al. (2003); Hooper and Weaver (2000)). The need for this investigation was particularly high as the stick insect presents a very well explored system in terms of motoneuronal activity, however as yet little is known on the direct translation of motoneuronal action potentials into muscle activity with an exception for muscle force generation in response to chordotonal organ stimulation (Storrer (1976); Storrer and Cruse (1977); Bässler and Stein (1996)). The extensor tibiae is a particularly good candidate, as it is innervated by just three motoneurons (Bässler and Storrer (1980)), but also well understood in lots of aspects: its pattern of muscle fibre innervation (Bässler and Stein (1996)) and muscle fibre composition (Bässler et al. (1996)), its role in rocking behaviour (Pflüger (1977)), or its role as an effector in response to local feedback from sensory neurons about movements (e.g. Bässler (1967); Bässler and Büschges (1998); Büschges (2005)) or forces (e.g. Akay et al. (2001); Akay and Büschges (2006)). Most biomechanical investigations are either focussed on one topic like e.g. the force-velocity relationship (Edman (1988)) or they are performed on muscles not being involved in leg movement (typically flight muscles, like e.g. Machin and J. W. Pringle (1960); Malamud (1989); Malamud and Josephson (1991)). This thesis presents a broad insect leg muscle description that comprises examinations on many muscle physiological and biomechanical aspects. The richness of muscle data from over half a century (e.g. Hill (1938)) allows classification and comparison to other muscle-joint systems. The data gathered within this thesis provide enough aspects to begin modelling the muscle with more than 20 parameters (Ekeberg et al. (2004); Blümel et al. (2007a;b; 2008b;a)). Experiments mimicking physiological motoneuronal firing patterns further deepened the understanding of the extensor tibiae's role in behaviour (Hooper et al. (2006; 2007a;b)).

D1 Femoral geometry

Summary

There is a clear linear dependence between femur length and muscle length of extensor and flexor tibiae for all three legs, tibial front leg muscles are notably shorter. It was shown that extensor tibiae muscle length changes with the cosine of the FT joint angle and flexor tibiae length changes with the negative cosine, except for extreme angles (close to 30° or 180°). Flexor tibiae moment arm length of all three legs (0.564 mm) is twice the moment arm length of all three legs' extensor tibiae muscles (0.282 mm). Proximal and medial flexor tibiae fibres are approximately 1.5 times longer (2.11 mm) than proximal and medial extensor tibiae fibres (1.41 mm). Preliminary phalloidin stainings could show that the percental length changes that extensor and flexor tibiae fibres experience within the muscles' working range of 150° deviate from the percental sarcomere length changes for their sarcomeres. Standardisation of sarcomere lengths result in means of 5.4 μm for the extensor and 6.9 μm for the flexor tibiae. Further examination is required in order to make a clear statement to this issue. Femoral cross-sectional area is about 0.5 mm^2 and extensor tibiae cross-sectional area about 1.9 mm^2 .

Discussion

Randomly picked sturdy looking female stick insects had body masses around 1 g (0.94 ± 0.07 g, N=10) and body lengths of 77.1 ± 2.28 mm (N=10), about the same values found by Burrows and Wolf, 1.1 ± 0.004 g and 78 ± 0.15 mm (N=10, Burrows and Wolf (2002)). The small inter-animal variation (small S.D. values) and the similarity to the values of another institute's breeding suggests stick insects from the Cologne institute's breeding to be representative for muscle examinations. This fact is particularly important in respect to the issue of data variability, see chapters D2 and D4. The proportion of relative femur lengths of the three legs presented in chapter C1 aligned with the findings from Burrows and Wolf: front leg femur is the longest, hind leg femur almost as long and middle leg femur about $\frac{2}{3}$ the front leg femur length (Burrows and Wolf (2002)).

Flexor and extensor tibiae muscle rest lengths of all three legs were shown to be proportional to femur length (see Fig. C.1). The specialisation of the front legs causes tibial muscles to fill out only three quarters of the femur length (76 % for the extensor tibiae and 73 % for the flexor tibiae, see Tab. C.1). Stick insects have a narrow, red coloured femur base in each front leg that allows them to hold their front legs rostrally over the animal's head and thus to mimic twigs (Marquardt (1940); Bässler and Wegner (1983). Opening the proximal femur reveals no tibial muscle fibres to be in the proximal part.

Investigating the dependence of muscle length on joint angle is considerably simplified by the fact that arthropod apodemes are 40 times as stiff as mammalian tendons (Ker (1977); Full and Ahn (1995); Full et al. (1998)) as this allows an unambiguous relation. Taking the muscle reference length as the muscle length when its moment arm is perpendicular to the long axis of the segment comprising the muscle in focus (Full et al. (1998)), in this case the femur, seemed to be reasonable although this may not be the actual 'rest length'. The real 'rest length' is likely to be different for every individual muscle and would have required cutting the distal apodeme at the beginning of each experiment and looking to which length the muscle shrinks.

The deviations of normalised muscle length (see Fig. C.2) changes from a fitted cosine function (and the negative cosine function respectively) that can be found in the extensor tibiae (and flexor tibiae respectively) can be interpreted simply by considering mechanical laws and truly make sense as the muscle would be unable to move the tibia out of extreme positions (where these deviations occur, e.g. during thanatosis (Bässler (1972); Godden (1974))). The fitted cosine function does not properly describe the range of angles close to the endpoint at 180°, the values still show a slope different from zero and not a horizontal tangent as would be described by a cosine function. This avoids the problems of a mechanical dead point for the tibial muscles at extended joint angles. Within the range of joint angles occurring in most physiological situations, the relationships between joint angle and muscle length were approximately linear, very similar to data shown for cockroach (*Blaberus discoidalis*) extensor muscles of all three segments (muscles 87 (prothoracic), 137 (mesothoracic) and 179 (metathoracic), Full et al. (1998)). It has to be mentioned that the moment arm orientation arrangement of extensor and flexor tibiae was not explicitly checked. The assumption made

in this thesis (e.g. Fig. C.31) and in Guschlbauer et al. (2007) is the most simple arrangement, with both extensor and flexor tibiae moment arms being perpendicular to the long axis of the tibia (Fig. D.1a). It is equally conceivable to think of an arrangement with both moment arms being either tilted relative to the longitudinal axis of the tibia (Fig. D.1 b) or tilted relative to each other (Fig. D.1 c).

The fact that tibial muscles show a pinnate arrangement of their fibres enhances effective muscle cross-sectional area and the ability of the muscle (relative to muscle length) to generate force within a rigid, confined space (Full (1997)) as the exoskeleton would not allow volume changes like in a parallel fibred muscle such as the human triceps. With a parallel fibre arrangement, the effective cross-sectional areas of the middle leg extensor tibiae (1.9 mm^2) and estimated 4 mm^2 for the flexor tibiae would not have enough space in a middle leg femur that has a cross-sectional area of 0.5 mm^2 . Locust abdominal muscles M214 and M169 have cross-sectional areas of 0.09 mm^2 and 0.03 mm^2 respectively. Their force output is much smaller than the extensor or flexor tibiae's ($< 25 \text{ mN}$, Rose et al. (2001)).

The pinnate arrangement of extensor and flexor tibiae necessitated fibre length measurements. Extensor tibiae fibres showed to correlate significantly with muscle resting length, whereas flexor tibiae fibres did not (see Fig.C.4). This 'non-correlation' can have two reasons: either the sample-size was too low ($N=4$ compared to $N=5$ extensor measurements), or flexor fibre length is indeed independent from muscle resting length, which would suggest that an increased flexor muscle length is reflected in an increased number of fibres, and not in an increased fibre length.

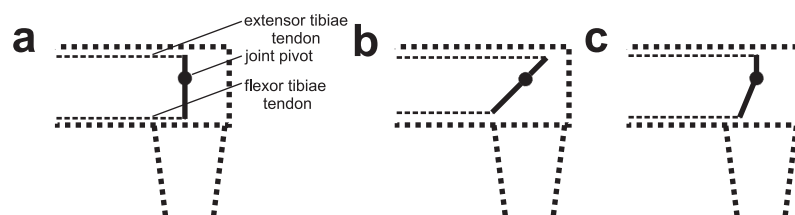


Figure D.1: Different conceivable moment arm orientation arrangements. (a) to (c) show schematic distal femur-proximal tibia drawings with joint arrangements at different orientations of the extensor and flexor tibiae moment arms, also shown schematically. Note that extensor tibiae moment arm is approximately half the flexor's.

Flexor tibiae fibres are nearly 1.5 times longer than extensor tibiae fibres. This finding becomes particularly important with respect to the maximum contraction velocity a fibre can bear, as it is dependent on its sarcomere number (Huxley and Niedergerke (1954a); Thuma (2007)) and will therefore be discussed below. The physiological significance of proximal extensor tibiae fibres being longer than medial ones and proximal flexor tibiae fibres being shorter than medial ones remains unclear. Determination of pinnation angles (see in the *Results* section) led to the conclusion, that measurement of fibre length changes is afflicted with an error of less than 3 % when calculated with a pinnation angle of zero, i.e. as if the fibre were arranged parallel to the muscle apodeme for both tibial muscles. Consistent with this calculation, a parameter study to calculate extensor mass of the dinosaur *Tyrannosaurus* showed that altering pinnation angle within a reasonable range of values had little or no effect (Hutchinson and Garcia (2002)).

The flexor tibiae's moment arm being twice as long as the extensor tibiae's seems to be an adaptation to the flexor's longer fibres (see Fig. C.3): extensor and flexor tibiae experience similar relative fibre length changes during walking. The middle leg flexor tibiae is mainly active during stance phase (Fischer et al. (2001); Schmidt et al. (2001); Gabriel et al. (2003)), it profits of a longer moment arm length in order to generate larger torques. The extensor tibiae in turn can take advantage of a shorter moment arm length in order to accomplish fast movements during swing phase (Bässler and Büschges (1998); Graham (1985)). Interestingly, middle leg extensor tibiae moment arm length can be very different in orthopteran insects, as femoral chordotonal organ apodeme movement of 0.2 mm in *Carausius morosus* (Weiland et al. (1986)), 0.4 mm in *Cuniculina impigra* and 0.6 mm in *Locusta migratoria* (Field and Pflüger (1989)) corresponds to a joint angle change of 40°, respectively (Bässler et al. (1996)). The determination of Weiland and colleagues (Weiland et al. (1986)) in *Carausius morosus* is in very good agreement with the examinations in this thesis: the same angular deflection of 40° around a centre position of 90° (like they did) results in an extensor tibiae excursion of 0.19 mm, when calculated with a moment arm length of 0.282 mm.

Sarcomere length measurements were conducted in order to answer two questions: Do sarcomeres of extensor and flexor tibiae experience the same percent length changes as do the fibres of both muscles? Do extensor and flexor tibiae sarcomeres differ in

their structural arrangement? Nissl sarcomere stainings of the extensor tibiae were difficult to interpret, because the procedure involved too many unpredictable factors (e.g. distortion of the material after paraffin treatment). As the quality of the stainings was not too good, the decision was made to take phalloidin as a classic muscle structure fluorescent dye. The outcome of these stainings was much better in quality and the sarcomere length changes quite close to the range of length changes that can be expected from the calculated fibre length changes. The fact that extensor tibiae sarcomeres experience 25 % less length change than the fibres and flexor tibiae sarcomeres experience 13 % more length change suggests that there could be some structural elements that cause this mismatch. For example, it is conceivable to think about the existence of proteins that connect the fibre with the cuticle or with the tendon. These proteins could cause only a few components of the fibre (e.g. some sarcomeres) to stretch more or less than the entirety of the fibre: this would necessarily lead to a certain mismatch. It was already discussed (see above in this 'Discussion' chapter) that muscle lengths show deviations from the cosine characteristic at extreme angles like 30° and 180° and that these deviations make sense from a physiological aspect. It is therefore also conceivable to trace the mismatch found between the calculated length changes of fibres and the measured length changes of sarcomeres back to the deviation from the cosine course.

The second issue to be solved with sarcomere length data concerned the comparison of the general structure of sarcomeres in different muscles. The standardisation technique by Thuma and colleagues (Thuma (2007); Thuma et al. (2007)) represents an appropriate tool to conduct this comparison. They compared different pyloric and gastric mill muscles in the lobster *Panulirus interruptus* and found large variability within a pool of nine muscles: the structure of sarcomeres can vary extremely between muscles accomplishing similar functions. The result of the standardisation procedure is to reduce each sarcomere to two times its thin filament length. The fact that standardised sarcomere lengths from a muscle fixed at 30° and from a muscle fixed at 180° are within a similar range, but still significantly different from one another again suggests that the existence of e.g. elastic proteins being responsible for the detected mismatch is likely. The examination revealed middle leg mean tibial sarcomere lengths of 5.42 μm for the extensor and 6.93 μm for the flexor tibiae (see Figs. C.5, C.6, C.7). Thuma (Thuma (2007)) investigated sarcomere lengths of nine muscles in the lobster stomatogastric system that have standardised lengths ranging from 3.25 μm to 12.29 μm

with four muscles having a length between 5 and 8 μm , similar to standardised tibial muscle sarcomere lengths. Other sarcomere lengths found: 2.20 μm (anterior *tibialis* muscle of *Rana temporaria*, Edman (2005)), 2.6-2.7 μm (*flexor digitorum brevis* muscle of the mouse), 2.45 μm (*semitendinosus* muscle of *Rana temporaria*, Edman (1966)), 2.5 μm (*psoas* muscle of the rabbit, Ranatunga et al. (2007)), 2.5 μm (*flexor halucis brevis* muscle of the rat, Roots et al. (2007)), 2.58 and 2.71 μm (*soleus* and *extensor digitorum longus* muscle in the mouse). The standardised sarcomere lengths of extensor and flexor tibiae are within the same ballpark than many other arthropod sarcomeres, however a direct comparison is impossible because the precise contraction state of each sarcomere is unknown. In general, longer sarcomeres with longer myosin filaments are capable of generating greater stress (Full and Ahn (1995)). This is confirmed by examinations on different crab closer muscles that revealed sarcomere lengths between 10 and 18 μm (Taylor (2000)). Taylor describes a linear relationship between resting sarcomere length and maximum muscle stress including arthropods (without crustaceans), crustaceans and vertebrates: the longer the sarcomere, the larger the maximum stress (Taylor (2000)). From this regression, tibial muscles should exert as much as 350 - 400 $\frac{\text{kN}}{\text{m}^2}$ in respect to their calculated standardised sarcomere lengths. However, maximal extensor tibiae stress is $79 \pm 23 \frac{\text{kN}}{\text{m}^2}$ (N=7, see Tab. C.7) and maximal flexor tibiae stress is $104 \pm 32 \frac{\text{kN}}{\text{m}^2}$ (N=8, see Tab. C.8): both tibial muscles deviate from this regression and exert less stress than expected. Apart from maximum muscle stress generation, another important parameter in terms of the functional relevance of sarcomeres is the maximal shortening velocity (V_0), which is supposed to be dependent on sarcomere number, as Huxley and Niedergerke (Huxley and Niedergerke (1954a)) predicted and later Thuma (Thuma (2007); Thuma et al. (2007)) showed. For both tibial muscles, sarcomere number can be calculated as follows: $\frac{(\text{fibre length at a particular contraction state})}{(\text{sarcomere length at a particular contraction state})} = (\text{sarcomere number at particular contraction state})$. For the extensor tibiae, the ratio is $\frac{1.65 \text{ mm}}{7.50 \mu\text{m}} = 220$ at 30° FT joint angle and $\frac{1.13 \text{ mm}}{6.21 \mu\text{m}} = 182$ at 180° (see Tab. C.2). For the flexor tibiae, the ratio is $\frac{1.62 \text{ mm}}{5.16 \mu\text{m}} = 314$ at 30° FT joint angle and $\frac{2.67 \text{ mm}}{9.16 \mu\text{m}} = 291$ at 180° (see Tab. C.2). Taking the means for both muscles gives $\sim 200 \frac{\text{sarcomeres}}{\text{fibre}}$ for the extensor tibiae and $\sim 300 \frac{\text{sarcomeres}}{\text{fibre}}$ for the flexor tibiae. Consequently, the sarcomere number predicts V_0 of the flexor tibiae to be about 1.5 times larger than V_0 of the extensor tibiae. Quick release experiments prove this predictions to hold true (compare Tabs. C.7 with C.8 in chapter C4): the ratio $\frac{V_0 \text{ of the flexor tibiae}}{V_0 \text{ of the extensor tibiae}}$ is with 1.38 close to the predicted value, calculated with $6.05 \frac{\text{mm}}{\text{s}}$ for the flexor tibiae (N=8) and $4.39 \frac{\text{mm}}{\text{s}}$ for the extensor tibiae (N=7). Although these data are intriguing, they should only be considered

preliminary because they come from only two animals for each muscle.

D2 Force measurements in the isometric domain

Summary

Extensor tibiae single twitch force is notably smaller than maximal tetanic force (2-6 mN compared to > 100 mN) and takes long to relax completely (> 140 ms). Flexor tibiae twitch force can become remarkably big (> 30 mN), depending on the degree of recruitment. These strong twitches show a steady amplitude decrease at continuous stimulation whose nature is unknown. Both increase in stimulation frequency and stimulation duration have a positive impact on the persistence of maximal force generation and on the relaxation decay dynamics in the extensor tibiae. The muscle appears to respond to a short-term altering stimulation in frequency or pulse number with an increased force level ('catch-like effect' or 'latch'). Thus, the muscle can compensate for stimulation intermissions to some extent. The extensor tibiae has its working range (30° to 180°, see also Friedrich (1932)) on the ascending limb of the force-length relationship described by Gordon et al. (Gordon et al. (1966b)). The maximally generated force was in most experiments shifted towards longer fibre lengths at lower stimulation frequencies.

Discussion

The method of examining forces the way it was done within this thesis differs essentially from the usual way the forces of most vertebrate muscles (e.g. frog in Hill (1938) or Edman (1988)) are measured. Single fibre measurements are most often performed on vertebrate muscle because their muscle fibre membranes normally feature voltage-dependent Na⁺- channels and are therefore able to be stimulated when placed between two small metal discs, which is methodologically a big advantage, because parameters like temperature or application of drugs can be controlled more accurately, and the muscle can be stimulated directly and not via the nerve. This kind of stimulation is not possible in invertebrates. The experimentalist has basically two possibilities: either eliciting motoneuronal action potentials with a monopolar suction electrode (Grillner et al. (1998)) or with a bipolar electrode. The main advantage

of the latter is that the generated electrical field is restricted to the nerve and the motoaxons therefore need presumably much less current to generate action potentials. Additionally, the fact that stick insect tibial muscles are pinnate and that single fibre forces are unmeasurably small make single fibre measurements inconceivable (at least with a force transducer like the Aurora 300 B dual-lever system). Apart from this aspect, whole muscle measurements have a clear advantage compared to single fibre measurements: it is very improbable that a muscle fibre, with a length hundreds of times its diameter, is supposed to have a constant strength throughout (Hill (1949)). In a whole muscle, with many fibres working in parallel, an average value is obtained being much more constant than in a single fibre (Abbot and Aubert (1952)).

Extensor tibiae nerve stimulation (*nl3*) was set to an amplitude that elicited a visible twitch in the force trace adding at least 50 %. With this stimulation, the FETi motoneuron was obviously excited and it is most likely to have activated the SETi and the CI₁ motoneuron simultaneously, a paradigm that comes close to the naturally occurring activation pattern during swing phase: excitatory and inhibitory extensor motoneurons are activated together with instantaneous frequencies of up to 200 Hz (Schmitz and Hassfeld (1989); Büschges (1995b); Kittmann et al. (1996)). Separate stimulation of individual excitatory motoneurons is not possible extracellularly (Bässler and Storrer (1980)). As was demonstrated in the *Materials & Methods* section (see also Fig. B.5), a set of 15 experiments was conducted to deal with the question whether simultaneous activation was achieved with at least 1.5 *T*, i.e. 50 % above the current amplitude to elicit a visible contraction. It turned out that either 1.5 *T* was sufficient to a) stimulate all three motoaxons or b) to recruit at least SETi in most cases. In 13 % of all test examinations, the incompleteness of a full recruitment (all three motoneurons together) was reflected in only a modest difference in terms of the total amount of isometrically developed force at 50 Hz stimulation frequency. Isotonic stick insect extensor tibiae data (*Carausius morosus*) further support this finding: addition of latter excited motoaxons little alters muscle contraction (Hooper et al. (2006; 2007a)). In these investigations, contractions of all seven muscles varied similarly in response to the variations in physiological burst input, which proves that either motoneuronal stimulation was consistent or the addition of SETi and / or CI₁ does not alter the output much, when FETi is active at similar frequency.

The role of slow motoneuron and common inhibitor activation during walking behaviour can vary largely among insects: High speed video motion analysis of the cockroach *Periplaneta americana* during intracellular stimulation showed that single action potentials in slow leg motoneurons are ineffective, only high frequency stimulation produces discernible joint movement (Watson and Ritzmann (1995)). This is in accordance with the observation that the fast motoneuron is not or barely active below walking speeds of 2-5 Hz (*Blaberus discoidalis*, Watson and Ritzmann (1998)) and that the slow motoneuron fires with a mean frequency of up to 200 Hz (Mu and Ritzmann (2005)). The (specialised) locust hindleg utilizes FETi motoneuronal output exclusively for kicking and SETi is accomplishing tibia extension during walking almost completely (*Schistocerca gregaria americana*, Burns and Usherwood (1979)). The locust middle leg extensor muscle is a stance phase muscle. SETi is active at the beginning of retraction and FETi (together with CI) becomes active only in the second half of retraction (Burns and Usherwood (1979)). In the stick insect middle leg, the situation is very different. FETi is always active when fast tibia extension occurs, i.e. generally in swing phase (evidence for this can be found in Büschges et al. (1994); v. Uckermann and Büschges (2008)). In *Cuniculina impigra*, extension movements during walking are reported to be exclusively generated by the fast contraction kinetics of the main (i.e. not the distal) part of the extensor tibiae (Bässler et al. (1996); Bässler and Stein (1996); Bässler et al. (2007)). Numerous examinations deal with the role of the SETi motoneuron and the force production involved when the chordotonal organ is stimulated with various stimulation regimes (Storrer (1976); Storrer and Cruse (1977); Cruse and Storrer (1977); Bässler and Storrer (1980); Bässler and Stein (1996); Bässler et al. (2007)). In these experiments, maximal force production is minor compared to the actively generated forces measured within this thesis. The role of CI₁ on extensor tibiae force production is thoroughly described in a 'bisected extensor tibiae' preparation that examines mostly the dually innervated muscle part, i.e. the most distal muscle fibres (Bässler and Stein (1996)). They used experimental paradigms that activate SETi much more strongly than FETi (Büschges (1995a); Hooper et al. (2007a)). Forces measured with the stimulation regime used for the investigations presented in the *Results* section of this thesis indicate that these forces are supposed to originate mainly from fast innervated fibres in the proximal part of the femur (Bässler et al. (1996)). The SETi innervated fibres are also innervated by CI₁ (Bässler and Storrer (1980)) and would presumably be blocked to a certain extent during walking or walking-like behaviour, as all three motoneurons are active during middle leg swing phase (FETi

together with SETi: Weiland and Koch (1987); Nothof and Bässler (1990); CI₁ active in active animals: Büschges (1995b); Bässler and Stein (1996); SETi almost always spontaneously active: Godden (1974); Bässler (1983)). In accordance with this, intracellular recordings from different muscle fibre types in the closely related stick insect *Cuniculina impigra* show that SETi - EJPs can be very small and are sometimes only visible due to facilitation. Their amplitudes can be massively reduced by IJPs elicited in the CI₁- motoneuron (Bässler et al. (1996)). Similarly, stimulation of a slow motoneuron in the spider crab closer muscle (*Chionectes tanneri*; Atwood (1965)) showed that intramuscular EPSPs were abolished completely as soon as the CI axon was stimulated simultaneously. The role of CI₁ is certainly an issue that needs to be examined further in the future: locust flight behaviour can be massively biased by manipulation of the common inhibitor (Wolf (1990a;b)) and locust mesothoracic extensor tibiae force elicited by SETi activity can be reduced during rise of isometric tension, relaxation phase can be accelerated and catch tension can be diminished due to CI stimulation (Burns and Usherwood (1978)). Recapitulatory, the extensor tibiae's net force output is likely to be mainly borne by the force of the fast innervated fibres, which might explain the small discrepancies between recruiting FETi alone or recruiting all three (see Fig.B.5). In *Carausius morosus*, the percentage of fast innervated fibres is always > 30%, even in the most distal part of the muscle (Bässler et al. (1996)).

Apart from motoneuron activation, it needs to be considered that the extensor tibiae additionally receives modulatory input from DUM neurons (Mentel et al. (2008)), which are known to enhance absolute muscle force amplitude and to make muscle relaxation faster in the locust *Schistocerca americana gregaria* (Evans and O'Shea (1977; 1978); Evans and Siegler (1982)). They can be rhythmically active during stepping movements (Hooper et al. (2007a); Mentel et al. (2008)). Hooper and collaborators raised the possibility that the modulatory effect of octopamine on the extensor tibiae might be the reason for their wide variation in delays to rapid relaxation and rise and relaxation time constants in the isotonic domain (Hooper et al. (2007a)). This might be taken as an alert that mere stimulation of the *nl3* nerve without any recording might be sort of 'uncontrolled' in respect to the various possibilities of axon recruitment. However, simultaneous recording would not have been possible without muscle damage and would have led to enormous time delays in respect to the muscle measurements (see Guschlbauer et al. (2007)) especially in regard to the *rigor mortis* phenomenon. DUM neuron action potentials have fairly small amplitudes (when

measured extracellularly, data not shown) and are very hard to detect in a F2 recording, hence a reasonable study of muscle properties would have been very difficult, at least not with as many successful experiments as presented in the thesis at hand.

Twitch force was measured in terms of maximum force development and its kinetics in both extensor (see Fig. C.8 and Tab. C.3) and flexor tibiae (see Fig. C.9 and Tab. C.4). Extensor tibiae single twitch time course is much slower than that of bi-functional flight/leg muscle Tcx_2 from *Schistocerca gregaria* (Malamud and Josephson (1991)) and flight muscle in *Manduca sexta* (Stephenson and Josephson (1990)). However, it is rather similar to time courses of cockroach *Blaberus discoidalis* (Ahn and Full (2002)) and to front and middle leg extensors of the locust *Schistocerca gregaria americana* (Burns and Usherwood (1978)). Interestingly, the extensor tibiae relaxes twice as fast as an asynchronous flight muscle in *Cotinus mutabilis* (metathoracic basalar muscle, Josephson (1993)). Twitch time kinetics change for the relaxation phase and become faster with increasing temperature, whereas twitch force rise time becomes only very modestly faster with increasing temperature (Josephson et al. (2000)). Tab. D.10 compares stick insect twitch kinetics with those of two different cockroach species in a functional context: latency depends on the location of muscle stimulation, for the stick insect the nerve ca. 6-7 mm from the proximal muscle end. T_{max} is very similar for *C. morosus* and *B. discoidalis*, *P. americana* develops max. twitch force in half as much time. The biggest differences arise in the relaxation phase: T_{50off} is about $\frac{2}{3}$ in *B. discoidalis*, but less than half in *P. americana*, at T_{90off} the discrepancy is even more. The large differences between these values can be interpreted in the functional

	Latency [ms]	T_{max} [ms]	T_{50off} [ms]	T_{90off} [ms]	max. step freq. [Hz]
Extensor tibiae <i>C. morosus</i>	8.5 ± 1.80	26.41 ± 6.3	60.69 ± 15.65	149.89 ± 67.93	3
Muscle 179 <i>B. discoidalis</i>	8.9 ± 0.9	26.5 ± 4.8	39.5 ± 6.2	60.2 ± 7.6	12
Muscle 137 <i>P. americana</i>	-	13.5	23.8	-	25

Table D.10: Twitch kinetics comparison of three different insect species. Maximum step frequency of *C. morosus* (Bässler (1983)), *B. discoidalis* data (Ahn and Full (2002)), *P. americana* data (Usherwood (1962); Delcomyn (1971); Full and Tu (1991); Full et al. (1998)). T_{max} = time to peak force, T_{50off} = time to relax to 0.5 P_{max} amplitude, T_{90off} = time to relax to 0.1 P_{max} amplitude.

context of each muscle: in respect to walking speed, *C. morosus* is by far the slowest of the three animals, *B. discoidalis* is four times faster and *P. americana* even more than 8 times faster. In respect to the entire animal kingdom, contraction times to peak force vary by over 200 fold: values range from 0.004 to 0.79 s, but the lack of standardisation of conditions makes direct comparison difficult (Full (1997)). Time to relax to half of the maximum force value varies by over 100-fold and ranges from 0.009 to as long as 1.1 s (Full and Meijer (1997)). Maximal flexor tibiae twitch force was shown to be remarkably high (see Fig. C.9 and Tab. C.4). Repetitive stimulation led to a steady decrease that could be fitted with a power-function. The mechanism appeared to be rather event-dependent than stimulation-frequency-dependent (see Fig. C.10). In the crab (*Cancer pagurus*), a similar phenomenon was detected: here, EJPs in the gm9 muscle are initially large and depress with repetitive stimulation (Stein et al. (2006)), presumably due to a presynaptic mechanism like transmitter depletion (Katz et al. (1993)). Given the enormous force increase that arose from recruitment of the last motoneuron (the fifth recruitment in the example of Fig. C.9, when further current amplitude increase did not lead to a further force increase), synaptic depression due to transmitter depletion is probable, because the stick insect most likely does not fire with this (obviously) fast motoneuron that often in a physiological situation (every fifth second in the experiment). Gradational tetanic extracellular flexor motoneuron recruitment with different current amplitudes was very difficult to achieve, because reliable repetitive stimulation of a particular set of motoneurons was nearly impossible at higher stimulation frequencies. Fig. C.12 shows one successful attempt. Consequently, stimulation current amplitude was chosen to be maximal (i.e. when no further isometrical force increase was detectable) in order to compare maximal flexor tibiae forces and contraction velocities with the corresponding extensor tibiae values, as those are particularly crucial muscle physiological parameters (e.g. for the Hill equation (Hill (1938))).

Compared to earlier studies from Storrer (Storrer (1976)), who measured extensor tibiae forces in response to sinusoidal femoral chordotonal stimulation, maximum tetanic force of the extensor tibiae is unexpectedly high. Nevertheless, normalized stress values ($4.2-10.5 \frac{N}{cm^2}$) are in the lower range of other insect muscles, compared e.g. to the Tcx₂ muscle in *Schistocerca americana* ($36.3 \frac{N}{cm^2}$, Malamud and Josephson (1991)) or two extensor muscles in *Blaberus discoidalis* (25 and $47 \frac{N}{cm^2}$, Ahn and Full (2002)). *Tetrigonia* wing muscles ($4-15 \frac{N}{cm^2}$, Josephson (1993)) and 4 of 6 leg muscles in *Periplaneta*

americana ($6.8-8.3 \frac{N}{cm^2}$, Smit et al. (1967); Jahromi and Atwood (1969)) lie in the range of the middle leg extensor tibiae. Different motor units of the cat tibialis anterior muscle show tensions starting from $17.4 \frac{N}{cm^2}$ (slow fibres) to $20.4 \frac{N}{cm^2}$ (fast, fatigue-resistant fibres) to $27.5 \frac{N}{cm^2}$ (fast, fatigable fibres), see Bodine et al. (1987). Mouse fibres from the hindlimb *flexor digitorum longus* muscle have a maximum tension of $36.8 \pm 5.7 \frac{N}{cm^2}$ (Edman (2005)), frog skeletal muscle fibres have $41.6 \pm 1.6 \frac{N}{cm^2}$ (*Rana temporaria*, Edman (2005)). Values of maximum isometric stresses within invertebrate species vary by 70-fold ($2-140 \frac{N}{cm^2}$, Ruegg (1968); Alexander (1985); Full and Ahn (1995); Full et al. (1995)) and can vary by more than twofold in mammals ($13.2-29.4 \frac{N}{cm^2}$, Josephson (1993); Powell et al. (1984); Close (1972); Full and Ahn (1995)). Surprisingly, absolute maximum forces of the middle and front leg extensor tibiae muscles of the locust (*Schistocerca gregaria*, Burns and Usherwood (1978)) are with 30-35 mN much below the corresponding muscles in the stick insect. Even though the locust is special in respect to its ability to kick, one might expect middle and front leg not to differ too much between species, as they are 'normal' walking muscles. However, length and particularly anatomy of the legs are quite different, considering the evolutionary process discussed by Burrows and Wolf (Burrows and Wolf (2002)). A detailed investigation dealing with the differences between FETi and SETi in the locust middle leg extensor is about to be accomplished in the Büschges working group.

Maximum isometric flexor tibiae force was shown to be more than two and a half times as large than maximum isometric force of the extensor tibiae (compare Tab. C.7 with C.8). This large discrepancy between two muscles operating at the same joint might be surprising but makes sense in respect to the muscles' 'jobs'. The extensor tibiae of the middle leg is mainly activated during swing phase (Büschges et al. (1994); Fischer et al. (2001)), thus the main force to be overcome is the dynamically generated flexor tibiae's passive force (see Fig. C.33) and the joint torques that have been shown to be very small (see Figs. C.38 and C.39). Eventually, as was demonstrated in chapters C2 and C6, the extensor tibiae has got to deal with sustained force levels due to history-dependent effects, so the very end of stance phase is in most cases characterised by a co-contraction of both tibial muscles (Fischer et al. (2001)). Sometimes only the extensor tibiae is active during stance end (Büschges et al. (1994); Fischer et al. (2001)) and pushes the animal forward right before tibia lift-off (Cruse (1976)). In this case, the extensor tibiae can take advantage of its force-length characteristic as it can generate the largest forces when being flexed, i.e. at the end of stance phase

(Cruse and Bartling (1995)). Gravity of the tibia is negligible, as it is for most small limbs (Hooper et al. (2009)). Middle leg's flexor tibiae is mostly active during stance phase (Schmidt et al. (2001)), so there is a natural requirement for a strong muscle to be able to achieve propulsion of the animal. Force disproportions between antagonists are not unusual: for example the human tibialis anterior / extensor hallucis longus muscle (1003 N) is only half as strong than its antagonist, the tibialis posterior / flexor hallucis longus (2149 N) (Anderson and Pandy (1999)). It has to be taken into consideration that human muscles often act in a more complex way than tibial stick insect muscles as they don't necessarily attach on one single joint. Some human muscles are bifunctional and hold geometries that make the mechanics of a joint much more difficult.

The twitch/tetanus ratio is a good measure to estimate a muscle's ability to fine-tune leg movement. From Tab. D.11, it becomes clear that the extensor tibiae holds the special ability of allowing better gradation of muscle force which is a feature that was already attributed to cockroach extensors, even though they have a ratio over 10 times bigger (Full et al. (1998)). This is a property that makes the extensor tibiae fairly unique and outstanding compared to most other leg muscles. This 'finetuning-capacity' is further supported by the existence of the inhibitory motoneuron (CI_1), a feature that lacks for instance in leg muscles like the anterior extensor muscles 87, 137, 179 and their antagonists, the posterior depressor muscles 86, 136 and 178 (Pearson (1972); Pearson and Iles (1971); Full et al. (1998)). The ability to grade force in that special manner is particularly advantageous in cataleptic behaviour: bending the FT-joint from an extended position to a particular angle and holding it in this position results in a quick extension after release followed by a returning movement with a velocity between 180 and $0.1 \frac{deg}{min}$, which is even slower than the hour hand of a clock (Bässler (1972); Godden (1974); Bässler (1983)). The data are in good agreement with requirements expected of a leg muscle in a slow walking and climbing insect: muscle forces reaching relatively high maximum values can be controlled by a broad range of motoneuron frequencies.

Isometric force generation of the middle leg extensor tibiae is characterised by a noticeably long lasting P_{max} after the end of stimulation followed by a slow relaxation phase, illustrated in Fig. C.13. In this example, force takes > 500 ms to decline com-

Table D.11: *Twitch/tetanus tension ratios of different muscles. The ratio of the extensor tibiae was determined using the mean twitch force (2.6 mN, N=12; see Tab. C.3) and mean P₀ (150.7 mN, N=7; see Tab. C.7).*

Extensor tibiae (<i>Carausius morosus</i>)	0.017
Extensor muscle 179 (<i>Blaberus discoidalis</i> , Ahn and Full (2002))	0.02
a single motor unit of the <i>tibialis anterior</i> muscle (cat, Bodine et al. (1987))	0.03
a different single motor unit of the <i>tibialis anterior</i> muscle (cat, Bodine et al. (1987))	0.17
Basalar muscle, a hindwing depressor (<i>Cotinus mutabilis</i> , Josephson et al. (2000))	0.19
T-F joint muscle 137/179 (<i>Blaberus discoidalis</i> , Full et al. (1998))	0.2
Extensor muscle 177c (<i>Blaberus discoidalis</i> , Ahn and Full (2002))	0.27
Tcx2 (<i>Schistocerca gregaria</i> , Malamud (1988); Malamud and Josephson (1991))	0.6
T-F joint muscle 137/179 (<i>Periplaneta americana</i> , Becht and Dresden (1956); Usherwood (1962))	0.67 - 0.83

pletely. In this context, force measurements on the hindleg extensor tibiae of the locust *Schistocerca gregaria* suggest a ‘recruitment of myofilaments in the core of the fibre’ involving a slower intrinsic relaxation rate of the later recruited contractile material of the core. There are not very much sarcoplasmatic reticula and few dyads in the core, therefore myofilaments in the core are farther away from calcium uptake sites. It takes a longer stimulation period for the calcium to reach core filaments and to be returned to storage areas than is the case in the periphery (Hoyle (1978)). Although these examinations were done on single bundles of slow muscle fibres, a similar mechanism is conceivable to be responsible for the stimulation history-dependent sustained maximum forces and slower relaxation rates described as well, described in chapter C2, see Figs. C.13, C.16, C.17, C.18 and chapter C6, see Figs. C.74, C.77, C.81. As mentioned in *Results*, exponential decay fits started at 95% P_{max} because Ca²⁺ takes a few milliseconds to be pumped back into the sarcoplasmatic reticulum (Abbot (1973); White and Thorson (1975)) and force decline cannot be expected to happen abruptly. A decline of 5 % seemed therefore reasonable to start fitting without losing too much of the information in focus. A mean ‘delay to rapid relaxation’ and the time constant

for relaxation after stimulating the muscle is already described for isotonic force experiments with physiological muscle activation performed in Hooper et al. (2007a): 52 ms (0.064 ± 0.014 s when the conductance delay is added) for the delay and 50-60 ms for the relaxation τ were calculated. This is in good agreement with the isometric force results shown in Figs. C.16 and C.18: when the muscle was stimulated at 200 Hz, relaxation had a delay of 43.3 ± 5.7 ms after stimulation with 40 pulses (N=5) and 47.9 ± 6.6 ms after 60 pulses (N=5). The mean linearised extensor tibiae burst consists of 46 (FETi-) spikes (see Hooper et al. (2007a)). When the muscle was stimulated with different frequencies, the minimal relaxation delay (data from N=7) was 33.4 ms (at 30 Hz) and the maximal value was 109.7 ms (at 200 Hz). Relaxation time constants in the isometric force domain resulted in 49.5 ± 10.8 ms at 40 pulses and 57.6 ± 12.0 ms at 60 pulses when stimulated at 200 Hz (N=5). Minimal τ was 30.9 ms at 50 Hz and maximal τ 145.7 ms at 200 Hz (data from N=7). The fact that both stimulation frequency and increasing pulse number (at constant frequency) were positively correlated with duration of sustained P_{\max} and relaxation τ suggests a clear stimulation history dependency of the extensor tibiae muscle which can be found in the isometrical domain and which is supported by data performed in the isotonical domain. The determined differences in relaxation following low or following high activation are definitely in an order of magnitude that is supposed to be physiologically relevant for the animal (considering a fast swing phase duration of 100-150 ms, Graham and Cruse (1981)). Interestingly, the history dependency does not affect twitch amplitude like in *Aplysia* (Zhurov and Brezina (2006)), otherwise the extensor tibia would not show spike-number coding (Hooper et al. (2007b)). A vertebrate muscle like the *lateral gastrocnemius* in the cat shows ‘an efferent delay’ (as the author calls a sustain in isometric tetanical force) of 18-30 ms when complete stimulation of five simultaneously activated motor units was stopped abruptly (Grillner (1972)). Thus, faster Ca^{2+} -dynamics, as can be expected from a typical vertebrate muscle, result in much shorter sustained force levels after stimulation compared to the stick insect extensor tibiae. However, post-stimulational half relaxation takes more than 50 ms, which is within the same range than stick insect values.

It was demonstrated that the extensor tibiae muscle shows enhancement of actively generated force after being presented to activation enhancements like either short bursts of different frequency or of different duration (C.19, C.20, C.21, C.22). The phenomenon was called ‘catch-like’, referring to publications from Blaschko and col-

leagues (Blaschko et al. (1931)) and Günzel and Rathmayer (Günzel and Rathmayer (1994)), which is on one hand the common term for such a mechanism but which can on the other hand be rather misleading as it refers to a term describing a completely different mechanism. The actual 'catch' phenomenon was found in the anterior byssus retractor of *Mytilus* and described the maintenance of actively developed force in the absence of any motoneuronal activity, which has nothing to do with the hysteresis effects shown in chapter C2 of this thesis (Figs. C.19, C.20, C.21, C.22). Just quite recently, it was found that *twitchin*, a member of the titin/connectin family is responsible for the actual 'catch' mechanism: the 'catch' state is induced by a decrease of intracellular Ca^{2+} after the active contraction and is terminated by the phosphorylation of twitchin by the cAMP-dependent protein kinase, PKA (Funabara et al. (2005); Hooper et al. (2008)). Günzel and Rathmayer suggest a development of non-uniformities of sarcomere lengths after the muscle had reached its peak force value in response to the inserted higher-frequent burst (Günzel and Rathmayer (1994)). They describe a cascade of active and passive force reactions finally leading to the force being enhanced compared to the force exerted before the high-frequent burst. This suggestion cannot be used to explain this thesis' observations. The assumption made by Günzel and Rathmayer requires a previously happened muscle stretch that brings the muscle into working on the descending limb of the force-length relationship (Gordon et al. (1966b)). As was demonstrated (see Figs. C.23, C.24 and Tab. C.6), the extensor tibiae operates on the ascending limb of the force-length curve and a previous stretch was not applied to the muscle within this experiments. The figures shown in a work about locust catch-like mechanism (*Schistocerca americana gregaria*) do not show such a stretch either (Evans and Siegler (1982)). As the non-uniformity hypothesis is the only attempt of an explanation to date (Hooper et al. (2008)), the conclusion must be drawn that the mechanism cannot be retraced. Functionally, the stick insect takes certainly advantage of the extensor's latch properties. As could be demonstrated in chapter C4 (Figs. C.46, C.44) and Hooper et al. (2006), natural motoneuronal output is highly variable and shows are very ragged instantaneous spike frequency profile. Apart from the extensor tibiae being slow, the latch effect could be responsible for the accomplishment of muscle movement being smooth, as large interspike gaps could be 'bypassed' by a few previously occurring spikes. Accordingly, most FETi bursts show a fast spike frequency increase which generally decreases steadily towards the end of the burst. It was demonstrated that octopamine is able to abolish catch-like effects observed in *Schistocerca americana gregaria* (Evans and Siegler (1982)) and in *Locusta*

migratoria (Stevenson and Meuser (1997)).

The classical relationship between active isometric contraction force and filament overlap is known for more than 40 years and is based on the sliding-filament hypothesis of muscular contraction (Huxley and Niedergerke (1954b); Huxley and Hanson (1954); Huxley (1957a;b; 1960)). The first publications on this topic (Edman (1966); Gordon et al. (1966b;a)) examined frog leg muscle fibres (dorsal *m. semitendinosus* in *Rana temporaria*), i.e. these investigations dealt with parallel fibred twitch muscles. The extensor tibiae, being pinnate, has to experience much larger length changes during contraction and relaxation (see chapter C1, Fig. C.2). The data presented in chapter C2 (see Figs. C.23, C.24 and Tab. C.6) shows the typical ascending-plateau-descending force versus muscle / fibre length relationship with the working range on the ascending limb, which is a common feature in most muscles in the animal's kingdom (Full and Meijer (1997); Blickhan et al. (2003)). Thus, muscle is not exposed to any possible instabilities resulting from working in a non-monotonic force-length domain. The change in extensor tibiae force from the FT-joint being extremely stretched (180°) to extremely flexed (30°) was in general 200% and sometimes up to 400%. There was never the occurrence of a real 'plateau' that arose from the measurements, as expected from the sliding filament theory. Maximum contraction force was normally generated in the upper third of the muscle's working range (see Fig. C.23, at 200 Hz), approximately half of the experiments demonstrated that maximum isometric force was still increasing when the muscle was stretched further than physiologically possible (see Fig. C.23 single twitch and 50 Hz, C.24 A), i.e. a shift of maximum force development towards longer fibre lengths was detectable at lower stimulation frequencies. This dependence of maximum contraction force on fibre length at different activation levels is known from other muscles like for example the feline *soleus* muscle (*Felis domesticus*, Rack and Westbury (1969)), amphibian muscles (Stevenson and Wendt (1984)), the rat medial *gastrocnemius* muscle (Roszek et al. (1994)), the mouse *flexor brevis* muscle (Balnave and Allen (1996)) or the feline *caudofemoralis* muscle (Brown et al. (1999)). There are several possible mechanisms suggested. A length dependent Ca^{2+} -release is conceivable, assuming that lower stimulus frequencies are associated with lower concentrations of Ca^{2+} (Balnave and Allen (1996); Brown et al. (1999)). These effects might be mediated by length dependent changes of cross bridge attachment/detachment rate (Yang et al. (1998); Brown and Loeb (1999)). Brown and colleagues could show that the site of Ca^{2+} -release is always located halfway along

the thin filament in the *caudofemoralis* muscle, thus the triads are independent of sarcomere length (Brown et al. (1998)). Consequently, there would be a length change of the site of Ca^{2+} -binding site to the Ca^{2+} -binding and uptake, the diffusion distances change with muscle length (Brown et al. (1999)). Another mechanism could consist in the process of activation functioning less effectively: each spike would give a smaller and perhaps briefer activation of the contractile machinery (Rack and Westbury (1969)). Alternatively, alterations in muscle length might well alter T-tubular geometry: they could become flattened during fibre shortening leading to a higher resistance to the inward spread of depolarising current, which could in turn account for an activation decline of the muscle fibre (Rack and Westbury (1969)). Furthermore, changing the length of a muscle fibre not only changes the degree of overlap between myofilaments but modifies other processes, like the myofilamental sensitivity to Ca^{2+} (Endo (1973); Stephenson and Wendt (1984)).

With respect to the force-length relationship, the extensor tibiae is a rather unspecialised muscle, which is supported by the following examples. Active force-length curves vary in the degree to which force decreases with changes in length. The largest differences are seen when comparing flight muscle, that can only generate maximum force over a very narrow range of strain (2-4 %) with body-wall muscle of animals that crawl using hydrostatic skeletons (Full (1997)), that can operate over a much broader range of strain (200 %). Abdominal muscle M214 in the locust (*Locusta migratoria migratorioides*), which is involved in oviposition, is able to tolerate extensions > 8 mm, when the animal is mature. The muscle can generate forces $> 0.2 \frac{P}{P_0}$ when being extended more than twice the length at which isometric force development is maximal. This might be due to a special mechanism, that allows z-line fragmentation into 'Z-bodies' and therefore provides an enormous dilatibility, see also Jorgensen and Rice (1983). *Connectin*, which connects myosin filaments with the Z-lines, is likely to play in concert with *Projectin* a major role in this context (Rose et al. (2001)). Chameleons are well known for their ability to project their tongue $> 1000\%$ of the resting length while catching large prey (Herrel et al. (2002)). They are able to generate constant force over a wide range of extension lengths *in vivo* (Herrel et al. (2001)). In this case, this is due to extensive overlap between thick and thin filaments at maximal extension and due to perforations in the Z-disks (Rice (1973); Herrel et al. (2001)).

D3 Passive forces I

Summary

Muscle stretch of different amplitude and duration demonstrates that both tibial muscles show a visco-elastic behaviour. The passive static force component increases exponential-like with increasing stretch although values within the working range do not exceed about 5 mN for the extensor and about 15 mN for the flexor tibiae. Dynamically flexor tibiae forces can become as big as 60-70 mN when ramps were mimicking middle leg swing. Photographical tracking could confirm the results from muscle stretch experiments in terms of suggesting passive forces to be the main actuators determining tibia rest position besides extensor and flexor tibiae joint tissues. Joint torque measurements demonstrated that torques are not dependent on the FT-joint angle within the range tested. However, joint torques are dependent on deflection amplitude (and velocity) and therefore suggest the joint to act like an attenuator that resists to fast tibia deflections.

Discussion

All muscles exhibit dynamic forces against passive lengthening. The amount of passively generated force is a topic getting mostly less attention, although an important component of the load on the contracting agonist (e.g. a human arm flexor) is represented by the passive stiffness of the stretching antagonist, e.g. a human arm extensor (Proske and Morgan (1999)). The biphasic passive tension rise in response to a ramp stretch (the dynamic passive force component, see Figs. C.25, C.32 and C.34) is stretch-history-dependent (Denny-Brown (1929)) and cannot be adequately described in terms of purely elastic behaviour (Lidell and Sherrington (1925); Proske and Morgan (1999)). The initial steep tension increase can be interpreted by the presence of crossbridges between actin and myosin within resting sarcomeres (Hill (1968); Proske and Morgan (1999)): D.K. Hill describes a 'spring-like' elastic resistance that is responsible for the early stages of a passive muscle stretch being due to the mechanical stiffness of a small number of cross-bridges in resting muscle. The tension rise and the size of the stretch are linearly related at the very beginning of stretch, as long as the cross-bridges do not significantly detach. After exceeding their elastic limit, cross-bridges start to detach and a slightly velocity-dependent, constant frictional resistance builds up (in respect to 'slightly velocity dependent', see Fig. C.34).

Filaments are responsible for at least 50 % of muscle compliance. The local spring in the crossbridge is half as compliant as previously assumed (Irving (1995)).

A more recent research for the major contributing factor to the passive-length-tension relation led to the insight, that the elastic gap filaments, composed of the extensible protein *Titin*, which links Z-lines with thick filaments, are an important source of passive tension in muscle (Wang et al. (1991); Proske and Morgan (1999)). Together with the 'viscous friction between the sliding filaments', cytoskeletal elements like *Titin* are supposed to contribute to tension responses observed during stretch (Proske and Morgan (1999)).

However, investigations like the creep experiment (Figs. C.64 and C.65) or the asymmetry of the tension responses to a ramp stretch and to a ramp release (Fig. C.68) show that the dependency of stretch responses on the immediate history of contraction and length changes (thixotropy) cannot be explained simply in terms of viscous and viscoelastic properties. A muscle that relaxes after contraction reforms its cross-bridges to develop a 'short-range elastic component' (see Hill (1968)). When the muscle is passively shortened, 'muscle slack' develops because compressive forces on sarcomeres lead to the detachment of some, but not enough cross-bridges to fully take up the shorter length. The bridges being responsible for the 'short-range elastic component' exert most likely a pushing action which opposes passive tension. Interestingly, these bridges have a low turnover rate and do not detach as rapidly in response to compression as do actively cycling bridges in response to stretch (Lakie et al. (1984); Morgan et al. (1984); Proske and Morgan (1999)). The shape in tension rise during passive muscle stretch can be altered by the presence or absence of slack (Proske and Morgan (1999)). This finding is further supported by examinations on the cat medial *gastrocnemius* muscle, where slack was intentionally evoked by prestretch and where passive tension rise showed a considerable delay compared to the 'non-slack' - situation (Whitehead, N.P. Gregory, J.E. Morgan, D.L. and Proske, U. (unpublished observations)).

Stick insect experiments investigating static passive muscle forces were normally done by setting the muscle to its resting length (by definition 90° FT joint angle), then shortening it and stretching it continuously in ramps afterwards (see *Materials and Methods*

section). Presumably, slack was induced by the initial passive shortening. As the aim of these studies was the assessment of static passive tension dependent on muscle length, the differences in dynamic tension development because of slack did not matter. When active muscle forces were investigated additionally, slack should have been removed by active cross-bridge cycling (Proske et al. (1993)) prior to a stretch. Dynamic passive force examinations (Figs. C.32, C.33, C.34) did not involve any pre-stretch and tension rises were not delayed as described for stretches following muscle slack (Whitehead, N.P. Gregory, J.E. Morgan, D.L. and Proske, U. (unpublished observations)).

As was shown, tibial muscles relax very fast right after having reached a new length level (i.e. after the end of the stretch, see Figs. C.25, C.26, C.27, C.28, C.29). This relaxation becomes slower and slower with time, i. e. the force decays less and less but it will never reach a constant equilibrium (Malamud (1989)). As this is an infinite process (Malamud reported having detected tensions to diminish even when stretch was maintained for 2-4 hours; Fig. C.27 shows a 45 min recording), this led to the decision to measure the values for the static component of the resting tension when the stress relaxation becomes less slower than approximately $0.3 \frac{mN}{min}$. Malamud tried to fit his relaxation data (measured in the locust flight muscle Tcx₂ in *Schistocerca americana*) with an exponential function with four or more time constants which were independent of strain, the slowest even had a value of more than 60 minutes (Malamud (1989)). The explanation to the use of multiple time constants is as follows: many biomaterials such as collagen, and even crystalline polymers such as polyethylene, show multiple-component relaxation spectra rather than simple one- or two-exponential relaxation curves (Wainwright and Gosline (1976)). It is proposed that the different domains of these large molecules relax at different rates, which leads to multiple-component relaxation spectra. Malamud mentioned that 'the relaxation curve formed by multiple spectra' will, under some circumstances, be fitted by a power function (Malamud (1989)). Thorson and Biedermann-Thorson suggested the use of a power function characteristic to fit their data (Thorson and Biederman-Thorson (1974)), too. They were studying relaxation processes in sensory adaption and state that power-law decays in general have been shown to be characteristic of 'small-signal' responses of many receptors (Thorson and Biederman-Thorson (1974)). White was also describing stress relaxations of insect fibrillar flight muscle with power functions (White (1983)), and so did Josephson with the stress relaxation of a beetle hindwing depressor

as well (*Cotinus mutabilis*, Josephson et al. (2000)). To sum up, the approach seemed to be reasonable to attempt fitting extensor and flexor tibiae stress relaxations with power functions which turned out to match pretty well (R values of ≥ 0.937). Extensor tibiae exponents of increase ($1 - k$) and decrease ($-k$) were shown to be different, which suggests that different processes happen during stretch and the subsequent relaxation (see Fig. C.26b).

The actual static portions of resting force in both tibial muscles increase almost exponentially with muscle length, see Figs. C.30 and C.31a, like e.g. metathoracic femoral extensor muscles 178 and 177d in *Periplaneta americana* or the meropodite-carpodite extensor and flexor of *Carcinus maenas* (Yox et al. (1982), the tergo-coxal flight muscle in *Schistocerca americana* (Malamud (1989)), various extensors of the cockroach hind leg (*Blaberus discoidalis*, Full and Ahn (1995)), as well as the feline hind limb muscle (*caudofemoralis* muscle, Brown et al. (1999)). Noticeably, resting tension of extensor and flexor tibiae is much weaker than in other systems: maximum static resting force of the extensor tibiae is only about 20% of the active muscle force (maximum static resting tensions at 140% muscle length stay below 20 mN, whereas the muscle's maximum tetanical contraction force was as large as 120-200 mN), much lower than the values presented by Malamud (Malamud (1989)) or Brown and colleagues (Brown et al. (1999)). Static passive tension can sort of 'compensate' for active forces: cockroach extensors operating on the descending limb of the force-length relationship when being flexed manage to vary their total musculo-apodeme force by less than 3 % over the entire working range because passive force increase compensated the decline in active force at highly flexed joint positions (Full and Ahn (1995)). For the stick insect, the relative weakness of extensor muscle static resting force is even more striking when considered within the muscle's working range, where it does not exceed 5 mN, very similar to the *soleus* muscle in the cat, where the muscle hardly exerts static passive tension within its range of operation (Rack and Westbury (1969)). The passive static tension curve in the *Cuniculina impigra* front leg extensor tibiae measured 1 min after a position step shows very similar values, i.e. < 10 mN up to 0.6 mm stretch (Bässler et al. (2007)).

However, during walking, the dynamic resistance to stretch is what is likely to have the greatest functional importance as it can be a multiple of the static component,

depending on the starting position of the stretch, its amplitude and the ramp speed. Flexor tibiae muscles were stretched with ramps of 0.5 mm in 100 ms (see Fig. C.32). This kind of stimulation was supposed to mimick an average middle leg swing phase of a freely walking stick insect in which the flexor tibiae is passively lengthened due to contraction of the extensor tibiae. Considering FT-joint angular deflections of $70.8^\circ \pm 10.7$ (n=27) to $90.6^\circ \pm 11.8$ (n=27) during single middle leg stepping on a treadmill (N=3, from v. Uckermann and Büschges (2008)), flexor tibiae stretches of 0.5 mm are close to the range of muscle length changes that would occur during step-like movements: 0.5 mm stretches starting at 60° FT-joint angle (see Fig. C.33, middle column) simulate a tibia deflection of 53° , 0.5 mm stretches starting at 90° FT-joint angle (see Fig. C.33 left column) simulate a tibia deflection of 63° . Hence, ramps of 0.5 mm correspond to tibial deflections smaller than those measured during treadmill walking. However, two things need to be considered. Firstly, swing phase time in the single-leg preparation is much longer than in freely behaving animals (compare Fischer et al. (2001) with Graham and Cruse (1981)). Secondly, FT-joint angles changes in freely walking animals are less than in the single leg preparation (compare Cruse and Bartling (1995) with v. Uckermann and Büschges (2008)). To sum up, the ramps used are close to mimick realistically occurring swing phases and elicit passive dynamic flexor tibiae forces that need a large amount of the actively generated extensor tibiae force to get overwhelmed in order to extend the tibia during swing, taking into account that the flexor tibiae's moment arm is twice the extensor tibiae's (see Fig. C.3).

The amount of dynamic passively generated force of the extensor tibiae (see Fig. C.33 right column) is not considerably smaller than the flexor tibiae's, as both values are not statistically different from one another. Interestingly, although the estimated cross-sectional area ratio of flexor tibiae to extensor tibiae is 2:1 (see chapter C1) and passive force is supposed to scale with cross-sectional area (see below for detailed explanation), passive dynamic force seems to be approximately equal. In respect to joint stabilisation, a large passive extensor tibiae force can be advantageous as maximal active flexor tibiae forces are much larger than the antagonist's and the flexor tibiae's moment arm length is double the extensor tibiae's anyway. In the cat, *triceps surae* passive tension in response to slow extension was shown to be sufficiently large to add significantly to the active tension (Grillner (1972)).

A reasonable extension of the ramp experiment mimicking swing would be to repeat it with simultaneous physiological stimulation of the CI_2 and / or CI_3 motoneurons that innervate parts of the flexor tibiae (Debrodt and Bässler (1989)) to examine to which extent dynamically generated passive flexor tibiae force can be reduced to facilitate tibia extension. Debrodt and Bässler could show that CI_2 or CI_3 stimulation produced IPSPs in extensive regions of the muscle. From locusts (*Schistocerca gregaria*), we know that relaxation after high frequent SETi activation of mesothoracic extensor tibiae fibres is clearly accelerated when the CI_1 motoneuron is stimulated (Burns and Usherwood (1978)).

Photographical tracking of tibial deflection to either maximal extension or flexion in cut middle legs demonstrated the individual impact of passive extensor and flexor tibiae muscle (see Fig. C.35) and the connective tissue sheath surrounding the outer (close to the extensor tibiae) and the inner (close to the flexor tibiae) FT joint (see Fig. C.36). Yox et al. (Yox et al. (1982)) suggested these elements to be the main cause for resting tension, a possibility that Berkowitz and Laurent raise as well (Berkowitz and Laurent (1996)). The latter ones reported observing locust grooming movements without muscle activity and suggested mechanical contribution due to energy transfer from movement of other leg segments, e.g. levation of the femur, that ‘flings’ the tibia into an extended position. It could be shown that the equilibrium joint angle after extension or flexion was slightly flexed ($89 \pm 1^\circ$ and $76 \pm 1^\circ$, respectively) and that this matched quite well with the intersection range of the average passive extensor and flexor tibiae forces ($65\text{-}85^\circ$ FT joint angle, see Fig. C.31a). Using the determination of torques acting on the joint (see Fig. C.31b), the intersection range shifts slightly towards a more flexed position (about $55\text{-}65^\circ$ FT joint angle), which is still close to the range of equilibrium joint angles after extension or flexion of the tibia (see above). It is possible that the presence of inner and outer joint tissues (see Fig. C.36b and c) in the intact joint ‘pushes’ the tibia towards the more extended range of equilibrium FT joint angles. In the locust (*Schistocerca gregaria*), a very similar resting angle of 70.9° was found (Zakotnik et al. (2006)). Further agreement shows the following data set: cockroach (*Periplaneta americana*) resting FT joint in amputated legs showed a mean value of $72 \pm 6^\circ$ with an equilibrium point (at which muscles 177d and 178 exerted equal tension) at 78° (Yox et al. (1982)). Crab (*Carcinus maenas*) resting meropodite-carpopodite joint in amputated legs showed a mean angle of $82 \pm 10^\circ$ and an equilibrium point (of the joint’s extensor and flexor) at 80° (Yox et al. (1982)). Yox and colleagues claim non-

neural resting tension to be used to maintain joint position and further to maintain posture at an energetically low cost in arthropods and found the equilibrium point resting tension to be approximately equal to the animals weight (Yox et al. (1982)). This is a calculation that may also be true for stick insects like *Carausius morosus*: with an average mass of 0.94 ± 0.7 g (N=10), an equilibrium point tension of 2.5 - 5 mN is certainly enough to maintain a gravity independent tibia position: protractor / retracor coxae and EMG recordings while rotating the animal in the air in all planes show that middle leg posture can be maintained throughout with motoneuronal activity being silent (Hooper et al. (2009)). When the animal is hanging in the vertical plane with its longitudinal axis parallel to the ground, the total FT-joint equilibrium point resting tension of all six legs is what is supposed to maintain animal posture, therefore the required resting tension would be $F = m \cdot a = 0.94 \text{ g} \cdot 9.81 \frac{\text{m}}{\text{s}^2} = 9.22 \text{ mN}$, i.e. 1.54 mN for each leg ($\frac{9.22 \text{ mN}}{6}$). This calculated value represents a coarse approximation which is, interestingly, in the same ballpark as the equilibrium point tension is of 2.5 - 5 mN (Fig. C.31). Observing stick insects hanging vertically with their longitudinal axis parallel to the ground reveals that they actually increase the FT-joint angles of all six legs (i.e. they extend the tibia compared to standing horizontally): this new joint position takes advantage of the flexor tibiae static tension characteristic increasing steeper than the extensor tibiae's (see Fig. C.31), which might support posture maintenance of the whole body. It is of special note that ablation of motoneuronal innervation in the front leg extensor tibiae of *Cuniculina impigra* can be compensated within 17 days by shifting the passive static force tension curve towards higher force values: this increase in passive tension shifts the FT joint's equilibrium point towards much more extended tibia positions (resting positions of 170-180° after 4-16 days, Bässler et al. (2007)). This new equilibrium point enables the animal to use the leg sometimes even during walking.

Removal of the connective tissue sheath alone had considerable impact on tibial equilibrium position as well (see Fig. C.36), although tendons of both tibial muscles were left intact. Generally, cuticular structures are known to participate in passive force generation in a major way: e.g. locusts (*Schistocerca gregaria*) can store previously generated large forces in elastic distortions of the tendons and the femoral cuticle required for rapid tibia extension (Bennet-Clark (1975); Sasaki and Burrows (2003)). During co-contraction, a locust's semi-lunar process between femur and tibia is bent progressively. A cuticular lump is able to lock the FT-joint until extensor tibiae force

overwhelms flexor tibiae force and finally loosens the lump leading to a kicking of the hindleg (Sasaki and Burrows (2003)). Another example for joint structures generating passive forces is the rubber-like protein *Resilin*, that contributes to elastic energy storage in the beetle wing (in *Pachnoda marginata* and *Coccinella septempunctata*, Haas et al. (2000)). Passive forces in general are suggested to initiate movements and passive properties of the musculoskeletal system cause large joint stiffness (Zakotnik et al. (2006)). For instance, passive force in locust is reported to be as high that the locust FT-joint can be extended without any motor activity during scratching (*Schistocerca gregaria*, Matheson and Dürr (2003)). Insufficient stiffness of the unloaded tibia is not big enough to stabilise the joint against the locust tibia's intrinsic moment of inertia. Even in larger animals like the cat, interactive torques are less during slow walking than during fast walking and passive -elastic forces of the posterior thigh muscles might be sufficient to decelerate knee extension without requiring muscle contraction (Smith and Zernicke (1987)).

Interpretation of the results presented in chapter C3 involves the insight that small animals like insects have to deal with large passive forces of their muscles. This leads to the question in which way locomotion is affected by these forces and which consequences can be expected in comparison to larger animals, like cats, horses or elephants: muscle scaling in relation to body size is the determining factor when comparing e.g. motoneuronal firing during movement, especially swing movement. The swing phase in human walking is a good example of a truly ballistic movement which should by no means be compared with stick insect swing phase.

In human walking, muscles act only to establish an initial configuration and velocity of the limbs at the beginning of swing phase. Leg and body move then through the rest of the swing phase under the action of gravity (Mochon and McMahon (1980)). Thus, in addition to the concept of the inverted pendulum which serves most often as an analog for walking but which, in fact, does not include a time of swing, one has to consider the analog of a compound pendulum to get the simplest representation of walking. This model is able to disregard muscle action entirely, except for setting the initial positions and velocities of the limbs at the beginning of swing phase (Mochon and McMahon (1980)). When walking down a hill, muscles can completely be abolished as leg swing can be achieved entirely by gravity. A freely oscillating human

leg shows a nonlinear behaviour as the second oscillation cycle period is significantly lower than that of the first, suggesting an increase in stiffness (Coveney et al. (2001)). The mere fact that the human leg has the ability to oscillate passively shows that the passive muscle forces are small compared to the forces of gravity. The inertial effects of upper and lower leg, foot and added mass are represented by a single mass with a parallel spring and a viscous damper, representative of the muscle tendon unit's behaviour.

In the stick insect, this model will not hold. The inertial effects of the tibia and the tarsus are negligible compared to the tibial muscles' strength. A ballistic movement is impossible, as neither extensor nor flexor tibiae can take advantage of the tibia's inertia. This can be verified by looking at motoneuronal activity among animals of different size: the middle leg extensor tibiae needs to be activated throughout swing phase (Fischer et al. (2001)) in order to extend the FT joint. The same is true for the *protractor coxae* of the middle leg (Hooper et al. (2009)). In contrast, human illipsoas muscle motoneurons fire only at the begin of swing phase in order to accelerate the lower leg, the rest of swing movement is done ballistically (Hooper et al. (2009)). The larger the animal, the heavier its limbs: in a horse, swing phase motoneuronal activation is even shorter than in man. This mechanism has further consequences: the smaller the animal, the more the relative strength. An often used example is the fact that ants have the capacity to carry a multiple of their own mass, because muscle force scales as $(\text{bodymass})^{0.67}$ and muscle mass scales as $(\text{bodymass})^{1.0}$ (Hutchinson and Garcia (2002), see also Schilder and Marden (2004)). Consequently, a human individual is just about able to carry the mass of another person, whereas an elephant will not be strong enough to carry another elephant on its back. Active force of a muscle scales with its cross-sectional area, i.e. the number of actomyosin cross-bridges working in parallel (Hill (1950)), as both muscle mass and muscle area ratio show strong positive allometry (Bennett and Taylor (1995)). Consequently, passive muscle force should correlate positively with cross-sectional area as well. Thus, passive muscle force gains importance in terms of limb's movement the smaller the animal. Relating the idea to stick insect locomotion, a large portion of the active forces exerted by a tibial muscle will have to be used to 'overwhelm' the antagonist's passive forces instead of actually moving the limb (i.e. the tibia), which is what one might think in the first place. However, tibia mass is so small that a ballistic movement is completely inconceivable. Even at ballistic movements like human forearm swing, the contribution

of viscoelastic forces alone can manage to brake slow swing if agonist force does not exceed passive force (Lestienne (1979)). To sum up, the actual ratio of limb mass to passive muscle force is crucial. If passive muscle force is larger than the gravitational forces acting on the limb, limb joint angle at rest will not change when the joint orientation is altered, like e.g. the stick insect FT joint, the cockroach TC joint (*Periplaneta americana*), or the human finger joints (Hooper et al. (2009)).

In addition to the massive differences in relevance of passive muscle force, the stiffness of muscle tendons is another parameter that bears large discrepancies between large vertebrates and small invertebrates (see e.g. Zajac (1989)). Interestingly, at the very beginning of a muscle stretch, most of it is taken up by the tendon and the muscle fibres themselves are stretched only when tension begins to rise (Proske and Morgan (1987; 1999)). Kangaroo hind limb muscle tendons (of the *gastrocnemius* muscle, *fds*, *fdp*) serve as major elastic strain energy stores and demonstrate how tissue elasticity is strongly mass dependent and elastic energy storage scales with body size (Bennett and Taylor (1995)). Thus, tendon elasticity can significantly reduce the cost of travel.

Arthropod apodemes being 40 times as stiff as mammalian tendons (Ker (1977); Full and Ahn (1995); Full et al. (1998)) cannot store energy to this extent. Consequently, in order to accomplish limb movement, the stick insect cannot take advantage of this kind of tendon elasticity storage as it has a) a small mass and b) a stiff tendon, which further stresses the necessity of continuous motoneuronal firing throughout limb movement in small invertebrates like the stick insect.

Examination of FT-joint torques with the Aurora 300 B system involved measurement artifacts that were bothersome, yet controllable (see red trace in Fig. C.37**(i)**, **(ii)**, **(i)** and **(ii)**). The mass of the custom-built measurement device (see Fig. B.4) was too large for the fine-tuned Aurora system that typically operates exclusively with the lever that is delivered from the manufactory (see Fig. B.7**(d)**). This mass bore a moment of inertia that could not be compensated by re-fine-tuning the Aurora controller. Subtraction of the torques exclusively elicited by the device resulted in a hardly overshooting signal in response to joint deflection (see black trace Fig. C.37**(i)**, **(ii)**, **(i)** and **(ii)**). The mean torque of the mere device was significantly different (***, $p < 0.001$) from the mean torque of both joint and device (see Fig. C.37). Thus, the

accuracy of the measurements was impaired, yet the signal resolution was clearly detectable.

Torque of the mere FT joint with both extensor and flexor tibiae muscle tendons cut was shown to be dependent on deflection amplitude (see Fig. C.39) but not on angular position (see Fig. C.38). Physiologically, this has two major consequences. First of all, the faster the tibial movement, the more it gets damped as friction is velocity dependent. Secondly, the data show that, within the range of FT angles tested (82° - 98°), the force required to deflect the tibia to an equal extent does not increase when the tibia is either stretched or flexed, i.e. the joint does not (or only slightly) get stiffer within a certain range of joint angles. Only a weakly significant (*, $p < 0.05$) linear increase could be detected (see Fig. C.38). Thus, the data provides good evidence that the FT-joint features the remarkable combination of being position independent and excursion dependent at the same time.

Such a special arrangement could as well be conceivable for horizontal eye ball movements. The muscle-eyeball system is dominated by muscle mechanics, inertia of the globe makes only minimal effects (Childress and Jones (1967)). However, the muscle-eyeball system is heavily damped. There are other biological examples of having no particular set point, but being resistant to fast changes: an untrained man walking fast from an altitude of 500 m up to 5000 m will get big difficulties with breathing, as the air gets thinner with increasing altitude. In contrast, when doing the whole process step by step (spending a week at 2000m, another week at 3000 m etc.), the number of erythrocytes will be adapted continuously and breathing will be possible even at high altitudes. Similarly, a person flying from middle Europe to Japan will suffer from jetlag in the first few nights. After a while, the circadian inner clock operates in the same way as in Europe, but with an offset of eight or nine hours. The same principle can also be explained with physical examples: the outer frame of a gyroscope can be positioned no matter how, it has no preferred position within one degree of freedom when the inner wheel is not turning. As soon as the inner wheel is turning, deflection of the outer rim becomes more difficult, i. e. is has become resistant to fast position changes.

D4 Force measurements in the isotonic domain

Summary

Isotonic extensor tibiae experiments in response to physiological motoneuronal input previously gained by recording nerve activity while the animal performed step-like movements suggests the muscle to respond highly variable in terms of the contraction shapes observed. Nonetheless, response to the same pattern is similar between animals. The muscle acts like a low-pass filter by contracting smoothly to a ragged stimulation pattern. Step-like movements arise in most cases from about 40-50 spikes of the FETi motoneuron, mean burst duration is about 0.41 s and mean interburst interval 2.3 s. Hill hyperbolas at 200 Hz vary much in terms of maximal force and vary less in terms of contraction velocity for both extensor and flexor tibiae. Maximally stimulated flexor tibiae muscles are on average 2.7 times stronger than extensor tibiae muscles (415 mN compared to 151 mN), but only 1.4 times faster contracting ($6.05 \frac{mm}{s}$ and $4.39 \frac{mm}{s}$). Both tibial muscles reveal deviations from the hyperbolic shape close to P_0 towards smaller contraction velocities. Isotonic lengthening experiments on the extensor tibiae show this deviation to persist at loads $> P_0$, further loading ($\gg P_0$) leads to a sigmoidal curve progression. Extensor tibiae Hill experiments at different stimulation frequencies reveal both V_0 and P_0 to become bigger with increased activation. The relation of stimulation frequency with V_0 and P_0 respectively can be described with an exponential saturation curve of the form $y_0 = y_{0_{max}}(1 - e^{-\frac{f}{f_0}})$, V_0 and P_0 correlate linearly. The relation between maximal contraction velocity and extensor tibiae muscle length can be described with a monotonic and nearly linear increase within the muscle's working range, followed by a plateau at longer fibre lengths. Velocity of a contraction's isometric force increase is much faster in a muscle being stretched than in relaxed state. Velocity of an isotonic muscle length change in turn is only slightly faster in the stretched state compared to the muscle being relaxed. The period in time to increase load to a shortening muscle is crucial: loading the muscle during the first 0.15 s of an isotonic contraction (depending on the load) leads to a shortening progression, the same load applied later in contraction leads to a muscle lengthening.

Discussion

A fourth of the steps analysed in Figs. C.41 to C.43 (22 out of 87) had interburst intervals > 2 s and were omitted because of the reasons described above (a robust walking sequence has a frequency of about 1 Hz). Removal of these step-like movements results in a mean interburst interval of 0.77 ± 0.39 s ($n=65$). With a mean burst duration of 0.41 ± 0.24 s ($n=87$), step frequency was a little bit less than 1 Hz, which is about the usual walking speed of adult freewalking *Carausius morosus* (Bässler (1983)). The discrepancy between the usual swing phase durations of 100-120 ms (Bässler (1983)) and the values measured from these steps might be due to fact that swing phases in tethered animals (single leg preparation, Fischer et al. (2001); Schmidt et al. (2001)) differ a lot in terms of sensory feedback. A tethered, supported stick insect gets different input from the trochanteral and femoral campaniform sensilla, the latter being mainly responsible for the switch from extensor tibiae to flexor tibiae activity (Akay et al. (2001)). Nonetheless, spike patterns from these steps were used to drive the extensor tibiae muscle for two reasons: first of all, many stick insect experiments over the last years were done with the single leg configuration in animals supported by a platform (e.g. Akay et al. (2004); Ludwar et al. (2005); Gabriel (2005); Borgmann et al. (2007); v. Uckermann and Büschges (2008)); secondly, there is no reason to believe that the actual spiking patterns during single-leg walking are much different from free walking except for the burst duration, as the animal truly performs the actual movement (therefore the extensor tibiae is obviously capable to do it). In general, the motor output has to adapt to changes in the biomechanical properties of the moving parts or to transfer functions of sensory systems, this was tested in several experiments investigating the ability to either adapt or recover, e.g. after surgical muscle manipulations (*cat*: Pearson et al. (1999); *Cuniculina impigra*: Bässler et al. (2007)). The step sequence presented in chapter C4 is one of seven sequences analysed in Hooper et al. (2006; 2007a;b). From these analyses, this sequence does not explicitly differ from the other six sequences used. It is essential to know how the output patterns generated by a representative animal look like in order to design reasonable, physiological relevant stimulation paradigms (nerve stimulation, muscle load, muscle strain) and for the interpretation of the muscle data presented in this thesis. The knowledge about the actual transformation into movement is of particular importance when analysing brisk motoneuronal output changes, as the muscle might not be able to follow to fast changes anyway. This might seem disadvantageous for the neuromuscular system at first. However, the extensor tibiae can take advan-

tage of the history-dependent effects described in chapter C2 in terms of producing a smooth movement in response to irregular input. Most of the analysed contractions are typically characterised by a steep increase of instantaneous FETi spiking frequency (see Fig. C.46 and Hooper et al. (2007a)), which decreases steadily and which features long interspike intervals in parts. Due to the initial high-frequent activation, such gaps could eventually be bridged, as isometric force data in chapter C2 demonstrate that relaxation is delayed the more the extensor muscle was activated before (reflected in either more spikes or higher spike frequency, see Figs. C.18 and C.16). Hence, a continuous shortening might be accomplished despite a lack of motoneuronal input. This could actually be a common strategy in small insect muscles in locomotion: posterior coxal levator muscles 182C and 182D in the cockroach *Periplaneta americana* show maximum frequency of the coxal depressor motoneuron D₈ to occur at the burst beginning as well (Pearson and Iles (1970)). In contrast, vertebrate muscle is likely to respond much faster (Edman (2005); Lappin et al. (2006)), i.e. the requirement of a persistent firing pattern is bigger in order to shorten smoothly, because large interspike intervals would immediately be transformed into a relaxation.

As described by Hooper and colleagues (Hooper et al. (2006)), stepping behaviour can be very different in terms of contraction shape, i.e. the muscle length changes that are finally move the limb. As was shown in chapter C4, the muscle shortenings can either have a rather trapezoidal or a rather triangular shape, they can either have a multi-sloped shortening phase or a multi-sloped relaxation phase. By many parameters (e.g. slope of the contraction rise or fall), extensor tibiae muscles from different individuals differ statistically from one another (detailed quantitative analysis in Hooper et al. (2006)). Overdrawn contractions allow the impression that extensor tibiae muscles of five exemplary animals respond similarly to the same physiological input at first sight (Fig. C.44). Having been subject to further more detailed analysis, extensor tibiae muscles responded indeed similarly to changes in neural input, at least on a burst-to-burst level (Hooper et al. (2006)). When contractions are plotted versus spike number, and not time, the rises per spike were identical (Hooper et al. (2007b)), which could already be shown for the lobster (*Panulirus interruptus*, Morris and Hooper (1997)). Hence, extensor tibiae muscles present a single population, even though there is considerable animal-to-animal variation. This is a very important finding as this enables averaging muscle data across animals (Hooper et al. (2006)), which was performed throughout this thesis. Driving the muscle with previously

recorded FETi motoneuron patterns recorded during step-like movement activity is supposed to mimick a physiological situation quite close. Although FETi, SETi and CI₁ are simultaneously active during middle leg swing (Büschges et al. (1994)), the SETi motoneuron's main role is most likely to maintain posture. In the locust middle leg, tension rise time in response to SETi stimulation is nearly 1 sec and cannot be the main determinant in walking (*Schistocerca gregaria*, Burns and Usherwood (1978)), although SETi is active with FETi being silent at the beginning of retraction (Burns and Usherwood (1979)). In the locust hind leg, SETi is the only excitatory extensor motoneuron to be active during walking (Burns and Usherwood (1979)). Physiological stimulation of the SETi motoneuron (previously recorded during walking and then played back) results in very smooth isometric force generation (*Schistocerca gregaria*, Evans and Siegler (1982)). This smoothness is very likely to be the consequence of the SETi's low fusion frequency (Burns and Usherwood (1978)). Similarly, isometric cockroach force traces of posterior coxal levator muscles 182C and 182D shown by Pearson and Iles (*Periplaneta americana*, Pearson and Iles (1970)) reveal these muscles to respond very slowly as well. Thus, the extensor tibiae is one among several invertebrate muscles that acts like a low-pass filter as it shows smooth contractions in response to rather ragged input (see Figs. C.44, C.45, C.46, C.47), comparing instantaneous frequency traces with muscle position traces (see Fig. C.46). Different from previous work, the extensor tibiae measurements were done in the isotonic force domain.

In order to reveal the extensor and flexor tibiae's force-velocity characteristic (Hill curve, Hill (1938)), a series of loaded release experiments was conducted with tonic input of different frequency. In contrast to the experiments with physiological stimulation, Hill experiments require tetanical stimulation before application of a clamped load level. The force-velocity curve can be considered as one of the many output characteristics of an underlying contraction principle (Ettema and Meijer (2000)). This is a major distinction from the length-tension curve, which is explained by structural models, e.g. the crossbridge theory (Huxley (1957a); Ettema and Meijer (2000)). Immediately after the transition from isometric to isotonic mode recording, contraction oscillations occurred (Jewell and Wilkie (1958); Edman (1988); Malamud and Josephson (1991); Edman and Curtin (2001); Siebert and Blickhan (2003)). Those may reflect the fast dynamic properties of the contractile mechanism under fast length change. Jewell and Wilkie explained those oscillations with the elastic properties of the series

elastic element represented by one of the springs in Hill's three component model (Hill (1938)). According to Podolsky and Nolan, an isotonic step change runs through different phases: between the original steady state with a certain distribution of attached cross-bridges and the final steady state featuring a different distribution of cross-bridges, there is a transitional state of zero-distortion, showing a distribution of negative distorted cross-bridges that equals the distribution of positively distorted ones. This 'gap' is the reason for the system's oscillatory response aided by the steep increase in stiffness of attached cross-bridges in the region of negative distorted cross-bridges (Podolsky and Nolan (1972)). Edman described the oscillatory course as a 'recoil of elastic structures, being situated in the inner sarcomere' (Edman (1988)). Oscillations in frog muscle fibres can have durations > 80 ms (Civan and Podolsky (1966); Sugi and Tsuchiya (1981)). Edman mentions experiments showing oscillations that persisted during the whole duration of load clamp, when the applied load was about $0.9 P_0$ (Armstrong et al. (1966); Edman (1988)). Extensor tibiae oscillations had durations from about 17 to 25 ms, depending on stimulation frequency. Isotonic extensor tibiae experiments being discarded because of the whole measuring system having been not stiff enough (the hooked-shaped insect pin pierced through the muscle tendon was attached to the servo motor via a silk filament and the mounting of the servo motor was more compliant) had durations from about 50-60 ms ($N=3$, data not shown). After these oscillations, initial contraction velocity which declines rather rapidly to zero is the result of the short fibre length and of the force-length characteristics of the extensor tibiae: by shortening, the muscle moves to a shorter length with reduced maximum force which results in a reduced contraction velocity. The contraction stops at the muscle length at which the maximum isometric force is equal to the load set in the experiment (see Fig. C.49. Thus, measuring the contraction velocity of a muscle yields automatically in getting active force - length data as well. This 'side-effect' was ignored within this thesis, but not in the data evaluation for the muscle model (Blümel et al. (2007a;b; 2008b;a)).

Extensor tibiae force-velocity curves show the well known hyperbolic shape of the Hill-curve, for which there are basically two main explanations. Firstly, the mean force that a single cross-bridge exerts decreases with increasing shortening velocity. This can be traced back to the fact that negatively distorted cross-bridges exert less force than positively distorted ones (see Huxley (1957a)). Secondly, the mean number of attached cross-bridges per time unit decreases with increasing shortening velocity as well. This can be traced back to the fact that negatively distorted cross-bridges are

more likely to detach than positively distorted ones (see Huxley (1957a)). Hill-curve measurements produced maximum isometric contraction forces that varied between 90 mN and 200 mN at activation of 200 Hz (see Fig. C.50 and Tab. C.7). The range of maximum contraction velocities was much narrower: $3.6 \frac{mm}{s}$ to $4.8 \frac{mm}{s}$. In respect to effective cross-sectional area (1.91 mm^2), tensions were 4.8 to $10.5 \frac{N}{\text{cm}^2}$. In respect to fibre length (1.41 mm), contraction velocities ranged from 2.6 to $3.4 \frac{FL}{s}$. Although absolute maximum isometric forces and contraction velocities were shown to differ a lot between extensor and flexor tibiae (compare Fig. C.50 and Tab. C.7 with Fig. C.51 and Tab. C.8), more detailed analysis of the data provides evidence that the muscles are not that different:

Similar to the extensor tibiae, the variation of maximum isometric flexor tibiae forces at 200 Hz was also much larger than the variation of maximum shortening velocities (see Fig. C.8). This result is hard to interpret because neither the measurement method should lead to more variability of one parameter compared to the other nor should differences in molecular processes (e.g. cross-bridge cycling) be responsible for such a discrepancy. Mean maximum flexor tibiae forces were more than two and a half times as large as extensor tibiae forces (see chapter D2). However, mean maximal flexor tibiae contraction velocities were only 1.4 larger than those of the extensor tibiae. Related to cross-sectional area and mean fibre length (4 mm^2 and 2.11 mm, see chapter C1), determined flexor tibiae tensions and velocities are very close to the ones determined for the extensor tibiae (determined using 1.94 mm^2 and 1.41 mm, see chapter C1). When normalised to fibre length, relative maximum velocities are $2.87 \pm 0.43 \frac{FL}{s}$ for the flexor tibiae compared to $3.12 \frac{FL}{s}$ for the extensor tibiae, when stimulated maximally. These values are rather at the lower end of the spectrum of data known for different muscles, indicating stick insect leg muscles are adapted to generate slow movements. In a similar range are mouse fibres from the hindlimb *flexor digitorum brevis* muscle ($4.0 \pm 0.3 \frac{FL}{s}$, Edman (2005)), frog fibres from the anterior *tibialis* muscle ($2.01 \pm 0.05 \frac{FL}{s}$, Edman (1988)). Clearly faster contracting are fibres from the Tcx₂ muscle in *Schistocerca americana* ($5.2 \pm 0.1 \frac{FL}{s}$, Malamud and Josephson (1991)), from cockroach extensors 177c and 179 (*Blaberus discoidalis*, $5.7 \pm 0.4 \frac{FL}{s}$ and $4.9 \pm 0.4 \frac{FL}{s}$, Ahn and Full (2002)), the cat *soleus* muscle ($4.82 \frac{FL}{s}$, Spector et al. (1980)) and skeletal muscles of the frog ($8.2 \pm 1.9 \frac{FL}{s}$, Edman (2005)). Much faster contracting are tentacle fibres from the squid *Loligo palei* with a maximum contraction velocity of $15.4 \pm 1.0 \frac{FL}{s}$ (Kier and Curtin (2002)) and fibres from the cat medial *gastrocnemius* muscle

(12.87 $\frac{El}{s}$, Spector et al. (1980)).

As already discussed in chapter D1, the comparison between extensor and flexor tibiae shows further similarities in respect to their maximum shortening velocities and the numbers of sarcomeres determined for the extensor tibiae (~ 200) and for the flexor tibiae (~ 300). Contraction velocity depends on sarcomere number (Huxley and Niedergerke (1954b); Thuma (2007); Thuma et al. (2007)) and the flexor tibiae having 1.5 times more sarcomeres than the extensor tibiae predicts therefore that the flexor tibiae shortens 1.5 times faster maximally than the extensor tibiae, which it almost does: $V_0 = 6.05 \frac{mm}{s}$ for the flexor tibiae (N=8) and $V_0 = 4.39 \frac{mm}{s}$ for the extensor tibiae (N=7), see Tabs. C.8 and C.7). An asymmetry of maximum shortening velocities in antagonistic muscles is not unusual: in the ghostcrab *Ocypode quadrata*, the *extensor carpopodite* has a V_0 of 4.6 - 4.7 $\frac{El}{s}$ and the *flexor carpopodite* has a V_0 of 5.6 - 7.0 $\frac{El}{s}$ (Perry et al. (2009)).

Measurements of contraction velocity at altered load levels $> P_0$ (i.e. stretch) can be described as being eccentric (the muscle is lengthened while being active), see Figs. C.52 and C.53. Muscle soreness is a painful experience that probably everyone might have experienced and which is known to be the consequence of eccentric exercise (Whitehead et al. (2003)). One might assume that such eccentric exercise occurs to a large amount when walking downhill ('when muscles have to absorb the momentum of the body during jumping and running', Edman et al. (1997)), which is supposedly more energy-consuming than going uphill. The theory behind this proposition comprises the occurrence of disrupted sarcomeres in series with still-functioning sarcomeres increasing series compliance and therefore reducing passive tension and shifting the optimum length for peak active force (toad *sartorius* muscle, Wood et al. (1993); amphibians and humans, Jones et al. (1997); humans, Whitehead et al. (1998)). In addition, factors such as metabolic exhaustion, structural filamental damage or electromechanical coupling failures contribute to a reduction in actively generated force (reviews by Morgan and Allen (1999); Proske and Morgan (2001)). With respect to the eccentric experiments presented in this thesis, care was therefore taken to stop the experiment when muscle rundown was obvious in terms of P_0 reduction exceeding 15%. Loads were therefore gradually increased until measurable muscle damage was appearing. Permanent after-effects indicating a weakening or complete break of some

contractile links were regularly found after application of several rapid stretches (*sartorius* muscles of *Rana temporaria* and *Rana esculenta*, Katz (1939)). Direct *in vivo* tendon force and indirect ground reaction force measurements on the ankle extensors of the kangaroo rat showed that a range of 45 to 175 % of the *in situ* measured isometric peak force are utilized by the animal during locomotion. The way the animal jumps involves rapid stretching of the muscles while being active (i.e. eccentric exercise), which comprises operations on the lengthening region of the force-velocity curve (Katz (1939); Biewener et al. (1988)). This is a good example of how force levels $> P_0$ are actually used and how they can become essential for the capacity of an animal's locomotory possibilities. The ankle joint dynamics of the cat paw-shake cycle are another good example for such eccentric exercise: active forces are derived primarily from lengthening contractions, assuring e.g. that extensor activity coincides with the development of peak extensor torque and the slowing of knee flexion (Smith and Zernicke (1987)).

Previous reports have shown that the Hill-curve deviates from a hyperbola when contraction velocity is very small and muscle force is close to being maximal (Edman et al. (1976) Edman et al. (1978) above force values of $0.65 P_0$, the corresponding velocity values are markedly lower than those predicted by the hyperbolic fit and that data from eccentric experiments cross the abscissa (zero velocity) with a slope near zero (Edman et al. (1976; 1978)) for single muscle fibres, the curve can be seen to be flat (Edman (1988)). Edman explains the deviations in the high force range as a reduced contraction velocity. In accordance to the findings in this thesis (Figs. C.52 and C.53), he sees no discontinuity in the force-velocity relation around P_0 (i.e. forces $< P_0$ and $> P_0$), as seen by e.g. Katz: a consistent divergence between the observed and calculated speed of isotonic lengthening; the actual velocities being several times smaller than the theoretical (Katz (1939)). There are two conceivable mechanisms that could be taken as a basis for the 'double-hyperbolic' shape of the Hill curve.

One explanation comprises the possibility that the deviation may result from an intrinsic Coulomb-friction in the muscle fibres. This would result in a reduced active contraction force and would lead to the sigmoid zero crossing of the Hill curve when changing the direction of movement. The consequence of this intrinsic friction would be that high passive forces would need to be overcome before movement could oc-

cur. Physiologically, this could be the case when the load affecting tibia movement changes, e.g. at the transition from swing to stance in walking of the stick insect middle leg (Karg et al. (1991); Bässler (1993a); Büschges (1995b); Fischer et al. (2001)).

Another explanation concerns cross-bridge cycling. Edman and colleagues describe a kind of a 'highly effective intracellular servomechanism' that is of particular significance in situations when the muscle is suddenly overloaded and claim that an extramuscular mechanism could hardly provide an equal protection from overstretch (Edman et al. (1997)): that is, the biphasic shape of the force-velocity curve can promote mechanical stability. They claim cross-bridges in striated muscle to act as independent force generators under various loading conditions of the muscle. The average force per cross-bridge is then reflected by the force/stiffness ratio. They further claim force output per bridge to be lower in the high-force range than expected from measurements at low and intermediate loads and suggest a model that can be aligned with the classical crossbridge works from Huxley (Huxley (1957a)) and Huxley and Simmons (Huxley and Simmons (1971)): force during shortening is a function of a cross-bridge's attachment rate constant, its traverse distance during a working stroke and its detachment rate constant. Force is assumed to be generated in several steps, where each step leads to a tighter binding between actin and myosin and therefore to a greater force production (Huxley and Simmons (1971); Eisenberg et al. (1980)). This binding sequence comprises three states of cross-bridge attachment during a working cycle (the powerstroke), the first two occurring proportionally more often during isometric conditions and during shortening at low velocity and the last one, being the strongest bound, mostly occurring during shortening (Lombardi and Piazzesi (1990); Piazzesi et al. (1992); Edman et al. (1997)). The beginning of the powerstroke features a region of slow cross-bridge attachment leading to a marked decrease in the number of attached cross-bridges and in further consequence to a fairly large drop in force (which can be measured in the Hill's curve flat region around P_0). This is the direct conclusion from the assumption that the attachment rate constant in the model by Edman and co-workers shows a Gaussian distribution in respect to the cross-bridge position (Edman et al. (1997)). Huxley (Huxley (1957a)) suggested that the force exerted by an attached bridge might be proportional to its distortion and that the probability for an attachment might be higher at positive crossbridge distortions. On the other hand, detachment might occur more often when filament sliding induces cross-bridges to attain small distortions and therefore to exert little forces. The higher the contraction velocity, the greater the proportion of cross-bridges hav-

ing negative distortions and resisting the shortening. The total amount of attached cross-bridges decreases. At maximum shortening velocity, forces from bridges with negative distortions equal the forces from bridges with positive distortions.

Looking at forces occurring in response to muscle lengthening, the increase to forces $> P_0$ can be explained again in terms of cross-bridge cycling. During lengthening, the number of crossbridges would be less than during isometric (increased probability of breakdown), but individual links would exert a larger force (Joyce et al. (1969)), just like springs would. If this extra force of individual links outweighed the reduction in their number, the tension during lengthening would exceed the isometric tension. The most strained (or distorted) bridges are the least stable ones and thus the first ones to break (Cavagna and Citterio (1974)).

While the length dependence of contraction force was a direct indication for the different degree of thick and thin filament overlap (Gordon et al. (1966b)), the question of whether the contraction velocity also depends upon fibre length is not as straightforward. White treated the contraction velocity according to Gordon et al. (1966b) as being independent of fibre length and coined the 'tug-of-war-concept': "The tension such a team can exert is proportional to the number of members in that team, but if the rope between two teams is cut, then the maximum rate at which the team can move is the speed with which any individual member can run (White (1977))." However, in doing so, White cited Gordon et al. (Gordon et al. (1966b)) incompletely: Gordon et al. stated for long fibre lengths beyond the resting length that V_0 changes only little (15%) with length, while isometric force P_0 declines from 100% to 40%. The data in chapter C4 show a similar broad plateau, much broader than the narrow maximum of the force-length curves presented in chapter C2 (compare Fig. C.56 with Figs. C.23 and C.24). But Gordon et al. show explicitly that for shorter fibre lengths the maximum contraction velocity V_0 decreases linearly with fibre length, in agreement with our findings. Abbot and colleagues (Abbot and Wilkie (1953)) also show this for short fibre lengths. Edman (1979) finds a similar result for short fibre lengths, but an increased V_0 in the range of long fibre lengths, presumably caused by the increased resting tension of the fibres. Although it was not possible to measure the contraction velocity without any load with the experimental design used within this thesis, the residual load was attempted to be kept as small as possible. The residual load at 200

Hz accounts for 1% (filled circles) and 3% (open circles) of the maximum contraction force P_0 (the values of the rest load are not shown). Under these conditions, the contraction velocity decreases to 50% at short fibre lengths, whereby the relative load increases to 1.6% (5%) because of the decreasing maximum contraction force. The minor rise in relative load is negligible, the length dependence is for real: it is highly improbable that the effect shown will turn into a completely different characteristic just because of this marginal increase.

The 50 Hz curve shows that an increase in relative load can indeed falsify the length dependence: here, the relative portion increases from 2% to 80% of the maximum contraction force. The contraction velocity falls back to almost zero, because the strongly reduced contraction force at this length has almost reached the force value of the residual load.

Especially in terms of aiming for muscle modelling, a very essential investigation concerned the dependence of the extensor tibiae Hill-curves across a range of stimulation frequencies that covered the physiological firing range (30-200 Hz) of the extensor motoneurons (see Fig. C.54 and Tab. C.9). Both maximum contraction force (P_0) and maximum contraction velocity (V_0) greatly increased with frequencies up to around 60 Hz and then began to level off, achieving near maximum values at frequency values beyond 100 Hz (see Fig. C.55a and b). This is consistent with the fact that contraction amplitude at large spike numbers does not increase in tonic stimulations at spike frequencies > 100 Hz, although spike frequencies up to 325 Hz can occur in real physiological bursts (see e.g. v. Uckermann and Büschges (2008)). As such bursts are usually highly variable, variation in average spike frequency above 100 Hz can still have functional effects (Hooper et al. (2007b)). The curvature of the Hill-characteristics is greater at low activation compared to higher activation (see 'c' - values for Fig. C.54 and Tab. C.9). Similar observations were made in the frog, where F-V curves were measured during different times after tetanus onset (13% P_0 , 25% P_0 and 100% P_0) and curvature was greater at lower activation, i.e. early in tetanus (Edman and Josephson (2007)).

Both P_0 and V_0 data sets were well fit with equations of the form $P = P_{0_{max}}(1 - e^{-\frac{f}{f_0}})$ and $V = V_{0_{max}}(1 - e^{-\frac{f}{f_0}})$ in which the mean 'frequency constants' f_0 were identical

(see Fig. C.55a and b). f_0 may reflect the time constant of a process common to both force production and contraction velocity such as Ca^{2+} -summation. Consistent with this common dependence, V_0 and P_0 were linearly correlated with each other in single preparations, although some animal to animal variability was present (see Fig. C.55c). Summarising, these data suggest that for the control of force and contraction velocity of the extensor tibiae, changes in motoneuron firing are most effective below 80 Hz. The differences between P_0 and V_0 at 80 Hz and 200 Hz activation are much less than between 30 Hz and 80 Hz activation. In great similarity with these observations, activation-frequency relationships of the caudofemoralis muscle in the cat show that differences in activation are strongest between 20 and 60 Hz (Brown et al. (1999)). Another examination on human wrist flexors demonstrates as well that maximum shortening velocity of muscle should be scaled with activation, 20-100% P_0 at intervals of 20%: P_0 and V_0 show an almost linear relationship ('best fit', Chow and Darling (1999)). The main interest of this particular set of experiments was to assess frequency-dependence of V_0 and P_0 and not to additionally look for the length dependence of this curve as Brown et al. (1999) or how maximum contraction velocity could be assessed using much higher stimulation frequencies (up to 400 Hz, De Haan (1998)). Rack and Westbury fitted their isometric muscle data similarly, except for describing the whole stimulation frequency - tension relation with a sigmoidal rather than an exponential function, as P_0 was maximal at 50 Hz (Rack and Westbury (1969)), instead of 200 Hz for the extensor tibiae. P_0 between 1 and 10 Hz seems to increase less than between 10 Hz and 20 Hz for the cat *soleus* muscle. As this range of stimulation frequencies was not tested for the extensor tibiae, it is hard to tell if a sigmoidal fit would have been the most reasonable fit for the extensor tibiae as well. Noticeably, the stick insect computer muscle model does operate with a sigmoidal fit, as single twitch data points (1 Hz) are included (Blümel et al. (2007a;b; 2008b;a)).

Similar to the parallel length dependence of V_0 and P_0 at shorter fibre lengths, the data provided shows that there is also an approximately parallel influence of excitation on V_0 and P_0 (Fig. C.55c). Experiments of Malamud and Josephson on the locust and of Jewell and Wilkie on the frog, where force-velocity curves were measured at different times during a single twitch provide suitable results: both V_0 and P_0 change similarly with excitation (Tcx₂ flight muscles in *Schistocerca americana*, Malamud and Josephson (1991); *sartorius* muscle in *Rana temporaria*, Jewell and Wilkie (1960)). Similar to variation of motoneuronal stimulation frequency, different times during a single twitch

represent different ‘degrees of activation’ (see Malamud and Josephson (1991)), referring to the term ‘active state’ (Hill (1938)). The ‘active state force’ is the force which the contractile component of a muscle could just maintain without shortening or being lengthened (Hill (1949); Edman (1970); Edman and Kiessling (1971); Malamud and Josephson (1991); Edman and Josephson (2007)).

The variability of the data, especially of P_0 - values is an issue that demands further interpretation. Maximum tetanical extensor tibiae force at 200 Hz has a S.D. of $\pm 29.8\%$ (see Tab. C.7), single twitch force varies even more (S.D. of $\pm 94\%$, see Tab. C.3) and maximum extensor tibiae contraction velocities feature a S.D. of $\pm 9.1\%$. For the flexor tibiae, a similar variability arises: at maximal recruitment, tetanical force at 200 Hz shows a S.D. of $\pm 30\%$ and maximum contraction velocities have a S.D. of 15% . In search of parameters that might justify these large variations, a set of ten extra animals (representative for animals used in all examinations within this thesis) were measured in size and mass and demonstrated mean body length to be $L=77.1 \pm 2.28$ mm and mean body mass to be $M=940 \pm 70$ mg (see *Materials and Methods* section). From these minor inter-animal variations (S.D.s of $\pm 3\%$ and 7% , respectively), it is hard to reason the discrepancies measured. There are two arguments that a systematic preparation error is rather unlikely. First, within sets of experiments, the magnitude of variation is not the same for different parameters: for both tibial muscles, maximum contraction velocity varies much less than maximum tetanical force. Second, in different sets of experiments, a large variation can be found as well: determination of extensor and flexor tibiae fibre lengths, extensor tibiae relaxation time constants after different activation, the extensor tibiae force-length characteristics, flexor and extensor tibiae dynamic passive forces, extensor tibiae contractions in response to physiological input and extensor and flexor tibiae quick-release experiments including determinations of P_0 , V_0 and the spring constant β . The magnitude between different sets is comparable, e.g. Tabs. C.7 and C.8, Figs. C.62 and C.60 or Fig. C.55. This large degree of variation is apparently a property of the extensor tibiae (Hooper et al. (2006); Guschlbauer et al. (2007); Hooper et al. (2007a;b)) and seems to apply for the flexor tibiae as well, other stick insect leg muscles are not yet examined. In the flexor tibiae, it could be argued that variation in P_0 or V_0 could arise from different levels of recruitment. As described in the ‘*Materials and Methods*’ section, stimulation current was set to an amplitude where further increase did not result in a further isometrical force increase. Hence, it was assumed that this current level was eliciting action potentials

in all flexor motoneurons, yet a test recording from the *ncr* nerve was not considered because of the high number of motoneurons (e.g. Goldammer et al. (2007)). As the degree of flexor tibiae force and contraction velocity variability was not higher than the extensor tibiae's, different levels of recruitment are apparently not the source of variability.

A very essential revelation is the finding that other insect leg muscles show considerable variability in contraction force as well, for example the extensor 117c in the cockroach (*Blaberus discoidalis*, Ahn and Full (2002)) or pro- and mesothoracic extensor tibiae in *Schistocerca gregaria* (Burns and Usherwood (1978)): relative standard deviations of force in the cockroach at twitch $\pm 38\%$, at tetanus $\pm 31\%$, and in the locust at twitch $\pm 30\%$ in response to prothoracic and $\pm 48\%$ in response to mesothoracic FETi stimulation. These specifications are in a similar range as some of the extensor tibiae forces measured in this thesis ($\pm 72.3\%$ at twitch, $\pm 47.9\%$ at 50 Hz stimulation and $\pm 29.8\%$ at 200 Hz stimulation (see C.6). In vertebrate muscles, high variability can be also found: passive force of the cat *soleus* muscle at optimal fascicle length had a S.D. of 120% (Scott et al. (1996)).

Investigating the kinetics of isometric force development and isotonic shortening at different muscle lengths (see Fig. C.57) led to several interesting insights. Extensor tibiae shortening velocities at 50 Hz against a small load were within the same range that might be expected from C.54: about $3 \frac{mm}{s}$ (see Fig. C.57a(ii)). From the length dependence of maximum shortening velocity (see Fig. C.56), one might expect the muscle starting at higher stretch to shorten faster. As the load applied was chosen to be equal to the passive force at the respective length, the slightly increased load obviously 'compensated' for the higher stretch and led to approximately the same shortening velocity. Edman and Josephson (Edman and Josephson (2007)) measured Hill curves in *Rana temporaria* at different times during isometric contraction rise and revealed V_0 to remain approximately the same and detected only a shift along the force axis. Interestingly, isometric contraction at larger stretch results in much larger velocity of force increase than at less stretch (see Fig. C.57a(i)). Using maximum velocity as a 'degree of activation' (see Hill (1949); Malamud and Josephson (1991) to this topic), activation is complete by the time that isometric force has risen to a quarter of its plateau value. This is faster than expected by the isotonic and isove-

locity experiments of Edman and Josephson, they claim activation to be complete by approximately half the plateau value (Edman and Josephson (2007)). The cause for the higher force rise velocity at larger stretch could be the series elastic component, as an increase in stiffness leads to a faster gain of force per time unit. The fact, that the ratios of isometric forces and isotonic shortening amplitudes $\frac{muscle_{stretched}}{muscle_{relaxed}}$ are very similar is a logical consequence of the force-length relationship: the muscle shortens by 'descending' the ascending leg of the force-length curve.

It was demonstrated that the time of externally applied forces during muscle contraction is crucial, especially in respect to the direction of a limb's movement. As could be shown in chapter C4, loading the extensor tibiae 0.12 s after the begin of an isotonic shortening will lead to a further shortening, whereas the same amount of load being applied after about 1 s of shortening will lead to a sudden lengthening (see Fig. C.58b). Dean could show that load changes are met with rapid adjustments (often < 20 ms; Dean (1984)). He measured stick insect protraction speeds in the presence of increased loads (up to 0.75 g, i.e. ca. 7.5 mN applied to the tibia) and concluded from the fact that protraction continued in spite of the opposing forces the occurrence of a motor output enhancement. Protraction speed was not maintained. Similarly, in locusts a high-gain position control loop is assumed to be responsible for load compensation (Matheson and Dürri (2003)). In general, muscles are thought to respond to perturbations by way of active neural reflexes. However, such more immediate responses can result from the muscle's intrinsic force-length and force-velocity properties (Rack (1970); Grillner (1972); Jindrich and Full (2002); Blickhan et al. (2003)) and were termed 'Preflexes' (Full and Koditschek (1999); Brown and Loeb (2000a)). In addition to such reflexes, there is the possibility that the morphology (leg geometry and skeleton properties) represents a mechanical feedback controller (Kubow and Full (1999)). Passive muscle properties can act qualitatively like a negative position feedback system (Polit and Bizzi (1978); Hogan (1982); Bartling and Schmitz (2000)) or can contribute to joint impedance in a stabilising way together with the connective tissue (Brown et al. (1982); Esteki and Mansour (1996); Hajian and Howe (1997); Jindrich and Full (2002)). Muscle properties constitute a peripheral feedback system that has the advantage of zero time delay. When perturbations during a movement paradigm are not too large, e.g. human vertical jumping, the task might be performed successfully without any necessity of adapting the muscle stimulation pattern (van Soest and Bobbert (1993)). Movement does not need to be actively controlled to exhibit

dynamic stability (Jindrich and Full (2002)). Even in vertebrate muscles (e.g. in the cat), which are in general faster responding than invertebrate ones, only muscle stiffness can provide a load compensation, because the delays between a change in motor unit discharge and tension development are too long to allow a reflexly induced load compensation during e.g. gallop (Grillner (1972)). In two experiments (exemplary figure of the principle mechanism given in chapter C4), investigations aimed to test how large a load increase during contraction had to be to cease the actual shortening procedure. Fig. D.2 shows that loads up to > 30 mN applied 0.12 s after contraction start do not prevent the extensor tibiae muscle from continuing to shorten.

The experimental paradigm used (Figs. C.58 and D.2) was designed to be close to Dean's, who applied loads opposing protractor coxae contraction directly on the hind leg, 0.1 to 0.2 s after protraction begin (from what could be estimated from the figure in the paper). Although loads were applied directly on the tendon (and not on the leg) and the muscle in focus was the extensor tibiae (and not the protractor coxae), the data provided in this thesis suggest the persistence of the protraction movement recorded by Dean to be rather a muscle property than a positive feedback reflex mechanism (as claimed by Dean (1984)). This suggests a new approach to the term of preflex behaviour: the middle leg extensor tibiae (or any 'slow contracting' muscle) can take advantage from its slowness and from the fact that it will only rarely reach a steady

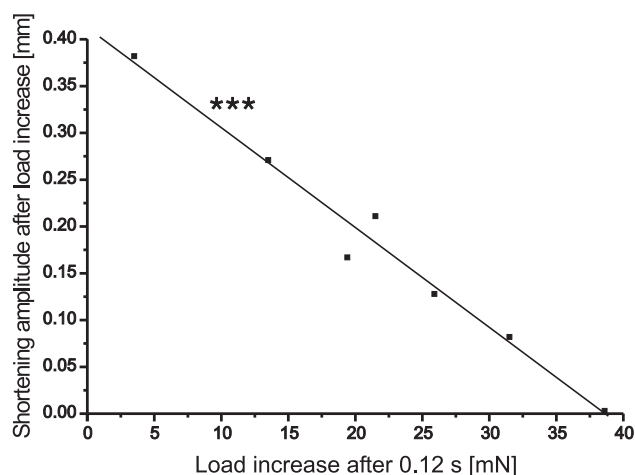


Figure D.2: Extensor tibiae shortening amplitudes after various load increases from two experiments ($N=2$, $n=7$). Load increase was applied 0.12 s after isotonic contraction begin. The linear regression fit (solid line) is highly significant (< 0.001 , ***, $R=-0.987$).

contraction state within a physiological situation like a fast swing phase consisting of about 40 FETi spikes (see chapter C4 and Hooper et al. (2007a)). Fig. C.11 and Tab. C.5 show the kinetics at different activation levels. As described earlier in respect to quick release experiments, the muscle ‘weakens itself’ by shortening and the contraction reaches a steady state when the applied load equals the force the muscle can exert at a particular length: it descends along the ascending leg of its force-length characteristic. Thus, the slowness of shortening development enables the muscle to resist loads for a longer period of time. As long as the load is not too large, the muscle will therefore nearly always continue to shorten when being perturbed. In contrast, frog skeletal muscle fibres (*Rana temporaria*) are much faster contracting: they need 59 ± 4 ms to reach 90 % of maximum tetanic force (Edman (2005)). This has dramatic consequences in respect to the reflex mechanism because a sudden perturbation > 0.06 s after contraction begin would lead to a fibre lengthening and the above described ‘zero delay peripheral feedback system’ (van Soest and Bobbert (1993)) would fail or rather would not exist. This effect is mimicked by stick insect loading experiments with load increases after nearly 1 s (see Fig. C.58b), that show that a perturbation leads to a fibre lengthening as the muscle is about to reach a steady state and is consequently weaker than before because of the force-length characteristic. Thus the particular time point of disturbance occurrence is crucial: whether the muscle is in the rising phase of an isotonic contraction or whether it has reached a constant length level. To the author’s knowledge, the currently suggested mechanisms describing the reflex behaviour do not yet consider that slow muscle kinetics are essential in order to benefit from the stabilising effect of the force-length characteristic.

D5 Passive forces II

Summary

Quick release experiments provide not only contraction velocity data (see chapter C4), but reveal also the properties of the muscle’s series elastic component. It turns out that extensor and flexor tibiae series elasticities act like nonlinear springs, data-points measured at a particular stimulation frequency can be fitted with a parabola: the muscle gains stiffness with increasing force. By shifting individual parabolas representing measurements at different activations, the series elasticity of a muscle can

be characterised with one single parabola. Flexor tibiae quadratic spring constants β are on average 1.6 times larger than those of the extensor tibiae. Creep experiments reveal the extensor tibiae to be neither a cross-linked, nor an uncross-linked polymer, its properties appear to be inbetween. Quantitative experiments demonstrate that creep can be described with a power-function in tibial muscles. When cross-sectional area and fibre length is taken into account, compliances of the extensor and flexor tibiae lie either within the same ballpark or the extensor tibiae is much less compliant than the flexor tibiae.

Discussion

When exercising 'quick release' experiments like in chapter C4, the initial fast length change upon switching to isotonic recording conditions represents the relaxation of a muscle's series elasticity (see Fig. C.49b). It was evaluated by measuring the muscle length difference between the isometric length (in position clamp mode) and the length value, where the actual muscle shortening is about to start ('T' in Fig. C.49b). It was calculated by extrapolation of the muscle shortening slope in a 50 ms time window immediately following the above described oscillations that are involved (see chapter D4). The series elasticity was non-linear with a quadratic length-force characteristic, i.e. the displacement from equilibrium (clamped position during tetanus) increases parabolically as the change in force increases. Wilkie (Wilkie (1956); Jewell and Wilkie (1958)) measured the spring properties of the frog sartorius (*Rana temporaria*) and fitted the individual measurements with a composite curve with an exponential slope at low forces and an almost linear shape at higher forces. Lappin and colleagues report river toad muscle displacement during elastic recoil to increase exponentially with the change in load as well (*depressor mandibulae* muscles of *Bufo alvarius*, Lappin et al. (2006)). In contrast to these data with a finite slope at low values, the curves depicted in Figs. C.59 and C.60 reach the zero point with horizontal slope. Tibial muscles were observed to shorten maximally by up to about 10 % FL (fibre length) in the extensor tibiae and 8 % FL in the flexor tibiae (compare upper abscissas in the figures). These are strain values that lie inbetween previous values of 2-6 % of the muscle length (*sartorius* muscle in *Rana temporaria*, Jewell and Wilkie (1958); skeletal muscle fibres in the horseshoe crab, Sugi et al. (2000); white myotomal muscle fibres in the dogfish *Scyliorhinus canicula*, Lou et al. (1999)) and 15.3-17.6 % of the muscle length (*depressor mandibulae* muscles of the river toad *Bufo alvarius*, Lappin et al. (2006) and

semimembranosus muscles in *Rana pipiens*, Pilarski and Pierotti (2003)). Exposing the extensor tibiae to forces $> P_0$ (see Fig. C.61) reveals the muscle to remain as stiff as before (up to $(P_0 + 40 \text{ mN})$, the slope does not change). This matches the findings described in chapter C4 (Fig. C.52) in respect to the deviations in the high force region: like the velocity data, the series elastic component length data cross zero with a slope near zero. Stiffness eventually starts to decline when $P \gg P_0$, as cross-bridges can only bear a certain amount of load.

The spring constants β were shown to vary drastically when related to muscle cross-sectional area and fibre length ($\beta^* = 15322 \pm 2655 \frac{\text{mN}}{\text{mm}^2}$ for the extensor and $\beta^* = 27285 \pm 5833 \frac{\text{mN}}{\text{mm}^2}$ for the flexor tibiae). The absolute values for maximal stiffness differ by a factor of 2: $\sim 3.1 \frac{\text{N}}{\text{mm}}$ for the extensor and $\sim 6.5 \frac{\text{N}}{\text{mm}}$ for the flexor tibiae. For comparison, the cat *soleus* muscle bears a stiffness of $11 \frac{\text{N}}{\text{mm}}$ (Proske and Morgan (1984); Siebert et al. (2008)). Hence, extensor and flexor tibiae are very different with respect to the amount of stiffness they can provide maximally. This fact can be interpreted by looking at the muscles' role in one step cycle: the middle leg flexor tibiae is exclusively active during stance, when a larger stiffness is advantageous in order to support a stable standing of the animal.

Fig. C.62 demonstrates that parabolas at different activation can be described by one common parabola, when data is shifted in x-direction. Similarly, investigations of frog *sartorius* muscle twitch at various times (\cong different activation) result in data that can be described with one common curve as well (Wilkie (1956)). Curves have been made to coincide at an arbitrary but clearly defined point. Conclusively, the series elastic component is present throughout contraction and relaxation, probably with constant properties.

The origin of series elasticity is not completely known: Wilkie suggests the series elastic component to reside at least partly in the tendons (*Rana temporaria*, Wilkie (1956)). This tendon elasticity can not be the main origin of the series elastic component in invertebrates: Zakotnik et al. (Zakotnik et al. (2006)) justified the omission of a series elastic element in their model (like Zajac did in his model, see Zajac (1989)) assuming the apodeme's stiffness to be as stiff as a cockroach's apodeme (*Blaberus discoidalis*), which is 40 times stiffer than a vertebrate tendon (Ahn and Full (2002)). Sugi and

colleagues suggest that series elastic component could be mostly due to the "elastic" thick filament misalignment in each A-band during isometric force generation. Titin filaments are likely to be involved in this alignment (Sugi et al. (2000)).

Creep experiments are a very common way of testing material's properties. The test series presented in this thesis revealed the extensor tibiae to be neither a cross-linked nor uncross-linked polymer as the material neither recovers completely, nor could the amount of its steady-state flow that is attained under constant stress be related to the amount of creep recovery (see Figs. C.64 and C.63). A perfect solid body features a direct proportionality between stress and strain (in accordance to Hooke's law) and a perfectly viscous liquid shows stress to be directly proportional to the rate of strain, in accordance to Newton's law (Ferry (1961)). When stress is dependent on both strain and rate of strain together (and even higher time derivatives of the strain), the material can be described as viscoelastic. Apart from such time anomalies, there can be also stress anomalies. In summary, the collected creep properties cannot be explained satisfactorily with a linear power function model. Linear viscoelastic behaviour is supposed to be simulated with an infinite number of springs and dashpots either being arranged in parallel (Voigt-Model, see D.3a) or in series (Maxwell-Model, see D.3b). Both models do not completely explain the muscle behaviour observed: the Maxwell model cannot predict creep since it describes the strain relationship with time being linear and the Voigt Model cannot sufficiently describe stress relaxation, i.e. after a stress load is removed. Even when spring and flow constants of each spring-and-dashpot-unit may be different, the analysed material is supposed to show a linear behaviour when each unit is linear. This is not the case with the extensor tibiae. In general, creep appears to be fundamentally more nonlinear and is likely to not obey the quasi-linear hypothesis. The microstructural process taking place in a material undergoing creep could be quite different from that undergoing relaxation or oscillation. Analogous situation is known for metals at higher temperature (Fung (2004)).

Creep was shown to recover completely when a short stimulus is presented to the muscle (see Fig. C.65). Similarly, Proske and colleagues report that slack can be removed by contraction at a given length previously showing slack (Proske et al. (1993)). Purposely induced slack causes detachment of cross-bridges previously being formed

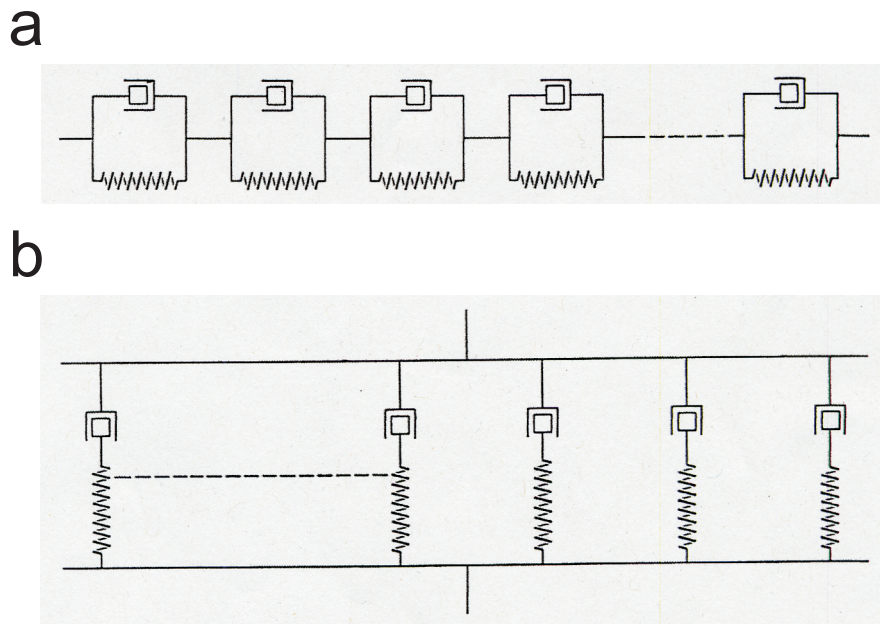


Figure D.3: Simplified Voigt - (a) and Maxwell - model (b). Drawings adapted after Ferry (1961).

during relaxation after a contraction. These bonds have a very low turnover rate (Lakie et al. (1984); Morgan et al. (1984)), so slack may persist for long periods when the muscle is not activated meanwhile. D.K. Hill describes the possibility that stimulation of a resting muscle causes a break-down of the comparatively stable bonds between the cross-bridges and the actin filaments (Hill (1968)). Similarly, the ‘catch’ mechanism in the anterior byssus retractor muscle of *Mytilus edulis* can be abolished by an alternating current stimulus and therefore the muscle is brought to relaxation (Winton (1937)). Altogether, a mechanism is conceivable where cross-bridges alter their current status and ‘abandon’ bonds which cannot be rebuilt passively because of muscle loading. Fig. D.4 displays the author’s suggestion of how to interpret this sort of ‘reset mechanism’ using a simple two-component spring-dashpot model (see Hill (1938)): first, loading the extensor tibiae with a step stimulus is supposed to stretch its series elastic component, represented by the spring. Then, delayed due to inner friction, persistent loading starts pulling the piston out of the dashpot, which represents the damping of the series elasticity. Unloading results in a complete relaxation of the spring but not of the dashpot, whose piston remains pulled further out than at the very beginning. Active muscle shortening, i.e. filament sliding, is the process that moves the piston back to its original position. In a strict sense, the piston is moving even further than initially, and is pulled out again as soon as the muscle stimulation

is over. In order to do so, the contractile component must be arranged parallel to the dashpot.

The quantitative comparisons of creep experiments in extensor tibiae compared to flexor tibiae data were based throughout on a time span of 85 ms immediately following oscillations that come along when applying a step stimulus (see Figs. C.66 and C.67). The choice to take 85 ms comes from trading off between taking a time span long enough to analyse reasonably the development of the length change and the desire to analyse as many creep developments as possible. As described in chapter C5 of the 'Results' part, many creeps can only be analysed within 85 ms because muscle length changes are fast and saturate when large stress levels are applied and the maximum muscle stretch level is reached. A test supported this notion: creep determination within 850 ms (10x longer) resulted only in a modest increase of the linear fit R value compared to analysis within 85 ms. The determined compliances for two extensor-flexor pairs show either the muscle values to be in good agreement, or the extensor tibiae to be much stiffer than the flexor tibiae, which is surprising. Theoretically, the exponents of each muscle pair (extensor-flexor) are expected to have the same value. More creep experiments would need to be done in order to make a clear statement. This preliminary finding (at least one of the two muscle pairs examined) joins the cognitions gained from experiments investigating maximum tetanical force output and maximum contraction velocity: related to cross-sectional area and fibre length, extensor and flexor tibiae reveal large similarities.

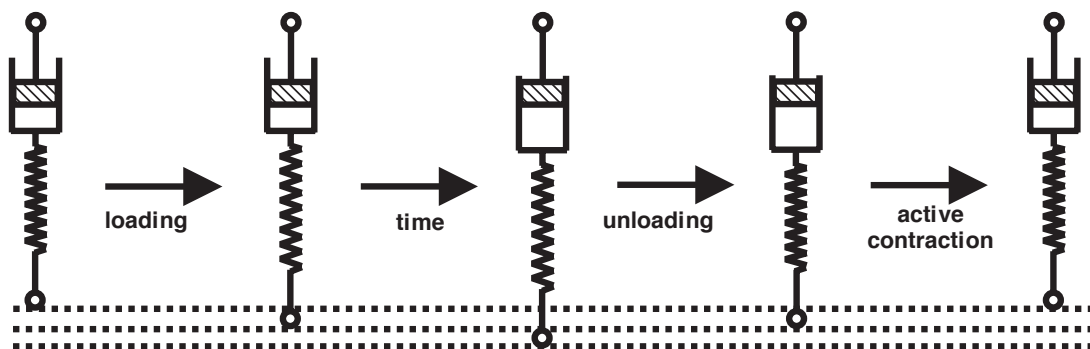


Figure D.4: *Simplified mechanism that attempts to interpret the 'reset' of muscle length with a short high frequency stimulation burst. The model used is a spring-dashpot two-component model, representing the damped series elastic component. The contractile component must be arranged parallel to the dashpot.*

The linear theory of distributed relaxation with a power-function characteristic leads to a common exponent k at **force** step application in the creep experiment (length $L = C \cdot t^k$) and for the relaxation after a **length** step (force $P = C \cdot t^{-k}$). k is the slope of the linear development when applied double logarithmically. This could not be verified in the measurements shown in chapters C3 and C5. This fact may suggest the existence of further nonlinearities in this system.

D6 Force generation under naturally occurring FT joint movement patterns

Summary

Investigation of extensor tibiae force increase (fitted with an exponential RC-type growth function) and relaxation (fitted with an exponential decay function) dynamics before, during and after muscle stretch and release gave several results: force increase time constants change only little whereas relaxation time constants are much more affected by the muscle length changes, maximal developed force P_0 confirms what one would expect from the extensor tibiae force-length characteristic described in chapter C2. Exerted forces of actively shortened extensor tibiae muscles in response to ramps mimicking middle leg stance phase are dependent from the muscle's activation state. From about 100 mN occurring 100 ms before the last stimulation pulse to 40 mN when ramps start right after the last pulse to about 80 ms after the last pulse, the muscle develops force that diminishes linearly with time after the end of stimulation. As expected from Hill experiments at loads $> P_0$, maximal developed force increases with ramp velocity as it is lengthened during active contraction. Video tracking of tibial movements in response to extensor and flexor tibiae stimulation reveals FT joint angular displacement to be pulse number dependent and the flexor tibiae to develop larger maximal shortening velocities than the extensor tibiae. When tibia movement was blocked with an obstacle, extensor tibiae relaxation dynamics changed with increasing pulse number. The combination of history - dependent isometric extensor tibiae force relaxation dynamics with passive dynamic flexor forces could reproduce the different time courses of the tibial relaxation movements observed. This calcula-

tion suggests the FT joint to be a mainly muscle-dominated system.

Discussion

In integrated daily-life movement, skeletal muscle contractions are most often dynamic and of short duration (Ettema and Meijer (2000)). However, so-called 'history of contraction phenomena' like stretch-induced force enhancement or shortening-induced force depression cannot satisfyingly be modelled with the classic Hill model. For instance, passive prestretch results in force enhancement of the extensor muscle 178 in the cockroach *Blaberus discoidalis* (Ahn et al. (2006)). The cat *soleus* muscle bears steady-state force enhancement following active stretching, which can be abolished instantaneously by shortening-stretching the passive muscle by an equivalent to the active stretch magnitude (Herzog et al. (2003)). As described in chapter D3, cross-bridges continuously detach and reattach during progress of a muscle stretch. During steady lengthening of single muscle fibres in *Rana temporaria*, the half-sarcomere stiffness becomes 1.25 times the isometric value (Linari et al. (2000)), similar to the results found in *Rana esculenta* (Lombardi and Piazzesi (1990); Piazzesi et al. (1992)), and the cross-bridge number rises to 1.8 times the original isometric value. This explains why after-stretch potentiation shows stiffness to remain on average 12 % higher. Contraction 2 (for the numbering, see Fig. C.68) in Fig. C.72c(ii) demonstrates that the maximum force value arising from stretching with fast ramps (0.5 and 0.75 $\frac{mm}{s}$) can become as high as almost 150%. The slower the stretch, the less the eccentric force production (about 105% P_{max} at ramp stretch of 0.1 $\frac{mm}{s}$ and 135 - 150% P_{max} at 0.5 - 0.75 $\frac{mm}{s}$): this is exactly what the results in chapter C4, Fig. C.52 would predict because of the course of the F-V curve at negative velocities. At , values of can be expected (see Fig. C.52). The amount of eccentric force that a muscle or a musclegroup can provide was already discussed in chapter D4: the kangaroo rat uses up to 175% of its maximum isometric force (Biewener et al. (1988)). In this case, the animal relies on the force enhancement that is involved with eccentric contractions, otherwise its locomotion behaviour would have to be different. Whether the stick insect actually takes advantage of this force enhancement is unclear. From the cockroach, we know that maximum power output of cockroach extensor muscles was attained with activation beginning during muscle lengthening: early activation (involving active stretch) increases muscle stiffness and facilitates storage of strain energy in tendons and cuticle (Full et al. (1998)). The variation of isometric force at rest (contraction 1) is within

the the expected range (90-190 mN, see chapter D4; here: 100-160 mN). In contrast, the degree of variation was much less pronounced in respect to exponential decay τ at rest (see Fig. C.72b(i), contraction 1). However, the relaxation τ data showed large alteration during and after ramps: time constants increased the more the larger the stretch, up to almost 200% during the largest ramp (0.75 mm, contraction 2, see Fig. C.72b(ii)). This may be due to muscle stiffness in response to a stretch being lowered during activation as crossbridges have a much higher turnover rate than in passive muscle (cat *soleus* muscle, Proske and Morgan (1999)). Consistently, the time constant of the RC-type force growth showed an increase in response to the stretch as well (see Fig. C.72a(ii), yet it was much less pronounced as the increase in relaxation τ and difficult to interpret because the variability of starting contractions (contraction 1 in Fig. C.72a(i)) was very large. The effects on the force rise time constant were generally rather weak (maximally 95 - 130% of the initial value).

After the ramp stretch (contractions 3-5), values for P_{max} confirmed the findings in chapter C2 in terms of the force-length relationship. Figs. C.23 and C.24 predict forces to decline drastically at stretches > 0.3 mm: forces after 0.5 mm stretch diminish to about 90% of the force initial value and forces after 0.75 mm stretch to about 50% of the initial force value (see Fig. C.72c(ii)). In contrast to values for P_{max} and force rise τ , relaxation τ continued increasing at stretches > 0.1 mm, even though stretch was completed and actual muscle length did not change (contractions 3-5). This may be due to RC-type growth τ and P_{max} being two parameters that are dependent on active processes in contrast to the relaxation phase being a passive process. However, attempts to align the time constant of the passive force decline from contractions 3 to 5 with the change in relaxation time constant of the isometric contractions were not successful: passive force decline τ is in the order of magnitude of several seconds whereas the relaxation τ change is in the size of 10-30 ms (see Fig. C.72b(i)). An alternative explanation for this kind of muscle behaviour could be that repeated activation during passive muscle stretch (i.e. contraction 2) leads to a rise in stiffness (Jones et al. (1987); Howell et al. (1993); Chleboun et al. (1998)) which is, interestingly, a sign of muscle damage. The theory behind this phenomenon comprises the assumption of particular damage of sarcoendoplasmic reticulum membranes and T-tubules, leading to an uncontrolled Ca^{2+} -release into the sarcoplasm (Morgan and Allen (1999); Proske and Morgan (2001); Whitehead et al. (2001; 2003)). The above described change in relaxation τ is in disagreement with the results of Jewell and Wilkie, who found that the

decay constant was independent of the sequence of changes in length and tension that the muscle had undergone (*sartorius* muscle in *Rana temporaria*, Jewell and Wilkie (1960)).

From experiments on the cat *soleus* muscle, it is known that full slack will develop when the muscle is held at the longer length for several seconds before returning to start length (Morgan et al. (1984)). Subsequent activation is lower than originally at the same length because of both the slow rate of cross-bridge formation and the delayed take-up time of the slack, so the muscle reveals to be more compliant (Proske and Morgan (1999)). This might explain the ongoing alterations in τ of the exponential RC-type growth and P_{max} (see Fig. C.72a(i), a(ii), c(i), c(ii)) from contractions 7 to 10. Relative P_{max} - values at contraction 7 (right after the descending ramp moving to original length) deviate from the relative initial P_{max} - value at contraction 1: P_{max} is close to 100% after the slowest ramp ($0.1 \frac{mm}{s}$), close to 90% at $0.25 \frac{mm}{s}$, between 80 and 90% at $0.5 \frac{mm}{s}$ and below 80% after the fastest ramp ($0.75 \frac{mm}{s}$), see Fig. C.72c(ii). Thus, the data provide evidence for the existence of a force-velocity history phenomenon that modulates thin filament activation, which could be already demonstrated to occur in frog muscle: the rate of force development after muscle fibre shortening was found to be increased after a slow ramp (and thus a larger isotonic force) compared to a fast ramp involving a smaller isotonic force (*tibialis anterior* muscle in *Rana temporaria*, Vandenboom et al. (2002)). Relaxation τ s were larger after the ramp down (contraction 6) compared to the initial value (contraction 1) and kept increasing after the largest ramps (red and green traces, contractions 7 to 10). According to Proske et al. (1993), muscle slack that might occur after the relaxation ramp should be abolished after the first muscle stimulation, i.e. contraction 7. However, P_{max} and time constants of both relaxation and force increase do not reach their initial values within the three following stimulations (contractions 8-10). This is in good agreement with data from Ahn and colleagues, who could show that active shortening leads to force depression (extensor muscle 179 in *Blaberus discoidalis*, Ahn et al. (2006)).

In order to investigate the interaction of muscle relaxation forces and the properties of the Hill-hyperbola at forces $> P_{max}$, stretch ramps were applied at different times during or briefly following stimulation of the extensor tibiae (see Figs. C.73, C.74, C.76, C.75). These ramps were supposed to mimick flexor activity during stance phase. The

transition from swing to stance features co-contraction in terms of an extensor and flexor tibiae activity overlap, which could be demonstrated to occur in the stick insect single leg preparation (*Cuniculina impigra*, Fischer et al. (2001)). Stiffness at step transitions is an important part of a successful control strategy used for dynamically stable three-dimensional hopping and running robots (Raibert et al. (1984); Jindrich and Full (2002)). Antagonistic muscle co-contraction attributable to long muscle time constants facilitates substantial load compensation (Zakotnik et al. (2006)), like in the stick insect (see Figs. C.16 and C.18 in chapter C2 and Hooper et al. (2007a)). Maximal extensor muscle excursions during stance can be calculated using the maximal FT-joint deflection values mentioned in chapter D3 (70.8 - 90.6° (N=3, v. Uckermann and Büschges (2008)), starting at either 140° or 160° FT-joint angle, resulting in deflections of 0.27 mm minimally and 0.4 mm maximally. Cycle duration in a freely moving animal is 0.3 - 2 s (Bässler (1983); Fischer et al. (2001)). In both single-leg walking (Gabriel and Büschges (2007)) and intact tetrapod gait walking (Graham and Cruse (1981); Bässler (1983)), only stance phase depends on cycle period (Hooper et al. (2006)). That is, as swing phase duration is independent from walking speed (tetrapod walk of adult stick insects, Wendler (1964); Graham (1972); Bässler (1983)), stance duration can be as variable as 0.19 - 1.89 s, when calculated with a mean swing duration of 112 ms (free walking, Graham and Cruse (1981)). Thus, extensor tibiae stretching velocities during stance can range from 0.14 to 2.13 $\frac{\text{mm}}{\text{s}}$ in a physiological context. Hence, the stretching velocities used during or following extensor tibiae shortening of 0.33 to 1.32 $\frac{\text{mm}}{\text{s}}$ are close to mimick a physiological situation (see Fig. C.75a and b). This determination is the basis for the assessment of the forces and the times obtained: up to 80 ms after stimulation end, the extensor tibiae exerts force. Consistent with the extensor tibiae Hill-curve at negative velocities (see Fig. C.52), the velocity of the ramp stretch is reflected in the amount of force generated (see Fig. C.75b). In a similar experimental arrangement, Grillner and Udo demonstrated that the stiffness of a contracting *soleus* muscle in the cat can account for the tension increase in the steep linear part of the stretch reflex up to maximum physiological extension (Grillner and Udo (1971)). They saw that the steep and almost linear part of the active tension increase starts at shorter muscle lengths as the stimulus frequency is changed (Grillner (1972)). The forces measured in Fig. C.75a and b are presumably highly relevant for the stick insect's behaviour, as co-contraction of antagonistic muscles is known to cause significant stiffness of the limb (*Schistocerca gregaria*, Zakotnik et al. (2006)). From the cockroach, it is reported, that co-contraction helps adapting to different surface com-

pliances and stabilizes the impact when the leg touches ground at the beginning of the stance movement (*Blaberus discoidalis*, Ahn and Full (2002)). This joint stiffness is actively affected by neuromodulation and neuromuscular inhibition (Matheson and Dürr (2003)) as the timing of common inhibitory neurons during active movements must lower joint stiffness by downregulating antagonistic contraction forces (Wolf (1990b)).

Remarkably, muscular co-contraction is possible without any motoneuronal input as well: in locust scratching for instance, there is no overlap of antagonistic motoneuron bursts, even when the tibia was additionally loaded (Zakotnik et al. (2006)). A possible reason may be the slow activation and deactivation of tibial muscle fibres (Bässler and Stein (1996); Hooper et al. (2007a)), which could be confirmed by analysis of isometric measurements in chapter C2 (see Figs. C.16 and C.18). Additionally, passive forces contribute as well (as could be reasoned in chapter C3 in great detail) and can potentially accomplish tibial movement without any motoneuronal input (see Zakotnik et al. (2006)). Consistently, during hindleg grooming in the locust (*Schistocerca americana*), tibial extension can begin often before tibial extensor muscle activity (Berkowitz and Laurent (1996)). Co-contraction can even be mediated by one single motoneuron: the FETi motoneuron makes excitatory output connections within the central nervous system that can be gained or diminished from the femoral chordotonal organ, i.e. depending on tibial position (hindleg in *Schistocerca gregaria*, Jellema and Heitler (1996)).

Investigations of the role of muscle impact on intact tibia movement (Figs. C.77, C.78) were undertaken in order to make a statement how to interpret the data achieved in chapters C1-C5. The experimental approach tested the interaction of two antagonistic muscles in a natural context (i.e. in an intact, unaffected FT joint system) and not being measured separately with the tendon hooked up to the Aurora force transducer. The main goal of these examinations was to test to which extent a combination of the investigated muscle characteristics would reflect the actual movement. Do eventual mechanical peculiarities of the whole joint (e.g. connective tissue, elastic properties of the cuticle) bias tibia movement markedly or is the movement muscle-dominated and additional joint mechanics can be neglected? Fig. C.78 shows calculated tibial muscle excursions when either extensor or flexor tibiae was stimulated with the an-

tagonistical motoneurons being either crushed or cut. A maximum extensor tibiae shortening velocity of $2.6 \frac{mm}{s}$ is within the range of expected velocities when the applied load is 10 - 40 mN (see Fig. C.50 and Tab. C.7), which would correspond to the dynamically generated passive flexor force that would occur during tibia extension. However, maximum flexor tibiae shortening velocity is with $8.3 \frac{mm}{s}$ in a range of velocities that would be expected in a completely unloaded situation (see C.51 and Tab. C.8), where no passive extensor force would be present. This surprisingly high value is hard to explain as the CI₁-axon, that might have facilitated flexor tibiae shortening due to inhibition of dually and triply innervated extensor tibiae fibres (Bässler et al. (1996)), was either crushed or cut and was not stimulated extracellularly.

As was shown in chapter C4, average FETi spike number from 87 putative steps is 44.2 ± 20.0 per step-like movement (see Fig. C.41). The rather large standard deviation indicates that FETi motoneuronal spiking is highly variable. Steps with up to 180 spikes can occur and therefore the use of the term 'step-like movement' seems more appropriate as it seems to be a fine line between walking and searching movements. 'Active sensing' might be an alternative way to describe this kind of behaviour (Hooper et al. (2006)), a conclusion that is consistent with the lack of clean separation between clear steps and clear searches in *Cuniculina impigra* (Bässler (1993b)) and which is also consistent with the fact that a single artificial network is able to produce both sings and searches (Dürr (2001)). Although most step-like movements will be carried out with less than 60 FETi motoneuron action potentials (see mean linearised extensor tibiae muscle burst in Hooper et al. (2007a)), much larger spike-numbers do occur as well (Hooper et al. (2007b)), which shows that the muscular system has to be able to deal with the changes involved (e.g. relaxation kinetics), as described in chapter C2 and C6. Extensor tibiae bursts routinely exceed spike numbers of 40 to 60 spikes Hooper et al. (2007b)). Thus, stimulation of 20 to 140 pulses seemed to be a reasonable range of stimulation input to test physiological motoneuronal output on its effect in respect to post-stimulational relaxation dynamics (see Figs. C.18, C.79, C.80, C.81).

The fact that the time course of passive flexor tibiae torque subtracted from active isometric extensor tibiae torque can satisfyingly well reproduce videotaped intact tibia movement in response to different extensor tibiae stimulation levels clarifies one main issue. It points out that the above made comparison of the FT-joint with the muscle-

eyeball system is justifiable (see chapter D3): tibial movement time course can be described with the mere dynamics of two antagonistic muscles without having to incorporate any joint torques into the calculations. Although examinations in chapter C3 resulted in a clear dependence of joint torque on deflection amplitude (and deflection velocity, as the deflection time was the same at all amplitudes), the measured torques were still very small in comparison to passive muscle forces (0.068 ± 0.057 $mN \cdot mm$, see Fig. C.37c). Thus, the system is apparently truly muscle dominated, as is the eyeball-muscle-complex (Childress and Jones (1967)).

General conclusions and future directions

With respect to the investigation of stick insect walking behaviour, the understanding of the neuromuscular transform was one of the most urgent topics that needed to be clarified. It turned out that the stick insect middle leg extensor tibiae is a muscle with the ability to operate over a large range of motoneuronal firing frequencies. The largest changes in terms of force production and shortening velocity happen within action potential frequencies of 30 to 80 Hz, less changes happen above 80 Hz up to 200 Hz. The combination of contraction velocity measurements that prove the extensor tibiae to be in the lower range compared to other arthropod muscles and contraction analysis in response to physiological input, demonstrates that the extensor tibiae can be considered a 'slow' muscle. This is further supported by the fact that the extensor's muscle fibre membrane is not able to generate action potentials (with respect to invertebrates, e.g. Hoyle (1966)). However, even though it is a 'slow' muscle, which smoothens fast interspike interval alterations in terms of its contraction movement, it has the ability to respond very sensitively to short-term firing frequency changes with an increased force level in the isometric domain, termed 'latch' phenomenon. This is in good agreement with the finding that the extensor tibiae is a spike number dependent muscle (within the physiologically relevant time frame; Hooper et al. (2007b)). Its antagonist, the flexor tibiae, is remarkably different in the amount of maximum force it can generate and in terms of the maximum contraction velocity. This asymmetry is further supported by large differences in fibre length, cross-sectional area and moment arm length, which might be well-founded in the roles of the two muscles during locomotion, i.e. being mostly active either during stance or during swing phase. The amount of time that the extensor tibiae takes to even start relaxing and to relax subse-

quently gives evidence that there must be a high level of stiffness at the transition from swing to stance, as the rest of these actively generated forces need to be overcome by the flexor tibiae. Additionally, the large dynamically generated passive muscle forces that occur when the antagonist shortens (either extensor or flexor tibiae), contribute as well to a large stiffness at the step transitions. In this context, the CI motoneurons (CI₁ for the extensor tibiae and CI₂ and CI₃ for the flexor tibiae) are very likely to play a major role in facilitating antagonistic shortening. Hence, investigations combining CI stimulation with force and length measurements are certainly a task for further examinations in the future. A conceivable experimental approach could comprise *nl2* or *nl5* stimulation (both containing the CI₁ axon) together with *nl3* recording (in order to control successful CI₁ stimulation) while measuring extensor tibiae force in response to stretches and relaxations of different amplitude and velocity. The role of the CI₁ neuron in force reduction of dually and triply innervated extensor tibiae fibres (see Bässler et al. (1996)) could also be an interesting future project: the CI₁ neuron is most likely responsible for the modest differences observed between full recruitment of all three motoneurons or only partial recruitment (see 'Materials and Methods' section). Another urgent topic would be the examination of P₀ and V₀ of the muscles in other leg joints like the thorax-coxa joint (protractor and retractor coxae) and the coxa-trochanter joint (depressor and levator trochanteris). Similar to the flexor tibiae, investigations of these muscles are limited by the existence of a large number of motoneurons (Goldammer et al. (2007)), which cause a problem in terms of a reasonable extracellular stimulation. In this context, measuring fibre and sarcomere lengths of these muscles could help comparing those muscles in terms of their maximal contraction velocities V₀ (see Thuma (2007)) just by comparing their structural anatomy. The preliminary determinations of extensor and flexor tibiae sarcomere lengths need to be finalised.

Appendix

1 Spike2 scripts

The following set of scripts represents a selection of the most important scripts written for either conductance of the experiments or analysis of the data presented in this thesis. Comments (written after semicolons on the right side) and output dialogs are mostly in German.

1.1 Sequencer scripts

Script to stretch and stimulate muscle in order to obtain an active force - length curve

Letters 'a' to 'e' initiate individual subscripts to stimulate the nerve (*nl3*) with pulse series of different frequency (single pulse, 30, 50, 80, 200 Hz). Letters 'A' to 'C' initiate individual ramps to stretch the muscle starting from -0.75 mm to -0.3 mm (0 mm \cong 90° FT-angle) with 0.15 mm ramps of 1.5 s duration. Only a selection of subscripts is shown.

```

SET 0.050 1 0 ;                               Get rate & scaling OK
VAR V45,LoopC=0 ;                             Define variable for section loops
VAR V46,RampC=0 ;                             Define variable for ramp loops
VAR V47,DelayC=0 ;                             Define variable for delay loops
VAR V52,count=0
DAC 0,0
DAC 1,0
HALT

'a DAC 0,5;                                   Einzelreiz
PULS1: DELAY s(0.0005)-1 ;                     definiert Pulsdauer (0.5ms)
DAC 0,0 ;Pulsende
HALT

```

APPENDIX

<pre>'b MOVI count,30 ; PULS30: DAC 0,5 DELAY s(0.0005)-1 ; DAC 0,0 ;Pulsende DELAY s(0.032833)-1 ; DBNZ count,puls30 ; HALT</pre>	<pre>30Hz definiert Pulsdauer (0.5ms) definiert Abstand zwischen Pulsen loop</pre>
<pre>'c MOVI count, 50 ; PULS50: DAC 0,5 DELAY s(0.0005)-1 ; DAC 0,0 ;Pulsende DELAY s(0.0195)-1 ; DBNZ count,puls50 ; HALT</pre>	<pre>50Hz definiert Pulsdauer (0.5ms) definiert Abstand zwischen Pulsen loop</pre>
<pre>'d MOVI count, 80 ; PULS80: DAC 0,5 DELAY s(0.0005)-1 ; DAC 0,0 ;Pulsende DELAY s(0.012)-1 ; DBNZ count,puls80 ; HALT</pre>	<pre>80Hz definiert Pulsdauer (0.5ms) definiert Abstand zwischen Pulsen loop</pre>
<pre>'e MOVI count, 200; PULS200: DAC 0,5 DELAY s(0.0005)-1 ; DAC 0,0 ;Pulsende DELAY s(0.0045)-1 ; DBNZ count,puls200 ; HALT</pre>	<pre>200Hz definiert Pulsdauer (0.5ms) definiert Abstand zwischen Pulsen loop</pre>
<pre>EA: 'A DIGOUT [.....00] ; DAC 1,-1.5 ; MOVI RampC,29999 ; RA0: ADDAC 1,1.0001e-005 ; DBNZ RampC,RA0 ;</pre>	<pre>zu -0.6 mm Start point for ramp Loop count for ramp Ramp the DAC Keep going till ramp done</pre>

HALT ;	End of this sequence section
EB: 'B DIGOUT [.....00] ;	zu -0.45 mm
DAC 1,-1.2 ;	Start point for ramp
MOVI RampC,29999 ;	Loop count for ramp
RB0: ADDAC 1,1.0001e-005 ;	Ramp the DAC
DBNZ RampC,RB0 ;	Keep going till ramp done
HALT ;	End of this sequence section
EC: 'C DIGOUT [.....00] ;	zu -0.3 mm
DAC 1,-0.9 ;	Start point for ramp
MOVI RampC,29999 ;	Loop count for ramp
RC0: ADDAC 1,1.0001e-005 ;	Ramp the DAC
DBNZ RampC,RC0 ;	Keep going till ramp done
HALT ;	End of this sequence section

Script to adjust load of the Aurora dual mode lever system for quick release experiments

VAR V54,maxval%,ok%;	'Definition der Variablen(V54=KRAFTAMPLITUDE)
WindowVisible(3);	'Scriptfenster in den Hintergrund
maxval%:=(Trunc(Pow(2,31)-1))/5;	'Umrechnungsfaktor von Volt in Sequencer-Einheiten
DlgCreate("Wähle Kraftamplitude");	'Dialog zur Wahl der Variablen
DlgReal(1, "Kraftamplitude",0,5);	'Spannung zwischen den Strompulsen
ok%:=DlgShow(V54);	
V54:=V54*maxval%;	'Umrechnen der Werte auf Sequencer-Einheiten
	'Schwelle, ab der der nächste Puls ausgelöst werden kann
SampleSeqVar(54,V54);	'schreiben der Variablen in Sequencer-Variablen
SampleKey("a");	'springe zu Label "a" in den Sequencer

Script to obtain a single Hill curve data point (exemplary at 80 Hz stimulation frequency)

The script needs the previously described script to work properly. It starts by setting a large counterforce level on the Aurora dual lever system and loops a certain number of instruction lines in order to generate the desired number of pulses at 80 Hz (in this example). There has to be a second stimulation loop (80Hz-II) in order to set a new

counterforce level (V54) between the two loops.

```

'a DIGOUT [.....00] ;                               Hill-80Hz
DAC 1,5
MOVI count,79 ;                                     80Hz-I
PULS15: DAC 0,5
DELAY ms(0.5)
DAC 0,0
DELAY s(0.0115)
DBNZ count,puls15
DAC 0,5
DELAY ms(0.5)
DAC 0,0
DELAY s(0.0054)
DAC 1,V54 ;                                         Kraftamplitude
DELAY s(0.006)
MOVI count,40 ;                                     80Hz-II
PULS16: DAC 0,5
DELAY ms(0.5)
DAC 0,0
DELAY s(0.0115)
DBNZ count,puls16
DELAY s(1.5)
DAC 1,5
HALT
    
```

Script to stretch muscle at particular times before or after the end of stimulation

The essential feature of this sequencer script is the output instruction 'Call', which saves the next step number to a return stack and jumps to the labelled instruction. That is, the script provides the opportunity to memorise a value that can be used to initiate a chain of instructions starting from this value.

APPENDIX

SET 0.100 1 0 ;	Get rate & scaling OK
VAR V1,poBase ;	Position OUT start level
VAR V2,piBase ;	Position IN start level
VAR V3,piCurr ;	Current IN position
VAR V58,poCurr ;	Current OUT position
VAR V5,deltaPi ;	IN Differenz (piBase-piCurr)
VAR V6,tmp	
VAR V7,rSlopeA=VDAC32(0.0042)	
VAR V8,rISlopeA=VDAC32(2)	
VAR V9,loopCnt	
VAR V11,delayRes=0	
VAR V12,delayStd=2000 ;	time after stimulation start
VAR V13,delaySub=0 ;	subtracted time from V12: controls the time of the ramp start
VAR V14,rampc=0	
VAR V15,Stufe ;	this value determines the ramp speed of the muscle stretch
VAR V16,tem	
VAR V17,delayS2=0	
VAR V50,force2=2	
VAR V33,piConAmp=0	
DAC 0,0.24	
DAC 1,0	
HALT ;	
'X CALL READPI ;	gereizt
MOV piBase,piCurr	
DIGOUT [.....01]	
DIGOUT [.....00]	
DELAY delayStd	
DELAY delaySub ;	0-x ms
CALL READPI	
MOV piConAmp,piCurr	
MOV deltaPi,piBase	
SUB deltaPi,piCurr	
NEG deltaPi,deltaPi	
DAC 1,deltaPi	
DAC 0,0.3	

```

ADDAC 1,Stufe ;                               VAR15: 0.00045 - 0.0018
DAC 0,0.5
ADDAC 1,Stufe
DAC 0,0.7
ADDAC 1,Stufe
DAC 0,0.9
ADDAC 1,Stufe
DAC 0,1.2
ADDAC 1,Stufe
DAC 0,1.5
ADDAC 1,Stufe
DAC 0,2
DELAY delayS2 ;                               x+y ms
RAMPX: ADDAC 1,Stufe ;                         VAR15: 0.00045 - 0.0018
CALL READPI
BLT piCurr,piBase,rampx
DAC 1,0
DELAY s(2)
DAC 0,0.24
HALT

READPI: CHAN tmp,3 ;                           ; reads the value of channel 3 (16 bit) into the piCurr variable, additionally
MULI tmp,65536 ;                               ; scales the input to into the DAC value range (32 bit)
MOV piCurr,tmp
RETURN

```

Script to stimulate the nerve with a physiological pattern

The following lines combine two different scripts: 'PlayWaveAdd' accomplishes access to an already existing waveform file (in this example: from 0s to 165s of the recording termed 'PhysCo') and calls this sequence 'A'. The output of this sequence ('A') can be initiated subsequently by 'WAVEGO'.

```

PlayWaveAdd ("A","PhysCo",0,0,165,3);
'P DIGOUT [.....00] ;                         physiologische Stim. ISOTONISCH
DAC 1,0.8 ;                                   40 mN counterforce

```

DELAY s(5)

WAVEGO A

DELAY s(5)

DAC 1,5

HALT

1.2 Analytical script

Script to determine shortening velocity and length of the series elastic component

This script needs a waveform channel with data, an event channel with the information about the muscle stimulation start, and a cursor (1) to step through the waveform data file. The script creates dialogue windows to get information about the begin and width of the time frame to calculate the contraction velocity from, and of the quick release start, i.e. when position control switches to force control. There are two calculations being done: a) determination of the slope that represents the muscle shortening velocity at a particular force level (see line: $\text{slope} := (y_2 - y_1) / \text{width}$), i.e. interpolating between begin and end of a desired time frame, and b) determination of the length change between length at the switch from position to force control and length being extrapolated from the earlier determined slope (see lines: $b := y_1 - \text{slope} * (\text{delay}_2 - \text{delay}_1)$; $c := b - \text{offset}$; $\text{delta} := \text{Abs}(c)$).

```
VAR n%,slope, anzahl%, evtch%, delay1, delay2, width, datach%, y1, y2, b, c, offset, delta;
```

```
DlgCreate("Wähle Eventkanal");
```

```
DlgChan(1, "Eventkanal", 2);
```

```
DlgChan(2, "Datenkanal", 1);
```

```
DlgShow(evtch%, datach%);
```

```
DlgCreate("Wähle Parameter");
```

```
DlgReal(1, "Beginn Geschwindigkeitsberechnung bei [ms]", 0, 3000);
```

```
DlgReal(2, "Zeitfenster [ms]", 0, 1000);
```

```
DlgReal(3, "Kraftsprung bei [ms]", 0, 3000);
```

```
DlgShow(delay2, width, delay1);
```

```
delay2:=delay2/1000;
```

```
width:=width/1000;
```


REFERENCES

```
delay1:=delay1/1000;
Cursor(1, 0);
anzahl%:=count(evtch%, 0, MaxTime());
printlog("Zeit",chr$(9), "Steigung", "erster Positionssprung");
for n%:=1 to anzahl% do
Cursor(1, Nexttime(evtch%, cursor(1)));
y1:=Chanvalue(datach%, cursor(1)+delay2);
y2:=Chanvalue(datach%, cursor(1)+delay2+width);
offset:=Chanvalue(datach%, cursor(1)+3);
slope:=(y2-y1)/width;
b:= y1-slope*(delay2-delay1);
c:=b-offset;
delta:=Abs(c);
printlog(cursor(1), slope,chr$(9), delta);
next
```

References

- Abbot, B. and Aubert, X. (1952). The force exerted by active striated muscle during and after change of length. *J Physiol*, 117(1):77–86.
- Abbot, B. and Wilkie, D. (1953). The relation between velocity of shortening and the tension-length curve of skeletal muscle. *J Physiol*, 120:214–223.
- Abbot, R. (1973). Does calcium affect the rate constants of muscle? In *37th Cold Spring Harbor Symposium of Quantitative Biology*.
- Ahn, A. and Full, R. (2002). A motor and a brake: two leg extensor muscles acting at the same joint manage energy differently in a running insect. *J Exp Biol*, 205:379–389.
- Ahn, A., Meijer, K., and Full, R. (2006). In situ muscle power differs without varying in vitro mechanical properties in two insect leg muscles innervated by the same motor neuron. *J Exp Biol*, 209(Pt 17):3370–3382.
- Akay, T., Bässler, U., Gerharz, P., and Büschges, A. (2001). The role of sensory signals from the insect coxa-trochanteral joint in controlling motor activity of the femur-tibia joint. *J Neurophysiol*, 85(2):594–604.
- Akay, T. and Büschges, A. (2006). Load signals assist the generation of movement-dependent reflex reversal in the femur-tibia joint of stick insects. *J Neurophysiol*, 96(6):3532–3537.
- Akay, T., Haehn, S., Schmitz, J., and Büschges, A. (2004). Signals from load sensors underlie interjoint coordination during stepping movements of the stick insect leg. *J Neurophysiol*, 92(1):42–51.
- Alexander, R. M. (1985). The maximum forces exerted by animals. *J Exp Biol*, 115:231–238.
- Anderson, F. and Pandy, M. (1999). A dynamic optimization solution for vertical jumping in three dimensions. *Comput Methods Biomech Biomed Engin*, 2(3):201–231.
- Armstrong, C., Huxley, A., and Julian, F. (1966). Oscillatory responses in frog skeletal muscle fibres. *J Physiol*, 186:26–27.
- Atwood, H. L. (1965). Excitation and inhibition in crab muscle fibres. *Comp Biochem Physiol*, 16(4):409–426.
- Balnave, C. D. and Allen, D. G. (1996). The effect of muscle length on intracellular calcium and force in single fibres from mouse skeletal muscle. *J Physiol*, 492 (Pt 3):705–713.
- Bartling, C. and Schmitz, J. (2000). Reaction to disturbances of a walking leg during stance. *J Exp Biol*, 203:1–13.
- Bässler, D., Büschges, A., Meditz, S., and Bässler, U. (1996). Correlation between muscle structure and filter characteristics of the muscle-joint system in three orthopteran insect species. *J Exp Biol*, 199:2169–2183.
- Bässler, U. (1965). Propriozeptoren am Subcoxal- und Femur-Tibia-Gelenk der Stabheuschrecke *Carausius morosus* und ihre Rolle bei der Wahrnehmung der Schwerkraftrichtung. *Kybernetik*, 2(4):168–193.
- Bässler, U. (1967). Zur Regelung der Stellung des Femur-Tibia-Gelenkes bei der Stabheuschrecke *Carausius morosus* in der Ruhe und im Lauf. *Kybernetik*, 4:18–26.
- Bässler, U. (1972). Der Regelkreis des Kniesehenreflexes bei der Stabheuschrecke *Carausius morosus*: Reaktionen auf passive Bewegungen der Tibia. *Kybernetik*, 12:8–20.
- Bässler, U. (1974). Vom femoralen Chordotonalorgan gesteuerte Reaktionen bei der Stabheuschrecke *Carausius morosus*: Messung der von der Tibia erzeugten Kraft im aktiven und inaktiven Tier. *Kybernetik*, 16:213–226.

REFERENCES

- Bässler, U. (1977). Sense organs in the femur of the stick insect and their relevance to the control of position of the femur-tibia-joint. *J Comp Physiol A*, 121:99–113.
- Bässler, U. (1983). *Stick Insect News. Annual Supplement to Neural Basis of elementary behavior in stick insects. No. 1-8.* Springer Verl.
- Bässler, U. (1993a). The femur-tibia control system of stick insects - a model system for the study of the neural basis of joint control. *Brain Research Reviews*, 18:207–226.
- Bässler, U. (1993b). The walking- (and searching-) pattern generator of stick insects, a modular system composed of reflex chains and endogenous oscillators. *Biol Cybern*, 69:305–317.
- Bässler, U. and Büschges, A. (1998). Pattern generation for stick insect walking movements - multisensory control of a locomotor program. *Brain Research*, 27:65–88.
- Bässler, U. and Stein, W. (1996). Contributions of structure and innervation pattern of the stick insect extensor tibiae muscle to the filter characteristics of the muscle-joint system. *J Exp Biol*, 199:2185–2198.
- Bässler, U. and Storrer, J. (1980). The neural basis of the femur-tibia-control-system in the stick insect *Carausius morosus*. I. motoneurons of the extensor tibiae muscle. *Biol Cybern*, 38:107–114.
- Bässler, U. and Wegner, U. (1983). Motor output of the denervated thoracic ventral nerve cord in the stick insect *Carausius morosus*. *J. exp. Biol.*, 105:127–145.
- Bässler, U., Wolf, H., and Stein, W. (2007). Functional recovery following manipulation of muscles and sense organs in the stick insect leg. *J Comp Physiol A Neuroethol Sens Neural Behav Physiol*, 193(11):1151–1168.
- Becht, G. and Dresden, D. (1956). Physiology of the locomotory muscles in the cockroach. *Nature*, 17:836–837.
- Becht, G., Hoyle, G., and Usherwood, P. (1960). Neuromuscular transmission in the coxal muscles of the cockroach. *J Insect Physiol*, 4:191–201.
- Bennet-Clark, H. C. (1975). The energetics of the jump of the locust *Schistocerca gregaria*. *J Exp Biol*, 63(1):53–83.
- Bennett, M. B. and Taylor, G. C. (1995). Scaling of elastic strain energy in kangaroos and the benefits of being big. *Nature*, 378(6552):56–59.
- Berkowitz, A. and Laurent, G. (1996). Local control of leg movements and motor patterns during grooming in locusts. *J Neurosci.*, 16(24):8067–8078.
- Biewener, A. A., Blickhan, R., Perry, A. K., Heglund, N. C., and Taylor, C. R. (1988). Muscle forces during locomotion in kangaroo rats: force platform and tendon buckle measurements compared. *J Exp Biol*, 137:191–205.
- Blaschko, H., Cattell, M., and Kahn, J. (1931). On the nature of the two types of response in the neuromuscular system of the crustacean claw. *J Physiol*, 73:25–35.
- Blickhan, R. (1986). Stiffness of an arthropod leg joint. *J Biomech*, 19(5):375–384.
- Blickhan, R., Wagner, H., and Seyfarth, A. (2003). *Recent research developments in Biomechanics. Vol. 1, chapter Brain or muscles.*, pages 215–245. India. Transworld Research Network, Thiru-ananthapuram (Trivandrum).
- Blümel, M., Guschlbauer, C., and Büschges, A. (2008a). Muscle and joint simulation. In *DFG meeting Cologne: Load and force control in walking pattern generation of animals and robots: From sensors to local and global control function.*
- Blümel, M., Guschlbauer, C., and Büschges, A. (2008b). Muscle properties in leg step control. In *MBI workshop 4/2008: Neuromechanics of locomotion.*
- Blümel, M., Guschlbauer, C., Gruhn, M., Scharstein, H., and A., B. (2007a). Predicting swing phase movements of the stick insect FT joint. In *100th annual meeting of the Deutsche Zoologische Gesellschaft (Köln).*

- Blümel, M., Guschlbauer, C., Zehl, L., Hooper, S., and A., B. (2007b). Investigating stick insect extensor muscle properties: an experimentally based muscle simulation. In *Proceedings of the 31st Göttingen Neurobiology conference and the 7th meeting of the German Neuroscience society*.
- Bodine, S. C., Roy, R. R., Eldred, E., and Edgerton, V. R. (1987). Maximal force as a function of anatomical features of motor units in the cat *tibialis anterior*. *J Neurophysiol*, 57(6):1730–1745.
- Borgmann, A., Scharstein, H., and Buschges, A. (2007). Intersegmental coordination: the influence of a single walking leg on the neighboring segments in the stick insect walking system. *J Neurophysiol*, 98:1685–1696.
- Boyd, I. and Davey, M. (1968). *Composition of peripheral nerves*. London.
- Brown, I. E., Cheng, E. J., and Loeb, G. E. (1999). Measured and modeled properties of mammalian skeletal muscle. II. the effects of stimulus frequency on force-length and force-velocity relationships. *J Muscle Res Cell Motil*, 20(7):627–643.
- Brown, I. E., Kim, D. H., and Loeb, G. E. (1998). The effect of sarcomere length on triad location in intact feline caudofemoralis muscle fibres. *J Muscle Res Cell Motil*, 19(5):473–477.
- Brown, I. E. and Loeb, G. E. (1999). Measured and modeled properties of mammalian skeletal muscle. I. the effects of post-activation potentiation on the time course and velocity dependencies of force production. *J Muscle Res Cell Motil*, 20(5-6):443–456.
- Brown, I. E. and Loeb, G. E. (2000a). *Biomechanics and neural control of movement.*, chapter A reductionist approach to creating and using neuromusculoskeletal models., pages 148–163. Springer Verlag, New York.
- Brown, I. E. and Loeb, G. E. (2000b). Measured and modeled properties of mammalian skeletal muscle: III. the effects of stimulus frequency on stretch-induced force enhancement and shortening-induced force depression. *J Muscle Res Cell Motil*, 21(1):21–31.
- Brown, I. E. and Loeb, G. E. (2000c). Measured and modeled properties of mammalian skeletal muscle: IV. dynamics of activation and deactivation. *J Muscle Res Cell Motil*, 21(1):33–47.
- Brown, T. I., Rack, P. M., and Ross, H. F. (1982). Electromyographic responses to imposed sinusoidal movement of the human thumb. *J Physiol*, 332:87–99.
- Burck, H. (1988). *Histologische Technik*. pp. 123-124. Stuttgart, New York: Thieme Verlag.
- Burns, M. and Usherwood, P. (1978). Mechanical properties of locust *extensor tibiae* muscles. *Comp Biochem Physiol*, 61A:85–95.
- Burns, M. and Usherwood, P. (1979). The control of walking in orthoptera. II. motor neurone activity in normal free-walking animals. *J Exp Biol*, 79:69–98.
- Burrows, M. and Wolf, H. (2002). Jumping and kicking in the false stick insect *Prosarthria teretrirostris*: kinematics and motor control. *J Exp Biol*, 205(Pt 11):1519–1530.
- Büschges, A. (1995a). Plasticity of neuronal networks that control posture and movement of leg joint in insects. *Verh Dtsch Zool Ges*, 88:139–151.
- Büschges, A. (1995b). Role of local nonspiking interneurons in the generation of rhythmic motor activity in the stick insect. *J Neurobiol*, 27(4):488–512.
- Büschges, A. (2005). Sensory control and organization of neural networks mediating coordination of multisegmental organs for locomotion. *J Neurophysiol*, 93(3):1127–1135.
- Büschges, A., Kittmann, R., and Schmitz, J. (1994). Identified nonspiking interneurons in leg reflexes and during walking in the stick insect. *J Comp Physiol [A]*, 174:685–700.
- Büschges, A., Ludwar, B. C., Bucher, D., Schmidt, J., and DiCaprio, R. A. (2004). Synaptic drive contributing to rhythmic activation of motoneurons in the deafferented stick insect walking system. *Eur J Neurosci*, 19(7):1856–1862.
- Büschges, A. and Schmitz, J. (1991). Nonspiking pathways antagonize the resistance reflex in the thoraco-coxal joint of stick insects. *J Neurobiol*, 22(3):224–237.
- Cavagna, G. A. and Citterio, G. (1974). Effect of stretching on the elastic characteristics and the contractile component of frog striated muscle. *J Physiol*, 239(1):1–14.

REFERENCES

- Childress, D. S. and Jones, R. W. (1967). Mechanics of horizontal movement of the human eye. *J Physiol*, 188(2):273–284.
- Chleboun, G. S., Howell, J. N., Conatser, R. R., and Giesey, J. J. (1998). Relationship between muscle swelling and stiffness after eccentric exercise. *Med Sci Sports Exerc*, 30(4):529–535.
- Chow, J. W. and Darling, W. G. (1999). The maximum shortening velocity of muscle should be scaled with activation. *J Appl Physiol*, 86(3):1025–1031.
- Civan, M. M. and Podolsky, R. J. (1966). Contraction kinetics of striated muscle fibres following quick changes in load. *J Physiol*, 184(3):511–534.
- Close, R. I. (1972). Dynamic properties of mammalian skeletal muscles. *Physiol Rev*, 52(1):129–197.
- Coveney, V. A., Hunter, G. D., and Spriggs, J. (2001). Is the behaviour of the leg during oscillation linear? *J Biomech*, 34(6):827–830.
- Cruse, H. (1976). The function of the legs in the free walking stick insect, *Carausius morosus*. *J Comp Physiol A*, 112:235–262.
- Cruse, H. (1985a). Which parameters control the leg movement of a walking insect? I. Velocity control during the stance phase. *J Exp Biol*, 116:343–355.
- Cruse, H. (1985b). Which parameters control the leg movement of a walking insect? II. the start of the swing phase. *J.exp.Biol.*, 116:357–362.
- Cruse, H. and Bartling, C. (1995). Movement of joint angles in the legs of a walking insect. *Carausius morosus*. *J Insect Physiol*, 41:761–771.
- Cruse, H. and Storrer, J. (1977). Open loop analysis of a feedback mechanism controlling the leg position in the stick insect *carausius morosus*: comparison between experiment and simulation. *Biol.Cybern.*, 25:143–153.
- De Haan, A. (1998). The influence of stimulation frequency on force-velocity characteristics of in situ rat *gastrocnemius* muscle. *J Exp Physiol*, 83:77–84.
- Dean, J. (1984). Control of leg protraction in the stick insect: a targeted movement showing compensation for externally applied forces. *J. Comp Physiol A*, 155:771–781.
- Debrodt, B. and Bässler, U. (1989). Motor neurones of the flexor tibiae muscle in phasmids. *Zool Jb Physiol*, 93:481–494.
- Debrodt, B. and Bässler, U. (1990). Responses of flexor motor neurons to stimulation of the femoral chordotonal organ of the phasmid *Extratosoma tiaratum*. *Zool. Jb. Physiol.*, 94:101–119.
- Delcomyn, F. (1971). Computer aided analysis of a locomotor leg reflex in the cockroach *Periplaneta americana*. *Z vergl Physiologie*, 74:427–445.
- Denny-Brown, D. (1929). On the nature of postural reflexes. *Proc R Soc Lond Ser B*, 104:252–301.
- Driesang, R. and Büschges, A. (1993). The neural basis of catalepsy in the stick insect. IV. properties of nonspiking interneurons. *J.Comp.Physiol.A*, 173:445–454.
- Dudek, D. M. and Full, R. J. (2006). Passive mechanical properties of legs from running insects. *J Exp Biol*, 209(Pt 8):1502–1515.
- Dürr, V. (2001). Stereotypic leg searching movements in the stick insect: kinematic analysis, behavioral context and simulation. *J Exp Biol*, 204:1589–1604.
- Dürr, V., Schmitz, J., and Cruse, H. (2004). Behavior-based modelling of hexapod locomotion: linking biology and technical application. *Arthropod Structure & Development*, 33:237–250.
- Edman, K. A. (1966). The relation between sarcomere length and active tension in isolated *semitendinosus* fibres of the frog. *J Physiol*, 183(2):407–417.
- Edman, K. A. (1970). The rising phase of the active state in single skeletal muscle fibres of the frog. *Acta Physiol Scand*, 79(2):167–173.
- Edman, K. A. (1979). The velocity of unloaded shortening and its relation to sarcomere length and isometric force in vertebrate muscle fibres. *J Physiol*, 291:143–159.

- Edman, K. A. (1988). Double-hyperbolic force-velocity relation in frog muscle fibres. *J Physiol*, 404:301–321.
- Edman, K. A. and Curtin, N. A. (2001). Synchronous oscillations of length and stiffness during loaded shortening of frog muscle fibres. *J Physiol*, 534(Pt. 2):553–563.
- Edman, K. A., Elzinga, G., and Noble, M. I. (1978). Enhancement of mechanical performance by stretch during tetanic contractions of vertebrate skeletal muscle fibres. *J Physiol*, 281:139–155.
- Edman, K. A. and Kiessling, A. (1971). The time course of the active state in relation to sarcomere length and movement studied in single skeletal muscle fibres of the frog. *Acta Physiol Scand*, 81(2):182–196.
- Edman, K. A., Mulieri, L. A., and Scubon-Mulieri, B. (1976). Non-hyperbolic force-velocity relationship in single muscle fibres. *Acta Physiol Scand*, 98(2):143–156.
- Edman, K. A., Månsson, A., and Caputo, C. (1997). The biphasic force-velocity relationship in frog muscle fibres and its evaluation in terms of cross-bridge function. *J Physiol*, 503 (Pt 1):141–156.
- Edman, K. A. P. (2005). Contractile properties of mouse single muscle fibers, a comparison with amphibian muscle fibers. *J Exp Biol*, 208(Pt 10):1905–1913.
- Edman, K. A. P. and Josephson, R. K. (2007). Determinants of force rise time during isometric contraction of frog muscle fibres. *J Physiol*, 580(Pt.3):1007–1019.
- Eisenberg, E., Hill, T. L., and Chen, Y. (1980). Cross-bridge model of muscle contraction. Quantitative analysis. *Biophys J*, 29(2):195–227.
- Ekeberg, Ö., Blümel, M., and Büschges, A. (2004). Dynamic simulation of insect walking. *Athropod Structure and Development*, 33:287–300.
- Ekeberg, Ö. (2002). Modeling of interactions between neural networks and musculoskeletal system. *Computational Neuroscience - Realistic modeling for Experimentalists*, pages 317–335.
- Endo, M. (1973). Length dependence of activation of skin muscle fibres by calcium. *Cold Spring Harbor Symposia on Quantitative Biology*, 37:505–510.
- Esteki, A. and Mansour, J. M. (1996). An experimentally based nonlinear viscoelastic model of joint passive moment. *J Biomech*, 29(4):443–450.
- Ettema, G. and Meijer, K. (2000). Muscle contraction history: modified hill versus an exponential decay model. *Biol Cybern*, 83:491–500.
- Evans, P. and O'Shea, M. (1978). The identification of an octopaminergic neurone and the modulation of a myogenic rhythm in the locust. *J Exp Biol*, 73:235–260.
- Evans, P. D. and O'Shea, M. (1977). An octopaminergic neurone modulates neuromuscular transmission in the locust. *Nature*, 270(5634):257–259.
- Evans, P. D. and Siegler, M. V. (1982). Octopamine mediated relaxation of maintained and catch tension in locust skeletal muscle. *J Physiol*, 324:93–112.
- Fenn, W. O. and Marsh, B. S. (1935). Muscular force at different speeds of shortening. *J Physiol*, 85(3):277–297.
- Ferry, J. D. (1961). *Viscoelastic properties of polymers*. New York, London; John Wiley & Sons, Inc.
- Field, L. and Pflüger, H. (1989). The femoral chordotonal organ: a bifunctional orthopteran (*Locusta migratoria*) sense organ? *Comp. Biochem. Physiol.*, 93A:729–743.
- Fischer, H., Schmidt, J., Haas, R., and Büschges, A. (2001). Pattern generation for walking and searching movements of a stick insect leg. I. Coordination of motor activity. *J Neurophysiol*, 85(1):341–353.
- Friedrich, H. (1932). Nervenphysiologische Studien an Insekten I. Untersuchungen über das reizphysiologische Verhalten der Extremitäten von *Dixippus morosus*. *Z vergl Physiol*, 18:536–561.
- Full and Ahn (1995). Static forces and moments generated in the insect leg: comparison of a three-dimensional musculo-skeletal computer model with experimental measurements. *J Exp Biol*, 198(Pt 6):1285–1298.

REFERENCES

- Full, Yamauchi, and Jindrich (1995). Maximum single leg force production: cockroaches righting on photoelastic gelatin. *J Exp Biol*, 198(Pt 12):2441–2452.
- Full, R. (1997). Invertebrate locomotor systems. In Dantzler, W., editor, *The Handbook of Comparative Physiology*, number 12, pages 853–930. Oxford University Press, Oxford.
- Full, R. and Koditschek, D. (1999). Templates and anchors: neuromechanical hypotheses of legged locomotion on hand. *J Exp Biol*, 202:3325–3332.
- Full, R. and Meijer, K. (1997). Metrics of natural muscle function. In *Electroactive polymer actuators as artificial muscles*, number 3, pages 67–83.
- Full, R., Stokes, D., Ahn, A., and Josephson, R. (1998). Energy absorption during running by leg muscles in a cockroach. *J Exp Biol*, 201:997–1012.
- Full, R. and Tu, M. (1991). Mechanics of a rapid running insect: two-, four- and six-legged locomotion. *J Exp Biol*, 156:215–231.
- Full, R. J. and Farley, C. T. (2000). *Biomechanics & neural control of posture & movement.*, chapter Musculoskeletal Dynamics in Rhythmic Systems: a comparative approach to legged locomotion., pages 192–203. Springer Verlag-New York, Inc.
- Funabara, D., Kanoh, S., Siegman, M. J., Butler, T. M., Hartshorne, D. J., and Watabe, S. (2005). Twitchin as a regulator of catch contraction in molluscan smooth muscle. *J Muscle Res Cell Motil*, 26(6-8):455–460.
- Fung, Y. C. (2004). *Biomechanics: mechanical properties of living tissues*, chapter Quasi-linear viscoelasticity of soft tissues. Springer Science + Business Media.
- Gabriel, J. (2005). *Activity of leg motoneurons during single leg walking of the stick insect: From synaptic inputs to motor performance*. PhD thesis, University of Cologne.
- Gabriel, J. and Büschges, A. (2007). Control of stepping velocity in a single insect leg during walking. *Philos Transact A Math Phys Eng Sci*, 365(1850):251–271.
- Gabriel, J., Scharstein, H., Schmidt, J., and Büschges, A. (2003). Control of flexor motoneuron activity during single leg walking of the stick insect on an electronically controlled treadmill. *J Neurobiol*, 56(3):237–251.
- Godden, D. (1974). The physiological mechanism of catalepsy in the stick insect *Carausius morosus* Br. *J Comp Physiol*, 89:251–274.
- Goldammer, J., Mentel, T., and Büschges, A. (2007). A tracing study of leg motoneurons in *Carausius morosus*. In *100th Annual meeting of the Deutsche Zoologische Gesellschaft (Köln) 2007*.
- Gordon, A. M., Huxley, A. F., and Julian, F. J. (1966a). Tension development in highly stretched vertebrate muscle fibres. *J Physiol*, 184(1):143–169.
- Gordon, A. M., Huxley, A. F., and Julian, F. J. (1966b). The variation in isometric tension with sarcomere length in vertebrate muscle fibres. *J Physiol*, 184(1):170–192.
- Graham, D. (1972). A behavioural analysis of the temporal organisation of walking movements in the 1st instar and adult stick insect (*Carausius morosus*). *J Comp Physiol*, 81:23–52.
- Graham, D. (1983). Insects are both impeded and propelled by their legs during walking. *J Exp Biol*, 104:129–137.
- Graham, D. (1985). Pattern and control of walking in insects. In *Advances in Insect Physiology*, volume 18, pages 31–140. Academic Press Inc., London.
- Graham, D. and Cruse, H. (1981). Coordinated walking of stick insects on a mercury surface. *J Exp Biol*, 92:229–241.
- Grillner, S. (1972). The role of muscle stiffness in meeting the changing postural and locomotor requirements for force development by the ankle extensors. *Acta Physiol Scand*, 86(1):92–108.
- Grillner, S., Parker, D., and Manira, A. E. (1998). Vertebrate locomotion—a lamprey perspective. *Ann N Y Acad Sci*, 860:1–18.

- Grillner, S. and Udo, M. (1971). Motor unit activity and stiffness of the contracting muscle fibres in the tonic stretch reflex. *Acta Physiol Scand*, 81(3):422–424.
- Gruhn, M., Hoffmann, O., Dübber, M., Scharstein, H., and Büschges, A. (2006). Tethered stick insect walking: a modified slippery surface setup with optomotor stimulation and electrical monitoring of tarsal contact. *J Neurosci Methods*, 158(2):195–206.
- Guschlbauer, C., Scharstein, H., and Büschges, A. (2007). The extensor tibiae muscle of the stick insect: biomechanical properties of an insect walking leg muscle. *J Exp Biol*, 210(Pt 6):1092–1108.
- Günzel, D. and Rathmayer, W. (1994). Non-uniformity of sarcomere lengths can explain the 'catch-like' effect of arthropod muscle. *J Muscle Res Cell Motil*, 15(5):535–546.
- Haas, F., Gorb, S., and Blickhan, R. (2000). The function of resilin in beetle wings. *Proc Biol Sci*, 267(1451):1375–1381.
- Hajian, A. Z. and Howe, R. D. (1997). Identification of the mechanical impedance at the human finger tip. *J Biomech Eng*, 119(1):109–114.
- Heide, G. and Götz, K. G. (1996). Optomotor control of course and altitude in *Drosophila melanogaster* is correlated with distinct activities of at least three pairs of flight steering muscles. *J Exp Biol*, 199(Pt 8):1711–1726.
- Herrel, A., Meyers, J. J., Aerts, P., and Nishikawa, K. C. (2001). Functional implications of supercontracting muscle in the chameleon tongue retractors. *J Exp Biol*, 204(Pt 21):3621–3627.
- Herrel, A., Meyers, J. J., Timmermans, J.-P., and Nishikawa, K. C. (2002). Supercontracting muscle: producing tension over extreme muscle lengths. *J Exp Biol*, 205(Pt 15):2167–2173.
- Herzog, W., Schachar, R., and Leonard, T. R. (2003). Characterization of the passive component of force enhancement following active stretching of skeletal muscle. *J Exp Biol*, 206(Pt 20):3635–3643.
- Hildebrand, M. (1988). *Analysis of vertebrate structure*. New York, Toronto: John Wiley & Sons.
- Hill, A. V. (1938). The heat of shortening and the dynamic constants of muscle. *Proc. R. Soc. Lond. B Biol. Sci.*, 126:136–195.
- Hill, A. V. (1949). The energetics of relaxation in a muscle twitch. *Proc R Soc Lond B Biol Sci*, 136(883):211–219.
- Hill, A. V. (1950). The dimensions of animals and their muscular dynamics. *Sci. Progr.*, 38:209–230.
- Hill, D. K. (1968). Tension due to interaction between the sliding filaments in resting striated muscle. the effect of stimulation. *J Physiol*, 199(3):637–684.
- Hodgkin, A. and Huxley, A. (1952). Currents carried by sodium and potassium ions through the membrane of the giant axon of *Loligo*. *J Physiol*, 116:449–472.
- Hogan, N. (1982). *Robot motion, Vol. 5*, chapter Mechanical impedance control in assistive devices and manipulators. Cambridge, MA: MIT Press.
- Hooper, S., Guschlbauer, C., Blümel, M., Rosenbaum, P., Gruhn, M., Akay, T., and Büschges, A. (2009). Neural control of unloaded leg posture and of leg swing in stick insect, cockroach, and mouse differs from that in larger animals. submitted.
- Hooper, S., Guschlbauer, C., von Uckermann, G., and Büschges, A. (2006). Natural neural output that produces highly variable locomotory movements. *J Neurophysiol*, 96(4):2072–2088.
- Hooper, S. L., Guschlbauer, C., von Uckermann, G., and Büschges, A. (2007a). Slow temporal filtering may largely explain the transformation of stick insect (*carausius morosus*) extensor motor neuron activity into muscle movement. *J Neurophysiol*.
- Hooper, S. L., Guschlbauer, C., von Uckermann, G., and Büschges, A. (2007b). Different motor neuron spike patterns produce contractions with very similar rises in graded slow muscles. *J Neurophysiol*, 97(2):1428–1444.
- Hooper, S. L., Hobbs, K. H., and Thuma, J. B. (2008). Invertebrate muscles: thin and thick filament structure; molecular basis of contraction and its regulation, catch and asynchronous muscle. *Prog Neurobiol*, 86(2):72–127. submitted.

REFERENCES

- Hooper, S. L. and Weaver, A. L. (2000). Motor neuron activity is often insufficient to predict motor response. *Curr Opin Neurobiol*, 10(6):676–682.
- Howell, J. N., Chleboun, G., and Conatser, R. (1993). Muscle stiffness, strength loss, swelling and soreness following exercise-induced injury in humans. *J Physiol*, 464:183–196.
- Hoyle, G. (1966). Interpreting muscle function in invertebrates. *Pflügers Arch Gesamte Physiol Menschen Tiere*, 291(1):12–27.
- Hoyle, G. (1978). Distributions of nerve and muscle fibre types in locust jumping muscle. *J Exp Biol*, 73:205–233.
- Hutchinson, J. R. and Garcia, M. (2002). Tyrannosaurus was not a fast runner. *Nature*, 415(6875):1018–1021.
- Huxley, A. and Niedergerke, R. (1954a). Measurement of muscle striations in stretch and contraction. *J Physiol*, 124(2):46–7P.
- Huxley, A. and Niedergerke, R. (1954b). Structural changes in muscle during contraction; interference microscopy of living muscle fibres. *Nature*, 173(4412):971–973.
- Huxley, A. F. (1957a). Muscle structure and theories of contraction. *Prog Biophys Biophys Chem*, 7:255–318.
- Huxley, A. F. and Simmons, R. M. (1971). Proposed mechanism of force generation in striated muscle. *Nature*, 233(5321):533–538.
- Huxley, H. (1960). *Muscle cells.*, volume 4. New York: Academic press.
- Huxley, H. E. (1957b). The double array of filaments in cross-striated muscle. *J Biophys Biochem Cytol*, 3(5):631–648.
- Huxley, H. E. and Hanson, J. (1954). Changes in the cross-striations of muscle during contraction and stretch and their structural interpretation. *Nature*, 173(4412):973–976.
- Inman, V. T. (1966). Human locomotion. *Can Med Assoc J*, 94(20):1047–1054.
- Irving, M. (1995). Muscle. Give in the filaments. *Nature*, 374(6517):14–15.
- Jahromi, S. and Atwood, H. L. (1969). Structural features of muscle fibres in the cockroach leg. *J Insect Physiol*, 15:2255–2262.
- Jellema, T. and Heitler, W. (1996). Peripheral control of the gain of a central synaptic connection between antagonistic motor neurones in the locust. *J Exp Biol*, 199:613–625.
- Jewell, B. and Wilkie, D. (1958). An analysis of the mechanical components in frog's striated muscle. *J Physiol*, 143(3):515–540.
- Jewell, B. and Wilkie, D. (1960). The mechanical properties of relaxing muscle. *J Physiol*, 152:30–47.
- Jindrich, D. L. and Full, R. J. (2002). Dynamic stabilization of rapid hexapedal locomotion. *J Exp Biol*, 205(Pt 18):2803–2823.
- Jones, C., Allen, T., Talbot, J., Morgan, D. L., and Proske, U. (1997). Changes in the mechanical properties of human and amphibian muscle after eccentric exercise. *Eur J Appl Physiol Occup Physiol*, 76(1):21–31.
- Jones, D. A., Newham, D. J., and Clarkson, P. M. (1987). Skeletal muscle stiffness and pain following eccentric exercise of the elbow flexors. *Pain*, 30(2):233–242.
- Jorgensen, W. K. and Rice, M. J. (1983). Morphology of a very extensible insect muscle. *Tissue Cell*, 15(4):639–644.
- Josephson, R. (1985). Mechanical power output from striated muscle during cyclic contraction. *J Exp Biol*, 114:493–512.
- Josephson, R. K. (1993). Contraction dynamics and power output of skeletal muscle. *Annu Rev Physiol*, 55:527–546.
- Josephson, R. K., Malamud, J. G., and Stokes, D. R. (2000). Power output by an asynchronous flight muscle from a beetle. *J Exp Biol*, 203(Pt 17):2667–2689.

REFERENCES

- Joyce, G. C., Rack, P. M., and Westbury, D. R. (1969). The mechanical properties of cat soleus muscle during controlled lengthening and shortening movements. *J Physiol*, 204(2):461–474.
- Karg, G., Breutel, G., and Bässler, U. (1991). Sensory influences on the coordination of two leg joints during searching movements of stick insects. *Biol Cybern*, 64:329–335.
- Katz and Gosline (1994). Scaling modulus as a degree of freedom in the design of locust legs. *J Exp Biol*, 187(1):207–223.
- Katz, B. (1939). The relation between force and speed in muscular contraction. *J Physiol*, 96(1):45–64.
- Katz, P., Kirk, M., and Govind, C. (1993). Facilitation and depression at different branches of the same motor axon: evidence for presynaptic differences in release. *J Neurosci*, 13:3075–3089.
- Ker, R. F. (1977). *Some structural and mechanical properties of locust and beetle cuticle*. PhD thesis, University of Oxford.
- Kier, W. M. and Curtin, N. A. (2002). Fast muscle in squid (*Loligo pealei*): contractile properties of a specialized muscle fibre type. *J Exp Biol*, 205(Pt 13):1907–1916.
- Kittmann, R., Schmitz, J., and Büschges, A. (1996). Premotor interneurons in generation of adaptive leg reflexes and voluntary movements in stick insects. *J Neurobiology*, 31(4):512–531.
- Kubow, T. M. and Full, R. J. (1999). The role of the mechanical system in control: a hypothesis of self-stabilization in hexapedal runners. *Phil. Trans. R. Soc. Lond. B*, 354:849–862.
- Lakie, M., Walsh, E. G., and Wright, G. W. (1984). Resonance at the wrist demonstrated by the use of a torque motor: an instrumental analysis of muscle tone in man. *J Physiol*, 353:265–285.
- Lappin, A. K., Monroy, J. A., Pilarski, J. Q., Zepnewski, E. D., Pierotti, D. J., and Nishikawa, K. C. (2006). Storage and recovery of elastic potential energy powers ballistic prey capture in toads. *J Exp Biol*, 209(Pt 13):2535–2553.
- Lestienne, F. (1979). Effects of inertial load and velocity on the braking process of voluntary limb movements. *Exp Brain Res*, 35(3):407–418.
- Lidell, E. G. T. and Sherrington, C. G. (1925). Further observations on myotactic reflexes. *Proc R Soc Lond Ser B*, 97:267–283.
- Linari, M., Lucii, L., Reconditi, M., Casoni, M. E., Amenitsch, H., Bernstorff, S., Piazzesi, G., and Lombardi, V. (2000). A combined mechanical and x-ray diffraction study of stretch potentiation in single frog muscle fibres. *J Physiol*, 526 Pt 3:589–596.
- Lombardi, V. and Piazzesi, G. (1990). The contractile response during steady lengthening of stimulated frog muscle fibres. *J Physiol*, 431:141–171.
- Lou, F., Curtin, N., and Woledge, R. (1997). The energetic cost of activation of white muscle fibres from the dogfish scyliorhinus canicula. *J Exp Biol*, 200(Pt 3):495–501.
- Lou, F., Curtin, N., and Woledge, R. (1999). Elastic energy storage and release in white muscle from dogfish scyliorhinus canicula. *J Exp Biol*, 202 (Pt 2):135–142.
- Ludwar, B., Westmark, S., Büschges, A., and Schmidt, J. (2005). Modulation of membrane potential in mesothoracic moto- and interneurons during stick insect front-leg walking. *J Neurophysiol*, 94(4):2772–2784.
- Machin, K. E. and J. W. Pringle, J. (1960). The physiology of insect fibrillar muscle. iii. the effect of sinusoidal changes of length on a beetle flight muscle. *Proc R Soc Lond B Biol Sci*, 152:311–330.
- Malamud, J. (1988). The effects of octopamine on contraction kinetics and power output of a locust flight muscle. *J Comp Physiol*, 162:827–835.
- Malamud, J. (1989). The tension in a locust flight muscle at various muscle lengths. *J Exp Biol*, 144:479–494.
- Malamud, J. and Josephson, R. (1991). Force-velocity relationships of a locust flight muscle at different times during a twitch contraction. *J Exp Biol*, 159:65–87.
- Marquardt, F. (1940). Beiträge zur Anatomie der Muskulatur und der peripheren Nerven von *Carausius Dixippus morosus*. *Zoologische Jahrbücher Abt. A nat.*, 66:63–128.

REFERENCES

- Matheson, T. and Dürr, V. (2003). Load compensation in targeted limb movements of an insect. *J Exp Biol*, 206(Pt 18):3175–3186.
- Mentel, T., Weiler, V., Büschges, A., and Pflüger, H.-J. (2008). Activity of neuromodulatory neurones during stepping of a single insect leg. *J Insect Physiol*, 54(1):51–61.
- Mochon, S. and McMahon, T. A. (1980). Ballistic walking. *J Biomech*, 13(1):49–57.
- Morgan, D. L. and Allen, D. G. (1999). Early events in stretch-induced muscle damage. *J Appl Physiol*, 87(6):2007–2015.
- Morgan, D. L., Prochazka, A., and Proske, U. (1984). The after-effects of stretch and fusimotor stimulation on the responses of primary endings of cat muscle spindles. *J Physiol*, 356:465–477.
- Morris, L. G. and Hooper, S. L. (1997). Muscle response to changing neuronal input in the lobster (*Panulirus interruptus*) stomatogastric system: spike number- versus spike frequency-dependent domains. *J Neurosci*, 17(15):5956–5971.
- Mu, L. and Ritzmann, R. E. (2005). Kinematics and motor activity during tethered walking and turning in the cockroach, *Blaberus discoidalis*. *J Comp Physiol A Neuroethol Sens Neural Behav Physiol*, 191(11):1037–1054.
- Neustadter, D. M., Herman, R. L., Drushel, R. F., Chestek, D. W., and Chiel, H. J. (2007). The kinematics of multifunctionality: comparisons of biting and swallowing in *aplysia californica*. *J Exp Biol*, 210(Pt 2):238–260.
- Nothof, U. and Bässler, U. (1990). The network producing the "active reaction" of stick insects is a functional element of different pattern generating systems. *Biol Cybern*, 62:453–462.
- Orlovsky, G., Deliagina, T., and Grillner, S. (1999). *Neuronal Control of Locomotion*. Oxford University Press.
- Page, S. and Huxley, H. E. (1963). Filament lengths in striated muscle. *J Cell Biol*, 19:369–390.
- Pearson, K. (1972). Central programming and reflex control of walking in the cockroach. *J Exp Biol*, 56:173–193.
- Pearson, K., Fouad, K., and Misiaszek, J. (1999). Adaptive changes in motor activity associated with functional recovery following muscle denervation in walking cats. *The American Physiological Society*, pages 370–381.
- Pearson, K. and Iles, J. (1970). Discharge patterns of coxal levator and depressor motoneurons of the cockroach, *periplaneta americana*. *J Exp Biol*, 52:139–165.
- Pearson, K., Stein, R., and Malhotra, S. (1970). Properties of action potentials from insect motor nerve fibres. *J Exp Biol*, 53:299–316.
- Pearson, K. G. and Iles, J. F. (1971). Innervation of coxal depressor muscles in the cockroach, *periplaneta americana*. *J Exp Biol*, 54(1):215–232.
- Perry, M. J., Tait, J., Hu, J., White, S. C., and Medler, S. (2009). Skeletal muscle fiber types in the ghost crab, *Ocypode quadrata*: implications for running performance. *J Exp Biol*, 212(Pt 5):673–683.
- Pflüger, H.-J. (1977). The control of the rocking movements of the phasid *Carausius morosus* Br. *J Comp Physiol*, 120:181–202.
- Piazzesi, G., Francini, F., Linari, M., and Lombardi, V. (1992). Tension transients during steady lengthening of tetanized muscle fibres of the frog. *J Physiol*, 445:659–711.
- Pilarski, J., Philipps, G. N. K. and Pierotti, D. (2003). Power amplification by pre-activation of hind limb muscle during jumping in frogs. *FASEB*, 17 17:A1287.
- Pipa, R. and Cook, E. (1959). Studies on the hexapod nervous system. i. the peripheral distribution of the thoracic nerves of the adult cockroach, *Periplaneta americana*. *Ann Ent Soc Am*, 52:695–710.
- Podolsky, R. and Nolan, A. (1972). Cross-bridge properties derived from physiological studies of frog muscle fibres. In Podolsky, R., editor, *Contractility of muscle cells and related processes*.
- Polit, A. and Bizzi, E. (1978). Processes controlling arm movements in monkeys. *Science*, 201(4362):1235–1237.

- Powell, P. L., Roy, R. R., Kanim, P., Bello, M. A., and Edgerton, V. R. (1984). Predictability of skeletal muscle tension from architectural determinations in guinea pig hindlimbs. *J Appl Physiol*, 57(6):1715–1721.
- Proske, U. and Morgan, D. L. (1984). Stiffness of cat *soleus* muscle and tendon during activation of part of muscle. *J Neurophysiol*, 52(3):459–468.
- Proske, U. and Morgan, D. L. (1987). Tendon stiffness: methods of measurement and significance for the control of movement. a review. *J Biomech*, 20(1):75–82.
- Proske, U. and Morgan, D. L. (1999). Do cross-bridges contribute to the tension during stretch of passive muscle? *J Muscle Res Cell Motil*, 20(5-6):433–442.
- Proske, U. and Morgan, D. L. (2001). Muscle damage from eccentric exercise: mechanism, mechanical signs, adaptation and clinical applications. *J Physiol*, 537(Pt 2):333–345.
- Proske, U., Morgan, D. L., and Gregory, J. E. (1993). Thixotropy in skeletal muscle and in muscle spindles: a review. *Prog Neurobiol*, 41(6):705–721.
- Rack, P. M. (1970). *The significance of mechanical properties of muscle in the reflex control of posture.*, chapter Excitatory synaptic mechanisms., pages 317–322. Universitetsforlaget, Oslo: Scandinavian University Books.
- Rack, P. M. and Westbury, D. R. (1969). The effects of length and stimulus rate on tension in the isometric cat *soleus* muscle. *J Physiol*, 204(2):443–460.
- Radnikow, G. and Bässler, U. (1991). Function of a muscle whose apodeme travels through a joint moved by other muscles: why the *retractor unguis* muscle in stick insects is tripartite and has no antagonist. *J Exp Biol*, 157:87–99.
- Raibert, M. H., Brown, H. J., and Chepponis, M. (1984). Experiments in balance with a 3d one-legged hopping machine. *Int J Robot Res*, 3:75–92.
- Raibert, M. H. and Hodgins, J. A. (1993). *Biological Neural Networks in Invertebrate Neuroethology and Robotics.*, chapter Legged robots., pages 319–354. Boston: Academic Press.
- Ranatunga, K. W., Coupland, M. E., Pinniger, G. J., Roots, H., and Offer, G. W. (2007). Force generation examined by laser temperature-jumps in shortening and lengthening mammalian (rabbit *psaos*) muscle fibres. *J Physiol*, 585(Pt 1):263–277.
- Rice, M. J. (1973). Supercontracting striated muscle in a vertebrate. *Nature*, 243(5404):238–240.
- Ritzmann, R. E. and Büschges, A. (2007). Adaptive motor behavior in insects. *Curr Opin Neurobiol*, 17(6):629–636.
- Roberts, T. J. and Marsh, R. L. (2003). Probing the limits to muscle-powered accelerations: lessons from jumping bullfrogs. *J Exp Biol*, 206(Pt 15):2567–2580.
- Roots, H., Offer, G. W., and Ranatunga, K. W. (2007). Comparison of the tension responses to ramp shortening and lengthening in intact mammalian muscle fibres: crossbridge and non-crossbridge contributions. *J Muscle Res Cell Motil*, 28(2-3):123–139.
- Rose, U., Ferber, M., and Hustert, R. (2001). Maturation of muscle properties and its hormonal control in an adult insect. *J Exp Biol*, 204:3531–3545.
- Roszek, B., Baan, G. C., and Huijing, P. A. (1994). Decreasing stimulation frequency-dependent length-force characteristics of rat muscle. *J Appl Physiol*, 77(5):2115–2124.
- Ruegg, J. C. (1968). Dependence of cardiac contractility on myofibrillar calcium sensitivity. *News physiol. Sci.*, 2:179–812.
- Sasaki, K. and Burrows, M. (2003). Proprioceptors monitoring forces in a locust hind leg during kicking form negative feedback loops with *flexor tibiae* motor neurons. *J Exp Biol*, 206(Pt 4):759–769.
- Schilder, R. J. and Marden, J. H. (2004). A hierarchical analysis of the scaling of force and power production by dragonfly flight motors. *J Exp Biol*, 207(Pt 5):767–776.
- Schindler, G. (1979). Funktionsmorphologische Untersuchungen zur Autotomie der Stabheuschrecke *Carausius morosus* Br. (insecta: Phasmidae). *Zool Anz*, 203:316–326.

REFERENCES

- Schmidt, J., Fischer, H., and Büschges, A. (2001). Pattern generation for walking and searching movements of a stick insect leg. II. control of motoneuronal activity. *J Neurophysiol*, 85:354–361.
- Schmidt, J. and Grund, M. (2003). Rhythmic activity in a motor axon induced by axotomy. *NeuroReport*, 14:1267–1271.
- Schmitz, J., Delcomyn, F., and Büschges, A. (1991). *Methods in Neurosciences. Vol. 4, Electrophysiology and Microinjection*, chapter Oil and hook electrodes for en passant recording from small nerves., pages 266–278.
- Schmitz, J. and Hassfeld, G. (1989). The treading-on-tarsus reflex in stick insects: phase dependence and modifications of the motor output during walking. *J Exp Biol*, 143:373–388.
- Scott, S. H., Brown, I. E., and Loeb, G. E. (1996). Mechanics of feline *soleus*: I. effect of fascicle length and velocity on force output. *J Muscle Res Cell Motil*, 17(2):207–219.
- Sensenig, A. T. and Shultz, J. W. (2003). Mechanics of cuticular elastic energy storage in leg joints lacking extensor muscles in arachnids. *J Exp Biol*, 206(Pt 4):771–784.
- Seyfarth, A., Friedrichs, A., Wank, V., and Blickhan, R. (1999). Dynamics of the long jump. *J Biomech*, 32(12):1259–1267.
- Siebert, T., Rode, C., Herzog, W., Till, O., and Blickhan, R. (2008). Nonlinearities make a difference: comparison of two common hill-type models with real muscle. *Biol Cybern*, 98(2):133–143.
- Siebert, T., W. H. and Blickhan, R. (2003). Not all oscillations are rubbish: forward simulation of quick-release experiments. *J Mech Med Biol*, 3:107–122.
- Smit, W. A., Becht, B., and Beenackers, A. M. (1967). Structure, fatigue, and enzyme activities in ‘fast’ insect muscles. *J Insect Physiol*, 13:1857–1868.
- Smith, J. and Zernicke, R. (1987). Prediction for neural control base on limb dynamics. *Trends Neurosci*, 10:123–128.
- Spector, S. A., Gardiner, P. F., Zernicke, R. F., Roy, R. R., and Edgerton, V. R. (1980). Muscle architecture and force-velocity characteristics of cat *soleus* and medial *gastrocnemius*: implications for motor control. *J Neurophysiol*, 44(5):951–960.
- Stein, R. and Pearson, K. (1971). Predicted amplitude and form of action potentials recorded from unmyelinated nerve fibres. *J theor Biol*, 32:539–558.
- Stein, W., Smarandache, C. R., Nickmann, M., and Hedrich, U. B. S. (2006). Functional consequences of activity-dependent synaptic enhancement at a crustacean neuromuscular junction. *J Exp Biol*, 209(Pt 7):1285–1300.
- Stephenson, D. G. and Wendt, I. R. (1984). Length dependence of changes in sarcoplasmic calcium concentration and myofibrillar calcium sensitivity in striated muscle fibres. *J Muscle Res Cell Motil*, 5(3):243–272.
- Stephenson, R. and Josephson, R. (1990). Effects of operating frequency and temperature on mechanical power output from moth flight muscle. *J Exp Biol*, 149:61–78.
- Stevenson, P. and Meuser, S. (1997). Octopaminergic innervation and modulation of a locust flight steering muscle. *J Exp Biol*, 200:633–642.
- Stevenson, R. and Josephson, R. (1990). Effects of operating frequency and temperature on mechanical power output from moth flight muscle. *J Exp Biol*, 149:61–78.
- Storrer, J. (1976). *Systemanalytische Untersuchungen am "Kniesehenreflex" der Stabheuschrecke Carausius morosus Br. (Orthoptera)*. PhD thesis.
- Storrer, J., Bässler, U., and Mayer, S. (1986). Motoneurone im Meso- und Metathorakalganglion der Stabheuschrecke *Carausius morosus*. *Zool Jb Physiol*, 90:359–374.
- Storrer, J. and Cruse, H. (1977). Systemanalytische Untersuchung eines aufgeschnittenen Regelkreises, der die Beinstellung der Stabheuschrecke *Carausius morosus* kontrolliert: Kraftmessungen an den Antagonisten *Flexor* und *Extensor tibiae*. *Biol Cybern*, 25:131–143.

REFERENCES

- Sugi, H., Akimoto, T., Kobayashi, T., Suzuki, S., and Shimada, M. (2000). Possible contribution of titin filaments to the compliant series elastic component in horseshoe crab skeletal muscle fibers. *Adv Exp Med Biol*, 481:371–80; discussion 381–2.
- Sugi, H. and Tsuchiya, T. (1981). Isotonic velocity transients in frog muscle fibres following quick changes in load. *J Physiol*, 319:219–238.
- Taylor, G. M. (2000). Maximum force production: why are crabs so strong? *Proc Biol Sci*, 267(1451):1475–1480.
- Thorson, J. and Biederman-Thorson, M. (1974). Distributed relaxation processes in sensory adaptation. *Science*, 183(121):161–172.
- Thuma, J. (2007). *Anatomy and lengthening velocity of muscles in the lobster stomatogastric system*. Master's thesis, Ohio University.
- Thuma, J. B., Harness, P. I., Koehnle, T. J., Morris, L. G., and Hooper, S. L. (2007). Muscle anatomy is a primary determinant of muscle relaxation dynamics in the lobster (*Panulirus interruptus*) stomatogastric system. *J Comp Physiol A Neuroethol Sens Neural Behav Physiol*, 193(11):1101–1113.
- Usherwood, P. (1962). The nature of "slow" and "fast" contractions in the coxal muscles of the cockroach. *J Insect Physiol*, 8:31–52.
- v. Uckermann, G. and Büschges, A. (2008). Role of premotor nonspiking interneurons in the control of stepping velocity of the stick insect *Carausius morosus*. Technical report, DFG workshop in Cologne 2008: Load and force control in walking pattern generation of animals and robots: From sensors to local and global function.
- van Soest, A. J. and Bobbert, M. F. (1993). The contribution of muscle properties in the control of explosive movements. *Biol Cybern*, 69(3):195–204.
- Vandenboom, R., Hannon, J. D., and Sieck, G. C. (2002). Isotonic force modulates force redevelopment rate of intact frog muscle fibres: evidence for cross-bridge induced thin filament activation. *J Physiol*, 543(Pt 2):555–566.
- Wagner, H., Siebert, T., Ellerby, D. J., Marsh, R. L., and Blickhan, R. (2005). Isofit: a model-based method to measure muscle-tendon properties simultaneously. *Biomech Model Mechanobiol*, 4(1):10–19.
- Wainwright, S.A., Biggs, W. C. J. and Gosline, J. (1976). Mechanical design in organisms. Technical report, Princeton: Princeton university press.
- Wang, K., McCarter, R., Wright, J., Beverly, J., and Ramirez-Mitchell, R. (1991). Regulation of skeletal muscle stiffness and elasticity by titin isoforms: a test of the segmental extension model of resting tension. *Proc Natl Acad Sci U S A*, 88(16):7101–7105.
- Watson, A. and Pflüger, H. (1994). Distribution of input synapses from processes exhibiting GABA- or glutamate-like immunoreactivity onto terminals of prosternal filiform afferents in the locust. *J Comp Neurol*, 343:617–629.
- Watson, J. and Ritzmann, R. (1995). Combined intracellular stimulation and high speed video motion analysis of motor control neurons in the cockroach. *J Neurosci Methods*, 61:151–157.
- Watson, J. and Ritzmann, R. (1998). Leg kinematics and muscle activity during treadmill running in the cockroach, *blaberus discoidalis*: I. slow running. *J Comp Physiol A*, 182:11–22.
- Weidler, D. and Diecke, F. (1969). The role of cations in conduction in the central nervous system of the herbivorous insect *Carausius morosus*. *Z vergl Physiol*, 64:372–399.
- Weiland, G., Bässler, U., and Brunner, M. (1986). A biological feedback control system with electronic input: the artificially closed femur-tibia control system of stick insects. *J Exp Biol*, 120:369–385.
- Weiland, G. and Koch, U. (1987). Sensory feedback during active movements of stick insects. *J Exp Biol*, 133:137–156.
- Wendler, G. (1964). Laufen und Stehen der Stabheuschrecke *Carausius morosus*: Sinnesborstenfelder in den Beingelenken als Glieder von Regelkreisen. *Z vergl Physiol*, 48:198–250.
- Wendler, G. (1977). Kybernetik der Bewegung. *Kybernetik*, pages 11–34.

REFERENCES

- White, D. (1977). *Mechanics and energetics of animal locomotion: Muscle mechanics pp.* 23-55. New York: John Wiley & Sons.
- White, D. and Thorson, J. (1975). *The kinetics of muscle contraction.* Pergamon Press.
- White, D. C. (1983). The elasticity of relaxed insect fibrillar flight muscle. *J Physiol*, 343:31–57.
- Whitehead, N. P., Allen, T. J., Morgan, D. L., and Proske, U. (1998). Damage to human muscle from eccentric exercise after training with concentric exercise. *J Physiol*, 512 (Pt 2):615–620.
- Whitehead, N. P., Morgan, D. L., Gregory, J. E., and Proske, U. (2003). Rises in whole muscle passive tension of mammalian muscle after eccentric contractions at different lengths. *J Appl Physiol*, 95(3):1224–1234.
- Whitehead, N. P., Weerakkody, N. S., Gregory, J. E., Morgan, D. L., and Proske, U. (2001). Changes in passive tension of muscle in humans and animals after eccentric exercise. *J Physiol*, 533(Pt 2):593–604.
- Wilkie, D. (1956). Measurement of the series elastic component at various times during a single muscle twitch. *J Physiol*, 134(3):527–530.
- Wilson, D. and Larimer, J. (1968). The catch property of ordinary muscle. *Proc Nat Acad Sci USA*, 61:909–916.
- Winton, F. R. (1937). The changes in viscosity of an unstriated muscle (*Mytilus edulis*) during and after stimulation with alternating, interrupted and uninterrupted direct currents. *J Physiol*, 88(4):492–511.
- Wolf, H. (1990a). Activity patterns of inhibitory motoneurons and their impact on leg movement in tethered walking locusts. *J Exp Biol*, 152:281–304.
- Wolf, H. (1990b). On the function of a locust flight steering muscle and its inhibitory innervation. *J Exp Biol*, 150:55–80.
- Wood, S. A., Morgan, D. L., and Proske, U. (1993). Effects of repeated eccentric contractions on structure and mechanical properties of toad *sartorius* muscle. *Am J Physiol*, 265(3 Pt 1):C792–C800.
- Yang, Z., Stull, J. T., Levine, R. J., and Sweeney, H. L. (1998). Changes in interfilament spacing mimic the effects of myosin regulatory light chain phosphorylation in rabbit *psoas* fibers. *J Struct Biol*, 122(1-2):139–148.
- Yox, D., DiCaprio, R., and Fournier, C. (1982). Resting tension and posture in arthropods. *J Exp Biol*, 96:421–425.
- Zajac, F. (1989). Muscle and tendon: properties, models, scaling and application to biomechanics and motor control. *Critical Reviews in Biomedical Engineering*, 17(4):359–411.
- Zajac, F. and Gordon, M. (1989). Determining muscle's force and action in multi-articular movement. *Exerc Sport Sci Rev*, 17:183–230.
- Zakotnik, J., Matheson, T., and Dürr, V. (2006). Co-contraction and passive forces facilitate load compensation of aimed limb movements. *J Neurosci*, 26(19):4995–5007.
- Zhurov, Y. and Brezina, V. (2006). Variability of motor neuron spike timing maintains and shapes contractions of the accessory radula closer muscle of *Aplysia*. *J Neurosci*, 26(26):7056–7070.

Abbreviations

β - spring constant

CI_{1,2,3} common inhibitor motoneurons 1, 2 and 3

EJP - excitatory junctional potential

FETi - fast extensor tibiae motoneuron

FT - femur-tibia

F2 - femoral nerve 2

IJP - inhibitory junctional potential

lin-lin - double linear

log-log - double logarithmic

LSM - laser scanning microscope

ncr - nervus cruris

nl3 - nervus lateralis 3

PBS - phosphate buffered saline

P_{max} , P_0 - maximal isometric contraction force

SETi - slow extensor tibiae

T_{max} - time to reach maximum force

$T_{50,90off}$ - time to relax to 50 or 10 % of the maximal force level

V_{max} , V_0 - maximal shortening velocity

List of Publications

Articles

Hooper S.L., **Guschlbauer C.**, Blümel M., Rosenbaum P., Gruhn M., Akay T., Büschges A. (submitted)

Neural control of unloaded leg posture and of leg swing in stick insect, cockroach, and mouse differs from that in larger animals.

Hooper S.L., **Guschlbauer C.**, von Uckermann G., Büschges A. (2007)

Slow temporal filtering may largely explain the transformation of stick insect (*Carau-sius morosus*) extensor motor neuron activity into muscle movement. *J Neurophysiol* 98(3): 1718-1732.

Guschlbauer C., Scharstein H., Büschges A. (2007)

The extensor tibiae of the stick insect: Biomechanical properties of an insect walking leg muscle. *J Exp Biol* 210(Pt6): 1092-1108.

Hooper S.L., **Guschlbauer C.**, von Uckermann G., Büschges A. (2007)

Different motor neuron spike patterns produce contractions with very similar rises in graded slow muscles. *J Neurophysiol* 97(2): 1428-1444.

Hooper S.L., **Guschlbauer C.**, von Uckermann G., Büschges A. (2006)

Natural neural input that produces highly variable locomotory movements. *J Neurophysiol* 96(4): 2072-2088.

Poster and Abstracts

Guschlbauer C., Blümel M., Hooper S. L., Büschges A. (2009)

Measuring and modelling biomechanical parameters using individual stick insect extensor tibiae muscles. *Proceedings of the 32nd Göttingen Neurobiology Conference and the 8th Meeting of the German Neuroscience Society 2009.*

Blümel M., **Guschlbauer C.**, Büschges A. (2008)

Muscle properties in leg stepping control. *MBI workshop 4/2008 in Columbus (Ohio, USA): Neuromechanics of locomotion.*

Blümel M., **Guschlbauer C.**, Büschges A. (2008)

Muscle and joint simulation. *DFG workshop in Cologne 2008: Load and force control in walking pattern generation of animals and robots: From sensors to local and global function.*

Blümel M., **Guschlbauer C.**, Gruhn M., Scharstein H., Hooper S. L. (2007)

Predicting swing phase movements of the stick insect FT joint. *100th Annual meeting of the Deutsche Zoologische Gesellschaft (Köln) 2007*

Blümel M., **Guschlbauer C.**, Zehl L., Hooper S. L., Büschges A. (2007)

Investigating stick insect extensor muscle properties: an experimentally based muscle simulation. *Proceedings of the 31st Göttingen Neurobiology Conference and the 7th Meeting of the German Neuroscience Society 2007.*

Mentel T., **Guschlbauer C.**, Büschges A. (2007)

Phasing of subsets of motoneurons in the lamprey spinal cord is gated by segmental activation. *Proceedings of the 31st Göttingen Neurobiology Conference and the 7th Meeting of the German Neuroscience Society 2007.*

Guschlbauer C., Hooper S.L., Scharstein H., Büschges A. (2005)

Contraction dynamics of the stick insect extensor tibiae muscle. *Proceedings of the 30th Göttingen Neurobiology Conference and the 6th Meeting of the German Neuroscience Society 2005.*

Guschlbauer C., Scharstein H., Büschges A. (2004)

Force production in the extensor tibiae muscle of the stick insect. *Proceedings of the 7th International Congress of Neuroethology 2004.*

Talks

- at the *Annual German Arthropods Meeting* in Daun (2004)
- at the Biological Cybernetics department of Prof. Dr. H. Cruse in Bielefeld (2004)
- at the *Annual German Arthropods Meeting* in Kleinwalsertal (2003)

Acknowledgements

Ich möchte mich bei folgenden Personen besonders bedanken:

- Prof. Dr. Ansgar Büschges für die sehr gute Betreuung, die Vergabe meiner Diplom- und Doktorarbeit und seinen ansteckenden Enthusiasmus.
- Prof. Dr. Peter Kloppenburg für die freundliche Übernahme des Zweitgutachtens.
- Prof. Dr. Siegfried Roth für die freundliche Übernahme des Prüfungsvorsitzes meiner Disputation.
- Dr. Hans Scharstein für die langjährige Zusammenarbeit, seine Unterstützung und seine Geduld, insbesondere in mathematischen Fragen.
- Prof. Dr. Scott L. Hooper für die publikationsreiche Zusammenarbeit, seine Hilfsbereitschaft und sehr viele inspirierende wissenschaftliche Diskussionen.
- Dr. Tim Mentel und PD Dr. Joachim Schmidt für allerlei Hilfestellungen und anregende Konversationen.

- Marcus Blümel für seine unermüdliche Hilfsbereitschaft, etliche zugleich nützliche wie auch witzige Gespräche und seine beruhigende Art.
- Dr. Sandra Westmark, Dr. Géraldine v. Uckermann, Dr. Anke Borgmann, Eugenio Oliveira, Sherylane Marasigan und Sharon Meyen-Southard für viele Jahre netten Zusammenarbeitens.
- Dipl.-Ing. Michael Dübbert, Jan von Sydow, Hans-Peter Bollhagen, Dr. Matthias Gruhn, Katja Hellekes, Arndt von Twickel, Christina Klein, Philipp Rosenbaum, Sonja Karpati, Nina Meier, Jens Goldammer, Anne Woisnitza, Eva Berg, Viviane Fischer, Dr. Björn Nadrowski, Dr. Jörg Albert, PD Dr. Volker Dürr, Debora Fusca und allen ehemaligen Mitarbeitern für allerlei Unterstützungen und die nette Atmosphäre.
- Meinen Eltern und meiner Schwester für ihr Interesse an meiner Arbeit und ihre uneingeschränkte Unterstützung.
- Meiner Band Kent Coda.

Erklärung

Ich versichere, dass ich die von mir vorgelegte Dissertation selbstständig angefertigt, die benutzten Quellen und Hilfsmittel vollständig angegeben und die Stellen der Arbeit - einschließlich Tabellen, Karten und Abbildungen -, die anderen Werken im Wortlaut und Sinn nach entnommen sind, in jedem Einzelfall als Entlehnung kenntlich gemacht habe; dass diese Dissertation noch keiner anderen Fakultät oder Universität zur Prüfung vorgelegen hat; dass sie - abgesehen von oben angegebenen Teilpublikationen - noch nicht veröffentlicht worden ist sowie, dass ich eine solche Veröffentlichung vor Abschluss des Promotionsverfahrens nicht vornehmen werde. Die Bestimmungen dieser Promotionsordnung sind mir bekannt. Die von mir vorgelegte Dissertation ist von Prof. Dr. Ansgar Büschges betreut worden.

Köln, den 09.02.2009

Curriculum vitae

Christoph Guschlbauer
Sülzburgstraße 99-101
50937 Köln
c.guschlbauer@uni-koeln.de
cguschlbauer@gmx.de
*07.05.1977 in Wien (A)
österreichischer Staatsbürger

Ausbildung

- seit 2004: Doktorarbeit an der Universität zu Köln, Abteilung für Tierphysiologie; Betreuer: Prof. Dr. A. Büschges

- 1997-2003: Biologiestudium an der Universität zu Köln; Erlangung des Diplomgrades 2003; Betreuer: Prof. Dr. A. Büschges. Titel der Diplomarbeit: *Untersuchungen zur Muskelgeometrie und Krafterzeugung tibialer Muskeln bei der Stabheuschrecke.*
- 1996: Abitur am Einstein-Gymnasium in Kehl / Rhein (D)

Berufserfahrung

- seit 2002: Praktikumsbetreuung in Grund- und Hauptstudiumskursen (Bachelor- und Masterkursen) in Tierphysiologie / Neurobiologie an der Universität zu Köln
- Sommersemester 2008: Lecturer - Position am Zoologischen Institut der Universität zu Köln
- Sommer 2000: Prä- und postoperative Augenbewegungsuntersuchungen an Patienten des Herz- und Diabeteszentrums Nordrhein-Westfalen in Bad Oeynhausen

